Department of Civil and Environmental Engineering
University College Cork

Observations and modelling of carbon dioxide and energy fluxes from an Irish grassland for a two year campaign

By

Vesna Jaksic

A Thesis submitted to the National University of Ireland
In part candidature for the Degree of Master of Engineering Science

May 2004

Acknowledgements

This thesis was developed at the department of Civil and Environmental Engineering at the University College Cork from October 2001 to May 2003.

This work has been prepared as part of the Environmental Research Technological Development which is managed by the Environmental Protection Agency and financed by the Irish Government under the National Development Plan 2000-2006, Project CELTICFLUX (Grant No. 2001-CC/CD-(5/7)).

I would like to thank **Prof. Dr. J. P. J. O'Kane** for the use of the facilities of the Civil and Environmental Engineering Department.

I would like to express my profound thanks to **Teagasc Walsh Fellowship Programme** and **Dr. O. Carton** and **Dr. D. Fay**, from Environment and Land Use Department, Research Centre Johnstown Castle, for their support of the research programme and encouragement to present my work at Walsh Flellowships Seminar in Dublin (11th November 2003).

I would like to express my profound gratitude to my project supervisor **Prof. Dr. Gerard Kiely,** who initiated experiment in July 2001. His interest and the exchange of ideas were always stimulating and were encouraging me all the way throughout my study. He also brought me in contact with many scientists and encouraged me to participate at the AGU conference in Nice, France (April 2002) and at the Workshop on IEA Bioenergy Implementing Agreement in Dublin (20th November 2003).

I would like to thank **Dr. Gabriel Katul**, **Dr. Ram Oren** and **Dr. John D. Albertson** from Nicholas School of the Environment and Earth Science, Duke University, NC, USA, for the stimulating e-mail discussions during preparation of this thesis and work on the journal paper (to be submitted).

I would like to thank **Dr. Cheng-I Hsieh,** from Department of Bioenvironmental Systems Engineering, National Taiwan University, Taipei, Taiwan**,** for his helpful advice on the fetch subject.

I would like to acknowledge all who have contributed to this work with discussions, ideas and moral support during this project, and especially **Charlotte Le Bris**, **Ciaran Lewis**, **Fahmida Khandokar**, **Adrian Birkby**, **Todd Scanlon**, **Niall Bourke**, **Roberto Amboldi**, **Matteo Sottocornola,** **Marie Berthier**, **Gary Corcoran**,

Kenneth Byrne, **Paul Leahy** and **Anna Laine,** for their permanent help, and friendship.

I also would like to thank my husband **Aleksandar Jakšić** for his support, encouragement and love.

Abstract

An eddy covariance (EC) system for CO_2 fluxes was used continuously for two years (2002 and 2003) to study the interannual variability of net ecosystem exchange (NEE) and energy balance (EB) at a humid grassland site in South West Ireland. The climate is temperate and humid with mean annual precipitation of about 1470 mm for the area. Over 90% of Irish agricultural land is under grassland, suggesting the importance of quantifying the carbon fluxes in this ecosystem type. The grassland type can be described as moderately high quality pasture and meadow classified into the C_3-grass category. The farmland management practices in both years were similar, with intensely grazed (2.2 livestock units/ha) grassland fields subject to nitrogen fertilisation rates of approximately 300 kg.N/ha per year. The experimental grassland encompasses eight small dairy farms (of size 10 to 40ha each) with approximately 2/3$^{rd's}$ of the area grazed for eight months of the year while in the other 1/3rd the grass was cut (harvested for winter feed) twice per year in June and September. The year 2002 was wet (precipitation at 1785mm, ≈ 22% above average) and 2003 was dry (precipitation at 1185mm, ≈ 15% below average). The annual evapotranspiration (ET) was similar in both years, 370mm and 366mm in 2002 and 2003, respectively. We found that the wet year of 2002 had a NEE of -1.9 T.C/ha (uptake) compared to -2.6 T.C/ha for the dry year of 2003 (a 27% difference). One impact of 2002 being wet was that the first cut of silage was two weeks late (July 1) by comparison with the more normal date of June 15 for 2003. The NEE for June (July) 2002 was -75 (+2) g.C/m^2 and for June (July) 2003 was -31 (-23) g.C/m^2. The sum of the NEE for the eight months (February to September) was -340 g.C/m^2 for 2002 and -345 g.C/m^2 for 2003. The difference in NEE between the years was in the winter months (October to January) with 2002 having an NEE of +148 g.C/m^2 and 2003 with an NEE of + 85 g.C/m^2.The rainfall in these four months was 903mm in 2002 and 435mm in 2003. The rainfall of 2002 caused the soil moisture status to be more frequently saturated than in 2003. This resulted in a wetter soil environment that respired more. We conclude that the wetter winter of 2002 with its saturating effect on soil moisture caused enhanced ecosystem respiration which was responsible for the lower NEE of 2002.

Two semi-empirical models were then applied to simulate the net ecosystem CO_2 flux different time steps. The model proposed by Collatz *et al* [1991] considers the full biochemical components of photosynthetic carbon assimilation from Farquhar *et al.* [1980], and an empirical model of stomata conductance from Ball *et al*. [1987]. The model proposed by Jacobs [1994] is based on the empirical model of stomatal conductance from Jarvis [1976], and on a less detailed assimilation model from Goudriaan *et al*. [1985]. Both models satisfactorily predict CO_2 fluxes over the seasons for the grass catchment.

Contents

Chapter 3 The Eddy Covariance Method

Chapter 4 General meteorological data

Chapter 1
Introduction

Chapter 1 Introduction

1.1 Some ecology terms

1.1.1 Global climate change

The term 'climate change' is sometimes used to refer to all forms of climatic inconsistency [*Kyoto protocol*, 1997; *Hall et al.*, 2000; *Schimel at al.*, 2000a;*Schimel at al.*, 2000b], but because the Earth's climate is never static, the term is more properly used to imply a significant change from one climatic condition to another. In some cases, 'climate change' has been used synonymously with the term, 'global warming'. Scientists, however, tend to use the term in the wider sense to also include natural changes in climate [*Post at al.*, 1990; *Royer at al.,* 2001, *Sarmiento and Gruber*, 2002].

1.1.2 Greenhouse gases

Greenhouse gases include carbon dioxide (CO_2), methane (CH_4), nitrous oxide (N_2O), chlorofluorocarbons, and water vapour (H_2O). Carbon dioxide, methane, and nitrous oxide have significant natural and human sources while only industries produce chlorofluorocarbons [*Kiely*, 1997]. Water vapour has the largest greenhouse effect, but its concentration in the troposphere is determined within the climate system. Water vapour will increase in response to global warming, which in turn may further enhance global warming [*Campbell and Norman*, 1998].

Trace gases are both emitted and absorbed at the earth surface [*Dabberdt et al.*, 1993] and contribute to the greenhouse effect. Greenhouse gases (GHG) are transparent to certain wavelengths of the sun's radiant energy, allowing them to penetrate deep into the atmosphere or all the way to the Earth's surface [*Kiely*, 1997]. Greenhouse gases and clouds prevent some of infrared radiation from escaping, trapping the heat near the Earth's surface where it warms the lower atmosphere [*Kiely*, 1997; *Sarmiento and Gruber*, 2002]. Alteration of this natural barrier of atmospheric gases can raise or lower the mean global temperature of the Earth. This makes our planet about 30 ºC warmer than if those gases were not present, warm enough to support life as we know it [*Campbell and Norman*, 1998].

1.1.3 Photosynthesis

Photosynthesis, also called 'primary production', is the production of organic molecules from inorganic molecules by the plants [*Budyko*, 1974]. In plants, cell pigments called chlorophylls trap light from the sun. The photochemical reactions in this first phase of photosynthesis produce energy-rich compounds and release oxygen. In the second phase, enzymes in the plant use these compounds to 'fix' carbon dioxide [*Campbell and Norman*, 1998] (see section 7.1.1). That is, they combine atmospheric CO_2 with these other compounds to form organic matter for plant nutrition and growth. Much of this locked-up carbon is recycled into the soil as plant matter. Leaves die and decay, as worms and microorganisms like bacteria break down the organic matter [*Batjes*, 1999].

1.1.4 The temperate grassland ecosystems

Grassland biomes are large, rolling terrains of grasses, flowers and herbs. Latitude, soil and local climates for the most part determine what kind of plants grow in a particular grassland [*Encyclopedia Britannica*]. A grassland is a region where the average annual precipitation is great enough to support grasses, and in some areas a few trees [*Encyclopedia Britannica*]. Temperate grasslands are composed of a rich mix of grasses and forbs and underlain by some of the world's most fertile soils. In temperate grasslands the average rainfall per year ranges from 250-1000 mm [*Radford University*, 2000]. The amount of rainfall is very important in determining which areas are grasslands because it's hard for trees to compete with grasses in places where the upper layers of soil are moist during part of the year but deeper layers of soil are always dry [*UC Berkeley*, 2000].

1.1.5 C_3 plants

Most plant species fall into one of the two major groupings (C_3 and C_4 plants) with respect to carbon assimilation [*Encyclopedia Britannica*]. In the most common group, the primary product of photosynthesis is a three-carbon sugar, so these species are called C_3 plants. The CO_2 is directly introduced into the Calvin cycle [*Kozaki and Takeba*, 1996]. C_3 plants include most temperate plants, more than 95% of all earth's plants.

In our case, the metabolic pathway for carbon fixation is assumed to be a C_3 Cycle [*Le Bris*, 2002] (see section 7.1.1).

1.1.6 Carbon cycle

The movement of carbon, in its many forms, between the biosphere, atmosphere, oceans, and geosphere is described by the carbon cycle (a network of interrelated processes that transport carbon between different reservoirs on Earth) [*Schimel at al.*, 2000a; *Hall et al.*, 2000; *Sarmiento and Gruber*, 2002], illustrated in the Figure 1.1. The carbon cycle is one of the biogeochemical cycles [*Campbell and Norman*, 1998]. In the cycle there are various sinks (see section 1.1.8), or stores of carbon (represented by the boxes) and processes by which the various sinks exchange carbon (the arrows).

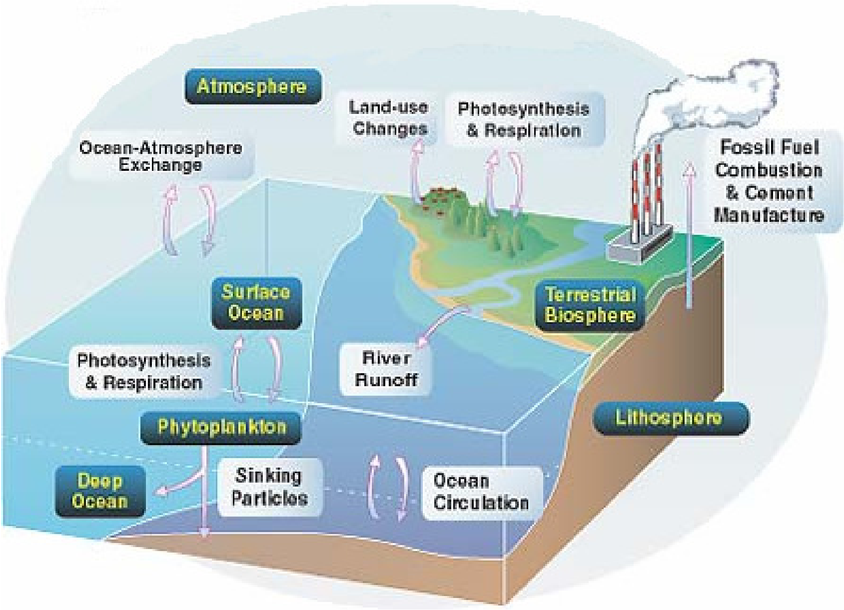

Figure 1.1: The Global carbon cycle
(www.lbl.gov/.../Archive/ sea-carb-bish.html)

1.1.7 Carbon source or carbon emission

Carbon emission is a process of releasing CO_2 flux in the atmosphere. Two major sources of carbon are the burning fossil fuels and clearing of tropical rainforests. About half of emitted CO_2 accumulates in the atmosphere, prompting concerns about global warming [*Kyoto protocol*, 1997].

1.1.8 Carbon sink or carbon sequestration

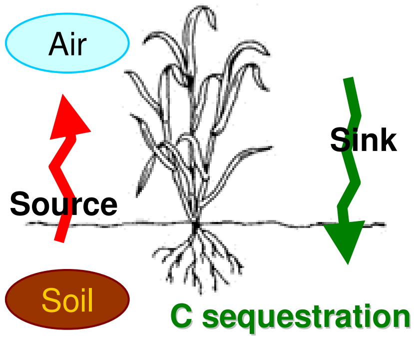

Figure 1.2: Sink and source definition

Plants through photosynthesis transform CO_2 into organic matter, which either stays in the plants or is stored in the soils. The process of storage of CO_2 in the soil as carbon (C) is called carbon sequestration [*Bruce et al.*, 1999], (see Figure 1.2).

In the case of the wood in trees, carbon may remain sequestered for centuries [*Jacksonet al.*, 2002]. In the case of grasses, carbon from the plant matter will return to the atmosphere in only a matter of years [*Jackson et al.*, 2002]. However the soil forms yet another carbon sink where organic carbon can stay for a long time, longer than in the plant [*Jackson et. al.*, 2002]. The global soil carbon pool is about twice as large as the plant pool [*Cruickshank et al.*, 1998; *Schimel at al.*, 2000a].

1.2 General Background

Many climate experts believe that the increased concentrations of Greenhouse gases are magnifying to dangerous levels an otherwise beneficial natural phenomenon known as the greenhouse effect [*Kyoto protocol*, 1997; *Sarmiento and Gruber*, 2002; *Schimel at al.*, 2000a].

Although greenhouse gases together make up less than 0.1% of our atmosphere [*Encyclopedia Britannica*], they act as a kind of thermal blanket around the whole earth, preventing a significant amount of incoming solar energy from being radiated back out into space [*Kiely*, 1997; *Sarmiento and Gruber*, 2002]. Unfortunately this blanket is getting thicker as the proportion of greenhouse gases increases because of human influences [*Kyoto protocol*, 1997], which may be causing a dangerous increase in the average temperature of our planet's atmosphere. It is estimated that the global temperature would increase by between 1 and 3.5 ºC if CO_2 concentration were to double. It is projected that this will happen before the end of the 21st century [*Houghton*, 1990]. Such changes could trigger major disruptions around the world: food production patterns could shift as agriculture becomes more difficult in some areas and easier in others, large numbers of plant and animal species could become extinct, forests and water supplies could be threatened etc [*Kyoto protocol*, 1997; *EMS*, 2003].

The Kyoto Protocol for Ireland requires that emissions of GHG must be no more than 13% above the 1990 levels. As of 2001, emissions are 31% greater than the 1990 levels [*EPA*, 2000]. By 2008 – 2012 the "business as usual" scenario forecast (produced in 2000 based on 1998 data) is that emissions may be more than 37% greater than the 1990 levels [*EPA*, 2003]. Agriculture is estimated to be responsible for about 27% (soils 5.5%) of total emission in 2001 [*EPA*, 2003].

The earth's vegetative cover is a key component in the global carbon cycle due to its dynamic response to photosynthetic and respirative processes. The increase of carbon emissions from fossil fuels into the atmosphere as well as deforestation processes during the last century are accountable for most of the estimated 0.4 % annual increase in concentration of atmospheric CO_2 [*IPCC*, 1997; *McGettigan and Duffy*, 2000]. Oceanic and forestry ecosystems have been studied in much detail because of their significant carbon sink attributes [e.g., *Post et al.,* 1990; *Cruickshank et al.,* 1998; *Valentini et al.,* 2000; *Berbigier et al.,* 2001; *Falge et al.,* 2002]. Studies of carbon fluxes in temperate grassland have been overlooked due to the perception that this ecosystem is in equilibrium with regard to carbon fluxes [*Hall et al.*, 2000; *Ham and Knapp*, 1998; *Hunt et al*., 2002]. However, representing 32 % of earth's natural vegetation, the carbon fluxes of grasslands are now being revisited [*Saigusa et al*., 1998; *Frank and Dugas*, 2001; *Hunt et al*., 2002; *Jackson et al*., 2002; *Novick et al*., 2004] and may yet play a role in the missing global carbon sink [*Ham & Knapp*, 1998; *Robert*, 2001; *Pacala et al*., 2001; *Goodale and Davidson*, 2002] of the global carbon balance. Grasslands are the dominant ecosystem in Ireland representing 45% of the total landmass (with 26% for mountains and lakes, 17% for peat lands, 7% for forests and only 5% for cultivated fields) [*Gardiner and Radcliffe*, 1980].

Several short-term studies have shown that grassland ecosystem can sequester atmospheric CO_2 [e.g. *Bruce et al*., 1999; *Batjes,* 1999; *Conant et al*., 2001; *Soussana et al*., 2003], but few multi-annual data sets are available [*Frank et al*., 2001; *Frank and Dugas,* 2001; *Falge et al*., 2002; *Knapp et al*., 2002; *Novick et al*., 2004]. To quantify the source-sink potential of grasslands in different climatic zones, long-term surface flux measurements are required [*Goulden et al*., 1996; *Ham and Knapp*, 1998; *Knapp et al*., 2002; *Baldocchi*, 2003] to build and test models that represent the biological and physical processes at the land surface interface. Such models (e.g. BIOME3, Pnet, PaSim, Canveg) [*Aber and Federer*, 1992; *Wilkinson and Janssen*, 2001; *Soussana et al*., 2003] can be used to examine scenarios of changing land use and management practices as well as climate change.

Many atmospheric, hydrological and biogeochemical processes are influenced by the partitioning of available energy into the fluxes of sensible and latent heat from the land surface [*Humphreys et al*., 2003]. A better understanding of how energy and mass are partitioned at the earth's surface is necessary for improving regional weather and global climate models [*Twine et al*., 2000; *Humphreys et al*., 2003]. These models are used to assess the impact of societal choices, such as abiding by the Kyoto Protocol for carbon sequestration. Based on numerous measurements, carbon dioxide fluxes which are measured by eddy covariance, are underestimated by the same factor as eddy covariance evaporation measurements when energy balance closure is not achieved [*Twine et al*., 2000; *Wever, et al*., 2002]. Therefore, dealing with lack of energy balance closure should be also considered in the standards for a long term, flux measurement networks even though it has received little attention so far [*Baldocchi et al.*, 1996; *Twine et al.*, 2000].

1.3 Methods

The Dripsey flux site in Cork, Southwest Ireland, is a perennial ryegrass (C3 category) pasture, very typical of the vegetation of this part of the country, and is grazed for approximately 8 months of the year. The lands are fertilised with approximately 300kg/ha.year of nitrogen. The flux tower monitoring CO_2, water vapour and energy was established in June 2001 and we have continuous data since then. The site also includes streamflow hydrology and stream water chemistry. We present the results and analysis for CO_2 for the years 2002 and 2003.The climate is temperate with a small range of temperature during the year and abundant precipitation. Several methods can be used to measure CO_2 fluxes. Here, CO_2 and H_2O fluxes between the ecosystem and the atmosphere as well as other meteorological data were recorded continuously at 30 minutes intervals by an aerodynamic method (Eddy Covariance method) over two years. No device has been set up to measure specific soil respiration and LAI (Leaf Area Index). Once collected, data were filtered and filled when found inadequate or suspect, as it is generally the case with tower-based flux measurements.

Two different semi-empirical models were tested in comparison with the measurements. The first is a model proposed by Collatz *et al* [1991] that considers the full biochemical components of photosynthetic carbon assimilation from Farquhar *et al.* [1980], and an empirical model of stomata conductance from Ball *et al*. [1987]. The second is a model proposed by Jacobs [1994], which is less demanding in terms of inputs parameter and often linked with meteorological research [*Calvet et al.*, 1998]. It is based on the empirical model of stomatal conductance from Jarvis [1976], and on a less detailed assimilation model from Goudriaan *et al*. [1985].

This work is part of a five-year (2002-2006) research project funded by the Irish Environmental Protection Agency.

1.3 Objectives

The objective of the project was to determine the energy and CO_2 fluxes over two years (2002 and 2003) using an eddy covariance (EC) system to measure CO_2 and water vapour fluxes in a humid temperate grassland ecosystem in Ireland. The central to this objective is investigation of seasonal, annual and interannual variation in terrestrial (grassland ecosystem) CO_2 and energy fluxes and to determine possible meteorological and phonological controls on net CO_2 and energy exchange. Long-term measurements of this kind are essential for examining the seasonal and interannual variability of carbon fluxes [*Goulden et al.*, 1996; *Baldocchi*, 2003]. Another aim of this project was to study the interannual variability of CO_2 flux relative to the climatic and agricultural forcing.

The modelling part of this work is just the first step of what could be achieved with such a tool. In this study, the models help to get a better understanding of processes at work, and try to give a faithful description of the reality. The comparison of two models is a good method to understand the most adapted description, and the level of complexity needed to fit CO_2 fluctuations.

1.4 Layout of thesis

Chapter 2 describes studied site and instruments used in experiment.

Chapter 3 describes eddy covariance method used for measuring CO_2 and water vapour fluxes.

Chapter 4 analyses the meteorological data measurements.

Chapter 5 provides estimates of the energy fluxes, energy balance closure and evapotranspiration.

Chapter 6 contains a discussion and analysis of CO_2 flux during two year studies.

Chapter 7 contains modelling of CO_2 flux using Jacobs's (A-g_s) and Collatz's models.

Chapter 8 presents the conclusions and recommendations and makes suggestions for continuing research.

The Appendices include Hsieh's model matlab codes, Penman-Monteith equation matlab codes, Priestley-Taylor equation matlab codes, contribution of Webb correction to CO_2 flux, Daytime fitting for 2002 and 2003, parameters for CO_2 flux modelling, analyses of measurements of CO_2 and energy fluxes for Wexford grassland during 2003, and complementary production.

Chapter 2
Data Collection

Chapter 2 Data collection

2.1 Site description

2.1.1 Location

The Dripsey experimental grassland is located near the town of Donoughmore, Co Cork in South West Ireland, 25 km northwest of Cork city (52º North latitude, 8º 30' West longitude), (see Figure 2.1).

Figure 2.1: Location of the site area

The Dripsey grassland at an elevation of 220 m above sea level has a gentle slope to a stream of 3% grade (see Figure 2.2). The soil is classified as brown-grey podzols [*Daly*, 1999]. The topsoil is rich in organic matter to a depth of about 15cm (about 12% organic matter, [*Daly*, 1999]), overlying a dark brown B-horizon of sand texture. A yellowish brown B-horizon of sand texture progressively changes to a brown, gravely sand which constitutes the parent material at a depth of approximately 0.3m. The underlying bedrock is old red sandstone [*Scanlon et al.*, 2004]. Depth averaged over the top 30cm the volumetric soil porosity was 0.49 (m^3/m^3), the saturation moisture level was 0.45, the field capacity was 0.32, the wilting point was 0.12, and the air dried moisture was 0.02.

Figure 2.2: Dripsey site

2.1.2 Field history and Grassland management

The site is agricultural grassland, typical of the land use and vegetation in this part of the country.

The vegetation cover at Dripsey is grassland of moderately high quality pasture and meadow, whereas the dominant plant species is perennial ryegrass. Considering the environmental conditions, warm but not hot temperatures and high humidity with very good airflow and the latitude of Ireland, the metabolic pathway for carbon fixation is assumed to be a Calvin-Benson Cycle (C3 grass) [*Le Bris*, 2002].

Like much of the surrounding rural area, the landscape near the tower is partitioned into small fields. Management strategies for boosting grassland production varied according to the individual farmers. The land use is a mixture of paddocks for cattle grazing (approximately 2/3^{rds} of fields) and fields for cutting (silage harvesting) (approximately 1/3rd of fields).

Cattle grazing begins in March and ends in October (approximately 8 months). The rotational paddock grazing periods last approximately one week in four. The grass height in the grazing fields varies from 0.05m to 0.2m. With wet fields in the autumn of 2002, cattle were not grazing (as cattle damage the fields in wet times) but were housed indoors from early October leaving the standing biomass to its own devices. By contrast, the autumn of 2003 was dry and cattle were grazing (at least during the day) up to December.

Livestock density at the site is 2.2 LU/ha [*Lewis*, 2003], where Livestock Units (LU) is the basis of comparison for different classes and species of stock. A dairy caw is taken as the basic grazing livestock unit (1 LU) that requires approximately 520 kg of good quality pasture dry matter per year.

In the cut fields the grass is harvested in the summer, first in May or June and second time in September, and exported as silage from the pastureland for winter feed. For the two years of the study, the first annual cutting was in July of 2002 and June of 2003. The height of grass just before cutting in silage fields reaches about 0.5 m in summer, whereas it is down to 0.15 m in wintertime during the resting period. Due to the mild climatic conditions the field stays green all year. No measurement of the biomass or of the Leaf Area Index (LAI) of grass has been made on this site. The annual yield of silage in the region has been 8 to 12 Tonnes of dry matter per hectare per year depending on the weather. The dry matter is composed of 46% carbon (Kiely, Teagasc, personal communication).

Grass productivity is enhanced with the application of approximately 300kg of nitrogen in fertiliser and slurry, spread at intervals of approximately six weeks between February and September [*Lewis*, 2003]. Nitrogen in chemical fertilizer was applied at the rate of 214 and 210 kg of N/ha, and nitrogen in slurry approximately at 91 and 80 kg of N/ha in 2002 and 2003, respectively. The monthly rates of chemical fertilizer and slurry for 2002 and 2003 [*Lewis*, 2003] are given in Figure 2.3 and 2.4 respectively, while exact values in kg/ha.month are given in Table 2.1.

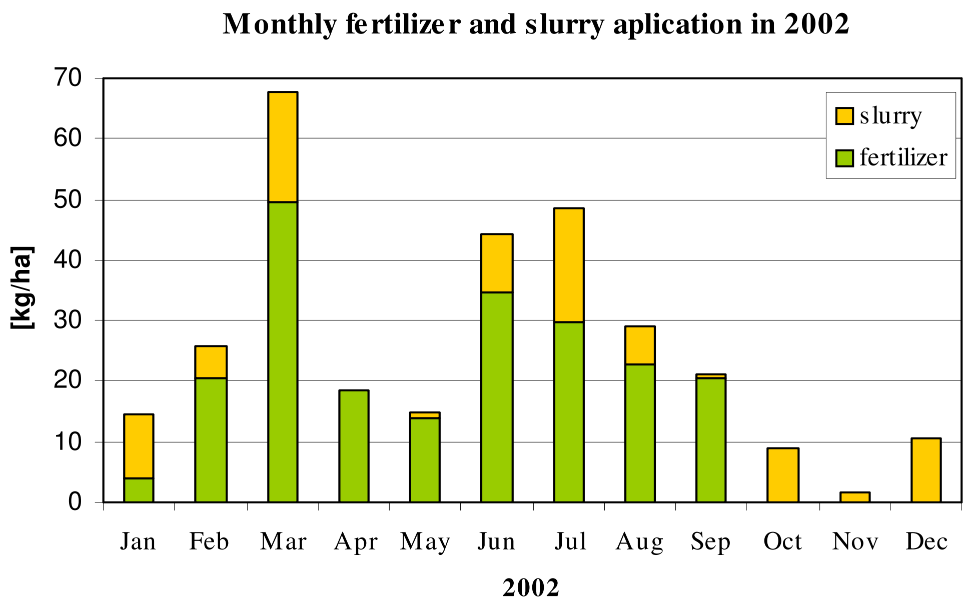

Figure 2.3: Monthly application of nitrogen fertilizer (green) and slurry (yellow) for year 2002 at Dripsey site

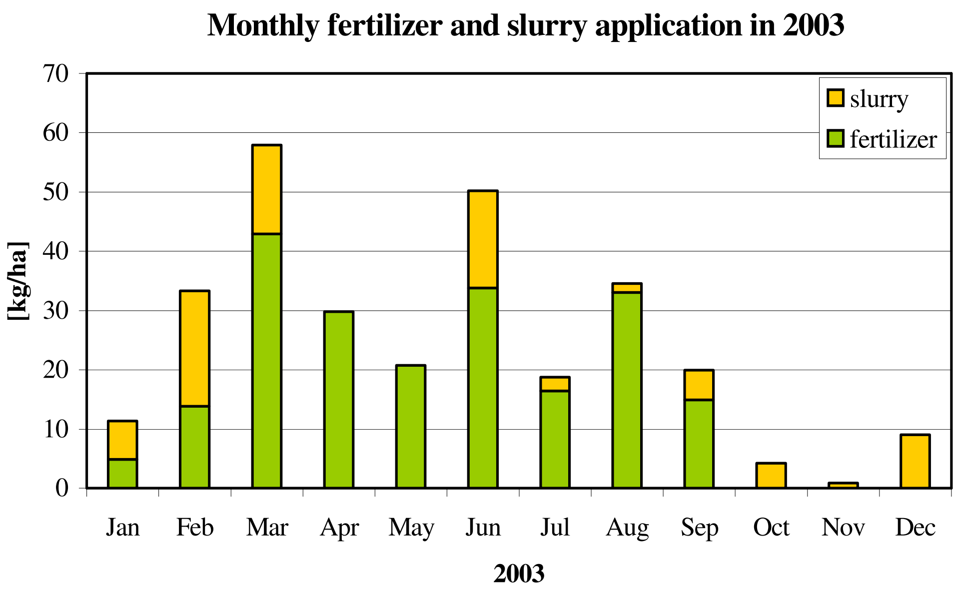

Figure 2.4: Monthly application of nitrogen fertilizer (green) and slurry (yellow) for year 2003 at Dripsey site

Table 2.1: Monthly application of nitrogen fertilizer and slurry in [kg/ha]

Year	2002			2003		
Month	**Fertiliser [kg/ha]**	**Slurry [kg/ha]**	**SUM [kg/ha]**	**Fertiliser [kg/ha]**	**Slurry [kg/ha]**	**SUM [kg/ha]**
January	3.9	10.7	14.6	4.9	6.4	11.3
February	20.6	5.0	25.6	13.8	19.5	33.3
March	49.6	18.0	67.5	42.9	15.0	57.9
April	18.4	0	18.4	29.8	0	29.8
May	13.9	0.8	14.8	20.7	0	20.7
June	34.5	9.7	44.3	33.7	16.5	50.2
July	29.8	18.7	48.4	16.4	2.3	18.8
August	22.9	6.3	29.2	33.0	1.5	34.6
September	20.6	0.4	21.0	14.9	5.1	20.0
October	0	9.1	9.1	0	4.2	4.2
November	0	1.7	1.7	0	0.9	0.9
December	0	10.5	10.5	0	9.0	9.0
SUM	214.1	90.9	305.0	210.3	80.5	290.8

2.1.3 Climate

The climate is temperate and humid (from the influence of the warm Gulf Stream in the North East Atlantic Ocean) with mean annual precipitation in the Cork region of about 1200 mm. The rainfall regime is characterized by long duration events of low intensity (values up to 40 mm/day). Short duration events of high intensity are more seldom and occur in summer.

Daily air temperatures have a very small range of variation during the year, going from a maximum of 20ºC to a minimum of 0ºC, with an average of 15ºC in summer and 5ºC in winter. This part of Ireland is windy with a mean wind velocity of 4 m/s at the site with peaks up to 16 m/s. The main wind comes from the southwest.

2.2 Description of instruments

The flux tower monitoring carbon dioxide, water vapour and energy was established in June 2001 and we have continuous data since then. The site also includes streamflow hydrology and stream water chemistry. In this section we present an overview of the sensors and techniques used for data collection.

2.2.1 Weather station

The experimental system used in this study is composed of a 10 m high tower, which supports different types of sensors connected to a datalogger. The datalogger controls the measurements, data processing and digital storage of the sensor outputs. A secured perimeter has been defined with a wire fence to protect the tower sensors, as well as to define a setting up area for the soil devices (see Figure 2.5).

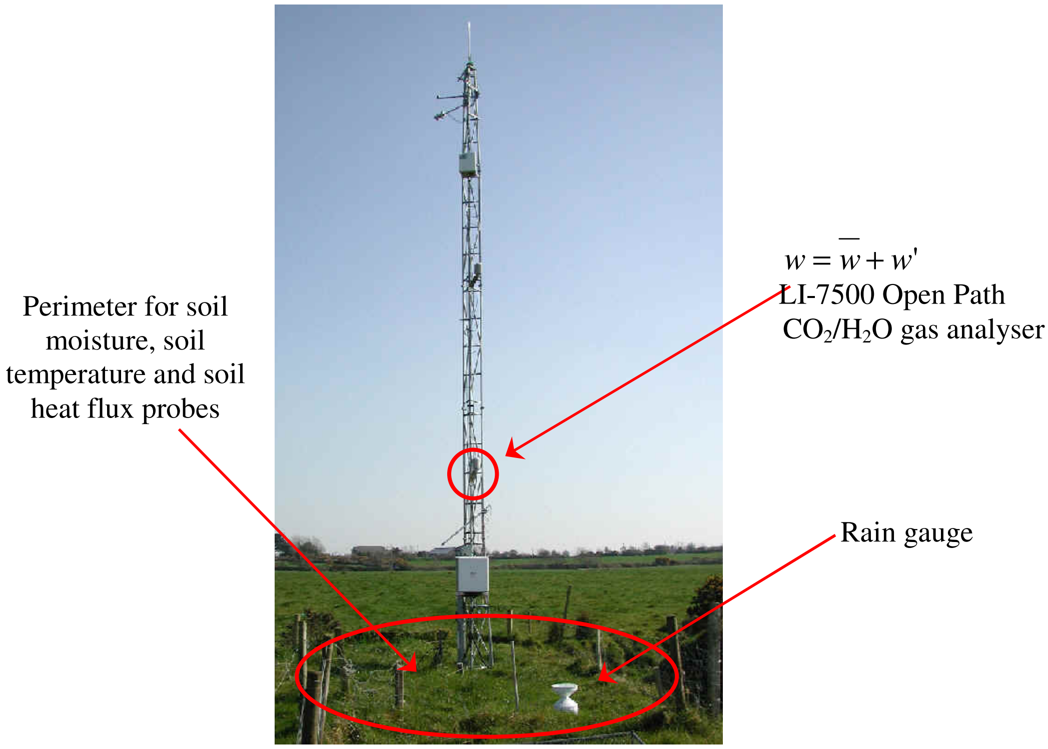

Figure 2.5: Tower at Dripsey site

Figure 2.5 shows tower in its full height and indicates position of the weather sensors. The tower supports sensors for measuring the relative humidity and air temperature at 3 m and various types of sensors at 10 m (see Figure 2.6). The rain gauge is located on the ground, while the soil moisture, soil heat flux plates and soil temperature probes are underground near the tower. The white box near the foot of the tower is called 'Campbell environmental box' and houses the datalogger, the multiplexer, the barometric pressure sensor, as well as a modem connection.

Figure 2.6 focuses on the top of the tower, showing the positions of net radiometer, sonic anemometer, and CO_2/H_2O gas analyser. On 22nd December 2003 the position of the sonic anemometer and the CO_2/H_2O gas analyser were moved from 10 m down to 3 m.

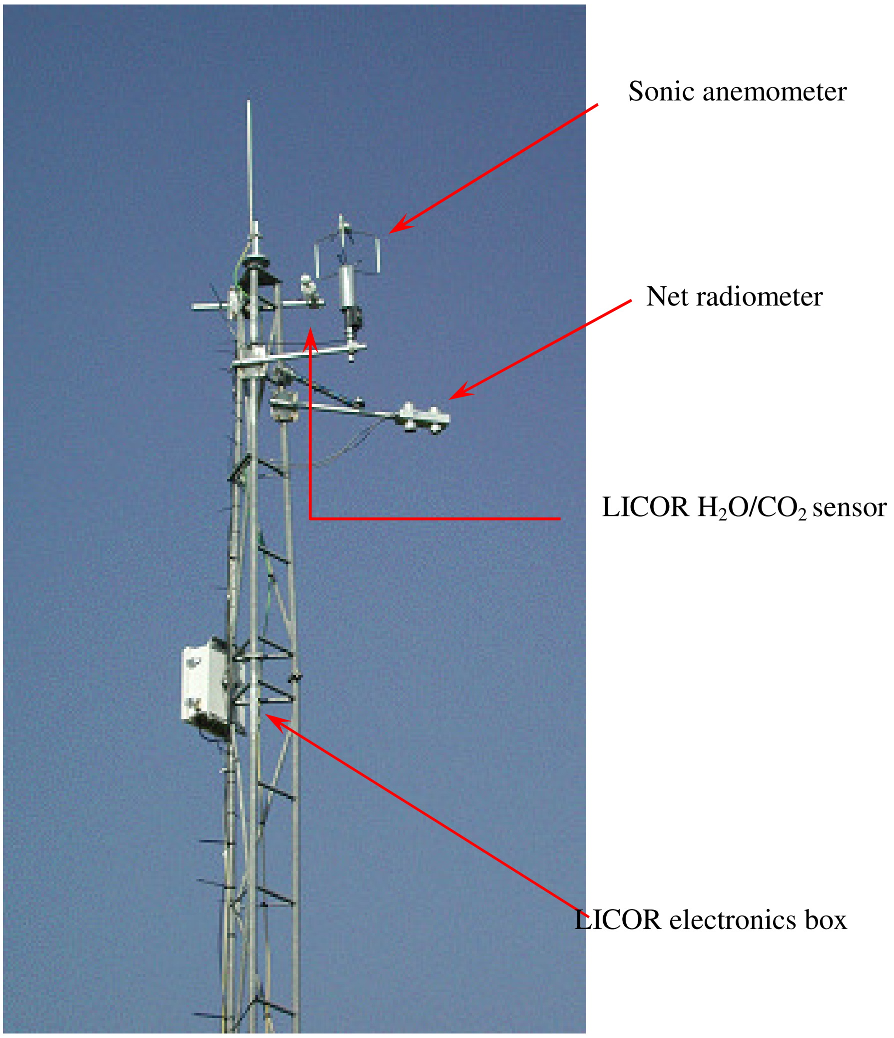

Figure 2.6: Top of the tower with instruments

Table 2.2 the sensors and logging devices that were used in the study. More details of the sensors are given in the following text.

Table 2.2: Equipment employed in the study

	Name	Model and manufacture
Sensors	1 Net radiometer	CNR 1 from Kipp & Zonen
	1 3D Sonic anemometer	Model 8100 from Young
	1 CO_2/H_2O gas analyser	LI-7500 from LI-COR Inc.
	1 PAR sensor	PAR LITE from Kipp & Zonen
	Combined humidity & temperature probes	HMP45C from Campbell sc.
	1 Barometric pressure sensor	PTB101B from Campbell sc.
	Soil heat flux plates	HFP01 from Campbell sc.
	Soil temperature probes	Model 107 from Campbell sc.
	6 Soil moisture monitors	CS616 from Campbell sc.
	1 Rain gauge	ARG100 from Campbell sc.
Logging devices	1 Datalogger	CR23X from Campbell sc.
	1 Multiplexer	AM 16/32 from Campbell sc.
	1 modem telephone connection	

2.2.2 Net Radiometer

Net radiation was measured with a net radiometer (CNR1 from Kipp & Zonen) positioned horizontally at 10 m above the ground. It is intended to analyse the radiation balance of solar and far infrared radiation. The most common application is the measurement of Net Radiation at the earth's surface. The Earth receives only one two-billionth of the energy the sun produces [*Encyclopedia Britannica*]. Much of the energy that hits the Earth is reflected back into space. Most of the energy that isn't reflected is absorbed by the Earth's surface. As the surface warms, it also warms the air above it. Net radiation is the difference between the incoming and outgoing radiation [*Campbell and Norman*, 1998].

The instrument consists of a pyranometer and pyrgeometer pair that faces upward and a complementary pair that faces downward. The pyranometers and pyrgeometers measure short-wave and far infrared radiation, respectively. All four sensors are calibrated to an identical sensitivity coefficient [*Kipp & Zonen*, 2000].

Pyranometer facing upward measures incoming radiation from the sky, and the other, which faces downward, measures the reflected solar radiation (see Figure 2.7). Thus the albedo (α), which is the short wave reflection factor for a particular ground surface, can also be determined [*Campbell and Norman*, 1998; *Kipp & Zonen*, 2000]:

$$\alpha = \frac{(\text{reflected solar radiations})}{(\text{incoming solar radiations})} \tag{2.1}$$

Since the albedo is the ratio of incoming and reflected solar radiation it is a between 0 and 1. Typical values are 0.9 for snow, and 0.3 for grassland [*Kipp & Zonen*, 2000]. A pyranometer consists of a thermopile sensor, housing, glass dome and a cable. The thermopile is coated with a black absorbent paint, which absorbs the radiations and converts them into heat. The resulting heat flow causes a temperature difference across the thermopile. The thermopile generates a voltage output. The absorber paint and the dome determine spectral specifications. The thermopile is encapsulated in the housing in such a way that its field of view is 180° degrees, and that its angular characteristics fulfil the so-called cosine response.

The conversion factor between voltage (V) and Watts per square metre of solar irradiance E (incoming or reflected in W/m^2), is the so-called calibration constant C or sensitivity [*Kipp & Zonen*, 2000].

$$E = \frac{V}{C} \tag{2.2}$$

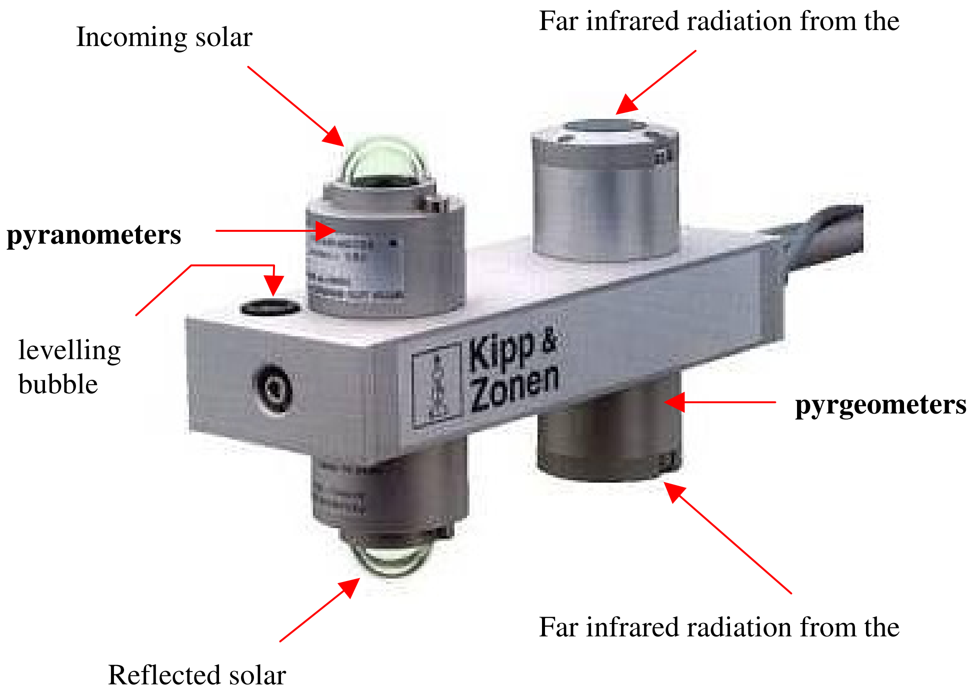

Figure 2.7: Net radiometer and its main components
(from Kipp & Zonen manual)

Far infrared radiation is measured by the mean of two pyrgeometers. One facing upward measures the far infrared radiations from the sky, the other, which faces downward, measures far infrared radiations from the soil surface (see Figure 2.7). A pyrgeometer consists of a thermopile sensor, housing, and a silicon window. The thermopile works the same way as for the pyranometer. The window serves both as environmental protection and as a filter. It only transmits the relevant far infrared radiation, while obstructing the solar radiation. The thermopile is encapsulated in its housing, so that its field of view is 150 degrees, and its angular characteristics fulfil the so-called cosine response as much as possible, in this field of view. The limited field of view does not produce a large error because the missing part of the field of view does not contribute significantly to the total, and is compensated for during calibration [*Kipp & Zonen*, 2000]. The pyrgeometer temperature (T) in ° K is needed for estimating the far infrared radiation from the voltage (V). Hence, a temperature sensor is located in the net radiometer body. The calculation of far infrared irradiance (E) in W/m^2 is given hereunder [*Kipp & Zonen*, 2000]:

$$E = \frac{V}{C} + 5.67 \times 10^{-8} \times T^4 \qquad (2.3)$$

The calculation of the net total radiation (Rn) is performed automatically by the instrument's [*Kipp & Zonen*, 2000] user's own processing software and is thus given in as an output in W/m^2:

$$Rn = E_{\text{incoming solar}}\downarrow + E_{\text{far infrared from sky}}\downarrow - E_{\text{reflected solar}}\uparrow - E_{\text{far infrared from ground}}\uparrow \qquad (2.4)$$

2.2.3 Ultrasonic Anemometer

Wind velocity, wind direction and virtual potential (sonic air) temperature measurements were performed by the model 81000 ultrasonic anemometer from Young (Figure 2.8) positioned at the top of the 10m tower.

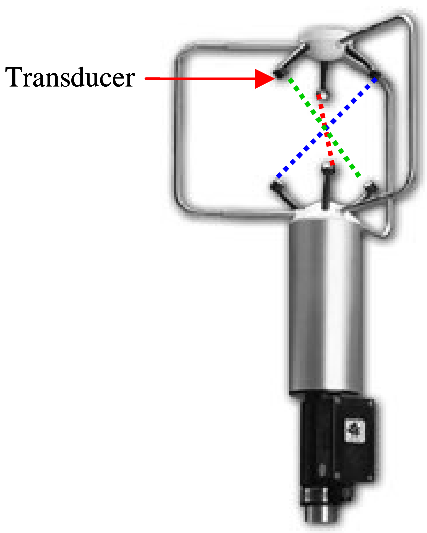

It is a 3-dimensional, no-moving-parts wind sensor. Whereas other 2D anemometers ignore the vertical wind component, the 81000 provide a complete picture of the wind. Robust construction, combined with 3 opposing pairs of ultrasonic transducers, provides accurate and reliable wind measurements [*Young*, 2001].

Figure 2.8: The sonic anemometer with the three paths shown in red (E -W), blue (SW-NE), green (NW-SE), as for a typical orientation of the device (From Young manual)

The instrument makes observations of the wind velocities by measuring the travel time of ultrasonic signals sent between the upper and lower transducers (see Figure 2.9). By measuring the transit time in each direction along all three paths, the three dimensional wind velocity and speed of sound may be calculated. From speed of sound, sonic virtual potential (sonic air) temperature is derived [*Young*, 2001].

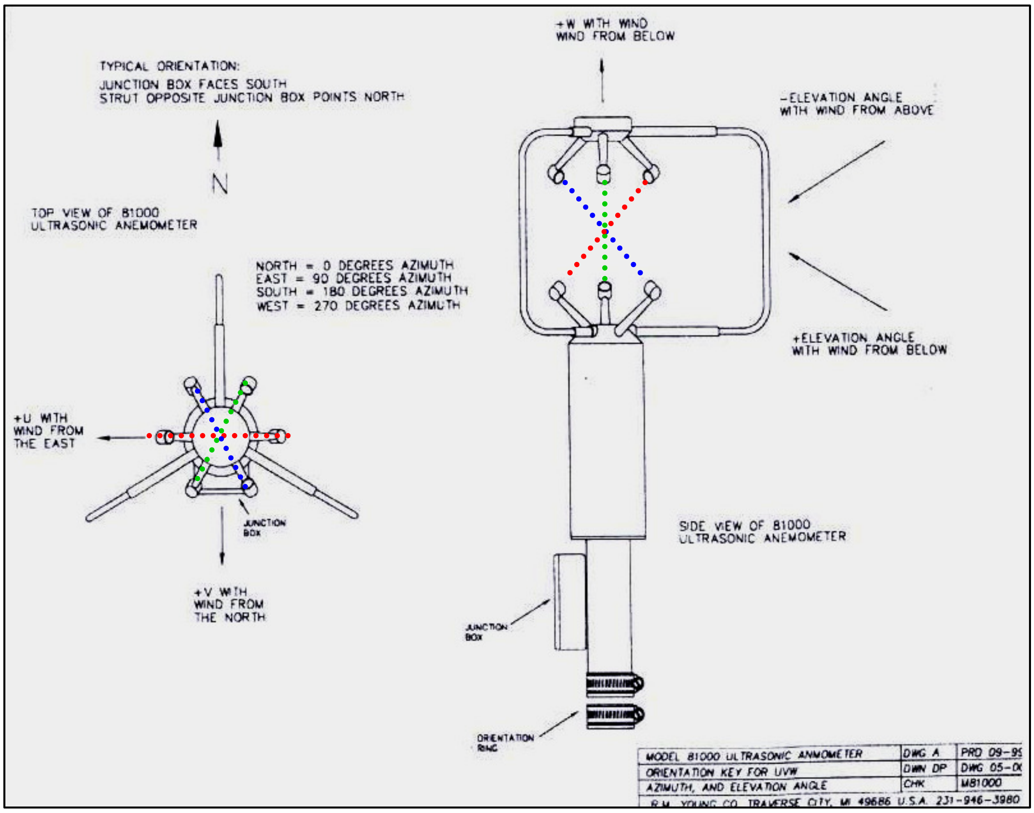

Figure 2.9: Ultrasonic Anemometer axis systems
(from Young manual)

2.2.4 Open path CO_2/H_2O gas analyser

Figure 2.10: LI-7500 Open path CO_2/ H_2O gas analyser (from LI-COR manual)

Carbon dioxide (CO_2) and water vapour (H_2O) densities in the turbulent air are monitored by a LI-7500 Open Path CO_2/H_2O non-dispersive, absolute infrared gas analyser from LI-COR (Figure 2.10). In the eddy covariance technique, these data are used in conjunction with sonic anemometer air turbulence data to determine the fluxes of CO_2 and H_2O [*LI-COR*, 2001]; the technique will be explained in detail in chapter 3. A high frequency (10 Hz) and high precision analyser such as LI-7500 is needed to correctly sample the turbulent eddies in the lower boundary layer [*Garratt*, 1992]. The sensor head has a smooth, aerodynamic profile, in order to minimize flow disturbance.

The open path analyser eliminates time delays, pressure drops, and sorption/desorption of water vapour on tubing employed with a closed path analyser [*LI-COR*, 2001]. The LI-7500 is placed within about 20 cm of the centroid of the air volume measured by the sonic anemometer.

The LI-7500 sensor head has a 12.5 cm open path, with single-pass optics and a large 1 cm diameter optical beam. The LI-7500 operates over a temperature range of -25°C to +50°C. Figure 2.11 shows a cutaway representation of the LI-7500 sensor head [*LI-COR*, 2001]. The Infrared Source emits radiation, which is directed through a Chopper Filter Wheel, Focusing Lens, and then through the measurement path to a cooled Lead Selenide Detector. Focusing the radiation maximizes the amount of radiation that reaches the detector in order to provide maximum signal sensitivity. The detector operates approximately as a linear quantum counter; that is, over much of its range the detector signal output ν is proportional to the number of photons reaching the detector. The existence of certain gas on the IR path reduces the photon flux reaching the other side. Each absorbing gas reacts at different wavelength of photon. Absorption at wavelengths centered at 4.26 µm and 2.59 µm provide for measurements of CO_2 and water vapor, respectively. Reference filters centered at 3.95 µm and 2.40 µm provide excellent rejection of IR radiation outside the desired band, allowing the analyzer to reject the response of other IR absorbing gases. Source and detector lifetimes are greater than 20,000 hours. A brush less Chopper Motor rotates the chopper wheel at 9000 rpm. The windows at both ends of the optical path are made of sapphire, which is extremely hard and starch resistant, allowing for worry-cleanup of dirt and dust accumulation.

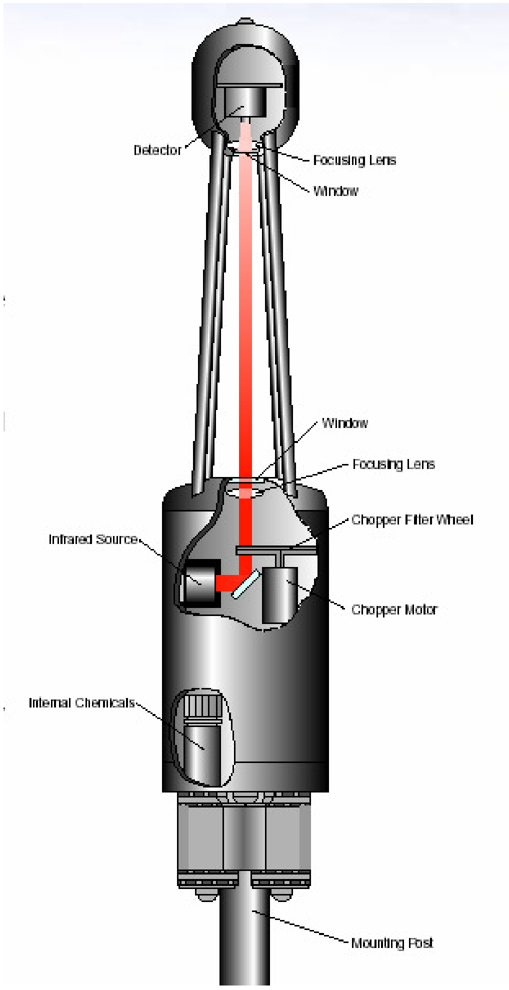

Figure 2.11: Cutaway representation of the LI-COR (from LI-COR manual)

2.2.5 PAR (Photosynthetic Active Radiation) sensor

The photosynthetic photon flux or PAR can be easily calculated with the incoming solar radiations, given some approximations [*Campbell and Norman*, 1998]:

- the energy content of photons is the same for all wave lengths. It is equal to the energy content of photons at the mean wavelength of the spectrum (green, 0.55µm) that is 3.6 10^{-19} J/photon (=0.217 J/µmol).
- about 45% of the incoming solar radiations are in the PAR wave length.

Then,

$$Q_{PAR} = \frac{0.45 \times E_{(incomingsolar)}}{0.217} = \left[\frac{W}{m^2} \times \frac{\mu mol}{J}\right] = \left[\frac{\mu mol}{m^2 \times s}\right] \quad (2.6)$$

Figure 2.12: PAR LITE (Kipp & Zonen)

In order to avoid those approximations, a sensor was used for the photosynthetic flux: PAR LITE from Kipp & Zonen (Figure 2.12). The sensor measures the PAR directly in µmol/m^2/s. For the periods when instrument did not perform well, Q_{par} was approximated as explained above. The PAR Lite is specifically engineered to measure PAR (photosynthetic active radiation) under naturally occurring daylight. The optical filter of the PAR Lite is designed to deliver a quantum response from 400 to 700 nm [*Kipp & Zonen*, 2001], which is the same spectral region responsible for stimulating plant photosynthesis [*Campbell and Norman*, 1998]. PAR LITE uses a photodiode sensor, which creates a voltage output that is proportional to the incoming radiation from the entire hemisphere. An especially optical filter has been designed to provide a quantum response in the photo synthetically active radiation (PAR) (between 0.4 and 0.7µm).

2.2.6 Humidity and temperature probe

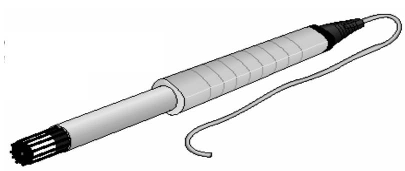

Figure 2.13: Model HMP45C Temperature and relative humidity probe (from Campbell Scientific manual)

Air temperature and humidity were monitored at 3m height and recorded continuously at 30 minute intervals. For that purpose the model HMP45C temperature and relative humidity probe from Campbell

Scientific was used. (Figure 2.13). Probe contains a Platinum Resistance Temperature detector (PRT) and a Vaisala HUMICAP® 180 capacitive relative humidity sensor [*Campell*, 2003a].

The HMP45C must be housed inside a radiation shield when used in the fields because it should be protected from the sunlight (Figure 2.14).

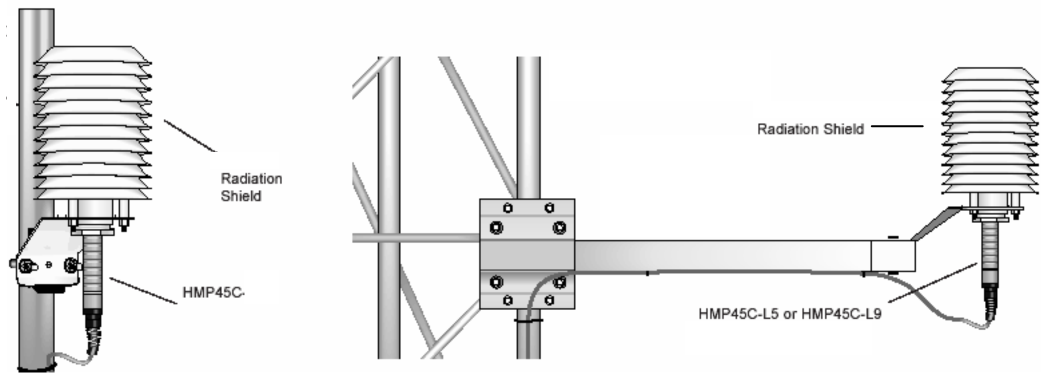

Figure 2.14: Model HMP45C housing
(from Campbell Scientific manual)

The HMP45C measures the relative humidity. Relative humidity is defined by the equation below [*Campell*, 2003a]:

$$RH = \frac{e}{e_s} \times 100 \tag{2.7}$$

where RH is the relative humidity, e is the vapour pressure in kPa, and e_s is the saturation vapour pressure in kPa. The vapour pressure, e, is an absolute measure of the amount of water vapour in the air and is related to the dew point temperature [*Garatt*, 1992; *Brutsaert*, 1991]. The saturation vapour pressure is the maximum amount of water vapour that air can hold at a given air temperature. When air temperature increases, so does the saturation vapour pressure [*Garatt*, 1992; *Brutsaert*, 1991]. Conversely, a decrease in air temperature causes a corresponding decrease in saturation vapour pressure. It follows then from equation (2.7) that a change in air temperature will change the relative humidity, without causing a change in absolute humidity [*Campell*, 2003a].

2.2.7 Barometric Pressure Sensor PTB101B

A PTB101B sensor from Campbell Scientific was used to measure barometric pressure. Data were collected and recorded in 30 minute intervals in mbar. The PTB101B Barometric Pressure Sensor is housed in an aluminium case

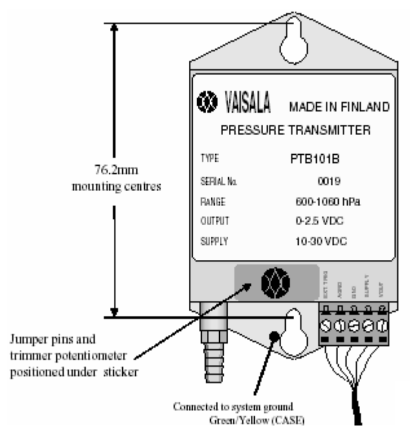

Figure 2.15: Model PTB101B
Barometric Pressure Sensor
(from Campbell Scientific manual)

fitted with an intake valve for pressure equilibrium (Figure 2.15). It uses the unique Barocap® silicon capacitive pressure sensor developed by Vaisala [*Campbell*, 2001]. The sensor is fabricated from two pieces of silicon, with one piece acting as a pressure sensitive diaphragm and the other acting as rigid support plate. Pressure variations deflect the sensitive diaphragm and change the sensor's capacitance. This capacitance is measured and linearised, and an analogue voltage output indicate the ambient pressure. The results given by the PTB101B are local pressure at the weather station and the measurements can be corrected to sea level if the altitude is known [*Campbell*, 2001]. The sensor has to be protected from condensation.

2.2.8 Soil heat flux plates HFP01 Campbell

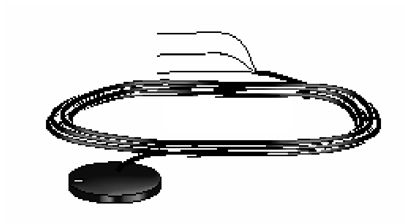

Figure 2.16: Soil heat flux plates HFP01 (from Campbell Scientific manual)

Soil heat flux (see chapter 5) was monitored by heat flux plates HFP01 from Campbell scientific (Figure 2.16). Typically, two sensors are buried in the ground around a meteorological station at a depth of 50mm below the surface.

A sensor is based on a thermopile, a number of thermocouples connected in series, placed in a material acting like a thermal resistance [*Campbell*, 1998]. When heat is flowing through the sensor, a temperature gradient takes place flowing from the hot to the cold side of the sensor. Thermocouples then generate an output voltage that is proportional to the temperature difference between its ends. Using more thermocouples in series will enhance the output signal [*Campbell*, 1998].

2.2.9 Soil temperature probes Model 107 Campbell

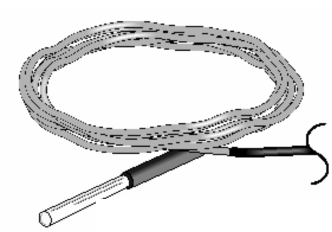

Figure 2.17: Soil temperature probes Model 107 (from Campbell Scientific manual)

Soil temperatures were measured in °C with buried temperature probes Model 107 [*Campbell*, 2003b] (Figure 2.17), two 2.5 cm deep and one 7.5 cm deep, and were recorded in 30 minute intervals by Campbell Scientific datalogger.

2.2.10 Soil moisture monitors CS615 Campbell

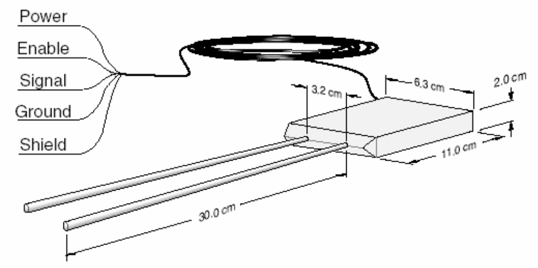

Figure 2.18: CS615 Soil moisture (water content) reflectometer (from Campbell Scientific manual)

Volumetric water content of the soil profile was measured at depths of 5, 10, 25 and 50 cm with CS615 water content reflectometers from Campbell Scientific set horizontally (Figure 2.18). Two CS615 water content reflectometers were installed vertically, one from 0 to 30 cm, and another from 30 to 60 cm depth. This type of sensor uses time domain reflectometry (TDR) methods that are based on the propagation characteristics of an electromagnetic wave on a transmission line [*Campbell*, 2002a]. The probe consists of two 30 cm long stainless steel rods connected to a printed circuit board. High-speed electronic components on the circuit board are configured as a bistable multivibrator. The output of the multivibrator is connected to the probe rods, which act as a wave travel guide. The travel time of the signal on the probe rods depends on the dielectric permittivity of the material surrounding the rods and the dielectric permittivity depends on the water content. Therefore the oscillation frequency of the multivibrator is dependent on the water content of the media being measured [*Campbell*, 2002a]. The CS615 output is essentially a square wave with amplitude of ±0.7 Volts with respect to the system ground. The period is then converted into volumetric water content using a calibration equation [*Campbell*, 2002a].

2.2.11 Rain gauge ARG100 Campbell

Rain gauge ARG100 Campbell Measures total rainfall in mm. Gauges used do not measure snowfall. A conventionally shaped raingauge interferes with the airflow so that the catch is reduced [*Campbell*, 2000]. The ARG100 gauge has been designed to minimise this effect by presenting a reduced area to the wind (see Figure 2.19).

Figure 2.19: ARG100 Rain gauge (from Campbell Scientific manual)

The ARG100 is manufactured in UV-resistant plastic. The amount of rain collected is measured by the well-proven tipping bucket method. The contact closure at each tip is recorded by Campbell Scientific datalogger. Standard setting is used of 0.2mm of rain per tip [*Campbell*, 2000].

2.2.12 Stream flow

Figure 2.20: V notch weir

In the small adjacent stream, about 10m from the tower, a Thalimedes (011 Hydrometry, UK) device collects the height of water at the 90º V notch weir section (see Figure 2.22). The catchment area at this point is 15 ha. Data are recorded at 15 minute intervals, and then transformed into 30 minute intervals in order to be used with the meteorological measurements.

The formula to convert height (m) into flow (L/s) is:

$$Q = 1390 \times h^{2.5} \qquad (2.8)$$

2.2.13 Datalogger CR23X Campbell

Dataloggers provide sensor measurement, time keeping, data reduction, data or/and program storage and control functions. In this study CR23X datalogger from Campbell Scientific was used (see Figure 2.21).

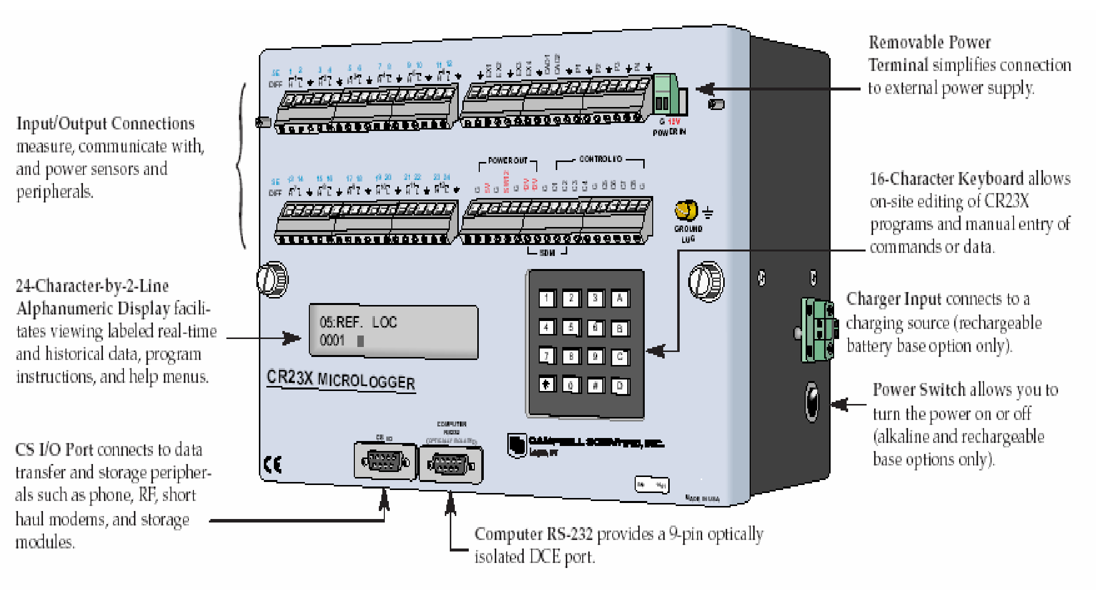

Figure 2.21: CR23X Datalogger (fom Campbell Scientific manual)

2.2.14 Multiplexer AM 16/32 Campbell

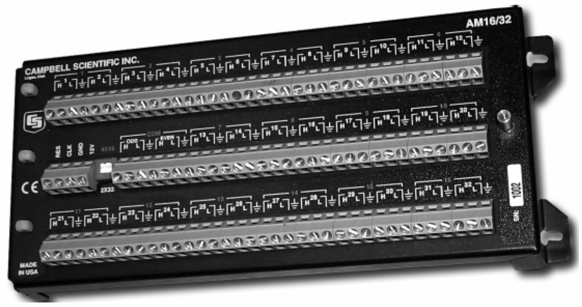

Figure 2.22: AM 16/32 Multiplexer
(From Campbell Scientific manual)

Multiplexer device increases the number of sensors that may be scanned by the dataloggers. For our needs AM 16/32 Multiplexer from Campbell Scientific was used (see Figure 2.22).

2.2.15 Telephone connection

The weather station was connected by modem to a network, and was feeding weather data into a retrieval system consisting of a personal computer and telephone communications link.

Chapter 3
The Eddy Covariance Method

Chapter 3 The Eddy Covariance Method

3.1 Basic theory

The Eddy Covariance or Eddy Correlation (EC) method is a statistical tool, used to analyse time series of Eddy high frequency wind and scalar atmospheric data [*Baldocchi*, 2003], to yields values of fluxes of these properties representing quite large areas [*Campbell*, 1998].

The atmosphere near the earth's surface is almost always turbulent, and trace gases are rapidly diffused to (or from) the surface by irregular or random motions generated by wind shear and buoyancy forces [*Dabberdt et al.*, 1993]. The boundary layer defined by Garratt [1992], is the layer of air directly above the Earth's surface in which the effect of the surface (friction, heating and cooling) are felt directly on time scales less than a day, and in which significant fluxes of momentum, heat or matter are carried by turbulent motions on a scale of the order of the depth of the boundary layer of less.

Transport in the boundary layer of heat, moisture, momentum and pollutants are governed almost entirely by turbulence [*Campbell*, 1998]. Using the Reynolds decomposition it is possible to quantify turbulent transport given a high enough sampling rate and fast response instruments [*Garatt*, 1992].

The instruments employed by this technique are the LI-7500 Open Path CO_2/H_2O non-dispersive, absolute infrared gas analyser, measuring densities of CO_2 and water vapour, and the 3D sonic anemometer measuring the vertical wind velocity fluctuations (Figure 3.1). The details about these instruments are given in chapter 2.

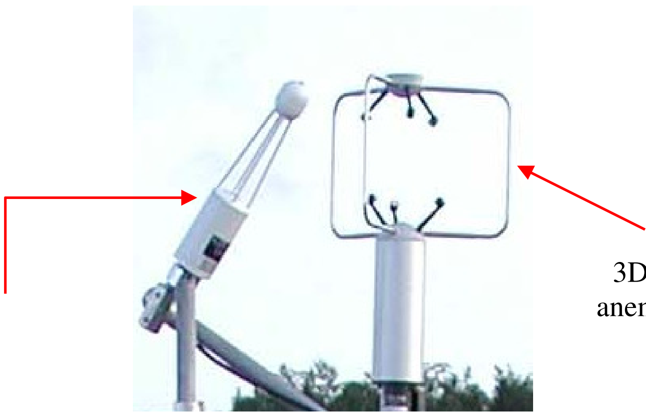

Figure 3.1: Eddy Covariance set up

The EC method is used worldwide to study carbon dioxide, and water vapour, in the atmosphere over the course of year or more [*Baldocchi*, 2003].

3.2 Definition of flux

The composition of the major components of dry air is relatively constant, their percent by volume is given in the Table 3.1:

Table 3.1: The components in dry air

name	[%]
nitrogen	78.084
oxygen	20.946
argon	0.934
carbon dioxide	0.033
neon	0.0018
helium	0.000524
methane	0.00016
krypton	0.000114
hydrogen	0.00005
nitrous oxide	0.00003
xenon	0.0000087

The transport of trace gas molecules through the air space of canopies is due to a combination of the mean wind (wind motions that occur at cyclic frequencies greater than one hour) and the turbulent wind (wind motions that occur at cyclic frequencies less than one hour).

Transport in the boundary layer is dominated by turbulence. Horizontal momentum of the air is transferred toward the ground where it is dissipated in frictional drag [*Garatt*, 1992]. Energy is transferred from larger eddies aloft downward to smaller eddies by turbulent mixing. The eddy velocities are departures from a characteristic mean. Thus, in a turbulent atmosphere, the instantaneous vertical transport of an atmospheric constituent (e.g. CO_2) is given by the product of the fluctuation of the concentration and the fluctuation of the vertical wind velocity [*Moncrieff et.al*, 1997; *WCRP/SCOR*, 2000; *Baldocchi*, 2003].

Consider the vertical velocity component of the wind vector w (m/s). The instantaneous velocity can be written as the sum of the mean velocity ($\overline{w}$) and a turbulent part (w’) (Reynolds rules of averaging) [e.g. *Reynolds*, 1895; *Moncrieff et.al*, 1997; *WCRP/SCOR*, 2000]:

$$w = \overline{w} + w' \tag{3.1a}$$

The turbulent eddies from the specific humidity (q), carbon dioxide concentration (CO_2) and temperature (T) can be separated exactly in the same way [e.g. *Reynolds*, 1895].

$$q = \overline{q} + q' \qquad CO_2 = \overline{CO_2} + CO_2' \qquad T = \overline{T} + T' \qquad \text{(3.1b, 3.1c \& 3.1d)}$$

In this study we are only interested in vertical fluxes. Since mean vertical wind speeds in the boundary layer are very close to zero under most circumstances, the vertical average value of turbulent parts is usually found to be very small. By definition, the average value of the turbulent parts of the velocities and scalars equals zero [*Moncrieff et.al*, 1997]:

$$\overline{w'} = \overline{q'} = \overline{T'} = 0 \qquad (3.2)$$

If the site is horizontally uniform, and atmospheric conditions are assumed steady over the averaging period (30 minutes), it is expected that: $\overline{w} = 0$.

The measurement of a vertical flux by eddy correlation requires careful physical alignment of the vertical velocity sensor (3D sonic anemometer) in the field and analytical rotation of the coordinate axes during post processing of data [*Dabberdt et al*., 1993]. This is necessary to avoid contamination of the vertical flux by the streamwise flux, which is opposite in sign to the vertical flux and can be as much as three times greater [*Dabberdt et al*., 1993].

In order to adjust measurements with eddy covariance basic principles, axis rotation was performed with the raw data set [*Guenther and Hills*, 1998], i.e. mean wind, its standard deviations, and all fluxes were rotated as follows:

- First rotate axes so that +U is pointing north, and +V is pointing west (see Figure 2.9 in chapter 2 for description of +U and +V).

- Then rotate mean wind so that mean vertical wind velocity is set to zero.

3.2.1 Latent heat flux and sensible heat flux

The sensible heat flux H (W/m^2) and the latent heat flux λE (W/m^2) are not measured directly but calculated using the eddy correlation technique with air temperature and air specific humidity [*WCRP/SCOR*, 2000; *Wever et al*., 2002].

The product of the vertical wind speed w (m/s), and the density of moist air ρ_a (kg/m^3), is the mass flux of moist air, $\rho_a w$ (kg/m^2/s). With q the relative humidity and λ the latent heat of vaporization (λ = 2450 kJ/kg), the latent heat flux can be written $\lambda\rho_a wq$ (W/m^2). The mass flux of air may be related, as well, to a specific property of the air such as the specific heat per unit mass, c_pT (J/kg), to give the sensible heat flux $\rho_a w c_p T$ (W/m^2) with c_p the specific heat capacity of moist air in J/kg/K.

Considering the atmospheric density as constant for the lower part of the atmospheric boundary layer (ρ_a =1.29kg/m^3), and applying Reynolds averaging to the property flux, the average flux of a constituent X can be written [*Garatt*, 1992]:

$$\overline{\rho_a wX} = \overline{(\overline{\rho_a} + \rho_a')(\overline{w} + w')(\overline{X} + X')} = \rho_a \overline{w'X'} \qquad (3.3)$$

Then the average latent heat flux becomes:

$$\lambda E = \lambda \rho_a \overline{w'q'} \qquad (3.4)$$

And the average sensible heat flux

$$H = \rho_a \overline{w'(c_p T)'} \qquad (3.5a)$$

This equation is often simplified, considering c_p as constant (c_p=1005 J/kg/° K) [*Garatt*, 1992]:

$$H = \rho_a c_p \overline{w'T'} \qquad (3.5b)$$

3.2.2 Carbon dioxide flux

In the eddy correlation method, the flux, Fc of gas is given by [*Webb et al.*, 1980; *Guenther and Hills*, 1998; *Baldocchi*, 2003]:

$$F_c \cong -\overline{w'\rho_c'} \qquad (3.6)$$

where ρ_c' is the density fluctuation of CO_2 gas (mol/m^3), measured with the LI-7500 at 10Hz speed, and w' is the vertical wind velocity fluctuation (m/s) measured at 10 Hz speed, given by the sonic anemometer.

3.2.3 Webb correction

When the atmospheric turbulent flux of a minor constituent such as CO_2 (or water vapour) is measured by the eddy covariance technique, account may need to be taken of variations of the constituent's density due to the presence of a flux of heat and/or water vapour [*Webb et al.*, 1980; *Kramm et al.*, 1995]. The total vertical flux of any entity has contributions from two terms, an advection term (that is the product of the average vertical velocity and the average flux concentration) and an eddy flux term (that is the flux measured by eddy correlation) [*Dabberdt et al.*, 1993]. The eddy correlation method described above uses some close approximations to end up with the simple equations (3.4, 3.5 and 3.6). So the advection term is neglected with assumption that the average vertical velocity is zero at or near the surface, however Webb et al. [1980] point out that the proper assumption is that the vertical flux of dry air is zero at the surface. As a consequence, there is small nonzero average vertical velocity equal to the negative of the eddy density flux divided by the density of dry air, where the eddy density flux has contributions from the sensible heat and water vapour fluxes.

Thus, the full equation for CO_2 should be written [*Webb et al.*, 1980]:

$$F_{c\,webb} = -\overline{w'\rho_c'} - \overline{w} \times \overline{\rho_c} \tag{3.7}$$

where the average wind velocity should be replaced by [*Webb et al.*, 1980]:

$$\overline{w} = \frac{\overline{w'\rho_v'}}{m_v} \times \frac{R \times T}{(p-e)} + \frac{p}{(p-e)} \times \frac{\overline{w'T'}}{T} \tag{3.8}$$

where p is the atmospheric pressure (in mbar), e the vapour pressure (in mbar), the air temperature (in Kelvin), m_v and ρ_v the molecular weight and density of water vapour constituent, w' the instantaneous wind velocity and R the gas constant.
So that the 'Webb' corrected expression of the CO_2 flux is:

$$F_{cwebb} = -\overline{w'\rho_c'} - \frac{R \times T \times \overline{\rho_c}}{m_v \times (p-e)} \times \overline{w'\rho_v'} - \frac{p \times \overline{w'T'} \times \overline{\rho_c}}{T \times (p-e)} \tag{3.9}$$

The Webb correction is used to perform correction of the water vapour flux in the same way [*Webb et al.*, 1980; *Foken and Wichura*, 1996].

In CO_2/H_2O flux measurements, the magnitude of the correction will commonly exceed that of the flux itself [*Webb et al.*, 1980].

The F_{cwebb} best represents the surface flux for steady state, planar homogeneous and well-developed turbulent flow [e.g. *Goulden et al.*, 1996; *Moncrieff et al.*, 1997; *Falge et al.*, 2001].

3.3 Accuracy of Eddy Covariance measurements

There are a number of diagnostic test statistics, which illustrate the correct functioning of individual components of an eddy covariance technique [*Gash et al.*, 1999; *Moncrieff et al.,* 1997]. Two useful statistics are the ratio of the standard deviation of vertical wind speed (σ_w) to the friction velocity (u_*) and the ratio of standard deviation of a scalar concentration (σ_c) to the relevant scalar concentration (c_*) [*Moncrieff et al.*, 1997].

In order to test performance of the anemometer that was used in this experiment we plot the standard deviation of the vertical velocity fluctuations (σ_w) against the friction velocity (or momentum flux) u_* (Figure 3.2) [*Gash, et al*. 1999; *van der Tol, et al.*, 2003]. The resultant mean values of σ_w/u_* are 1.25 for dry periods for both studied years (fig. 3.2(a&c)), which is in agreement with the Monin-Obukhov similarity theory where σ_w/u_* in neutral conditions is a universal constant. Observed values for σ_w/u_* are typically about 1.25 [*Garatt*, 1992; *Gash, et al.*, 1999; *van der Tol, et al.*, 2003]. Our results of σ_w/u_* for wet periods are greater than the 1.25 and are 1.4 and 1.35 for 2002 and 2003, respectively (Figure. 3.2 (b & d)).

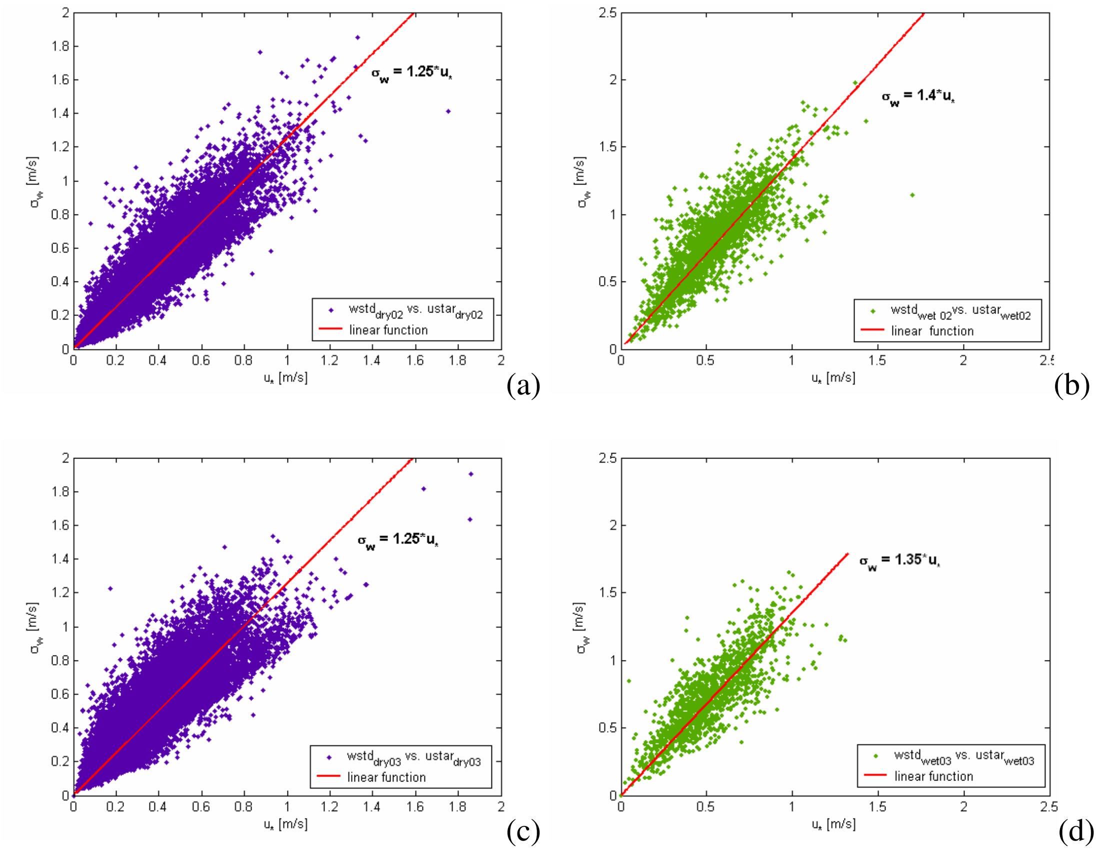

Figure 3.2: Scatter diagram of the standard deviation of the vertical velocity fluctuations (σ_w) with friction velocity (u_*) - half an hour data: (a) dry and (b) rainy conditions for 2002 and (c) dry and (d) rainy conditions for 2003

3.3.1 Precipitation filter

Since the test described above is a sensitive indicator of the anemometer's performance and the ability of the instrument to measure σ_w/u_* in both wet and dry conditions, one can conclude that performance of the instrument during the rain events was unsatisfactory. Raindrops on the open-path LI-COR can produce unreliable signals (see section 2.2.4).

As described in section 2.2.11 precipitation was monitored by rain gauge set on the ground which had resolution of 0.2 mm. Examining the half hour precipitation measurements, it was noticed that on occasions in the early hours in the morning and in the evening the rain gauge had registered 0.2 mm precipitation even when there was no rain. It was concluded that the effect was condensation. Therefore threshold for precipitation of 0.4 mm was adopted.

It should also be noted that approximately one hour was needed for the eddy covariance set to dry out after rain events and thereby reestablish reliable measurement by LI-COR. Therefore, the flux data (i.e. CO2 flux, latent heat flux (LE), and sensible heat flux (H)) measured during the rain events and one hour thereafter were treated as bad data and filtered out. Details about application of this filter will be given in chapter 5 for LE and H and in chapter 6 for CO_2.

3.4 Footprint and fetch

3.4.1 Definition of footprint and fetch

The eddy covariance method depends on turbulence to carry scalar entities past the measurements sensors and roughly mix the air so that the scalar of interest does not accumulate in the canopy air space [*Campbell and Norman*, 1998; *UMIST*, 2002].

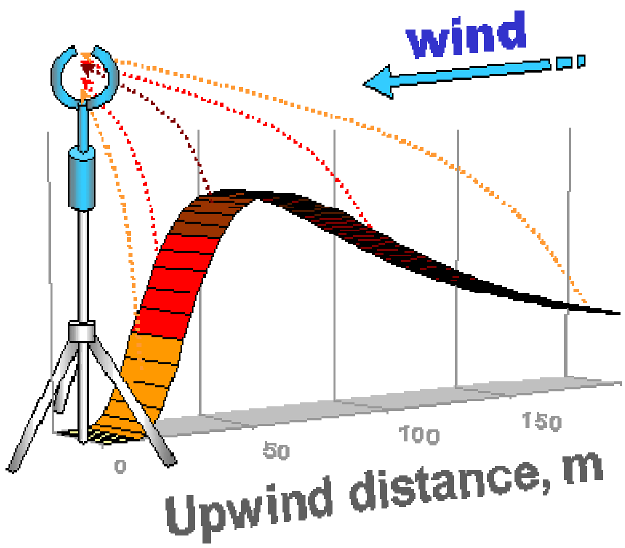

Figure 3.3: Fetch
(http://snrs1.unl.edu/georgeb/footprint/fp-title.html)

The area of the ground actually sensed in a tower-based flux measurement is known as the sampled footprint [*Hsieh et al.*, 1997; *Schmid*, 2002].

The fetch is the upwind horizontal distance from the sensor to the edge of the area contributing to the measured flux [*Hsieh et al.*, 1997; *Schmid*, 2002; *UMIST*, 2002] (Figure 3.3).

Each of these terms, even though slightly different in exact meaning) describes the characteristics of the upwind area, which is expected to influence most of the downwind measurements at a certain height. Three main factors affecting the station footprint at a flux measurement site are measurement height, surface roughness and atmospheric stability [*Leclerc and Thurtell*, 1990].

It has been shown [*Hsieh at al.*, 1997; *Hsieh et al.*, 2000; *Schmid*, 2002] that the size of footprint increases with:

- Increased measurement height
- Decreased surface roughness
- Change in stability from unstable to stable

And that the area nearest the tower contributes most if the:

- Measurement height is low
- Surface roughness is high
- Conditions are very unstable

3.4.2 Footprint estimation

Numerous models have been developed to investigate the relationship between scalar flux and its source areas, e.g. Eulerian analytical model [*Gash*, 1986; *Horst and Weil*, 1994], Lagrangian stochastic dispersion model [*Hsieh et al.*, 1997].

To interpret the eddy correlation measured scalar flux and understand the fetch requirement and contributing source areas for these measurements, the flux footprint model developed by Hsieh et al. [2000] was adopted. Model describes very well the relationship between footprint, atmospheric stability, observation height, and surface roughness. For this purpose, the fetch length (requirement), xf, for reaching the 90% constant flux layer and the peak source distance, xp, which has the maximum contribution to the flux measurement are considered. In Hsieh et al.'s model, xf and xp are calculated as:

$$xf = \frac{D}{0.105k^2} \mid L \mid^{1-P} \; z_u^P \tag{3.10}$$

$$xp = \frac{D z_u^P \mid L \mid^{1-P}}{2k^2} \tag{3.11}$$

where z_u is a length scale defined as $z_m(\ln(z_m/z_o)-1+z_o/z_m)$, z_m (=10m) is measurement height, z_o (=0.03) is surface roughness, k (= 0.4) is von Karman constant, and L is Obukhov length [*Brutsaert*, 1991] :

$$L = \frac{-u_*^{\,3} \times \rho}{k \times g \times \left(\dfrac{H}{T_a \times c_p} \right)} \tag{3.12}$$

where u_* is friction velocity (m/s), ρ is air density (1.2 kg/m^3), g is gravity (9.81 m/s^2), H is sensible heat flux (W/m^2), Ta is air temperature (K), and c_p is specific heat for dry air (1005 J/(kgK)). L is positive for stable, negative for unstable and infinitely large for neutral conditions [*Brutsaert*, 1991].
In (3.10) and (3.11), D and P are constants [*Hsieh et al.*, 2000] defined as:

a) D = 0.28; P = 0.59 for unstable condition;
b) D = 0.97; P = 1 for near neutral and neutral conditions; $|z_u/L| < 0.04$;
c) D = 2.44; P = 1.33 for stable condition.

The stable condition of the boundary layer forms over land in the evening as the ground cools, mixing is reduced and concentrations of trace gases released (or deposited) at the surface are likely to be larger (or smaller) [*Dabberdt et al.*, 1993].

The xf values give an indication how far the eddy-correlation system can sense the scalar flux measurement from the measurement tower. The xp values give an indication how far the source area, which has the maximum contribution to the scalar flux measurement, is from the measurement tower. Details about the derivation of (3.10) and (3.11) can be found in [*Hsieh et al.*, 2000]. Codes for the computation of fetch and footprint used in this study are given in Appendix 1.

Using (3.10) and (3.11) and measured u_* (friction velocity) and Hr (reasonable sensible heat flux (see chapter 5)) at 10 m height, scatter plots of xf and xp versus wind direction are shown in Figures 3.4 and 3.5 for 2002 and 2003, respectively. Table 3.2 show percentage of the measurements during the neutral, unstable and stable atmospheric condition.

Table 3.2: Atmospheric conditions occurrence in % for 2002 and 2003

Atmospheric condition	2002	2003
Neutral	23%	19%
Unstable	39%	40%
Stable	38%	41%

In Figure 3.4, for 2002, it is shown that for unstable (and neutral) conditions (62% of time), the fetch requirements are less than 2500 m and the strongest source areas are within 150 m from the tower. For stable conditions (38% of time), xf and xp are within 7km and 270m, respectively, except for some (~18%) very stable cases. Also, notice that 90% of the xf and xp values are less than 7 km and 370 m, respectively, for the whole year 2002.

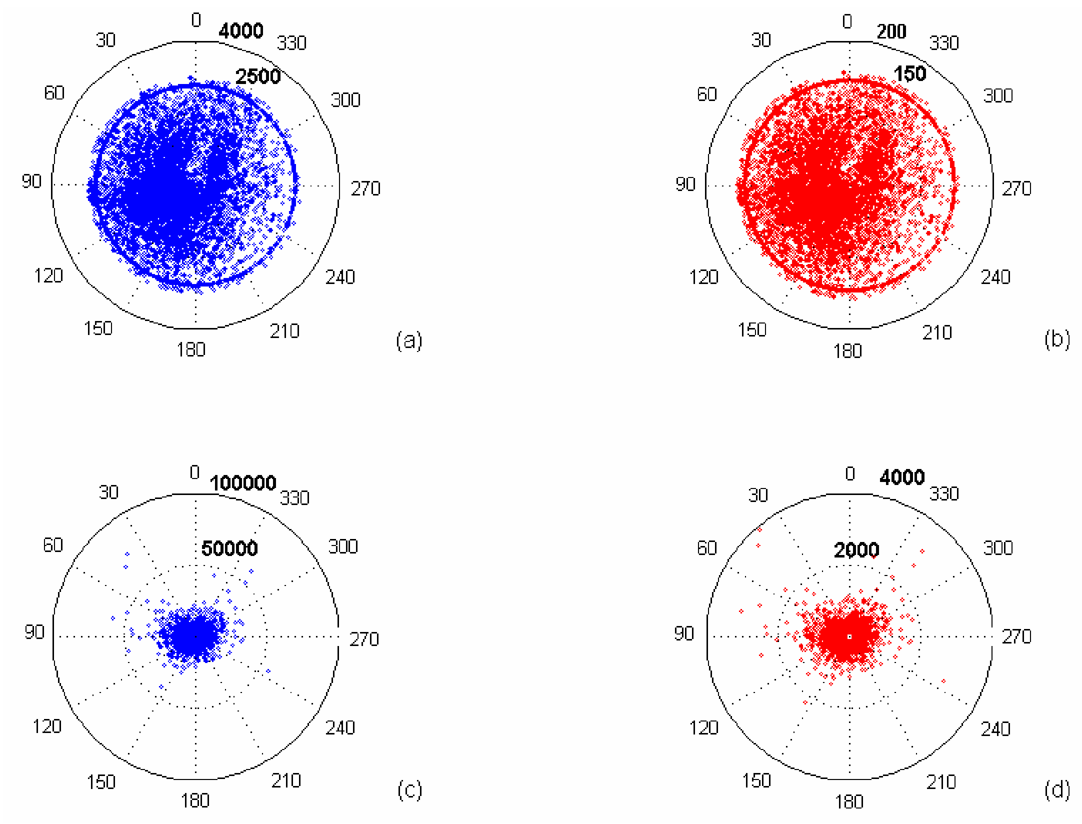

Figure 3.4: Fetch requirement for 2002: (a) fetch and (b) peak locations for unstable conditions; (c) fetch and (d) peak locations for stable conditions

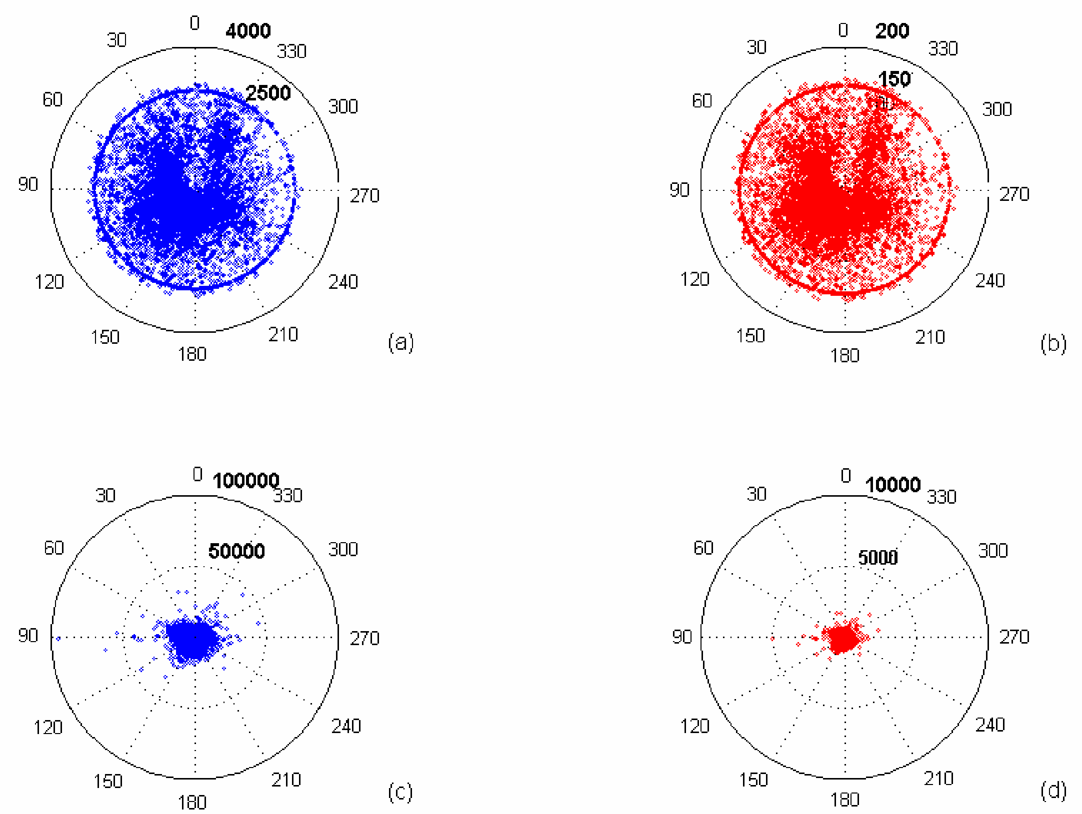

Figure 3.5: Fetch requirement for 2003: (a) fetch and (b) peak locations for unstable conditions; (c) fetch and (d) peak locations for stable conditions

In Figure 3.5, for 2003, it is shown that for unstable and neutral conditions (59% of time), the fetch requirements are less than 2500 m and the strongest source areas are within 150 m from the tower. For stable conditions (41% of time), xf and xp are within 7.5km and 390m, respectively, except for some (~ 18%) very stable cases. Also, notice that 90% of the xf and xp values are less than 7 km and 370 m, respectively, for the whole year 2003.

With these footprint analyses, it can be interpreted that most of the time (~ 82%) the eddy-correlation scalar flux measurements (i.e., sensible heat, latent heat, and CO_2 fluxes) represent the space averaged fluxes resulted from the circle area 7 km in radius from the tower, and the strongest source area is just 370m away for both years. Also, from the information given by the wind direction histogram shown in Figure 3.6, it is clear that the eddy correlation measured fluxes are mainly from the southwest part of the field. That brings conclusion that footprint is changeable during the time and it is not a circle around the tower, but it shaped according to the wind direction and wind speed. That fact is also noticeable in figures 3.4 and 3.5 since the plot is more scattered in directions other than S-W.

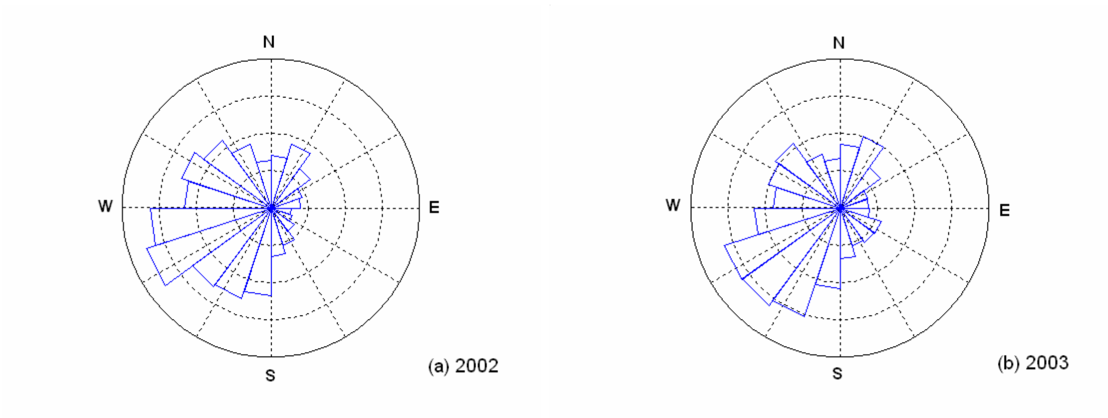

Figure 3.6: **Wind rose: (a) for 2002 and (b) for 2003**

Novick et al. [2004] propose additional meteorological constraints that only accept fluxes when atmospheric stability conditions are near-neutral and when the xp lies within the dimensions of the study site. Namely they suggest using the atmospheric stability parameter in the atmospheric surface layer ($\varsigma = (z-d)/L$) which is near neutral condition defined as $|\varsigma| < 0.1$ and xp (here 370m) together with u_* to filter night time data. This way they reduced footprint to the dimensions of the study site.

Leclerc and Thurtell [1990] applied a Lagrangian particle trajectory model to examine 'rule of thumb' fetch requirement and found that the 100 to 1 fetch to height ratio underestimates fetch requirements when observations are carried out above smooth surfaces, in stable conditions, or at high observation level. Hsieh et al. [2000] found that height to fetch ratio is about 1:100, 1:250, and 1:300 for unstable, neutral, and stable conditions, respectively.

Applying 1:100 height (here 10m) to fetch ratio, combined with information from the probability density function of the wind direction [*Hsieh et al.*, 2000], on our case we found that footprint for unstable condition can be reduced to the dimensions of the study site. The map of the tower with footprint is shown in figure 3.7.

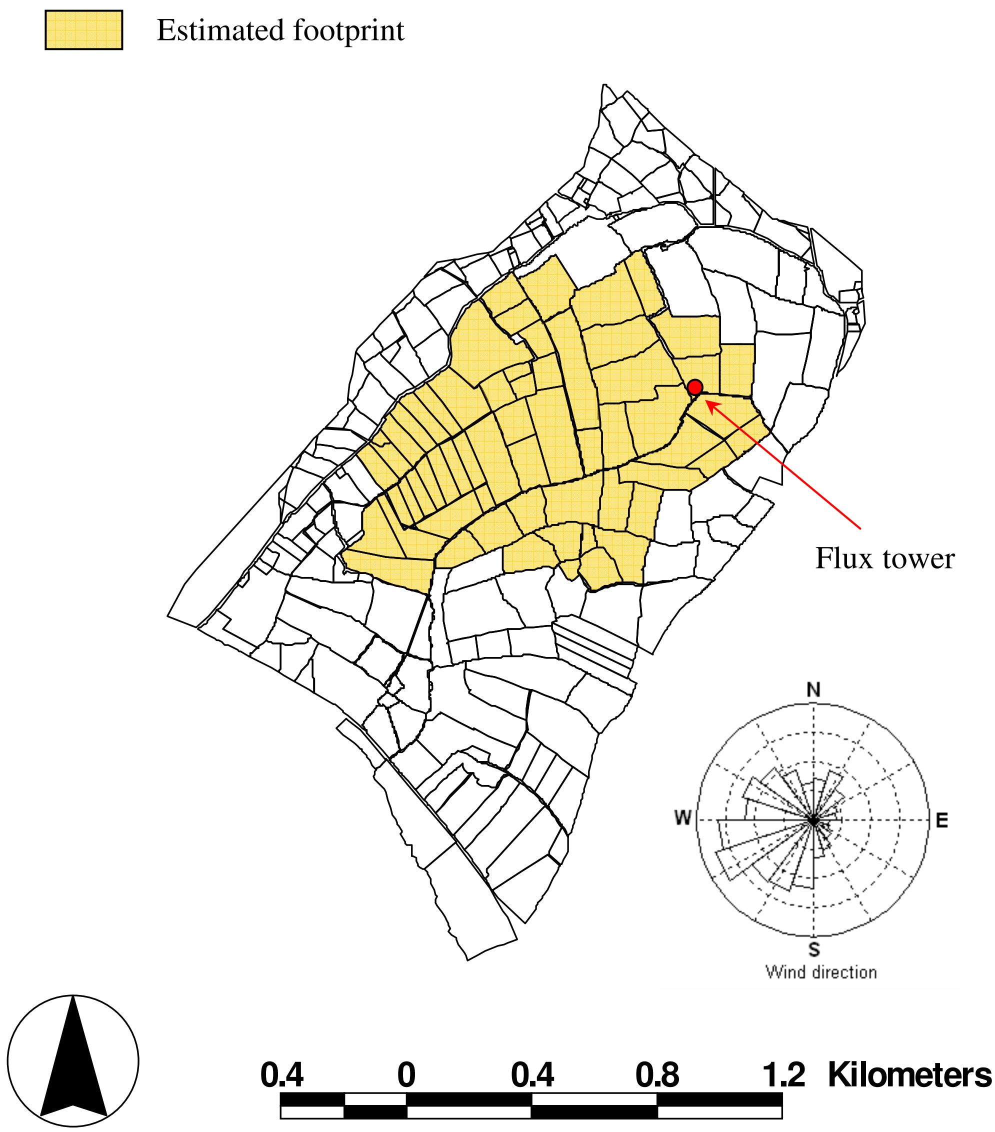

Figure 3.7: Map of the grassland catchment with eddy covariance tower location and the shaded fields indicative of the flux footprint. There are many small fields in the footprint varying in size from 1 to 5ha. The prevailing wind direction is from the south-west.

Chapter 4
General meteorological data

Chapter 4 General meteorological data

4.1 Data collection

Meteorological data were monitored since July 2001 and we have continuous data since then. In this thesis whole year data sets for years 2002 and 2003 were analysed. Precipitation and meteorological measurements were read at one minute and recorded at 30-minute intervals. The experimental system used in this study is described in chapter 2.

For year 2002 we have whole data set without gaps, while in 2003 a gap appears due to the electricity failure from 16th (00:00) to 19th (12:00) September.

Meteorological data for this period were filled following these steps:

- Data from 15/09/03 were used to fill missing data for 16 and 17/09/03,
- Gap for the first 12 hours of 19/09/03 were filled with data for the same period from 20/09/03,
- Missing data for 18/09/03 were filled up with data from 19/09/03.

Precipitation for this period was filled up with data from a nearby rain gauge.

4.2 Precipitation

4.2.1 Annual precipitation

The long-term annual average rainfall for Dripsey site is 1470mm. The year 2002 was wet, with an annual rainfall of 1785mm (~ 17 % above mean annual precipitation) and 2003 was dry, with an annual rainfall of 1185mm (~ 19% less than average). The first half of 2002 was particularly wet with 975mm compared to 610mm for 2003 (see Figure 4.1). It should be noted that there was no snow during the study period.

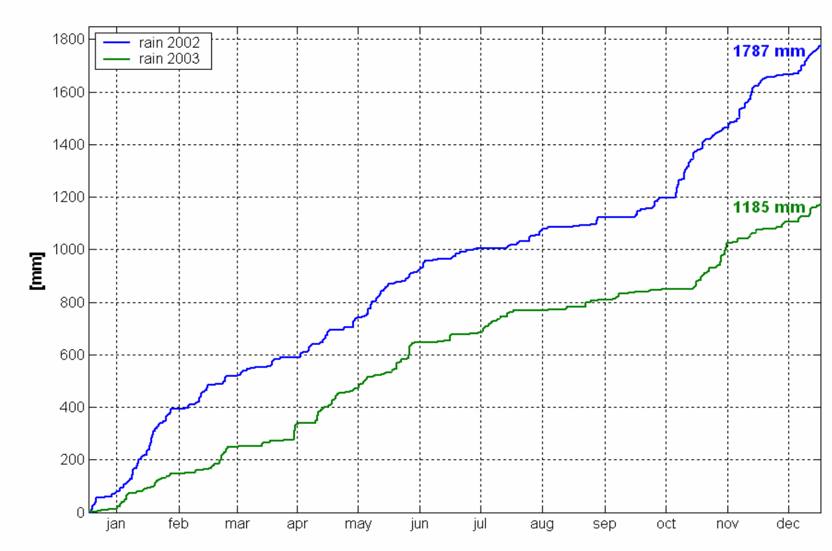

Figure 4.1: Cumulative precipitations in mm for 2002 and 2003.

4.2.2 Monthly precipitation

There is no clear seasonality in precipitation. Monthly precipitation (Figure 4.2) shows that the winter and autumn months of 2002 with values up to 255mm/month (Table 4.1) were with more precipitation than the same months of 2003. In spring, the average monthly rainfall was 130mm (126mm) while the average monthly summer rainfall was 73mm (82mm) for 2002 (2003).

Table 4.1: Monthly precipitation in mm

[mm]	jan	feb	mar	apr	may	jun	jul	aug	sep	oct	nov	dec
2002	254	231	73	137	178	99	48	73	45	244	255	150
2003	95	71	106	143	128	140	91	15	56	46	192	102

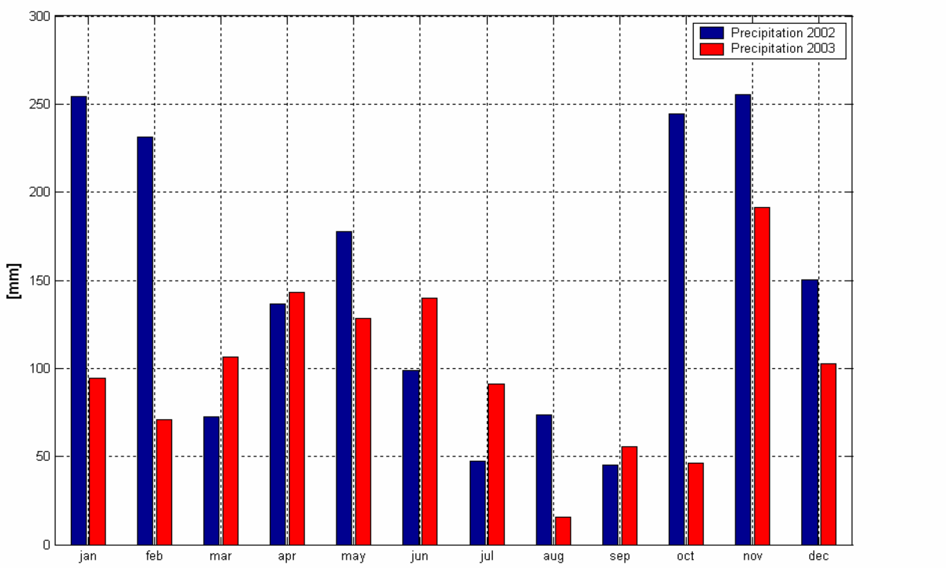

Figure 4.2: **Monthly precipitation in mm for 2002 (blue) and 2003 (red)**

4.2.3 Daily precipitation

Figure 4.3 (a) and (c) shows daily precipitation. It can be seen that maximum daily precipitation in 2002 was 40mm/day (October), while in 2003 maximum was 57mm/day (April). We note that in the summer months of both years have continuous periods of more days with no rain at all. The rainfall regime for the winter in both years is characterized by long duration events of low intensity. Short duration events of high intensity are more seldom and occur in summer. Summer rains are more intermittent and intense but no dry season is evident.

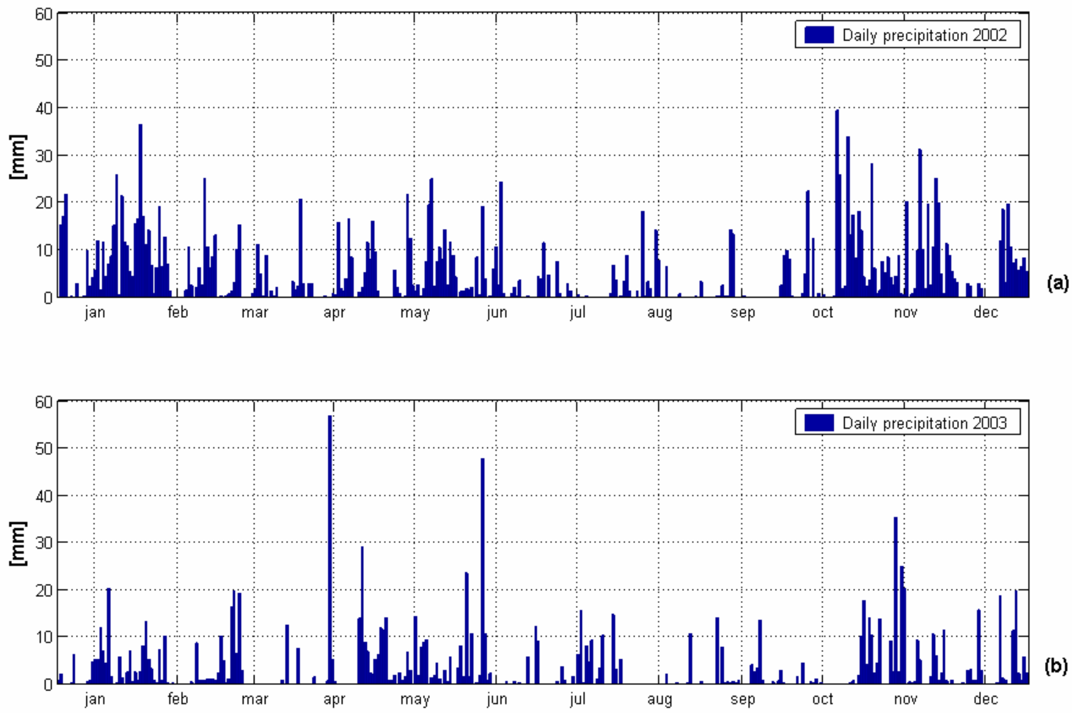

Figure 4.3: Daily precipitation in mm: (a) for 2002 and (b) for 2003

Rains are usually of small intensity with rainfalls below 0.2 mm per 30 minutes 91 % (2002) and 94% (2003) of the time. Rains are likely to occur more in the morning, with a lower frequency after mid-afternoon.

4.3 Soil moisture

The volumetric soil moisture in the topsoil at 5 cm (Figure. 4.4 (b)) shows that in both years during the period November to May levels are near saturation at approximately 0.6 m^3/m^3, and in spring the levels fall on occasion to near 0.4 m^3/m^3.

The main differences between the two years are for the period June to October. In the dry 2003, the soil moisture for the period June to October was at a low level (near 0.2 m^3/m^3) while for the wet 2002 the corresponding soil moisture rarely falls below 0.3 m^3/m^3 and in October the value is near saturation.

Near surface soil moisture shows a strong relationship with precipitation, and has a fast response to rain events. This is particularly visible during dry periods for both years. After each rain event there is a water stress in soil moisture.

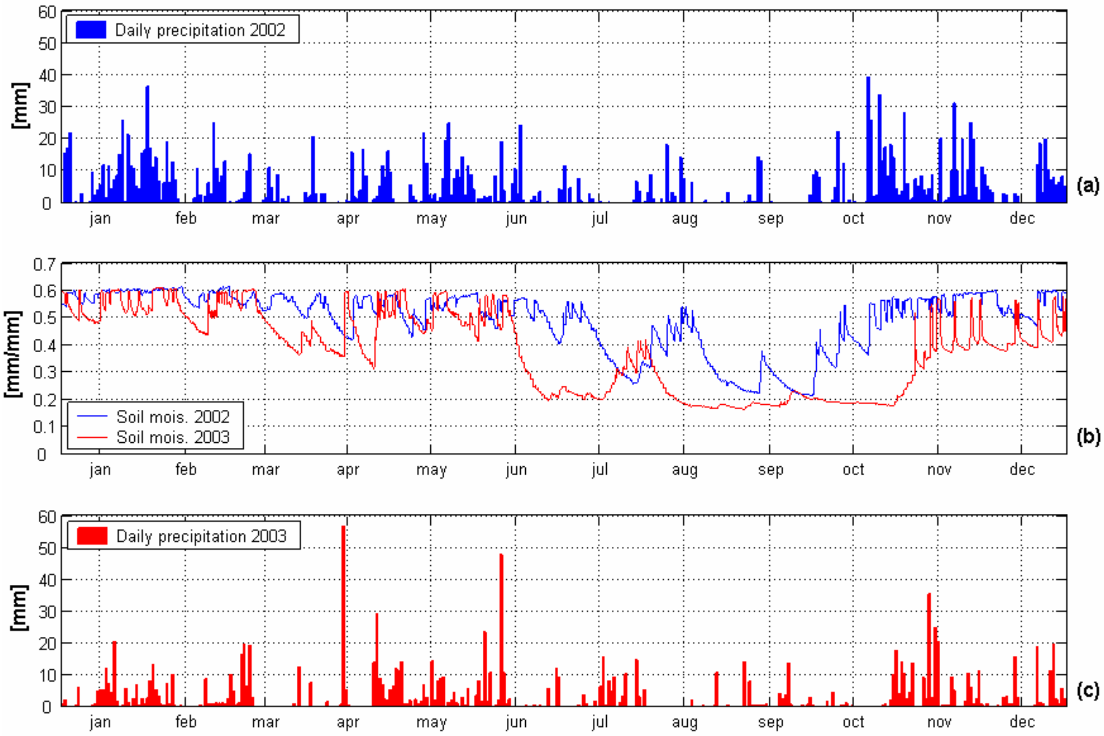

Figure 4.4: Soil moisture dependence on precipitation: (a) daily precipitation in mm for 2002; (b) soil moisture in mm/mm at 5cm depth (30min interval) in 2002 (blue) and 2003 (red); and (c) daily precipitation in mm for 2003

The lowest record of soil moisture is ~ 20% and the states at which soil moisture becomes limiting and eventually causes vegetation to wilt (θ_{wilt}) is ~ 8% [*Albertson and Kiely*, 2001]. The system was not water limited during the study period and its growth/production is not water limited.

4.4 Relative air humidity and atmospheric pressure

The relative air humidity (Figure 4.5 (a)) stays high throughout the year, and fluctuates a lot on a daily basis. However, spring distinguishes itself from the other seasons with drier peaks down to 33 % of relative humidity. Those points correspond to lows in the precipitation and soil moisture curves.

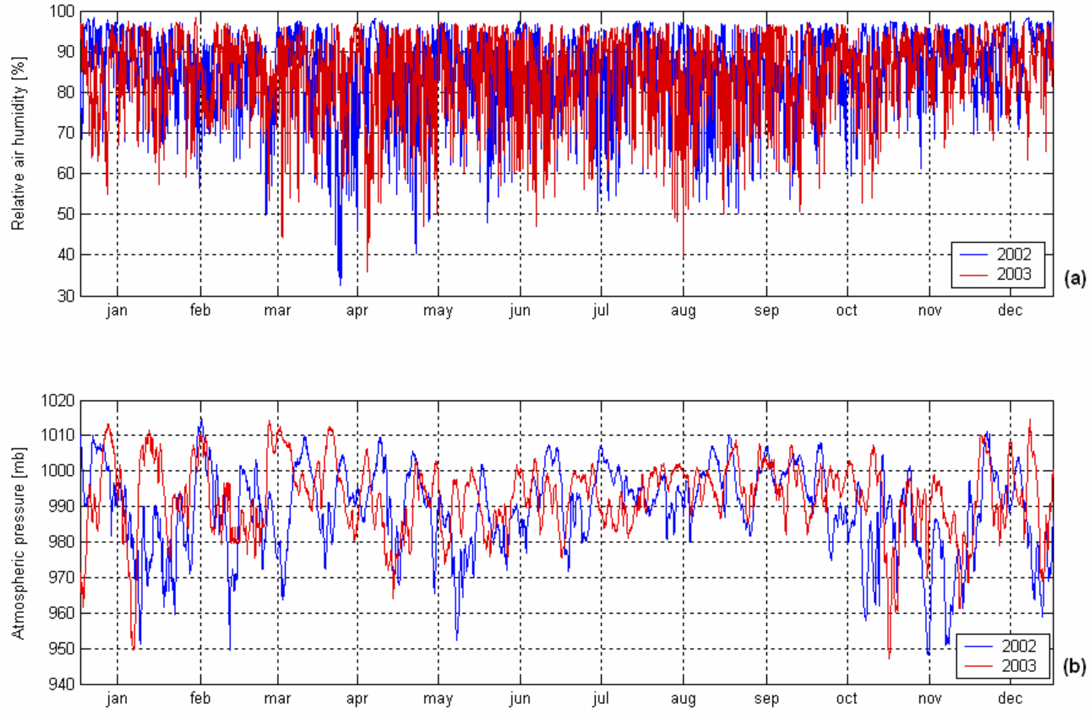

Figure 4.5: 30 minutes (a) Relative air humidity in % for 2002(blue) and 2003(red); and (b) Atmospheric pressure in mbar for 2002 (blue) and 2003 (red)

Atmospheric pressure (Figure 4.5 (b)) fluctuates a lot on a daily basis, and those fluctuations are bigger for winter period. In wintertime atmospheric pressure ranges from 950 to 1010mb, and in summertime from 980 to 1000mb. The mean atmospheric pressure was 989mb and 993mb for 2002 and 2003, respectively. (Note the site is at an elevation of 200m above sea level).

4.5 Air and soil temperature

The half hour air temperatures have a small range of variation during the year, going from a maximum of 21ºC (August 2002) and 25ºC (August 2003) to a minimum of 0ºC (January 2002) and -2ºC (January 2003). The average half hour temperature is 15º C in summer and 5º C in winter.

The daily air temperatures (Figure 4.6(a)) range from a maximum of 17ºC (August 2002) and 20ºC (August 2003) to minimum of 1ºC (January 2002) and 0ºC (January 2003).

The local climate is humid temperate, with very few days with temperature under 4°C (the lower threshold temperature for the photosynthetic process). For instance, grass growth was still measurable for December of 2003. No frost has been noticed during the study period.

The soil temperature at 5 cm depth follows the same annual pattern as air temperature, except for the night data where the soil doesn't cool down as quickly as the air (Figure 4.6(b)). The soil has a bigger inertia than the air. The soil temperature at 5 cm depth was used for the nighttime fitting function in the case of bad CO_2 flux data.

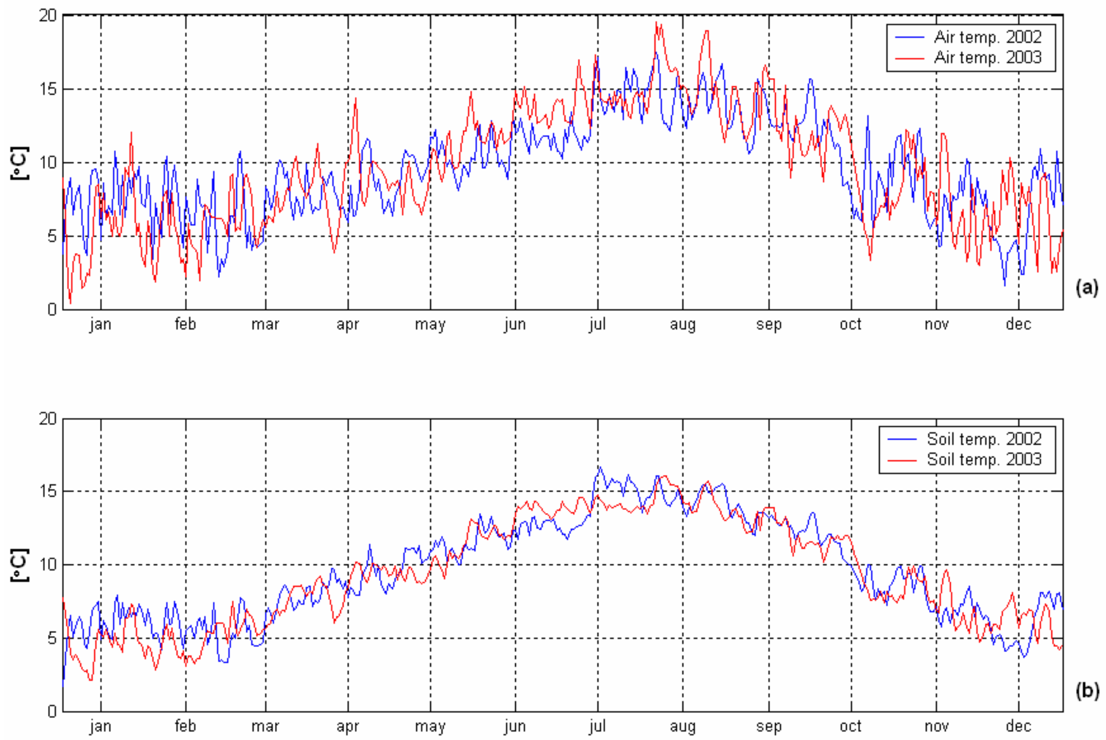

Figure 4.6: Daily average over 30min in °C: (a) air temperature for 2002 (blue) and 2003 (red); and (b) soil temperature at 5 cm depth for 2002 (blue) and 2003 (red)

From Figure 4.7 (a) and (b) we note that the year 2003 was warmer. The beginning of the 2003 (January and February) was colder compared with the same period in 2002. In March mean temperature in 2003 is a bit higher compared with 2002. After March increase in the air temperature for 2003 is rapid, and temperature reaches maximum in August with mean value of approximately 15.5°C±3°C. Air temperature from March 2002 increases with less steep slope, and reaches maximum also in August of 14.5°C±2.5°C, with deviation between 12°C and 17°C). From September to the end of the year mean air temperatures for two seasons do not differ a lot.

Mean soil temperature at 5 cm depth and its standard deviation are shown in Figure 4.7 (c) and (d). It is noticeable that soil temperature follows the same pattern as air temperature, but has lower values. As the air temperature for January and February 2003 was low, soil temperature for these months is also low with mean value less than 5°C (air and soil temperature for some days can be lower than 4°C, thus temperature can be limitation factor for photosynthesis for this period). The maximum mean soil temperatures are about 15°C for both years and occur in August.

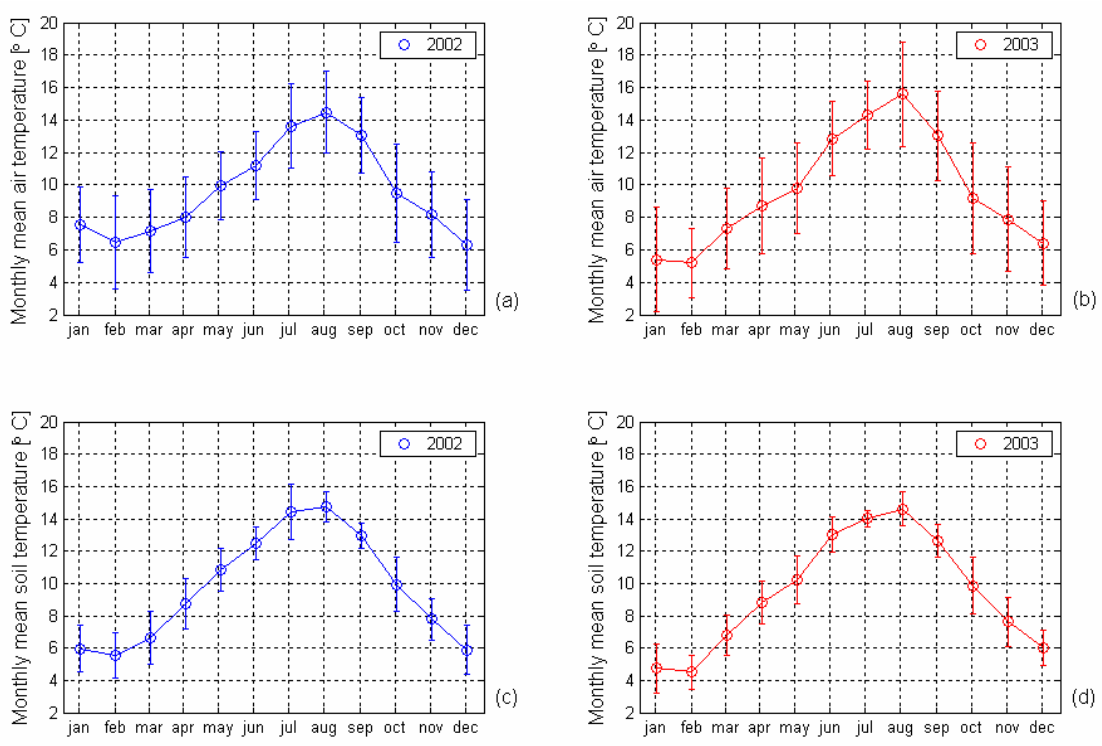

Figure 4.7: Monthly mean and standard deviation of (a) air temperature in 2002; (b) air temperature in 2003; (c) soil temperature at 5cm depth in 2002; and (d) soil temperature at 5 cm depth in 2003.

4.6 Photosynthetic photon flux (Q_{par})

The photosynthetic photon flux density (Figure 4.8(a)) shows the clear annual pattern with averaged 30-minute values reaching the maximum in summer months and minimum over the winter period. Those values were used for finding the function for CO_2 flux at daytime during the periods with bad CO_2 flux data.

The average monthly Q_{par} (Figure 4.8(b)) shows difference in monthly distribution within the year and between the same months for two different years. Average monthly values are given in Table 4.2. It can be noticed that Q_{par} values for most of the months are about the same. The months with difference of more than 50µmol of quantum/m^2/s are January, March, June and August, with Q_{par} in 2003 greater than in 2002. This may suggest more photosynthesis in those months during 2003.

Table 4.2: Monthly Q_{par} in µmol of quantum/m^2/s

	jan	feb	mar	apr	may	jun	jul	aug	sep	oct	nov	dec
2002	175	302	388	567	558	552	545	527	480	329	217	135

2003	225	268	461	545	587	638	497	625	463	343	210	147

Cumulative Q_{par} for 2002 (4775 μmol of quantum/m^2/s) is 5% less than for 2003 (5009 μmol of quantum/m^2/s).

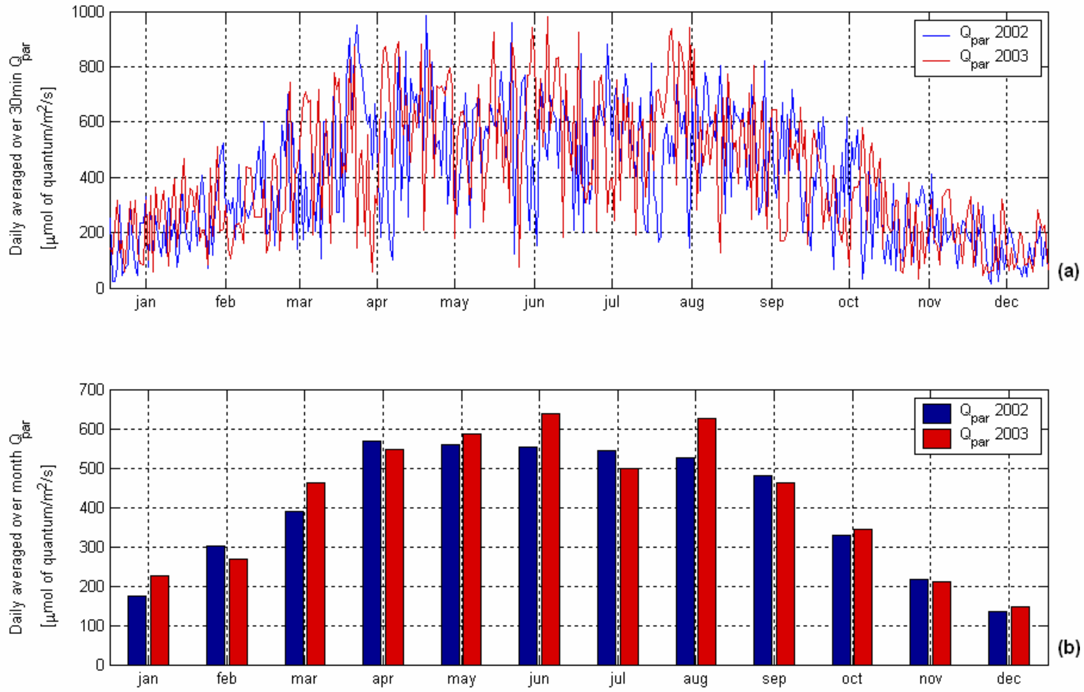

Figure 4.8: Photosynthetic photon flux in μmol of quantum/m^2/s: (a) daily averaged over 30min for 2002 (blue) and 2003 (red); and (b) daily averaged over month for 2002 (blue) and 2003 (red)

4.7 Wind velocity

Thirty-minute averages of wind direction were from the southwest most of the time for both studied years (see section 3.4.2). The mean wind velocity in m/s is derived as resultant of the wind speed in two horizontal directions, u and v, measured with sonic anemometer:

$$U = \sqrt{u^2 + v^2} \tag{4.1}$$

The mean wind velocity at 10 m is approximately 4.0 m/s (2002) and 3.5 m/s (2003) with peaks in wintertime up to 16 m/s (2002) and 14 m/s (2003) (Figure 4.9 (a) and (b)).

Note that there is a gap in wind speed (Figure. 4.9 (b)) from 10 (12:00) until 12 (17:00) February 2003. The reason is bad measurement by sonic anemometer, which gave unreasonable values of wind speed during that period. The gap was filled with averaged values for wind speed for the rest of February 2003 in order to perform calculations that use wind speed as variable.

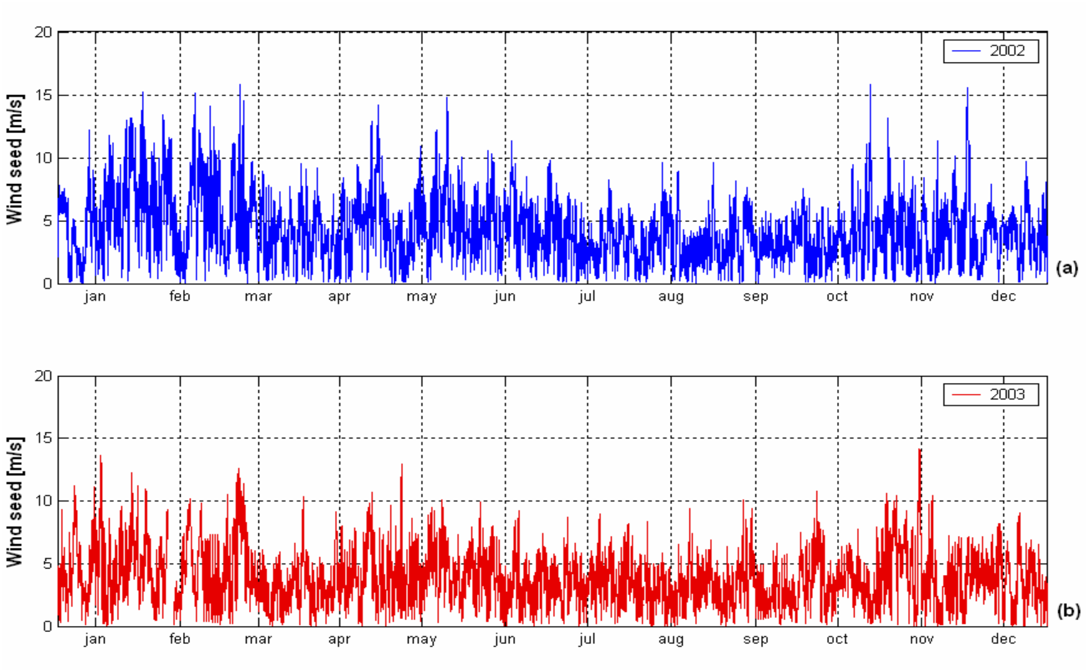

Figure 4.9: Wind speed in m/s in 30 min intervals: (a) for 2002 and (b) for 2003

4.8 Cloudiness

Clouds form when water vapour condenses to form water droplets. This happens when air cools to a temperature equal to its dew point (when saturation vapour pressure is equal to the actual vapour pressure of the air). Further decrease of temperature would lead to condensation of water vapour as liquid water droplets.

Clouds are important in the climate system because they reflect a significant amount of radiation back in the space, which acts as cooling mechanism. However, clouds also absorb outgoing long wave radiation, which is a heating mechanism. Hence clouds can reduce photosynthetic photon flux, which is necessary for the process of photosynthesis, and thereby reduced carbon dioxide uptake of the plants during the day.

The climate in Ireland is such that we cannot overlook the cloud effects. We can expect that during the wet season 2002 cloudiness played role in reduction of radiation that comes from the sun, compared with dry year 2003.

Chapter 5
Energy balance

Chapter 5 Energy balance

5.1 Energy fluxes

5.1.1 Net radiation (R_{net})

When the sun shines on the soil surface, some of the energy is absorbed, heating the soil surface. This heat is lost from the surface through conduction to lower layers of the soil [*Campbell and Norman*, 1998].

The energy balance at the surface is given by [*Brutsaert*, 1991; *Garratt*, 1992]:

$$R_{net} = G + H + \lambda E \tag{5.1}$$

where R_{net} (W/m^2) is net radiation given by the net radiometer (see chapter 2), G (W/m^2) is the ground heat flux given by heat flux plates (see section 2.2.8), H (W/m^2) is the sensible heat flux, and λE (W/m^2) is the latent heat flux. Net radiation (R_{net}) is usually positive during the day when the sun heats the surface and is negative during the night as the surface cools (returning 'heat' to the lower boundary layer).

5.1.2 Soil heat flux (G)

Soil (or ground) heat flux involves exchanges of energy between the earth's surface and subsurface. These energy flows affect temperature. If ground heat flux is positive, the earth's surface will cool and the subsurface will warm. If it is negative, the earth surface will warm and subsurface will cool (Figure 5.1).

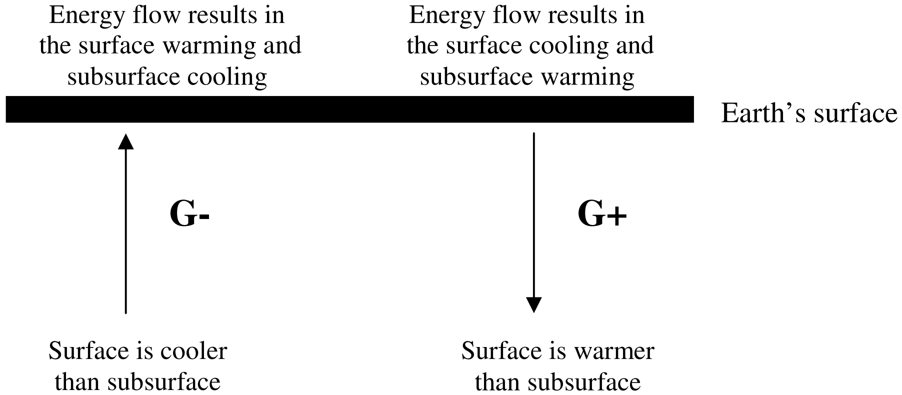

Figure 5.1: Flow of Soil heat flux

Soil heat flux is often ignored because its magnitude is very small, compared to the other terms of the energy balance equation (about 10% of the net radiation). However over shorter periods it can be quite important [*Brutsaert*, 1991] and must be taken into account [*Garratt*, 1992]. It was monitored in this study by means of heat flux plates HFP01 from Campbell scientific (see section 2.2.8). The two sensors are buried in the ground near the meteorological station at a depth of 50mm below the surface. In order to adjust the soil heat flux measured by the plates for change in storage, the following correction was preformed:

$$G_i = G_i m + G_i adj, \qquad i=1,2 \tag{5.2}$$

where $G_i m$ is measured soil heat flux in W/m^2 and $G_i adj$ is adjusted part of soil heat flux [*Brutsaert*, 1991, pp. 145-148]:

$$G_i adj = rho_{scs} \times dTs_i \times d \qquad i=1,2 \tag{5.3}$$

where dTs [K/s] is the difference in soil temperature in time, d=0.05m is the depth of soil heat flux plates and rho_{scs} [kJ/(m^{3}K)] is calculated after Brutsaert [1991, pp. 145-148]:

$$rho_{scs} = (\theta_m \times 2.31 + \theta_w \times 4.18) \times 10^6 \tag{5.4}$$

θ_m = (1-porosity), is fraction of soil volume that is solid (porosity in this case is 0.5 [*Le Bris*, 2002]). θ_w [m^3/m^3] is volumetric soil moisture (horizontal on 5cm depth). The volumetric heat capacity of soil minerals is 2.31 MJ/m^3/K. The specific heat of water is 4.18 J/g/K, [*Campbell and Norman*, 1998].

Since there are two measurements of soil heat flux, final heat flux into the soil was calculated as average of them:

$$G_{avg} = (G_1 + G_2) \times 0.5 \tag{5.5}$$

Values of the soil heat flux at the interface or at a shallow depth, as seen above, depend on many factors, including solar radiation (hence time of day), soil type (hence physical properties) and soil moisture content [*Garratt*, 1992].

Figure 5.2 shows the half hour soil heat flux for 2002 and 2003. It can be seen that the maximum soil heat flux is 190 W/m^2 (April and May) and 135 W/m^2 (May) (i.e. heat from the surface to the subsurface) and minimum is –70 W/m^2 (April and

May) and –50 W/m^2 (May) for 2002 and 2003, respectively. It can be seen also that during wet year (2002) more of the heat available at the surface went in the lower layer of soil compared with dry year (2003).

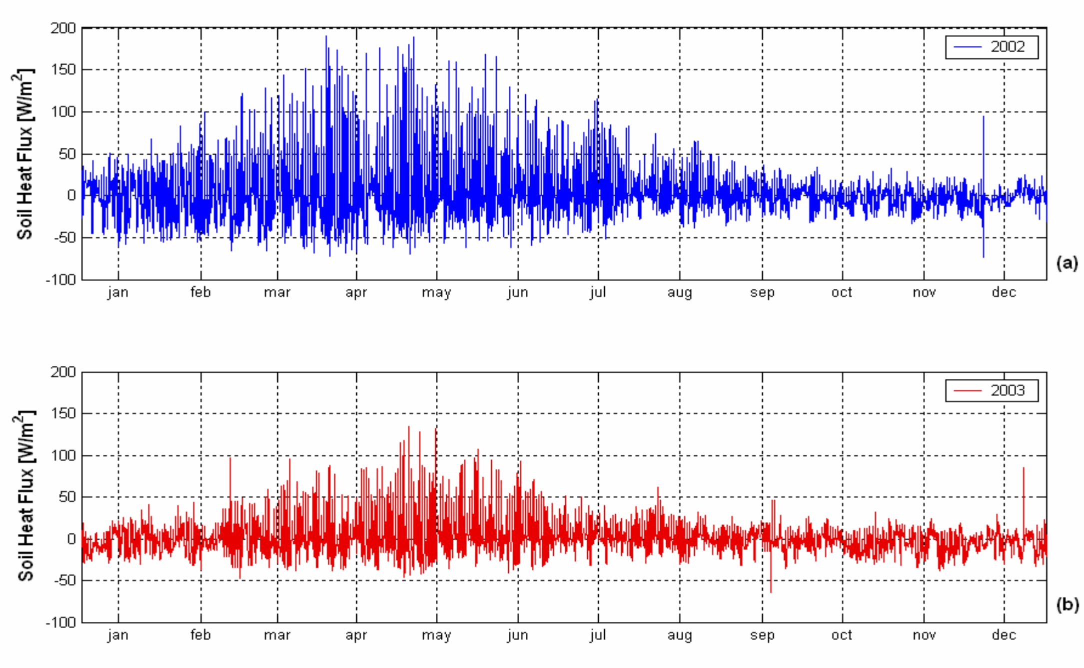

Figure 5.2: 30 minute soil heat flux in [W/m^2]: (a) for 2002 and (b) for 2003

5.1.3 Sensible heat flux (H)

Sensible heat flux is a part of solar radiation used for warming the air. The turbulent sensible heat flux into the atmosphere (H) is small, random vertical motion of the air, associated with the fact that the turbulent wind carries heat either away from or towards the surface [*Campbell and Norman*, 1998]. The magnitude of the sensible heat flux gives indication of how much energy is being used to change the temperature of the air.

During the day, H is often positive (i.e. heat is carried away from the surface) and at night it is negative (Figure 5.3).

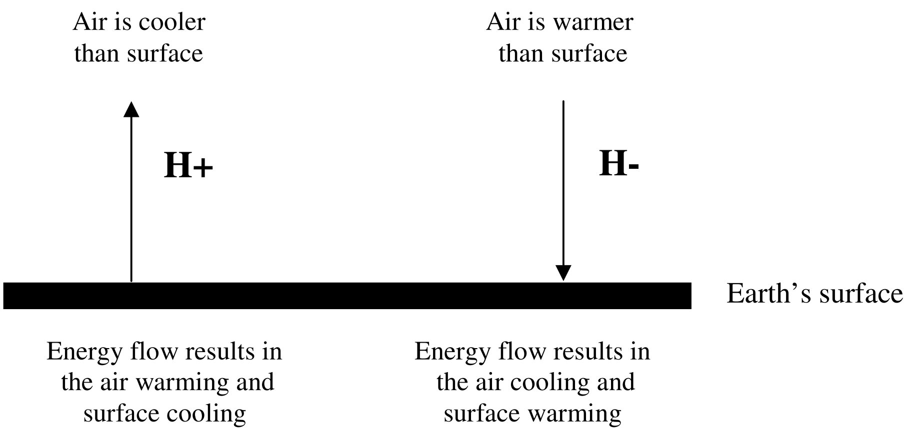

Figure 5.3: Flow of Sensible heat flux

5.1.4 Latent heat flux (LE)

Latent heat flux is that part of solar radiation that isused for water evaporation and plant transpiration. It is heat energy stored in water. The turbulent latent heat flux into the atmosphere is the latent heat capacity of water, λ, multiplied with the surface evaporation rate, E. Latent heat capacity of water (vaporization) λ depends on air temperature and can be calculated [*FAO*, 1998]:

$$\lambda = 2.501 - \left(2.361 \times 10^{-3}\right) \times ta \qquad [\mathrm{MJ/kg}] \tag{5.6}$$

where ta is air temperature in °C. As the value of latent heat varies only slightly over normal temperature ranges, a single value may be taken (for ta = 20°C): λ = 2.45 MJ/kg [*Garratt*, 1992; *FAO*, 1998].

Latent heat is required to evaporate water and water vapour is carried away from the surface by turbulent motions [*Campbell and Norman*, 1998]. The latent heat flux is positive (i.e. away from the surface) unless there is condensation taking place on the surface; in that case stored heat energy is released and becomes sensible heat (the earth's surface temperature increases (Figure 5.4).

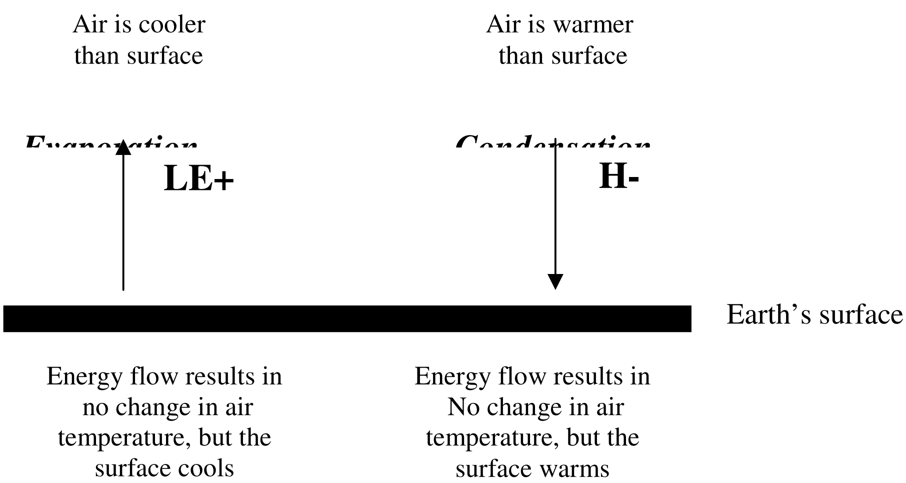

Figure 5.4: Flow of Latent heat flux

5.1.5 Evapotranspiration (E)

Evapotranspiration is the collective term for all the processes by which water in the liquid or solid phase at or near the earth's land surfaces becomes atmospheric water vapour [*Dingman*, 1994]. Most of the water 'lost' via evapotranspiration is used to grow the plants that form the base of the earth's land ecosystems, and understanding relations between evapotranspiration and ecosystem type is a requirement for predicting ecosystem response to climate change [*Dingman*, 1994].

Evapotranspiration can be estimated using the Penman-Monteith or Pristley-Taylor equation.

Penman-Monteith equation

The Penman-Monteith equation estimate the evapotranspiration rate from a vegetated surface [*Monteith*, 1965; *FAO*, 1998].

$$ET = \frac{\Delta \times (R_n - G) + \frac{\rho_a c_p}{r_a} \times (e_s - e_a)}{\left(\Delta + \gamma \times \left(1 + \frac{r_s}{r_a}\right)\right) \times \lambda} \qquad (5.7)$$

where R_n [W/m^2] is the net radiation, G [W/m^2] is the soil heat flux, (e_s-e_a) [kPa] represents the vapour pressure deficit of the air, ρ_a [kg/m^3] is the mean air density at constant pressure (density of dry air is 1.29 kg/m^3 [*Brutsaert*, 1991]), c_p [MJ/kg/°C] is specific heat of the air, Δ [kPa/°C] represents the slope of the saturation vapour pressure temperature relationship, γ [kPa/°C] is the psychrometric constant, and r_s and r_a [s/m] are the (bulk) surface and aerodynamic resistances, respectively.

The saturation pressure can be calculated [*FAO*, 1998]:

$$e_s = 0.6108 \times \exp\left(\frac{17.27 \times t_a}{t_a + 237.3}\right) \quad \text{[kPa]} \qquad (5.8)$$

where t_a [°C] is air temperature.

Actual vapour pressure can be calculated using the relative humidity of the air (RH) and saturation vapour pressure, calculated as in (5.8) [*FAO*, 1998]:

$$e_a = \frac{RH \times e_s}{100} \quad \text{[kPa]} \qquad (5.9)$$

The vapour pressure deficit is the difference between the saturation vapour pressure (e_s) and actual vapour pressure (e_a) for a given time period.

Slope of saturation vapour pressure curve, represents the slope of the relationship between saturation vapour pressure and temperature [*FAO*, 1998]:

$$\Delta = \frac{4098 \times e_s}{(t_a + 237.3)^2} \qquad [\mathrm{kPa/°C}] \qquad (5.10)$$

where e_s is saturation vapour pressure, calculated as in (5.8) and t_a is air temperature in [°C].

The psychrometric constant can be calculated [*FAO*, 1998]:

$$\gamma = \frac{c_p \times p_a}{\varepsilon \times \lambda} \times 10^{-3} \qquad [\mathrm{kPa/°C}] \qquad (5.11)$$

where c_p (= 1013 [J/kg/°C]) is specific heat of moist air, p_a [kPa = 10 mbar] is atmospheric pressure, ε (=0.622) is ratio of molecular weight of water vapour/dry air and λ [MJ/kg] is latent heat of vaporization calculated as in (5.6).

The aerodynamic resistance is defined as:

$$r_a = \frac{\ln\left[\frac{z_m - d}{z_{om}}\right] \times \ln\left[\frac{z_h - d}{z_{oh}}\right]}{k^2 \times u_2} \qquad [\mathrm{s/m}] \qquad (5.12)$$

where z_m [m] is height of wind measurements, z_h [m] is height of humidity measurements, d = (2/3*h) [m] zero plane displacement height estimated from crop height (h, which is in average from 0.12m to 0.15m for our case), z_{om} = (0.123*h) [m] is the roughness length governing momentum transfer, z_{oh} = (0.1*z_{om}) [m] is roughness length governing transfer of heat and vapour, k = 0.41 is von Karman's constant, u_2 [m/s] is wind speed at height z (= 2 [m] proposed by FAO).

To adjust wind speed data obtained from instruments placed at elevations other than the standard height of 2m (in our case instrument is placed at 10m height), logarithmic wind speed profile may be used for measurements above a short grassed surface [*FAO*, 1998]:

$$u_2 = u_z \frac{4.87}{\ln(67.8 \times z_m - 5.42)} \qquad [\mathrm{m/s}] \qquad (5.13)$$

where u_2 [m/s] is wind speed at 2m above ground surface, u_z [m] is measured wind speed at z [m] above ground surface, and z_m [m] is height of measurement above ground surface (in our case 10 m).

The ‘bulk’ surface resistance describes the resistance of vapour flow trough the transpiring crop and evaporating soil surface [*FAO*, 1998]:

$$r_s = \frac{r_l}{LAI_{active}} \qquad [s/m] \tag{5.14a}$$

where r_l [s/m] is bulk stomatal resistance of the well-illuminated leaf (it has a value of about 100 s/m for a single leaf under well-watered conditions [*FAO*, 1998], as it is case here) and LAI_{active} [m^2 (leaf area)/m^2(soil surface)] is active (sunlit) leaf area index (for bulk surface resistance for a grass reference crop LAI_{active} = 0.5LAI [*FAO*, 1998]). For clipped grass generally LAI = 24*h (h is the crop height [m]).

If we assume that study site is reference surface, the ‘bulk’ surface resistance can be calculated with approximations:

$$r_s = \frac{100}{0.5 \times 24 \times 0.12} \approx 70 \text{ s/m} \tag{5.14b}$$

The reference surface closely resembles an extensive surface of green grass of uniform height, actively growing, completely shading the ground and with adequate water [*FAO*, 1998]. The requirements that the grass surface should be extensive and uniform results from the assumption that all fluxes are one-dimensional upwards [*FAO*, 1998].

The ‘bulk’ surface resistance is highly dependant on the interactions (in many cases non linear) of soil, plant genotype, and atmospheric factors [*Ortega-Farias et. al.*, 1996]. If the ‘bulk’ surface resistance (r_s) is greater than zero and if we know its actual value over time, then calculating Penman-Monteith equation (5.7) estimate the the actual evapotranspiration or EA. Actual evapotranspiration is the quantity of water that is actually removed from surface due to the process of evaporation and transpiration [*Dingman*, 1994; *Pidwirny*, 2004].

If the ‘bulk’ surface resistance (r_s) equals zero, then the Penman-Monteith equation (5.7) estimates the potential evapotranspiartion or PE for open water surfaces (e. g. sea, lake, pan). Potential evapotranspiration is a measure of the ability of the atmosphere to remove water from the surface through the process of evaporation and transpiration assuming no control on water supply [*Dingman*, 1994; *Pidwirny*, 2004]. Factors influencing potential evapotranspiration are energy from the sun (80% variations in PE are caused by energy received from the sun) and wind (enables water molecules to be removed from the ground surface by eddy diffusion).

The rate of evapotranspiration is associated with the vapour pressure deficit (VPD). Vapour pressure deficit is the difference between actual and maximum vapour pressure (saturation vapour pressure) [Nederhoff, 2004]:

$$VPD = (e_s - e_a) = -\frac{RH}{100} \times (e_s - 1) \qquad [kPa] \tag{5.15}$$

where e_a is actual vapour pressure, RH [%] is relative humidity, and e_s is saturation vapour pressure calculated by (5.8).

Low VPD means a high air humidity, and vice-versa. The higher the VPD the stronger the drying effect, so the stronger the driving force on evapotranspiration.

The Matlab code for calculating Penman-Monteith equation is given in Appendix 2.1.

Priestley-Taylor equation

The Priestley-Taylor equation is a simplification of the Penman-Monteith equation. It negates the need for any other measured data than the radiation for calculating potential evapotranspiration [*Priestley and Taylor*, 1972]. It assumes that air travelling over a saturated vegetation cover will become saturated and the actual rate of evaporation (AET) would be equal the Penman rate of potential evapotranspiration. Under those conditions evapotranspiration is referred to as equilibrium potential evapotranspiration (PET_{eq}). The mass transfer term in the Penman-Monteith equation approaches zero and the radiation terms dominates. Priestley and Taylor [1972] found that AET from well watered vegetation was generally higher than the equilibrium potential rate and could be estimated by multiplying the PET_{eq} by factor α (=1.26):

$$PET = \alpha \times \frac{\Delta}{\Delta + \gamma} \times (Rn - G) \times \frac{1}{\lambda} \tag{5.16}$$

where Δ [kPa/°C] is slope of saturation vapour pressure curve at air temperature, γ [kPa/°C] is psychrometric constant, Rn [W/m^2] is net radiation, G [W/m^2] is ground heat flux, λ [=2.45 MJ/kg] is latent heat of vaporization.

The saturation vapour pressure curve is given by [*Brutsaert*, 1991]:

$$\Delta = 373.15 \times \frac{e_s}{(t_a + 273.15)^2} \times \left(13.3185 - 3.952 \times t_r - 1.9335 \times t_r^2 - 0.5196 \times t_r^3\right) \tag{5.17}$$

where t_a [°C] is air temperature, e_s is saturation vapour pressure [*Brutsaert*, 1991]:

$$e_s = 1013.25 \times \exp\left(13.3185 \times t_r - 1.9760 \times t_r^2 - 0.6445 \times t_r^3 - 0.1299 \times t_r^4\right) \tag{5.18}$$

where $t_r = 1-(373.15/(t_a+273.15))$. (5.18a)

α is factor which value has been tested to be 1.26 over a wide range of conditions for short vegetation [*Garratt*, 1992]. Over land, α varies with soil moisture although at saturation it approaches the value 1.26 [*Rind*, 1997].

Actual evapotranspiration (AET) takes into account water supply limitations and represents the amount of ET that occurs under field conditions. The most widely used method to incorporate the effects of soil moisture on evapotranspiration is through the use of soil moisture factor [*Albertson and Kiely*, 2001]:

$$\mathrm{PETa} = \beta(\theta_{rel}) \times \mathrm{PET} \tag{5.19}$$

where PET_a is the actual evapotranspiration, PET is potential evapotranspiration calculated in our case using the Priestley-Taylor equation and θ_{rel} is relative water content, defined as:

$$\theta_{rel} = \frac{1}{d_z}\int_0^{d_z} \theta(z)d_z \tag{5.20}$$

where z is depth of soil moisture measurements, so in our experiment relative water content represents average of soil moisture measured on 5, 10 and 25 cm depths. Then reduction factor β is found to be [*Albertson and Kiely*, 2001]:

$$\beta = \beta(\theta_{rel}) = \begin{cases} 0, & \theta_{rel} \le \theta_{wilt} \\ \dfrac{\theta_{rel} - \theta_{wilt}}{\theta_{lim} - \theta_{wilt}}, & \theta_{wilt} < \theta_{rel} < \theta_{lim} \\ 1, & \theta_{rel} \ge \theta_{lim} \end{cases} \tag{5.21}$$

where θ_{lim} and θ_{wilt} are parameters that define the states at which soil moisture becomes limiting and eventually causes vegetation to wilt and transpiration to cease, respectively [*Albertson and Kiely*, 2001]. In our case for θ_{lim} and θ_{wilt} values of 0.48 and 0.08 were adopted.

In this experiment it was found that reduction factor was never equal to zero, so during the study period soil moisture was never limiting in terms of causing vegetation to wilt. Only in 0.4% cases soil moisture was limiting in terms of case of transpiration.

The Matlab code for calculating Priestley-Taylor equation is given in Appendix 2.2.

5.2 Estimation of H and LE

H (W/m^2), the sensible heat flux and λE (W/m^2), the latent heat flux are not measured directly by any device, but calculated using the eddy correlation technique with air temperature and air specific humidity, as it is explained in chapter 3. Webb correction was applied to H and LE calculated by the eddy correlation technique. After this correction some bad points in H and LE data remained.

Hence bad data needed to be corrected. Webb corrected LE and H were filtered when:

- Eddy covariance performance failed due to rain events, precipitation filter (see section 3.3.1) was used

- Net radiation (Rn) and sensible heat flux (H) have different sign, i.e.

$$Rn \times H < 0 \tag{5.22}$$

- Absolute sum of energy fluxes is greater than net radiation, i.e.

$$|H + LE + Gavg| > |Rn + S| \tag{5.23}$$

where S = 50W/m^2 which is a part of energy balance equation that is negligible and represents the heat storage in the canopy.

Latent heat flux (LE) was corrected using the Priestley-Taylor equation (5.19) and sensible heat flux (H) was calculated as residual from energy balance equation (5.1) [*Wilson et al.*, 2000]. Figure 5.5 shows the LE half hour data which were replaced with PT.

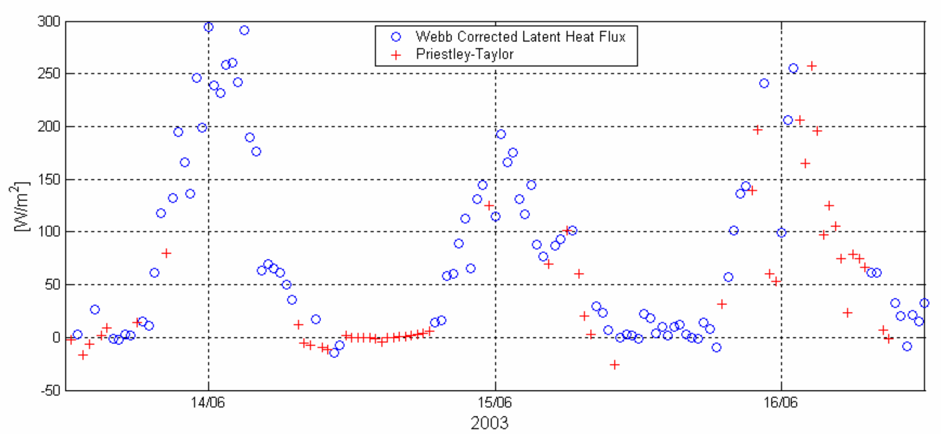

Figure 5.5: The corrected half hour Latent heat flux from 14th to 16th June 2003

Derived sensible heat flux was named reasonable sensible heat flux (Hr).

$$Hr = (Rn - LEpt - Gavg) \tag{5.24}$$

5.2.1 Accuracy of Eddy covariance

57% and 56% of the sensible heat data were good for 2002 and 2003, respectively. 43% and 44% of data were bad for 2002 and 2003, respectively. In those cases flux was corrected as explained above.

5.3 Energy balance

5.3.1 Energy balance closure

Independent measurements of the major energy balance flux components do not always balance [*Twine*, 2000]. This is referred to as lack of closure of the surface energy balance. Energy balance closure is used to assess the performance of eddy covariance flux system. Under perfect closure, the sum of the sensible and latent heat flux (H+LE) measured by eddy covariance is equal to the difference between net radiation and ground (soil) heat flux (Rn-G) measured independently from the meteorological sensors (see chapter 2) [*McMillen*, 1988].

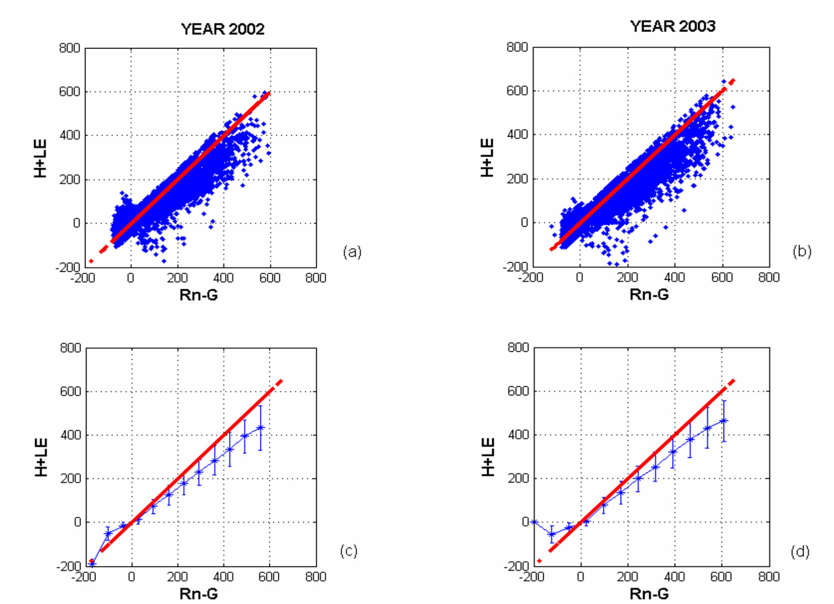

Figure 5.6: Relationships between (Rn-G) and (H+ λE): (a) 30 minute data for 2002; (b) 30 minute data for 2003; (c) average with standard deviation for 2002 and (d) average with standard deviation for 2003. The solid line represents the case of perfect energy balance closure, i.e. H+LE=Rn-G.

The slopes 0.8 and 0.81 for 2002 and 2003 respectively of the relationships between (Rn-G) and (H+λE) in Figure 5.6 indicate that the eddy covariance measurements underestimated sensible and/or latent heat fluxes in both years (or (Rn-G) was overestimated).

The lack of energy closure has also been reported in other long-term studies using eddy covariance [*Wever et al.*, 2002], although the reasons for this discrepancy are not completely understood [*Aubinet et al.*, 2000; *Twine et al.*, 2000]. A portion of the discrepancy may relate to the different locations of the footprints for the measurements of net radiation and soil heat flux, which are close to the instrument tower, while the footprint for the latent and sensible heat fluxes are larger and upwind of the tower (see section 3.4.2). This may in part be due to the heterogeneity of soil moisture status in the near surface and root zone.

5.3.2 Energy balance fluxes

Observing the monthly averaged net radiation and sum of monthly averaged energy fluxes (Figure 5.7), it can be seen that for 2002 and 2003 there is agreement in energy balance during the winter months. Difference between net radiation and sum of energy fluxes becomes greater going from spring to summer, when it reaches maximum, and than again becomes small as autumn comes (see Table 5.1 for the values).

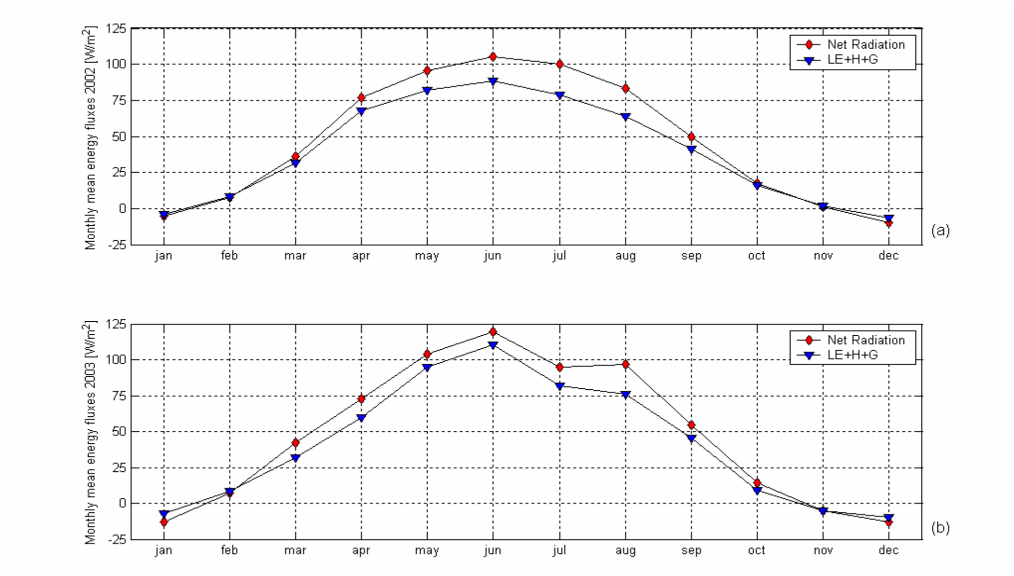

Figure 5.7: Monthly mean net radiation and sum of the energy fluxes; (a) for 2002 and (b) for 2003

Table 5.1: **Average monthly net radiation and sum of energy fluxes in [W/m^2]**

	[W/m^2]	jan	feb	mar	apr	may	jun	jul	aug	sep	oct	nov	dec
2002	**Rn**	-5	7	36	77	96	105	100	83	50	17	1	-10
	LE+H+G	-4	8	32	68	82	88	79	64	41	16	2	-6
2003	**Rn**	-12	7	42	73	104	120	95	97	54	14	-5	-13
	LE+H+G	-7	8	32	50	95	110	82	76	45	9	-5	-9

The underestimation of energy fluxes occurs during the spring-summer time in both years.

The monthly distribution of net radiation and energy fluxes for 2002 is shown in Figure 5.8, and their values in Table 5.2. There is a clear seasonality in distribution of net radiation with maximum values reached in the summer. Latent heat fluxes follow that seasonal trend and on average represent 60% of net radiation. That means that about 60% of net radiation in 2002 was spent on evaporation. Sensible heat flux is negative during the winter months, as the air is warmer than surface. In the spring air above ground becomes warmer and sensible heat flux changes its sign. In average 25% of net radiation in 2002 represents sensible heat flux. Soil (ground) heat flux is positive from March to August and in that period heat was going downwards, as the surface was warmer than subsurface. On average ground flux is about 5% of net radiation.

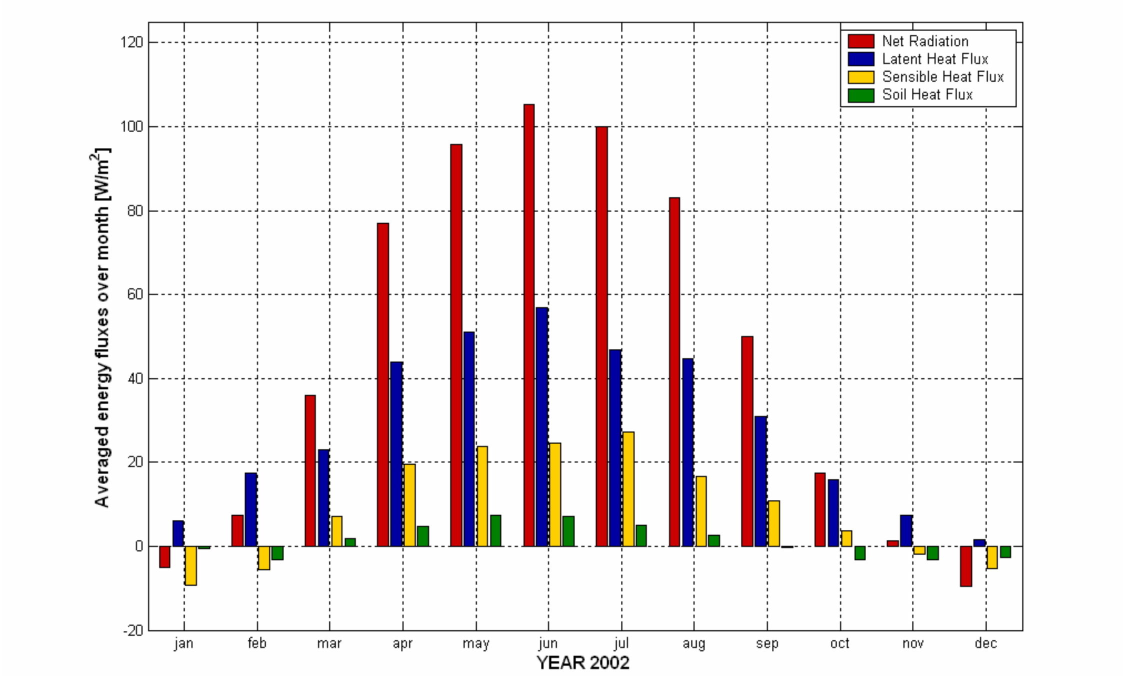

Figure 5.8: Average monthly distribution of Rn (red), LE (blue), H (yellow) and G (green) for 2002

Table 5.2: **Average monthly Rn, LE, H and G in [W/m^2] for 2002**

[W/m^2]	jan	feb	mar	apr	may	jun	jul	aug	sep	oct	nov	dec
Rn	-5	7	36	77	96	105	100	83	50	17	1	-10
LE	6	17	23	44	51	57	47	45	31	16	7	2
H	-9	-6	7	19	24	25	27	17	11	4	-2	-5
G	-1	-3	2	5	7	7	5	3	0	-3	-3	-3

The average monthly distribution of net radiation and energy fluxes for 2003 is shown in Figure 5.9, and their values in Table 5.3. There is a clear seasonality in distribution of net radiation with maximum values reached in the summer. Latent heat fluxes in 2003 follow that seasonal trend. Sensible heat flux in 2003 is negative during the winter months, as the air is warmer than surface. In the spring, air above ground becomes warmer and sensible heat flux changes its sign. Soil heat flux is positive from March to August and in that period heat was going downwards, as the surface was warmer than subsurface. On average in 2003, 5% of net radiation (Rn) was partitioned into soil heat flux (G), while Sensible (H) and latent (LE) hetat flux consumed nearly 30% and 60% of Rn, respectively.

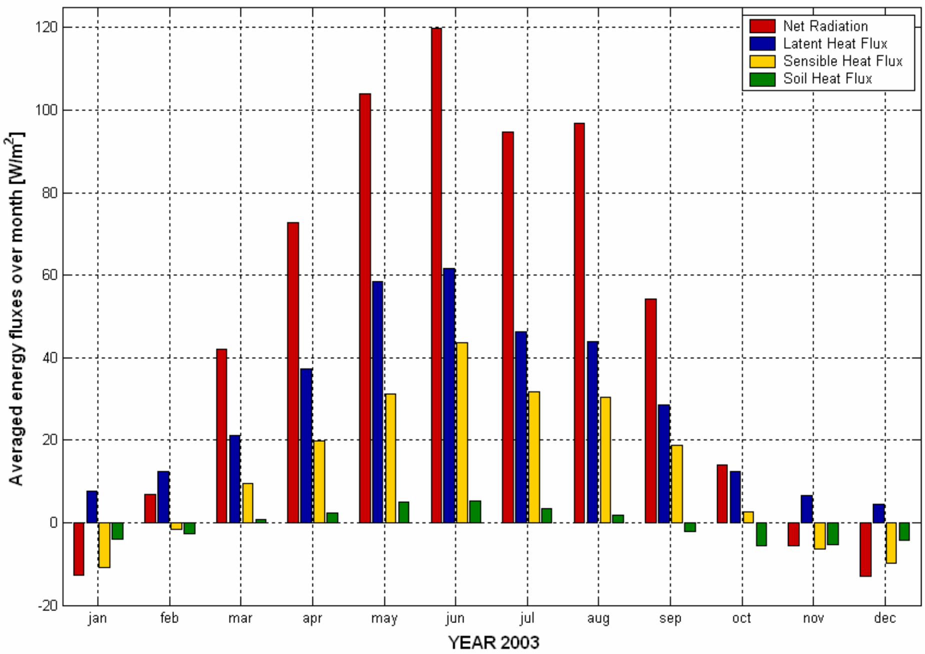

Figure 5.9: Average monthly distribution of Rn (red), LE (blue), H (yellow) and G (green) for 2003

Table 5.3: **Average monthly Rn, LE, H and G in [W/m^2] for 2003**

[W/m^2]	jan	feb	mar	apr	may	jun	jul	aug	sep	oct	nov	dec
Rn	-13	7	42	73	104	120	95	97	54	14	-5	-13
LE	8	12	21	37	59	62	46	44	29	12	7	4
H	-11	-2	10	20	31	44	32	30	19	3	-6	-10
G	-4	-3	1	2	5	5	3	2	-2	-5	-5	-4

Comparing the average monthly values of net radiation for two study years it can be noticed that the values are similar, with a bit higher values for summer months and a bit lower values for a winter time in 2003 compared with 2002. The net radiation can be expressed [*Campell and Norman*, 1998]:

$$Rn = S \times (1 - \alpha) + Ln \qquad (5.25)$$

where S is incoming solar short-wave radiation, α is albedo (αS is reflected short wave radiation) and Ln is incoming long wave radiation. Since the amount of reflected short wave radiation depends on whether the sky is covered by clouds (see chapter 4), clouds nature (high, middle, low), and type of the clouds (i.e. cirrus, cumulus, stratus) [*Campell and Norman*, 1998] we assume that cloudiness caused the difference in net radiation between two years. The same observation was reported by other researches [eg. *Wilson, et al*., 2000].

After this observation we can conclude that there is similar distribution of energy balance fluxes for both study years. Seasonal changes in solar angle and/or changes in cloudiness had a largest effect on sensible heat flux [*Wilson et al*., 2000], i.e. on average larger Rn and H in 2003 compared with 2002. In the partitioning of the water balance, the biggest part of the radiation is consumed in latent heat flux for both study years.

5.3.3 Bowen ratio

The Bowen ratio represents the ratio of sensible heat to latent heat [*Garratt*, 1992]:

$$B = \frac{H}{\lambda E} \qquad (5.26)$$

where H is sensible heat flux and λE is latent heat flux.

Negative values for Bowen ratio usually occur only when sensible heat (H) is low, around sunrise, sunset and occasionally at night [*Brutsaert*, 1991]. This situation does occur more often in cold weather [*Garratt*, 1992].

The seasonal variation of Bowen ratio is presented in Figure 5.10.

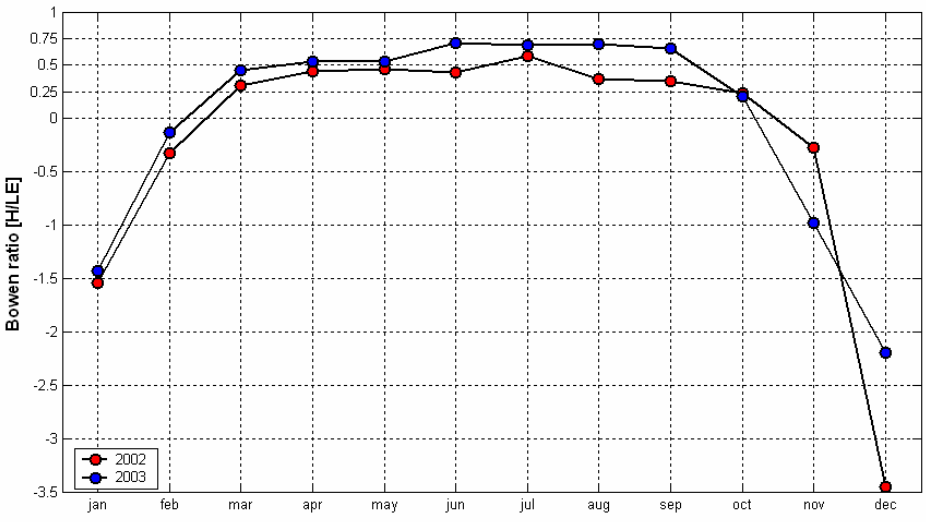

Figure 5.10: **Seasonal variation of Bowen ratio**

The Bowen ratio is negative during the winter season and positive from March to October for both study years. Generally, Bowen ratios for two observed seasons are in good agreement from January to October. From October, when the Bowen ratio was about 0.25 for both years, to December it drops to –3.5 and –2.2 for 2002 and 2003, respectively. The wet canopy tends to act as a sink for sensible heat flux (H was directed downwards, supplying the energy for evaporation of intercepted rainfall), especially throughout the winter months, resulting in the negative Bowen ratio. This contrasted dramatically with March to October turbulent exchange, which was usually dominated by upward sensible heat flux.

5.4 Evapotranspiration

5.4.1 Interannual variation in evapotranspiration

Evapotranspiration was obtained when corrected measured latent heat flux was divided with $\lambda = 2.45$ MJ/kg [*Garratt*, 1992; *FAO*, 1998].

Figure 5.11 shows the cumulative precipitation and evapotranspiration for 2002 and 2003. 2002 was wet with about 34% more annual precipitation than 2003. Nevertheless, Figure 5.11 shows that annual evapotranspiration measured using the eddy covariance techniques was 370 mm (2002) and 366 mm (2003) with little differences in the monthly ET between the two years. This evapotranspiration was 21% and 31% of annual precipitation in 2002 and 2003 respectively.

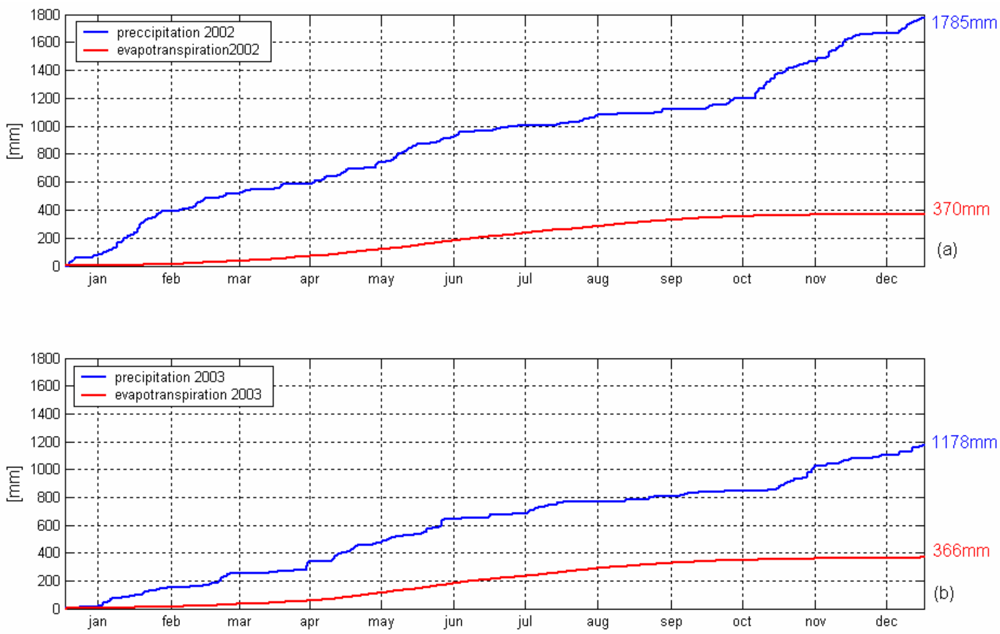

Figure 5.11: Cumulative precipitation (blue) and evapotranspiration (red): (a) for 2002, and (b) for 2003.

Therefore, although seasonal rainfall was higher in 2002 and evapotranspiration for both seasons is about the same, we can assume that more precipitation must have been exported as runoff or stored as soil moisture (as observed by the higher soil moisture and water table in summer months for 2002).

The monthly evapotranspiration shows a clear seasonal pattern (Figure 5.12) with maximum values reached during the summer months and minimum values in winter time for both study years (see Table 5.4). From February to April evapotranspiration for 2002 is greater by 29%, 7%, 15%, respectively than for the same months 2003. For May and June 2002 evapotranspiration is lower by 12% and 8% than for the same months 2002. For July and August for both years evapotranspiration is similar. For September and October, evapotranspiration is greater by 8% and 23%, respectively during 2002. January, November and December had evapotranspiration below 10 mm in both study years.

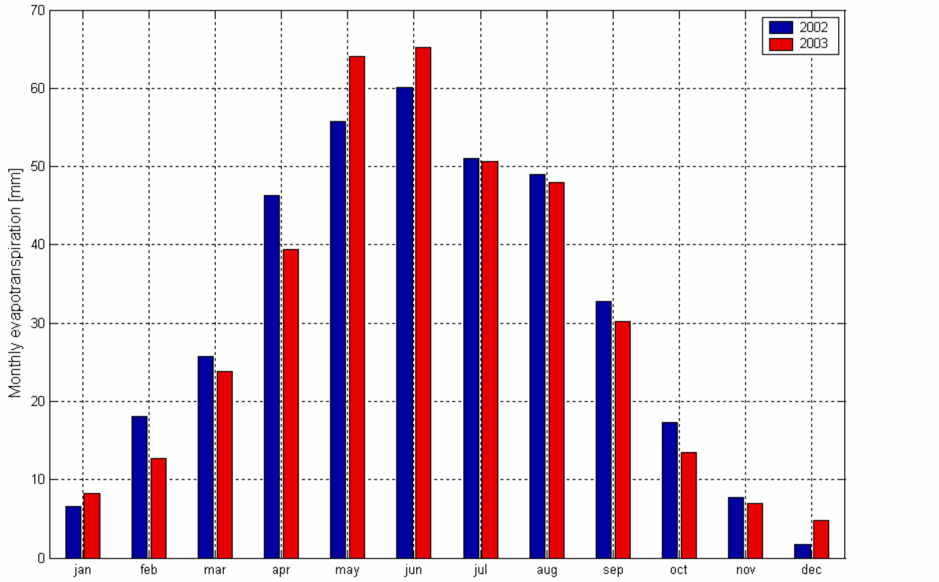

Figure 5.12: Averaged monthly evapotranspiration for 2002 (blue) and 2003 (red)

Table 5.4: Monthly averaged evapotranspiration in mm for 2002 and 2003

[mm]	jan	feb	mar	apr	may	jun	jul	aug	sep	oct	nov	dec
2002	6.6	18.0	25.8	46.3	55.8	60.1	51.1	49.0	32.7	17.3	7.7	1.7
2003	8.3	12.8	23.9	39.5	64.0	65.2	50.7	47.9	30.2	13.4	7.0	4.8

In summer, almost all of the precipitation is evaporated with hardly anything arriving to the stream except groundwater flow. A shift happens in late October when the stream flow becomes the main receiver of precipitation via the runoff phenomenon. Evaporation shows a flat part when radiation is lower in winter.

For both study years it can be noticed that maximum rates of evapotranspiration were recorded during the summer months, while rates near zero occurred during the winter months. Two main meteorological factors driving the evapotranspiration are Radiation and VPD [*Campell and Norman*, 1998], the increase of both enhancing evapotranspiration.

Figure 5.13 shows the monthly mean air temperature, precipitation and evapotranspiration for 2002. The beginning of the year is very wet, however despite that evapotranspiration is low due to the low air temperature and low VPD (see Figure 5.15 (a)) on one hand and the short height of grass (LAI is low) on the other. From March to June air temperature rises, average precipitation is above 100mm per month and evapotranspiration reaches the highest level in June (60mm). July, August and September are dryer and although the temperature reaches maximum in August, rate of evapotranspiration is smaller compared with June. Decrease of LAI caused by grass cutting in June and September could also contribute to decrease of evapotranspiration.

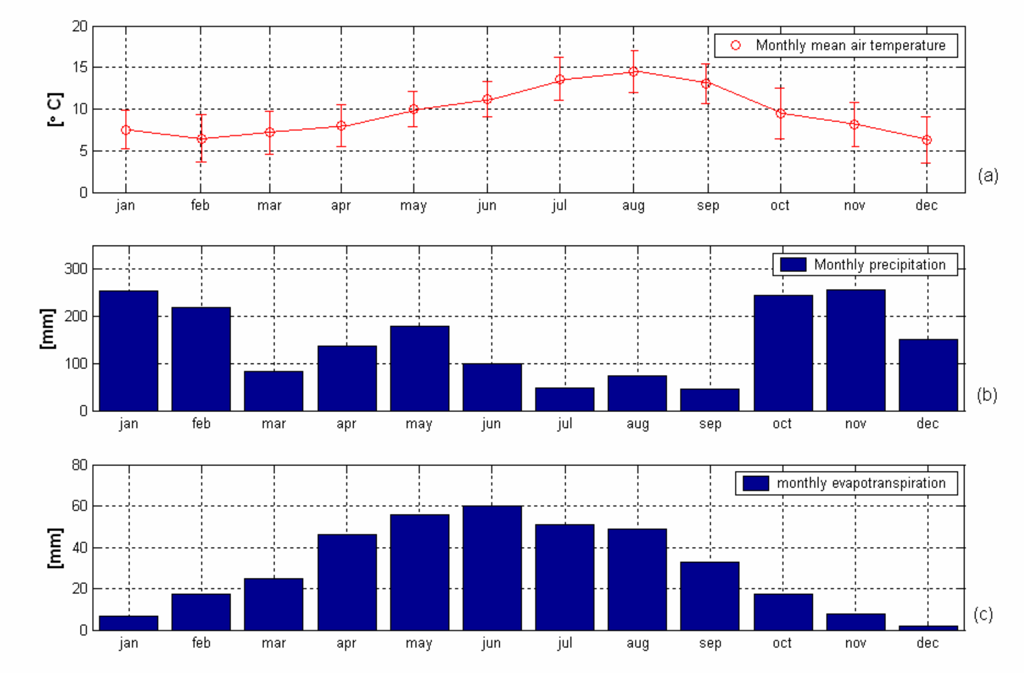

Figure 5.13: For 2002: (a) monthly air temperature with standard deviation; (b) monthly precipitation; and (c) monthly evapotranspiration

Figure 5.14 shows monthly mean air temperature, precipitation and evapotranspiration for 2003. At the beginning of the year evapotranspiration is low due to the low air temperature, short height of grass (LAI is low), and precipitation is low compared with the same period 2002. From March to June air temperature rises much faster than in 2002, precipitation in average is above 100mm per month and evapotranspiration reaches the highest level in June (65mm). July, August and September are dryer and although the temperature reaches maximum in August, rate of evapotranspiration is smaller compared with June. Decrease of LAI caused by grass cutting in July and September could also contribute to decrease of evapotranspiration. The end of the year is very wet, but because of low temperatures and low LAI evapotranspiratinon is low.

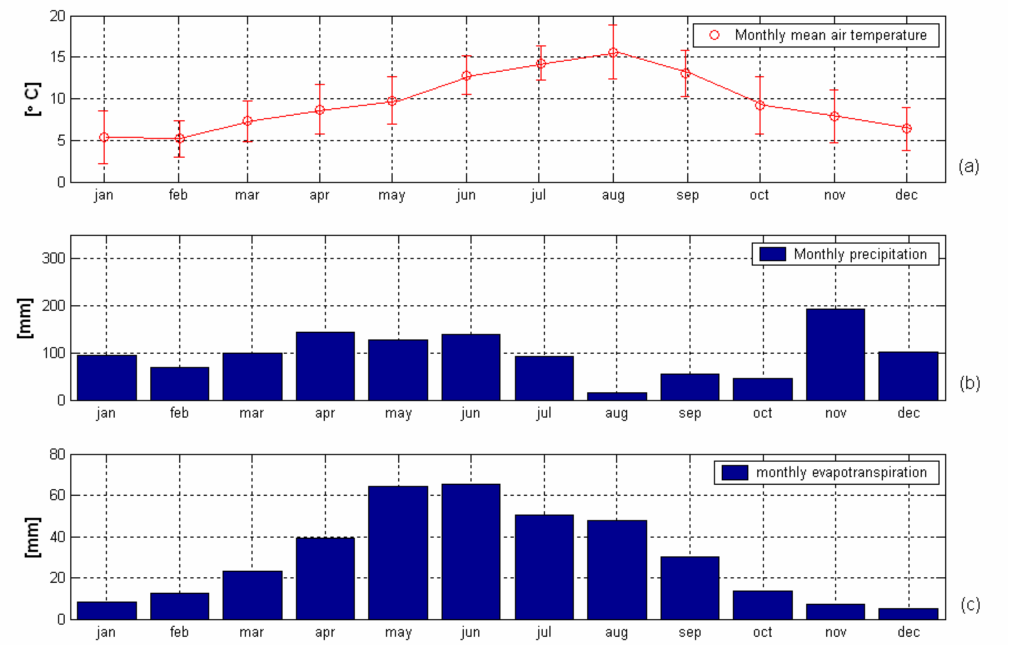

Figure 5.14: For 2003: (a) monthly air temperature with standard deviation; (b) monthly precipitation; and (c) monthly evapotranspiration

5.4.2 Measured and modelled evapotranspiration

The Penman-Monteith equation for reference grassland was used to compare with the evapotraspiration to a potential evapotraspiration. Their monthly values for 2002 and 2003 are given in the Table 5.5. Observed evapotranspiration between two years differ 4mm: 370mm (2002) vs. 366mm (2003). Cumulative potential evapotranspiration calculated for reference grassland using equation (5.7) is 423mm (2002) and 460mm (2003). The actual evapotranspiration was 88% (2002) and 81% (2003) of potential.

Table 5.5: Actual and potential evapotranspiration in [mm] for 2002 and 2003.

months	jan	feb	mar	apr	may	jun	jul	aug	sep	oct	nov	dec
ET 2002 (370mm)	6.6	18	25.8	46.3	55.8	60.1	51.1	48.9	32.7	17.3	7.7	1.7
ET 2003 (366mm)	8.3	12.8	23.8	39.4	64	65.2	50.6	47.9	30.2	13.4	6.9	4.8
PET 2002 (423mm)	9.2	18.3	27.6	46.5	55.7	62.4	66.5	59.7	40.6	20.6	10.4	5.1
PET 2003 (460mm)	8.8	14	31.6	46.9	65	75.1	64.8	75.3	42.6	22.2	9.1	4.8
PET/ET 2002	1.4	1.0	1.1	1.0	1.0	1.0	1.3	1.2	1.2	1.2	1.4	3
PET/ET	1.1	1.1	1.3	1.2	0.9	1.2	1.3	1.6	1.4	1.6	1.3	1

2003												

Figure 5.15 shows monthly vapour pressure deficit, evapotranspiration from the reference grassland, and measured evapotranspiration. The higher water pressure deficit, there is more space in the air for accepting the water vapour. The high humidity and low potential for evaporation of the region is evidenced by low VPD's with a maximum of 0.36kPa in August 2003 and as low as 0.1 kPa in the winter months. Calculated evapotraspiration closely follows this pattern and for that reason is higher than measured evapotraspiration. Namely, measured evapotraspiration mostly fallows the vapour pressure deficit pattern, but also shows discrepancies, particularly in August. For instance, examining August (Table 5.5) we note that the actual evapotranspiration was 49 mm (2002) and 48 mm (2003), while the potential was 60 mm (2002) and 75 mm (2003). This confirms that the evapotranspiration was water limited in both Augusts but more so in 2003.

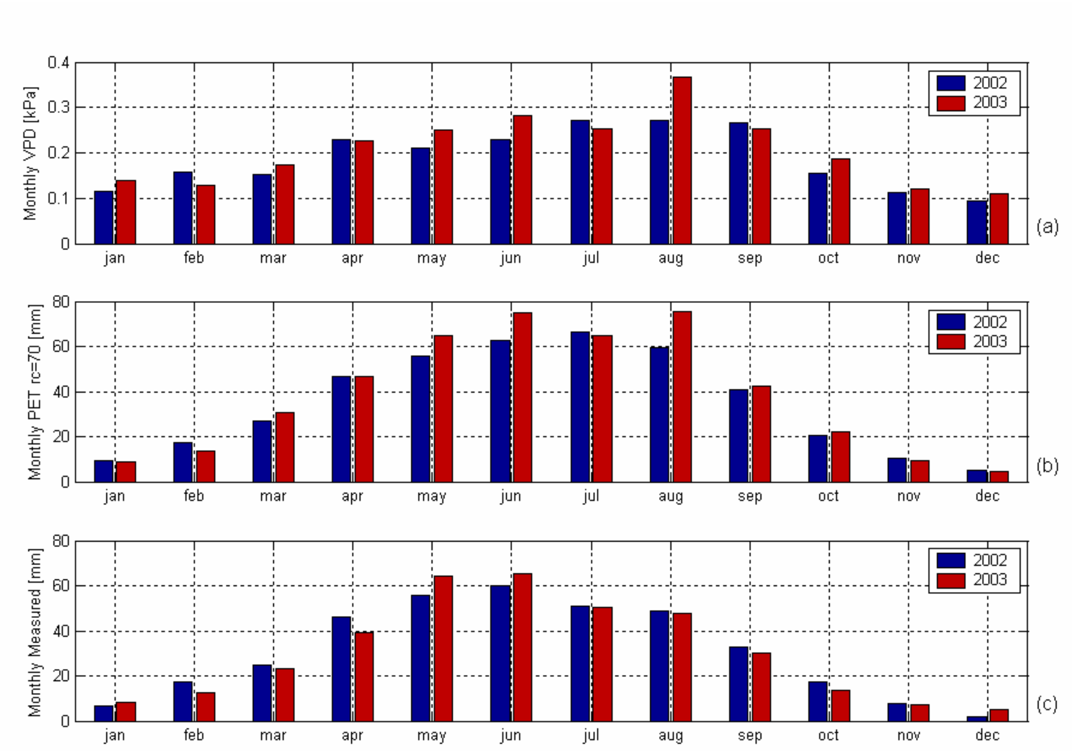

Figure 5.15: Monthly (a) averaged water pressure deficit [kPa]; (b) evapotranspiration from reference grassland (r_c = 70s/m); and (c) measured evapotranspiration.

Chapter 6
Carbon dioxide flux

Chapter 6 Carbon dioxide flux

6.1 Data analysis

6.1.1 Eddy covariance

The 3D wind velocity and virtual (sonic) air temperature were measured at 10 Hz with an RM Young Model 81000 3-D sonic anemometer positioned at the top of the 10 m tower (see section 2.2.3). CO_2 densities were measured at 10 Hz with an LI-7500 open path infrared gas analyser (LICOR Inc. USA) placed within 20 cm of the centre of the anemometer air volume (see section 2.2.4). The 30-minute CO_2 fluxes were calculated by the eddy correlation method defined by formula (3.6) in chapter 3. The fluxes were computed on line and logged every 30 minutes on CR23X datalogger. Post processing including Webb corrections, rotations, filtering etc.

6.1.2 Webb correction

All CO_2 flux data were firstly adjusted using the Webb correction [*Kramm et al.*, 1995; *Webb et al.*, 1980; *Baldocchi*, 2003], described in section 3.2.3. This corrects the turbulent flux measurements of a constituent by taking into account the simultaneous flux of any entity, in particular heat or water vapour, which cause expansion of the air and thus affect the constituent's density. This correction is important for CO_2 fluxes for which the density fluctuations range is comparable to the mean density value. Figure 6.1 shows measured and Webb corrected CO_2 flux for a few days in August 2002. The CO_2 flux is positive during the night (plants release CO_2 in the atmosphere in the process of respiration), and is negative during the day (plants are taking CO_2 flux from the air in the process of photosynthesis). It can be seen that the Webb correction reduces both the respiration and the photosynthetic component.

As it can be seen from the figure, after Webb correction there are still bad data.

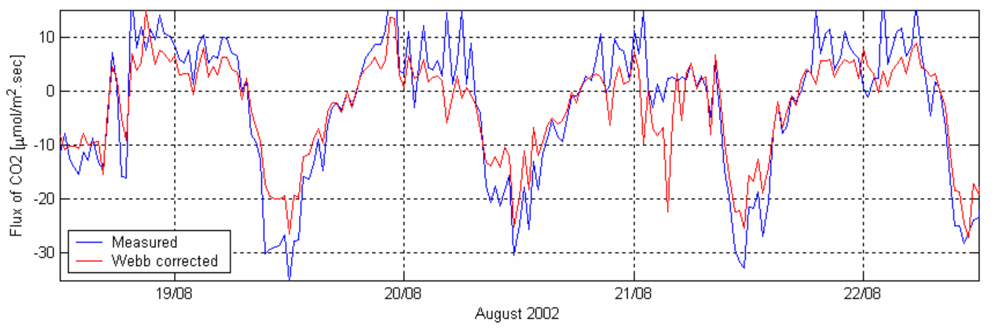

Figure 6.1: 30 minute measured flux (in blue) and Webb corrected flux (in red)

6.1.3 Defining the daytime and nighttime duration

One of the formulations of day/night duration is based on amount of incoming solar radiation [*Campbell and Norman*, 1998; *Lafleur et al.*, 2001]. If that amount is higher than a certain limit, it is a daytime, otherwise it is nighttime. This formulation allows seasonality in day length.

After observing the flux behaviour during the good days (no rain) we adopted that night begins when incoming radiation is below a very small value such as 20 W/m^2 (against average 950 W/m^2 at noon in summer). Observation was done for every month during the good days and here we present observations for one day in winter (Figure 6.2) and in summer (Figure 6.3). From the figures one can conclude that behaviour of incoming radiation describes well duration of the day length (i. e. day in February last approximately from 8:30 to 17:30, and in July from 5:30 to 20:30). The longer the night, the greater the part of respiration in the carbon budget and the smaller the cumulative uptake. The threshold of 20 W/m^2 describes well also the periods of carbon dioxide uptake (day) and release (night).

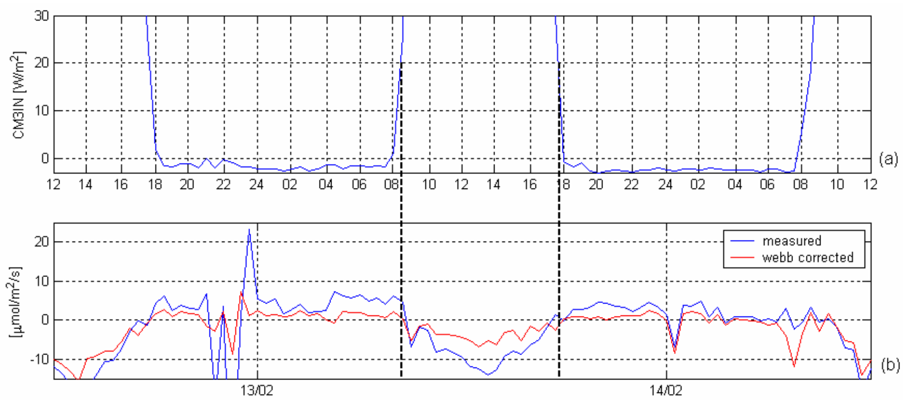

Figure 6.2: 30 minute: (a) Incoming solar radiation; and (b) measured (in blue) and Webb corrected (in red) CO_2 flux on 13th February 2002

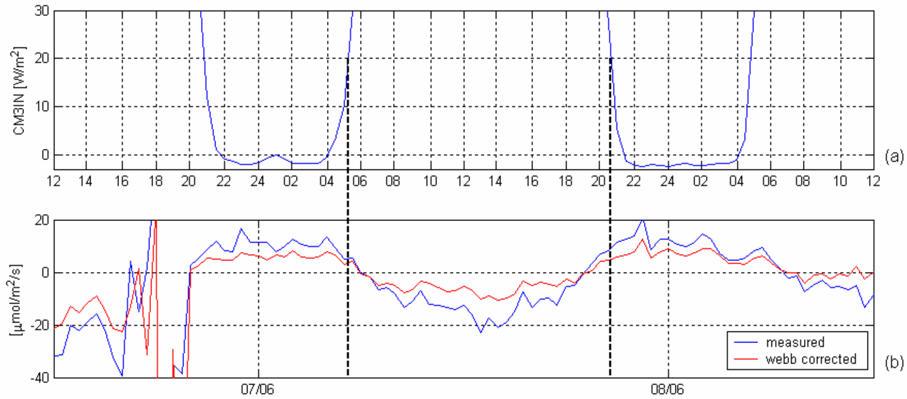

Figure 6.3: 30 minute: (a) Incoming solar radiation; and (b) measured (in blue) and Webb corrected (in red) CO_2 flux on 7th July 2002

The second definition of daylength is an astronomical definition where sunrise and sunset correspond to a zenith angle of 90°. The half daylength, which is the time (in degrees) from sunrise to solar noon, can be expressed as [Campbell and Norman, 1998]:

$$h_s = \cos^{-1}\left(\frac{\cos\psi - \sin\phi \times \sin\delta}{\cos\phi \times \cos\delta}\right) \tag{6.1}$$

where cosψ is null for the geometrical sunrise and sunset,ϕ is the latitude and δ is the solar declination. The time of sunrise (t_r) and sunset (t_s) are then:

$$t_r = t_o - \frac{h_s}{15} \qquad (6.2) \qquad\qquad t_s = t_o + \frac{h_s}{15} \qquad (6.3)$$

Using this approach it was found that night in Ireland fluctuates approximately between 8.30 pm and 5 am in summertime, and 17 pm and 8.30 am in wintertime. This is in agreement with what was found using the amount of incoming solar radiation to defined day length.

Using method based on amount of incoming solar radiation as definition of day and night it was found that 44.2% (2002) and 45% (2003) of data are day data (see Charts 6.1 and 6.2).

6.1.4 Precipitation filter

As it was shown in section 3.3.1 the eddy covariance system performed poorly during the rain events. This is a consequence of covering the LI-7500 probe head with water [*Mizutani et al.*, 1997]. Hence after the Webb correction, all data were filtered using the precipitation filter, described in section 3.3.1. In effect, all CO_2 data during and up to one hour after the rain events were rejected.

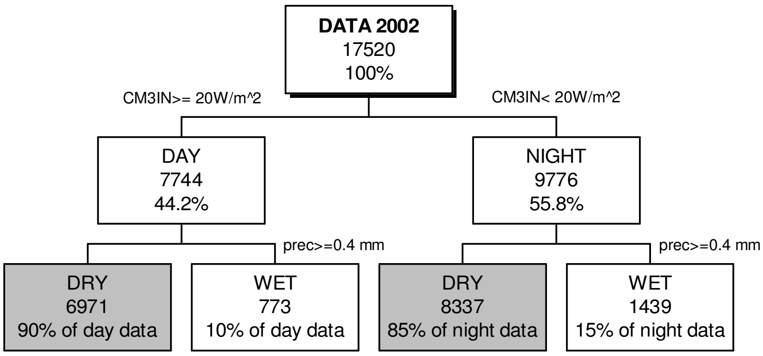

Chart 6.1: 2002 Day and Night data and percentage of their goodness regarding the precipitation filter

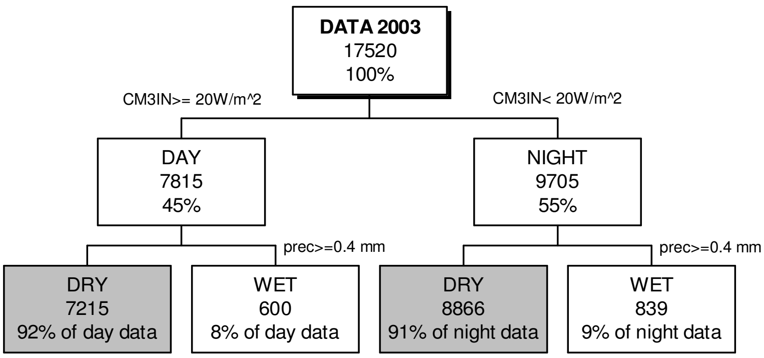

Chart 6.2: 2003 Day and Night data and percentage of their goodness regarding the precipitation filter

It was found that 10% of day and 15% of night data were rejected after application of precipitation filter in 2002 (see Chart 6.1). In 2003 only 8% of day and 9% of night data were rejected due to the rain (see Chart 6.2). The reason for this is

less precipitation during the 2003 season.

6.1.5 Momentum flux filter

The nocturnal period includes conditions such as cold air drainage, sporadic mixing, and fluctuations in vertical wind too small to be resolved by the sonic anemometer.

The eddy correlation method works best during windy periods [e.g., *Goulden, et al.*, 1996; *Moncrieff et al.*, 1997; *Falge et al.*, 2001]. During calm climatic conditions the measured fluxes are underestimated:

1) as the fluctuations in the vertical wind speed are too small to be resolved by the sonic anemometer [*Goulden, et al.*, 1996] and

2) for nocturnal and very stable conditions, the flow statistics may be dominated by transient phenomena or even lack of turbulence [*Cava et al.*, 2004].

Cava et al. [2004] found that when canopy waves dominate night-time runs, the local CO_2 production from ecosystem respiration and observed mean fluxes above the canopy are, to a first order, de-coupled presumably through a storage term. What is important here is that when canopy waves dominate, there is "gross" mass and heat exchange between the canopy and the atmosphere; however, the net exchange over the lifecycle of the wave is negligible. Occasionally, these waves are under-sampled because of a short flux averaging period leading to an apparent and spurious "photosynthesis" (or canopy C uptake) values at night in the case of CO_2. Correcting night-time fluxes with runs collected under high u_* (or more precisely for near-neutral to slightly stable conditions) ensures that the turbulent regime is fully-developed. Another reason why runs with high friction velocity (momentum flux), u_*, (or near-neutral conditions) are preferred for night-time flux corrections is a much smaller (and perhaps the more realistic) footprint.

Uncertainties in night-time fluxes have been examined by many researchers [Falge *et al.*, 2001; *Pattey et. al.*, 2002; *Baldocchi et al.*, 2003]. The nocturnal CO_2 flux is a critical issue regarding poorly mixed periods, since small underestimations of night-time CO_2 fluxes (respiration) imply overestimations of the annual carbon uptake [*Goulden et al.*, 1996; *Baldocchi et al.*, 1996; *Moncrieff et al.*, 1996; *Schmid et al.*, 2000; *Valentini et al.*, 2000]. In identifying calm conditions a lower boundary for u_*

was determined to filter transients and weak turbulence conditions [e.g., *Goulden, et al.*, 1996; *Moncrieff et al.*, 1996; *Falge et al.*, 2001; *Pattey et al.*, 2002]. In the literature, definitions of poor mixing use a condition on the momentum flux $u_* < u_{*critical}$, with $u_{*critical}$ varying from 0.15 m/s up to 0.6 m/s [*Baldocchi et al.*, 2003].

Observing the night time Webb corrected flux during the dry periods and corresponding values for friction velocity (Figure 6.4), we estimated the threshold for friction velocity as 0.2m/s. Therefore we filtered CO_2 fluxes at night when $u_* < 0.2$m/s [*Pattey et al.*, 2002; *Baldocchi et al.*, 2003].

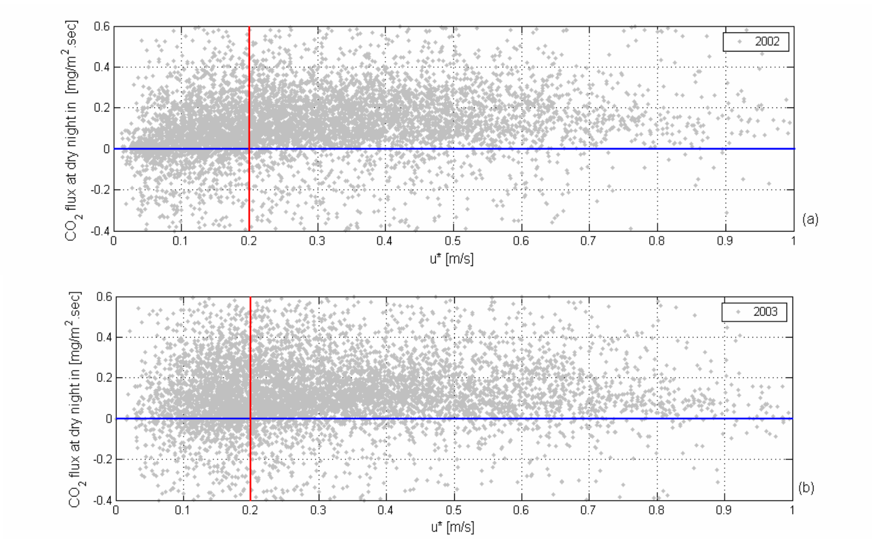

Figure 6.4: CO_2 flux during the dry nights in [mg/m^2/sec] versus friction velocity during the dry nights in [m/s]: (a) for 2002 and (b) for 2003

It can be seen from the frequency histogram (Figure 6.5) of the friction velocity for dry nights that values below 0.2m/s occur approximately 30% of dry nighttime. This value is consistent with the average data retrieved during a year for eddy covariance systems in the literature.

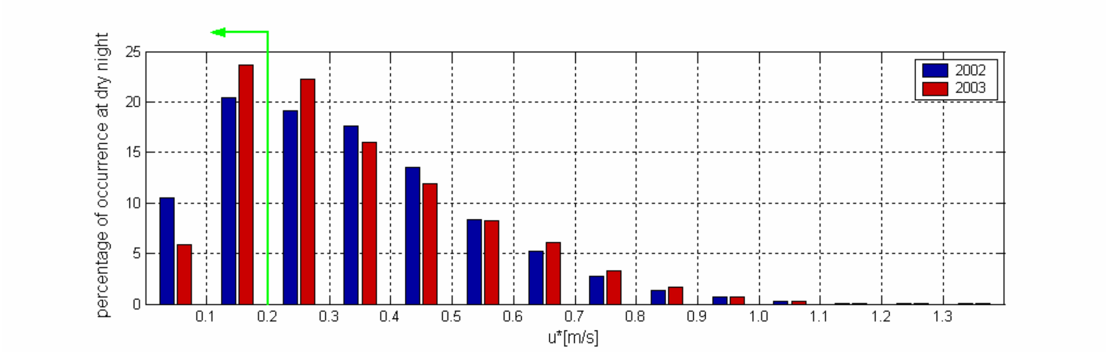

Figure 6.5: Frequency histogram of friction velocity during the nighttime without precipitation

6.1.6 CO_2 filter for nighttime

It has been shown in the last section that CO_2 flux measurements are sensitive to the physical environment and that consequently data corresponding to low wind conditions at nighttime must be removed. Those are not the only measurements that should be filtered. Indeed, a respiration flux above 15μmol/m^2/s (the convention in this thesis is that positive fluxes are net respiration - away from the surface) during the night cannot be seen on a grassland site. Although Baldocchi [2004] suggests that after rain events a significant pulse of respiration occurs which may exceed 15μmol/m^2/s. In the same way, photosynthesis cannot occur without any light. Thus negative flux should be filtered out at nighttimes.

We filtered nighttime fluxes when respiration exceeded predetermined threshold values for the season (see Table 6.1) and when the friction velocity was less than 0.2m/s.

Table 6.1: CO_2 filter for nighttime and data goodness for 2002 and 2003

(u*>=0.2m/s)	NEE limit [μmol/m^2/s]	2002			2003		
		good	bad	sum	good	bad	sum
Jan – Feb	up to 7	582	1432	2014	721	1232	1953
		29%	71%		37%	63%	
Mar – Apr	up to 10	578	906	1484	519	988	1507
		39%	61%		34%	66%	
May – Jun	up to 15	497	660	1157	391	773	1164
		43%	57%		34%	66%	
Jul – Aug	up to 15	645	620	1265	613	653	1266
		51%	49%		48%	52%	
Sep – Oct	up to 10	615	1071	1686	836	837	1673
		36%	64%		50%	50%	
Nov – Dec	up to 7	634	1535	2169	867	1275	2142
		29%	71%		40%	60%	
		3552	**6224**	**9776**	**3947**	**5758**	**9705**
		36%	**64%**		**41%**	**59%**	

For instance, the he night time summer fluxes were accepted if $u_* \geq 2$m/s, $f_c >$ 0μmol/m^{2}s (there is no photosynthesis) and $f_c <$ 15μmol/m^{2}s. The nighttime data were binned in two-month increments according to Falge et al., [2001]. After filtering of nighttime CO_2 flux data it was found that 36% (2002) and 41% (2003) of night data were good.

6.1.7 CO_2 filter for daytime

No physical environmental conditions were applied to filter CO_2 flux at day times. We filtered daytime fluxes when respiration and uptake exceeded predetermined threshold values for the season (see Tables 6.2 and 6.3).

The daytime data was binned in two-month increments according to Falge et al., [2001]. For instance the daytime summer fluxes were accepted if $f_c > -35\mu mol/m^2s$ and $f_c < 15\mu mol/m^2s$. Daytime data were good in 76% (2002) and 79% (2003) of all cases.

Table 6.2: CO_2 filter for daytime and data goodness for 2002

2002	NEE [µmol/m²/s]	NEE [µmol/m²/s]	good	bad	sum
Jan – Feb	-15	5	534	332	866
			62%	38%	
Mar – Apr	-25	10	1027	369	1396
			74%	26%	
May – Jun	-35	15	1339	432	1771
			76%	24%	
Jul – Aug	-35	15	1493	218	1711
			87%	13%	
Sep – Oct	-25	10	1037	205	1242
			83%	17%	
Nov – Dec	-15	5	452	306	758
			60%	40%	
			5882	**1862**	**7744**
			76%	**24%**	

Table 6.3: CO_2 filter for daytime and data goodness for 2003

2002	photosynthesis [μmol/m²/s]	respiration [μmol/m²/s]	good	bad	sum
Jan – Feb	-15	5	635	292	927
			69%	31%	
Mar – Apr	-25	10	1058	315	1373
			77%	23%	
May – Jun	-35	15	1305	459	1764
			74%	26%	
Jul – Aug	-35	15	1465	245	1710
			86%	14%	
Sep – Oct	-25	10	1082	173	1255
			86%	14%	
Nov – Dec	-15	5	607	179	786
			77%	23%	
			6152	**1663**	**7815**
			79%	**21%**	

6.1.8 Quality of data

After post-processing and filtering of spurious data, 54% of the CO_2 flux data for 2002 and 58% for 2003 were suitable for analysis. The percentage of usable data reported by other studies is approximately 65% [*Falge et al.*, 2001; *Law et al.*, 2002]. About 13% of our 2002 data and 8% of our 2003 data were rejected due to water drops on the LI-7500 during the rain and within hour after the rain. The rest of non-usable data (33% for 2002, and 34% for 2003) were rejected when found to be out of range or during periods of low nighttime friction velocity.

6.1.9 Contribution of Webb correction

After the Webb correction and filtering it was important to find out how big Webb correction contribution is to the CO_2 flux. We plotted measured CO_2 flux against Webb corrected and filtered CO_2 flux for all good daytime and night time data (Figure 6.6).

According to correlation found between these two fluxes (see Figure 6.6), average reduction of the flux after Webb correction is 25% (2002) and 23% (2003). The greatest reduction of the flux in average is for period July-August, when it is 37% (2002) and 41% (2003) and the smallest reduction is in wintertime. Plots of correlation between measured and Webb corrected flux for each two month period months are shown in Appendix 3. The Webb correction reduces the magnitude of the fluxes in both day and night periods.

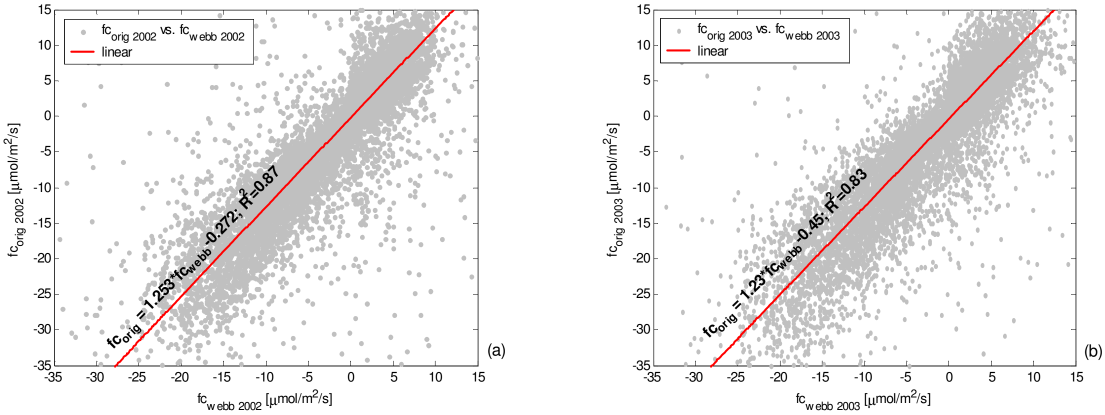

Figure 6.6: Correlation between measured and Webb corrected CO_2 flux for: (a) 2002 and (b) 2003

It is important to note for some particular cases 30 minute and daily CO_2 flux reduction by Webb correction may be much greater/smaller than the average reduction for the whole year or two month periods.

6.2 Gap filling

Once bad CO_2 flux data were removed in a satisfying way, methods have to be found to fill the gaps, in order to be able to establish the carbon balance for different time scales: from daily to annual budget. The gap filling functions tested were non-linear regressions [see *Goulden et al.*, 1996; *Falge et al.*, 2001; *Lai et al.*, 2002]. Those functions were determined based on good data and they preserve the relations between the fluxes and meteorological driving forces. To describe effects due to diurnal patterns, daytime and nighttime data were addressed separately.

6.2.1 Nighttime gap filling

For nighttime data, the ecosystem respiration is known to be linked to the soil temperature [*Lloyd and Taylor*, 1994; *Kirschbaum*, 1995] and to a lesser extent to soil moisture (consistent with the analysis of Novick et al. [2004] for warm temperate grassland). The correlation with different temperatures (air, surface, different soil depths) showed best results for soil temperature at 5 cm depth, whereas the data set was less well correlated to soil moisture. Different temperature response functions were tested (Tables 6.4 and 6.5) and parameterised statistically (Sum of Squares Error (SSE), Root-Square (R^2), adjusted Root Square (adjusted-R^2), and Root Mean Squared

Error (RMSE)). A linear relationship, an exponential relationship, 4th degree polynomial, the Arrhenius function and the so called Q10 (with 25°C as reference) relations were first considered.

The Matlab curve fitting toolbox was used to determine parameterisation of those functions, as well as the goodness of each fit in terms of SSE, R^2, adjusted-R^2, and RMSE. For SSE and RMSE the closer to 0 the better the fit, whereas for R^2 and adjusted-R^2 the closer to 1 the better the fit.

The best fit for nighttime was obtained for the exponential function defined as:

$$F_{ni} = a \times e^{(b \times t_{soil})} \quad (6.4)$$

where t_{soil} is the soil temperature at 5 cm depth in *ºC*, a=1.476 for 2002 and 1.109 for 2003, b=0.095 for 2002 and 3.389 for 2003. For the combined 2002 and 2003, a=1.485 and b=0.09575

Table 6.4: Fitting functions for nighttime for 2002

	Equation	Coefficients	SSE	R^2	Ad. R^2	RMSE
Arrhenius function	$F_{ni} = a \times e^{\left(b - \frac{c}{t_{soil}}\right)}$	a = 1.712 ± 4.253e6 b = 1.392 ± 2.485e6 c = 4.769 ± 0.403	1.39e4	0.2505	0.2505	2.017
Linear fitting	$F_{ni} = a \times t_{soil} + b$	a = 0.3561 ± 0.0176 b = 0.475 ± 0.176	1.27e4	0.3159	0.3157	1.927
4th degree polynomial	$F_{ni} = p_1 \times t_{soil}^4 + p_2 \times t_{soil}^3 + p_3 \times t_{soil}^2 + p_4 \times t_{tsoil} + p_5$	p_1 = -3.7e-4 ±3.0e-4 p_2 = 0.0114 ± 0.011 p_3 = -0.091 ± 0.142 p_4 = 0.336 ± 0.756 p_5 = 1.782 ± 1.404	1.24e4	0.3292	0.3284	1.909
Q_{10} func. 25°C	$F_{ni} = a \times b^{\left(\frac{t_{soil}-25}{10}\right)}$	a = 15.79 ± 1.04 b = 2.581 ± 0.125	1.25e4	0.3243	0.3241	1.915
Exp. fitting	$F_{ni} = a \times e^{(b \times t_{soil})}$	a = 1.476 ± 0.087 b = 0.095 ± 0.005	1.25e4	0.3243	0.3241	1.915

Table 6.5: Fitting functions for nighttime for 2003

	Equation	Coefficients	SSE	R^2	Ad. R^2	RMSE
Arrhenius function	$F_{ni} = a \times e^{\left(b - \frac{c}{t_{soil}}\right)}$	a = 2.38 ± 6.496e6 b = 1.111 ± 2.73e6 c = 5.154 ± 0.418	1.92e4	0.2835	0.2833	2.229
Linear fitting	$F_{ni} = a \times t_{soil} + b$	a = 0.42 ± 0.0184 b = -0.312 ± 0.177	1.70e4	0.366	0.366	2.097
4^{th} degree polynomial	$F_{ni} = p_1 \times t_{soil}^4 + p_2 \times t_{soil}^3 + p_3 \times t_{soil}^2 + p_4 \times t_{tsoil} + p_5$	p_1 = -3.5e-5 ±4.2e-4 p_2 = 0.0041 ± 0.016 p_3 = -0.068 ± 0.203 p_4 = 0.681 ± 1.098 p_5 = -0.103 ± 2.037	1.66e4	0.3819	0.3813	2.071
Q_{10} func. 25°C	$F_{ni} = a \times b^{\left(\frac{t_{soil} - 25}{10}\right)}$	a = 23.45 ± 1.66 b = 3.389 ± 0.178	1.66e4	0.3811	0.381	2.071
Exp. fitting	$F_{ni} = a \times e^{(b \times t_{soil})}$	a = 1.109 ± 0.072 b = 0.1221 ± 0.005	1.66e4	0.3811	0.381	2.071

Figure 6.7 shows that the regression of nighttime CO_2 fluxes against soil temperature is a very scattered plot. This is likely linked to the different respiration sources, leaf and soil. They have not been separated in this study but their contribution changes over time and in response to different developmental factors. However, this separation is not possible without independent measurements.

In using t_{soil} at one location near the tower, this does not represent the t_{soil} in the footprint. Akin to the debate about energy balance closure where Rn and G are measured at one point and may not represent the flux footprint.

An exponential function was applied to the good nighttime data for the full year (separately for 2002 and 2003 and for both years together, see Figure 6.7), because the range of nighttime soil temperature throughout the year was small (2 to 16° C) and its change gradual throughout the year (see section 4.5). The nighttime CO_2 flux for bad night data points was found using exponential equation 6.4 with coefficients in Tables 6.4 and 6.5 and the soil temperature for those data points.

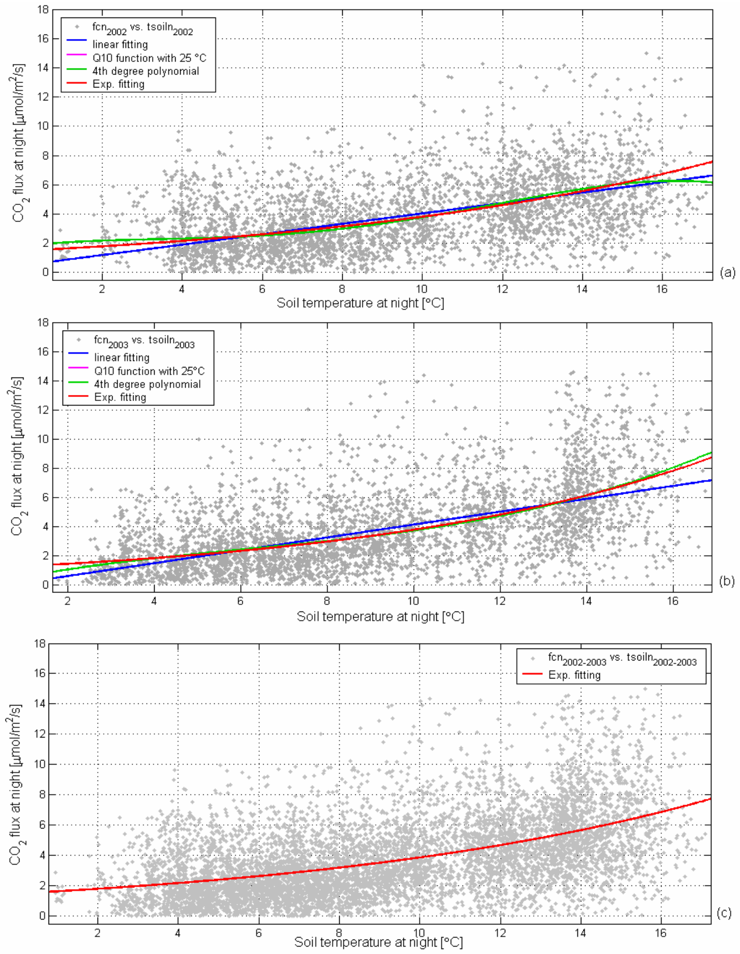

Figure 6.7: **Nighttime fitting: (a) for 2002; (b) for 2003 and (c) for 2002 and 2003**

6.2.2 Daytime gap filling

For daytime, the net ecosystem exchange of CO_2 is linked to the photosynthetic photon flux density Q_{ppfd} (photosynthetic active radiation Q_{par}) in µmol of quantum/m^2/s [e.g., *Michaelis and Menten*, 1913; *Smith*, 1938; *Goulden et. al.*, 1996]. The photosynthetic flux is obtained either by converting, with some approximations, 45% of the incoming solar radiation from W/m^2 into µmol of quantum/m^2/s or by using the PAR Lite instrument as explained in section 2.2.5.

Different light response functions tested included: a linear relationship, Smith formula [*Smith*, 1938; *Falge* et al., 2001], Michaelis-Menten formula sometimes referred to as a rectangular hyperbola [*Michaelis & Menten*, 1913; *Falge et al.*, 2001], Misterlich formula [*Falge et al.*, 2001], and Ruimy formula [*Ruimy et al.*, 1995; *Lai et al.*, 2002]. The Matlab curve fitting toolbox was used to parameterise those functions, and determine goodness of each fit. In the case of Misterlich, Michaelis and Smith formulas, the non-linear problem could only be resolved by setting some parameters constant. Indeed, the complete equations use the gross primary productivity at 'optimum' light $F_{GPP,opt}$, which is a function of the air temperature:

$$F_{GPP,opt} = \frac{F_{GPP,T_{ref}} \times e^{(\Delta H_a \times (T_k - T_{ref}) \div (R \times T_k \times T_{ref}))}}{1 + e^{((\Delta S \times T_K - \Delta H_d) \div (R \times T_K))}} \times \left(1 + e^{((\Delta S \times T_{ref} - \Delta H_d) \div (R \times T_{ref}))}\right) \quad (6.5)$$

where T_K is the air temperature (in K), R is the gas constant (8.314J/K/mol), ΔH_a is the activation energy in J/mol, ΔH_d is the energy of deactivation (set to 215,000J/mol), ΔS is an entropy term (set to 730J/K.mol) and $F_{GPP,ref}$ is the carbon uptake at optimum light and reference temperature T_{ref} (298.16K).

Matlab curve fitting toolbox cannot consider this kind of added variable data in a curve fitting study. However this variable does not fluctuate a lot, and has therefore been considered as a constant 'β' for Michaelis and Smith functions (see Tables in appendix 4.1 and 4.2) that was set by curve fitting, and replaced by its mean (-24 μmol CO_2 /m^2/s) for Misterlich function. In those three equations, 'α' is the ecosystem quantum yield and 'γ' is the daily respiration.

The best fit was obtained with the Misterlich formula defined as:

$$F_{day} = -24 \times \left(1 - e^{\left(\frac{\alpha \times Q_{par}}{-24}\right)}\right) + \gamma \quad (6.6)$$

where $Q_{par} \equiv Q_{ppfd}$ is the photosynthetic photon flux density in μmol of quantum/m^2/s . Since Q_{par} varies seasonally, data were analysed and the function was fitted to two-month data bins. Table 6.6 gives coefficients α and γ for adopted Misterlich function:

		Jan-Feb	Mar-Apr	May-Jun	Jul-Aug	Sep-Oct	Nov-Dec
2002	α	0.0173	0.031	0.030	0.018	0.029	0.019
	γ	0.217	2.525	3.703	3.501	3.24	1.212
2003	α	0.0171	0.0298	0.033	0.032	0.030	0.015
	γ	0.809	2.088	5.243	6.039	2.788	0.544

Table 6.6: Coefficients α and γ for Misterlich function for 2002 and 2003

Figure 6.8 shows best fits for daytime for May-June 2002 and 2003. All graphs with best fitting function for day and tables with fitting functions coefficients and statistical parameters (i.e. Sum of Squares Error (SSE), Root-Square (R^2), adjusted Root Square (adjusted-R^2), and Root Mean Squared Error (RMSE)) are given in appendix 4.1 and appendix 4.2 for 2002 and 2003 respectively. The CO_2 flux plot against the photosynthetic photon flux $Q_{ppfd} \equiv Q_{PAR}$ is much less scattered than plots for the nighttime data in figure 6.7, and the trend (i.e. Misterlich's formula) is easily noticeable even based on the visual aspect of the fits. Thus, Misterlich's formula was used to fill all missing or filtered data at daytime.

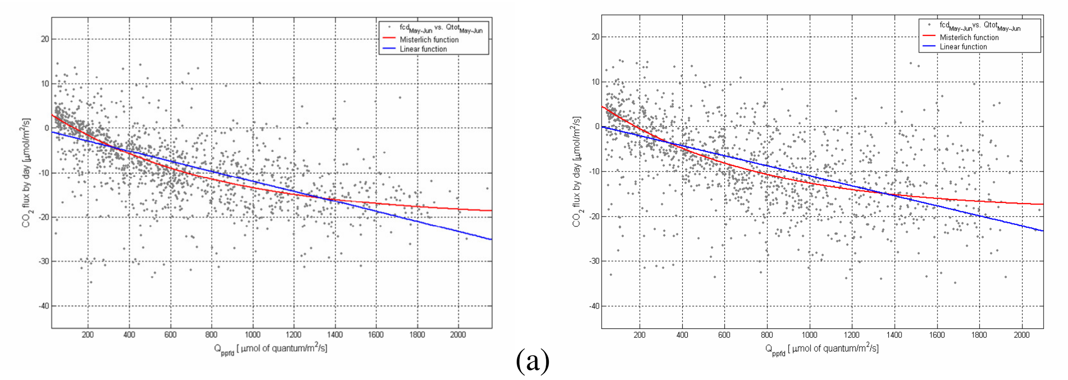

(a) (b)

Figure 6.8: Best daytime fitting curves for May - June: (a) 2002 and (b) 2003

The equations that have been chosen to fill daytime and nighttime gaps can be used for short time periods such as 1 or 2 hours, and also for long time gaps of the order of a month or more [*Falge et al.*, 2001; *Lai et al.*, 2002;].

6.3 Results and discussion

6.3.1 Daily flux

Two extreme days from year 2002 were selected to show the typical 30 minute averaged CO_2 fluxes throughout a winter and a spring day and compare them with average 30 minute fluxes for the corresponding months (Figure 6.9). In all figures, the photosynthesis flux is taken negatively, so that an uptake of carbon by the site is a negative value.

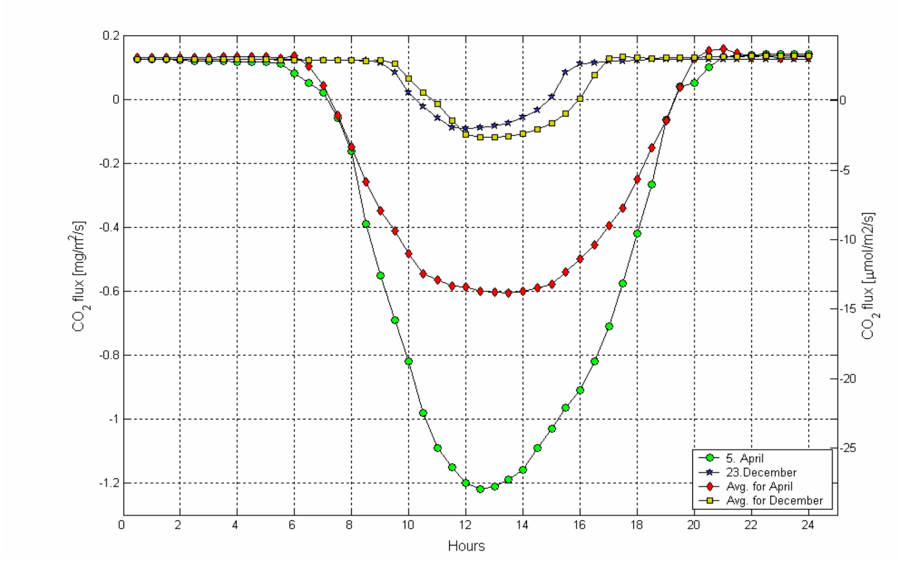

Figure 6.9: Representation of the daily CO_2 fluxes at 30 minutes intervals in 2002: for 5th of April (—○—); for 23rd of December (—☆—); averaged over month of April (—◊—) and averaged over month of December (—□—)

In Figure 6.9 the spring day curve (April the 5th) corresponds to the highest flux of the 2002 with a maximum of -1.2mg of CO_2 /m^2/s at midday and a nighttime flux of 0.14mg of CO_2 /m^2/s. This day was clear and the photosynthesis process lasted from about 5 am to 8.30 pm, that is a 15.5 hours daylength. In contrast, the winter day curve (December the 23rd), shows the smallest day flux of the study period with a maximum of only -0.09mg of CO_2 /m^2/s at midday and a nighttime flux of 0.12mg of CO_2 /m^2/s. The photosynthesis process lasted from about 8.30 am to 5 pm, that is an 8.5 hours daylength. The graph shows well the link between daylength and photosynthesis process, as well as the seasonal pattern for the CO_2 flux magnitude. The difference in the day part of the curves is much more pronounced than the one for the nighttime so, that the carbon budget for the 5th of April is a net uptake of 1.06mg of CO_2/m^2/s, whereas the 23rd of January corresponds to loss of 0.03mg of CO_2/m^2/s.

However, those kinds of extreme events do not last for many consecutive days. Let F_{30} be the 30 minute averaged CO_2 fluxes, Fd_{max} the daily maximum of F_{30}. Then, the mean of Fd_{max} over 30 consecutive days seems a more relevant indication for the seasonal fluctuation in magnitude, and a more reliable data to compare. For April 2002, averaged Fd_{max} is -0.61mg of CO_2 /m^2/s, whereas for December 2002, averaged Fd_{max} is -0.12mg of CO_2 /m^2/s. These values are consistent with what was found by other researches [*Frank and Dugas*, 2001; *Sims and Bradford,* 2001].

Figure 6.10 shows the daily uptake of CO_2 and the daily maximum temperature during 2002 and 2003.

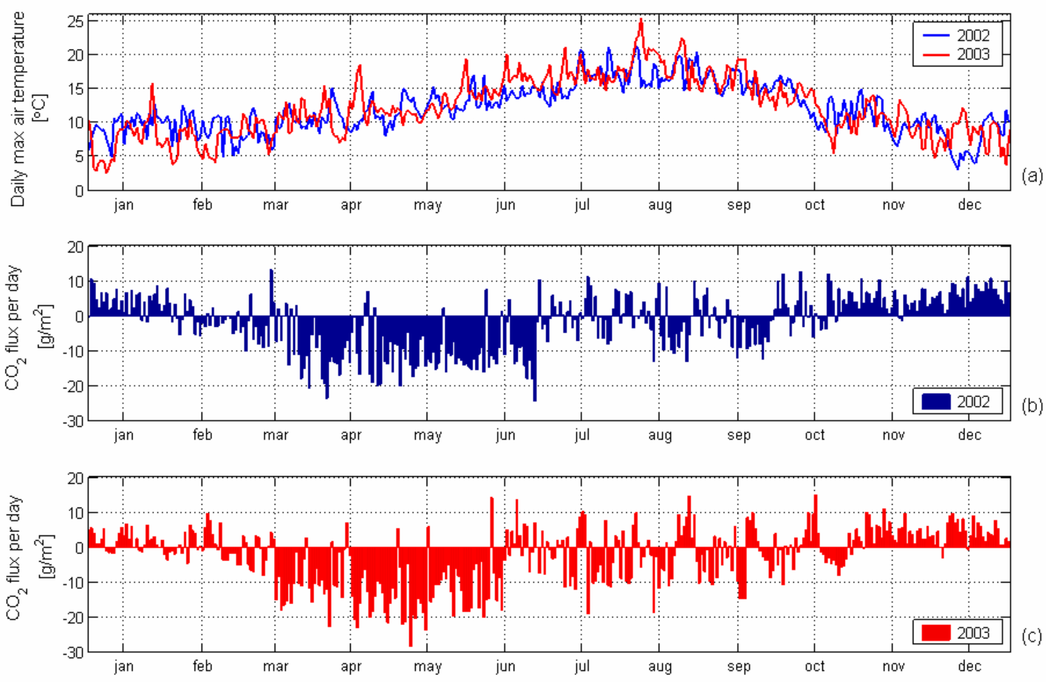

Figure 6.10: (a) daily maximum air temperature for 2002 (blue) and 2003 (red); (b) daily CO_2 flux in 2002; and (c) daily CO_2 flux in 2003

The maximum daily uptake is in late June 2002 and in the first half of May 2003 with values of -24g of $CO_2/m^2/d$ and -28g of $CO_2/m^2/d$, respectively, whereas the maximum daily release in winter is 12g of $CO_2/m^2/d$ for both study years. Those values are consistent with data found on other grassland sites [e. g. *Saigusa et al.*, 1998; *Dugas et al.,* 1999; *Frank and Dugas*, 2001; *Sims and Bradford*, 2001].

6.3.2 Monthly flux

Examining the monthly uptake of CO_2 shown (Figure 6.11) and its values (Table 6.7), the seasonal trend is clear. The part of the year for which the site behaves as a sink of carbon is from March to September and period that it behaves as a source of carbon is from November to January. In February and October the ecosystem is close to equilibrium. If we convert those data in average daily uptake during a month, we obtain for May, which is the biggest month as a sink for both studied years, -11.7g of $CO_2/m^2/d$ (2002) and -13.1g of $CO_2/m^2/d$ (2003). December is the biggest month as a source in 2002 with average daily release of 6.5g of $CO_2/m^2/d$, while the month with biggest release in 2003 is November with 4.4g of $CO_2/m^2/d$.

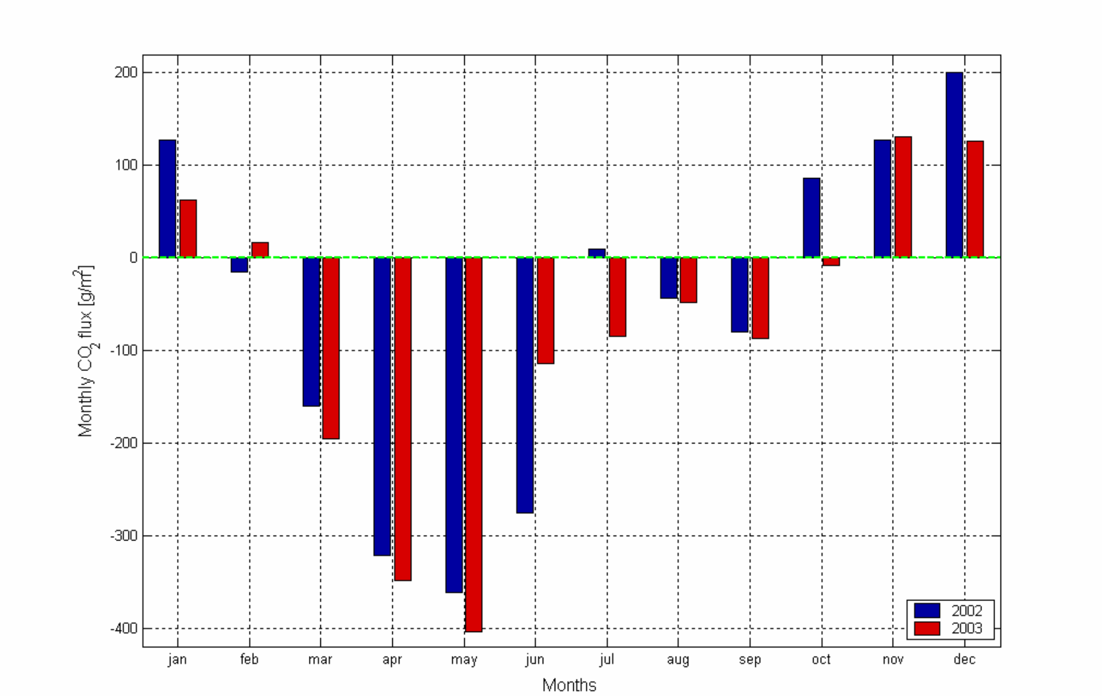

Figure 6.11: **Monthly CO_2 flux in g/m^2 for 2002 (blue) and 2003 (red)**

Table 6.7: **Monthly CO_2 flux in $[g/m^2]$ for 2002 and 2003**

$[g/m^2]$	jan	feb	mar	apr	may	jun	jul	aug	sep	oct	nov	dec
2002	128	-15	-160	-322	-362	-276	9	-44	-80	86	127	200
2003	63	17	-195	-348	-405	-114	-84	-48	-87	-8	131	126

Figures 6.12 – 6.15 show the mean daily courses of NEE with standard deviations month by month for both studied years. Plots on the left show 2002 data, and the ones on the right 2003 data.

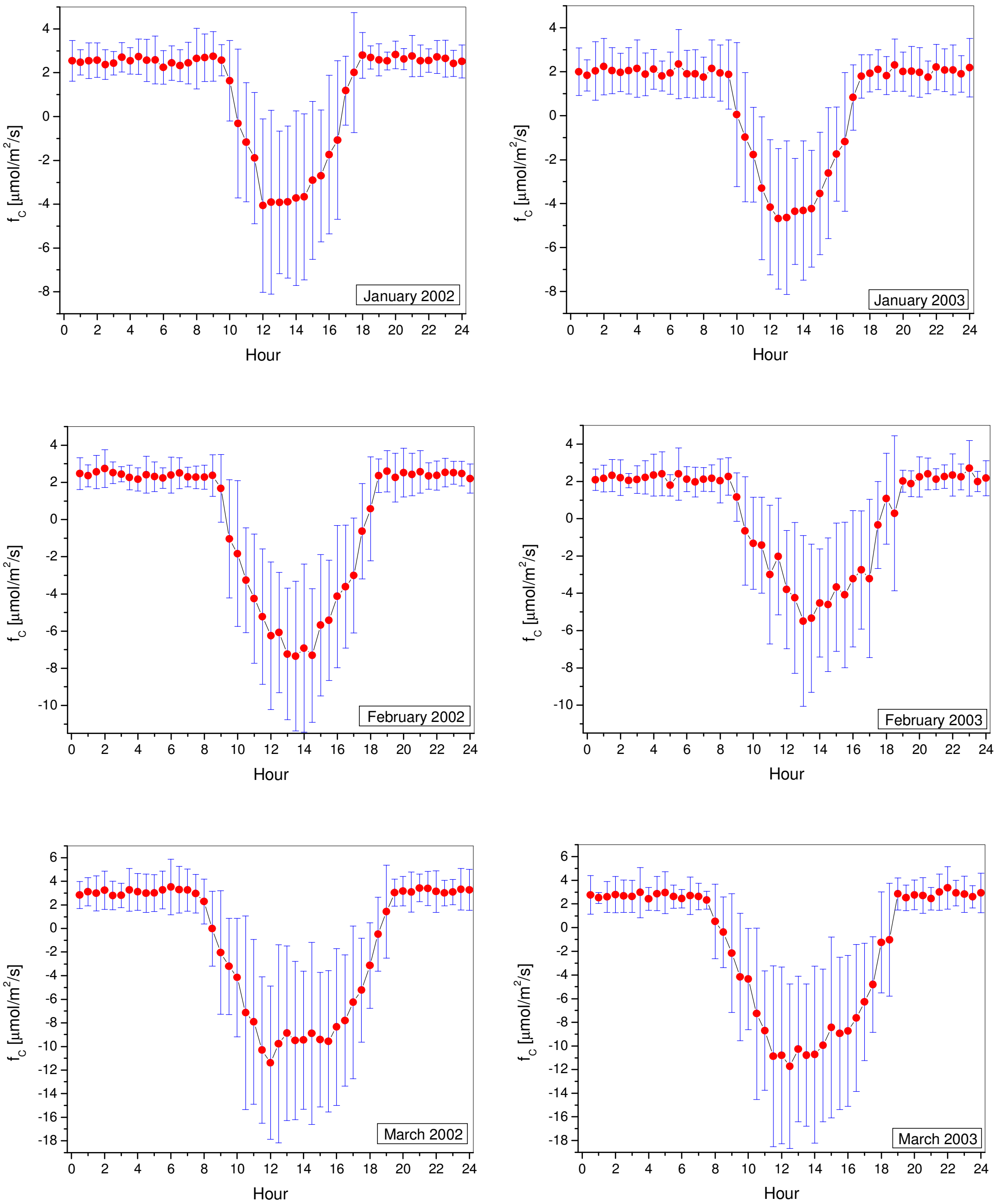

Figure 6.12: Mean daily courses of NEE with standard deviations for January, February and March for 2002 (left) and 2003 (right).

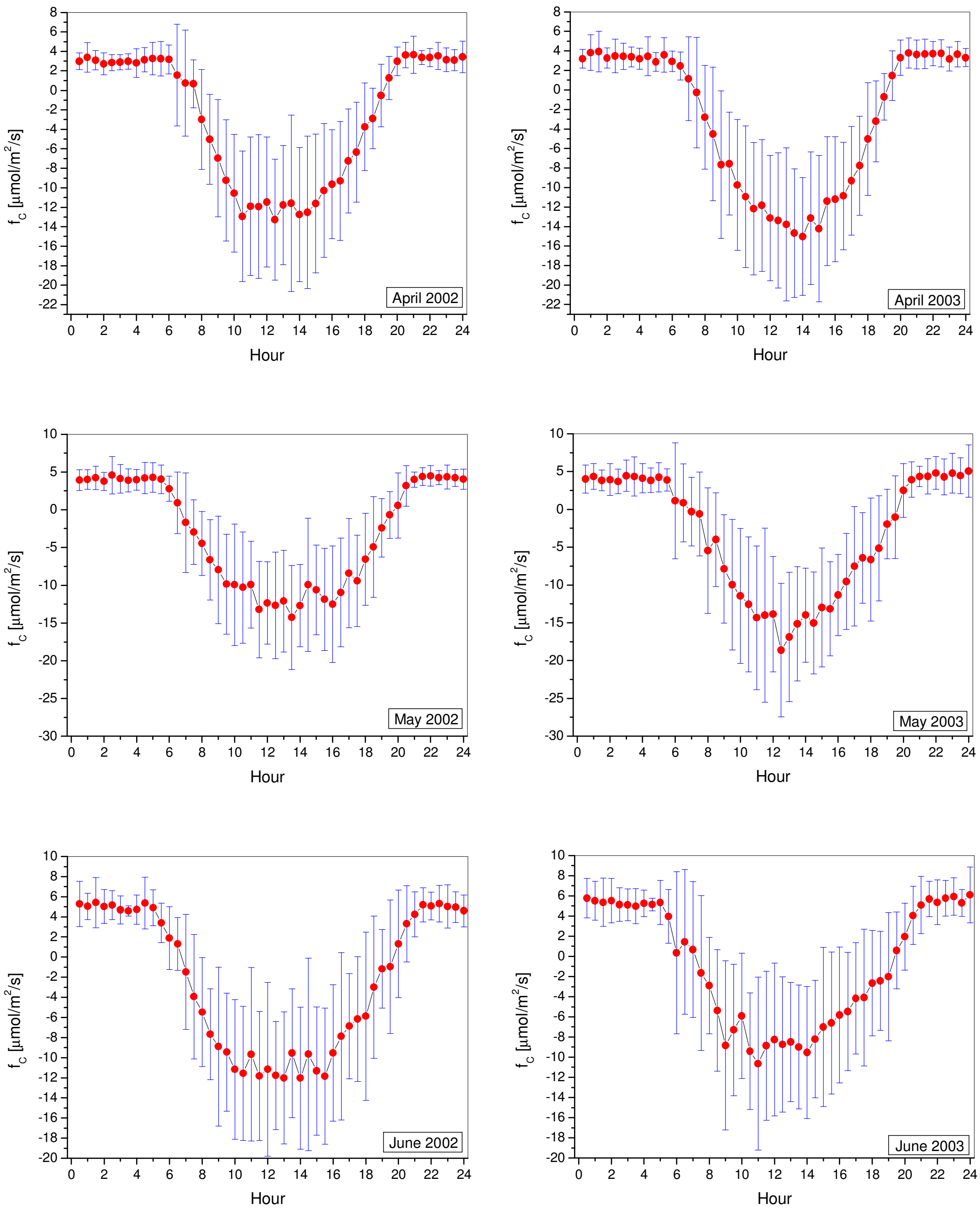

Figure 6.13: Mean daily courses of NEE with standard deviations for April, May and June for 2002 (left) and 2003 (right).

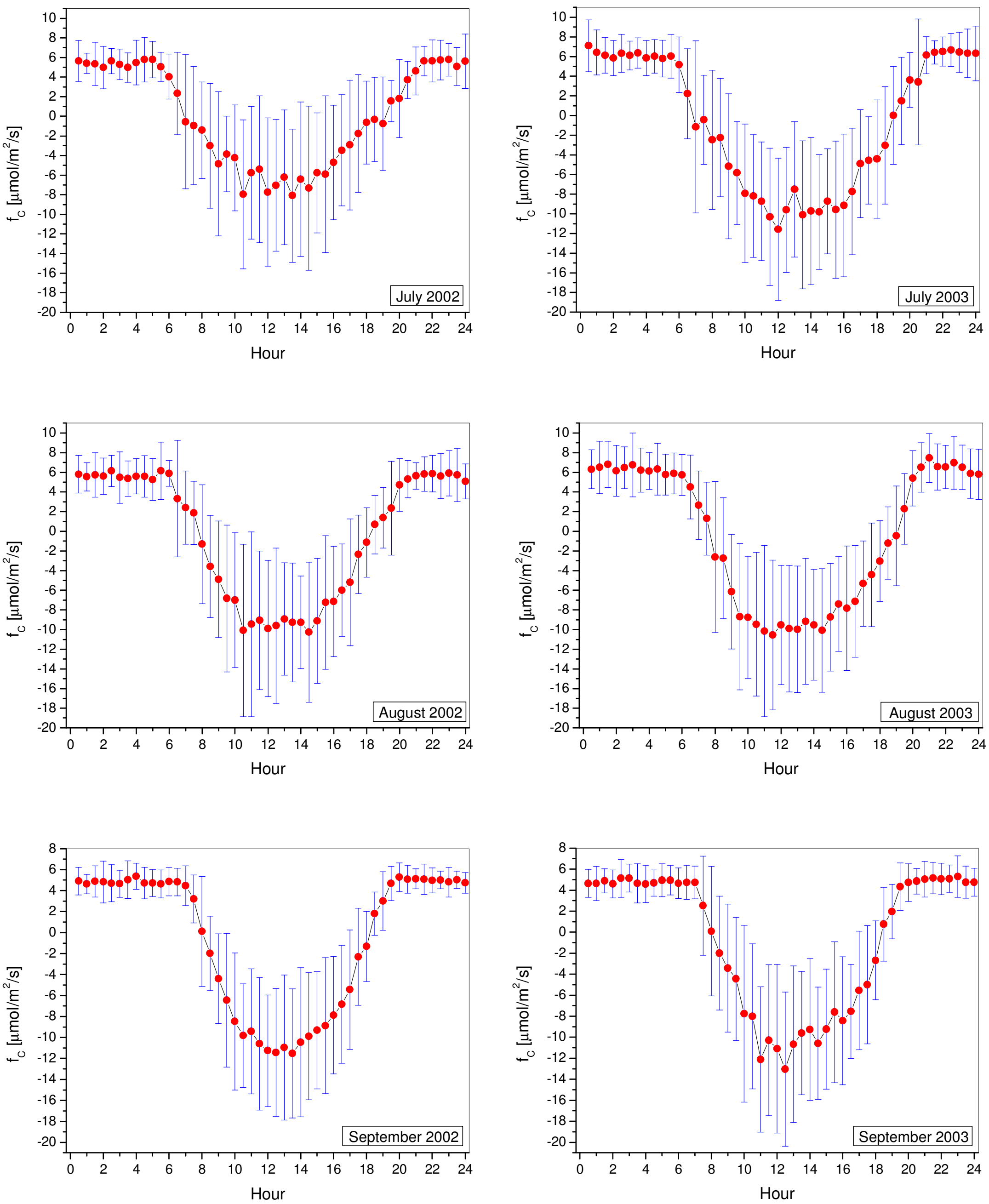

Figure 6.14: Mean daily courses of NEE with standard deviations for July, August and September for 2002 (left) and 2003 (right).

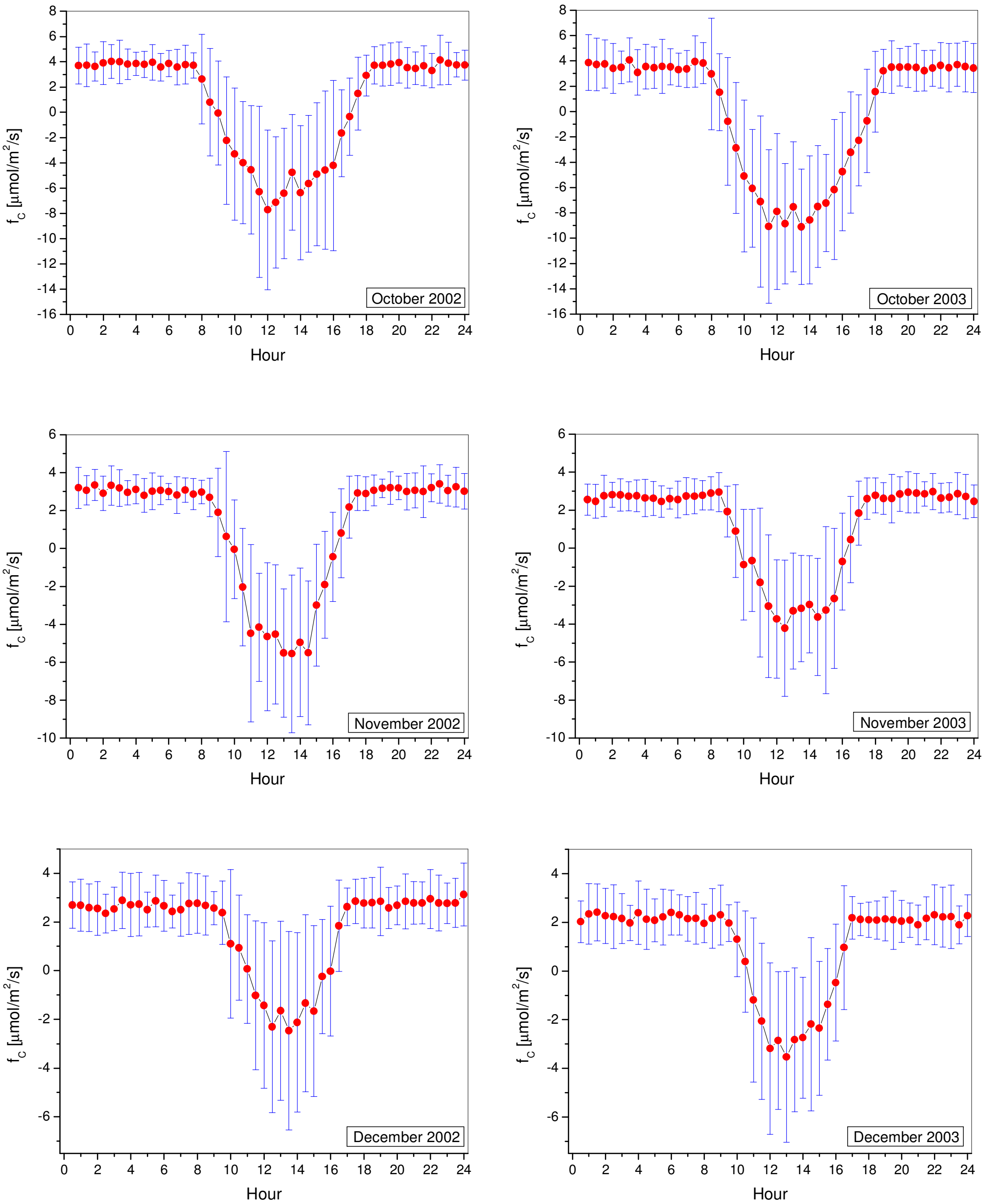

Figure 6.15: Mean daily courses of NEE with standard deviations for October, November and December for 2002 (left) and 2003 (right).

General observation is that the uptake of CO_2 is smaller during winter and autumn months and higher during spring and summer months. The variation in duration of the day during which there is a CO_2 uptake (i.e. photosynthesis process takes part) is clearly visible – it is the shortest during winter months and the longest during summer months. Variation of the flux between the days in the month is more pronounced for daytime than for nighttime.

Table (6.8) summarises some relevant parameters measured in 2002 and 2003 month by month.

Table 6.8: .Monthly precipitation, PAR, Ta (Ts), VPD, ET, PET, θ_{30}, LAI and f_{CO2} (f_c)

	Parameter	Jan	Feb	Mar	Apr	May	Jun	Jul	Aug	Sept	Oct	Nov	Dec	Sum
[mm]	02 Precip	254	231	73	137	178	99	48	73	45	244	255	150	1785
	03 Precip	95	71	106	143	128	140	91	15	56	46	192	102	1185
[W/m^2]	02 PAR	175	302	388	567	558	552	545	527	480	329	217	135	4805
	03 PAR	225	268	461	545	585	638	497	625	463	343	210	147	5007
[°C]	02 Ta (Ts)	8 (6)	7 (6)	7 (7)	8 (9)	10 (11)	11 (13)	14 (14)	15 (15)	13 (13)	10 (10)	8 (8)	6 (6)	
	03 Ta (Ts)	5 (5)	5 (5)	7 (7)	9 (9)	10 (10)	13 (13)	14 (14)	16 (15)	13 (13)	9 (10)	8 (8)	6 (6)	
[kPa]	02 VPD	0.05	-0.009	0.022	0.067	0.174	0.282	0.560	0.563	0.415	0.200	0.095	-0.019	
	03 VPD	-0.06	-0.09	0.022	0.104	0.179	0.389	0.540	0.635	0.434	0.170	0.087	-0.022	
[mm]	02 ET	6.6	18.0	25.8	46.3	55.8	60.1	51.1	49.0	32.7	17.3	7.7	1.7	370
	03 ET	8.3	12.8	23.9	39.5	64	65.2	50.7	47.9	30.2	13.4	7.0	4.8	366
[mm]	02 PET	9.2	18.3	27.6	46.5	55.7	62.4	66.5	59.7	40.6	20.6	10.4	5.1	422.6
	03 PET	8.8	14	31.6	46.9	65	75.1	64.8	75.3	42.6	22.2	9.1	4.8	455.2
[mm/mm]	02 θ_{30}	0.445	0.449	0.429	0.416	0.422	0.407	0.342	0.338	0.266	0.370	0.435	0.429	
	03 θ_{30}	0.426	0.426	0.400	0.380	0.409	0.336	0.282	0.238	0.227	0.233	0.359	0.380	
	02 LAI						-------	Cut 1st		Cut 30th	No grazing	No grazing	No grazing	
	03 LAI						Cut 15th	----------		Cut 15th	grazing	grazing	grazing	
[g/m^2]	02 fco_2	+128	-15	-160	-322	-362	-276	+9	-44	-80	+86	+127	+200	-709
	02 (fc)	(34.9)	(-4.1)	(-43.6)	(-87.7)	(-98.6)	(-75.2)	(2.5)	(-12)	(-21.7)	(23.5)	(34.6)	(54.6)	(-192.8)
	03 fco_2	+63	+17	-195	-348	-405	-114	-84	-48	-87	-8	+131	+126	-952
	02 (fc)	(17.1)	(4.6)	(-53.2)	(-95.0)	(-110.4)	(-31.1)	(-22.9)	(-13.1)	(-23.8)	(-2.2)	(35.8)	(34.4)	(-259.8)

The monthly magnitude of NEE varies between corresponding months in the two years. The net release of CO_2 in January 2002 of 128g/m^2 compares to 63 g/m^2 in January 2003. The reason for a difference is higher air temperature in winter of 2002 that can be driving force for greater efflux.

The net uptake of CO_2 in May 2002 of -362g/m^2 compares to -405g/m^2 in May 2003. The difference can be explained with more available photosynthetic flux during this month in 2003 (according to higher precipitation during May 2002 it is expected that cloudiness was reason for that) and air temperature in 2003 was higher.

The net uptake of CO_2 in June 2002 of -276g/m^2 compares to -114g/m^2 in June 2003.

The reasons for the differences in NEE in June was twofold: one was, that part of the grassland in the footprint was cut (harvested to within 5cm of the soil) in June 2003; and secondly, the last two weeks of June 2003 were dry and the soil moisture consequently dropped from 0.6m^3/m^3 to 0.2m^3/m^3 whereas in June 2002 there was no cutting and the rainfall was spread over the entire month keeping the soil moisture at near saturation (see section4.3). Similar reasons explain why in July 2002 there was a very small net respiration and in July 2003 a net uptake. July was dry in 2002 and cutting was performed (enabled in the dry fields), while the grass that was cut in June 2003 was then emerging growth (approximately 0.2m in height) in July 2003. It has been shown [*Frank and Dugas*, 2001] that short-term droughts during the growing season reduce CO_2 fluxes to near zero (photosynthesis balances respiration). Also, the timing and magnitude of precipitation events influence the total growing season flux and induce a considerable day-to-day variability in CO_2 fluxes. Decreases in LAI (Leaf Area Index) caused by the grass (silage) harvesting, reduce gross primary productivity (GPP) [*Budyko*, 1974].

The NEE (uptake) in August and September 2002 was the same as August and September 2003.

The sum of the NEE for the eight months (February to September) was –1247g.CO_2/m^2 (-340 g.C/m^2) for 2002 and –1265g.CO_2/m^2 (-345 g.C/m^2) for 2003. The difference in NEE between the years was in the winter months (October to January) with 2002 having an NEE of +543 g.CO_2/m^2 (+148 g.C/m^2) and 2003 with an NEE of +312 g.CO_2/m^2 (+ 85 g.C/m^2). The rainfall in these four months was 903mm in 2002 and 435mm in 2003. The rainfall of 2002 caused the soil moisture status to be more frequently saturated than in 2003. This resulted in a wetter soil environment that respired more. In addition, in the drier year (2003), cattle grazed the fields (during the daytime) during the parts of the months of October to January. By contrast, in the wet winter (2002) cattle did not graze the fields because to do so, they would have damaged the soil surface to an unacceptable level. So in the winter of 2002, there was a greater standing biomass (than in 2003), which enhanced the respiration. This suggests that the wetter winter of 2002 with its saturating effect on soil moisture, it’s higher standing biomass and enhanced ecosystem respiration was responsible for the lower NEE of 2002.

6.3.3 Annual flux

The cumulative NEE, expressed in Tonnes of carbon per hectare (TC/ha) for both years is shown in Figure 6.16. The NEE for 2002 was -1.9TC/ha while for 2003 it was -2.6 TC/ha. The cumulative uptake to From January 1 to June 27, 2002 was -2.7T.C. The cumulative uptake from January 1 to June 15, 2003 was also -2.7TC/ha. The uptake period, which continued longer by two weeks in 2002, was due to the delay in cutting (because of wet weather).

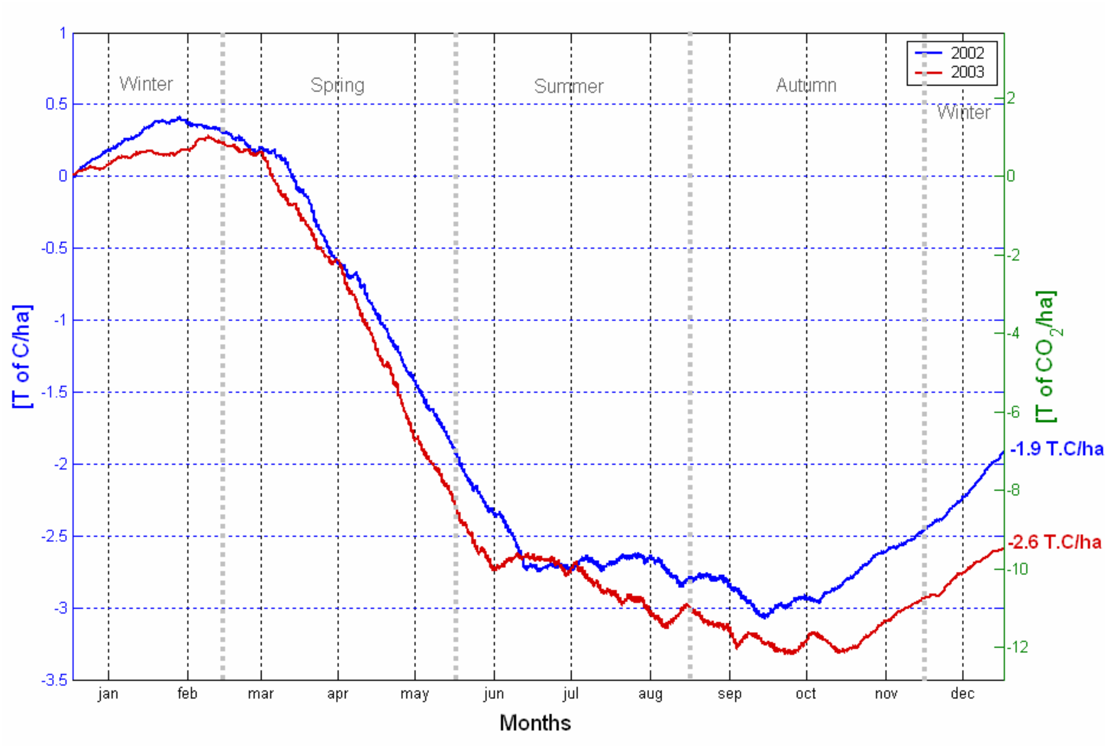

Figure 6.16: Cumulative uptake of carbon (C) and carbon dioxide (CO_2) in T/ha for 2002 (blue) and 2003 (red). The NEE for 2002 was -1.9TC/ha and for 2003 was -2.6TC/ha.

In Figure 6.17 we show the cumulative NEE for both years, for the months October, November, December and January. The NEE for these four months was +1.5 T.C./ha (respiration) for 2002 and +0.8 T.C/ha for 2003. The difference in the NEE between the two years was differences in these four winter months. Precipitation leading to near saturation soil moisture (as in 2002 but not in 2003), enhances the release of C, because of its effect on soil aeration and CO_2 transport within the soil profile [*Suyker, et al*., 2003].

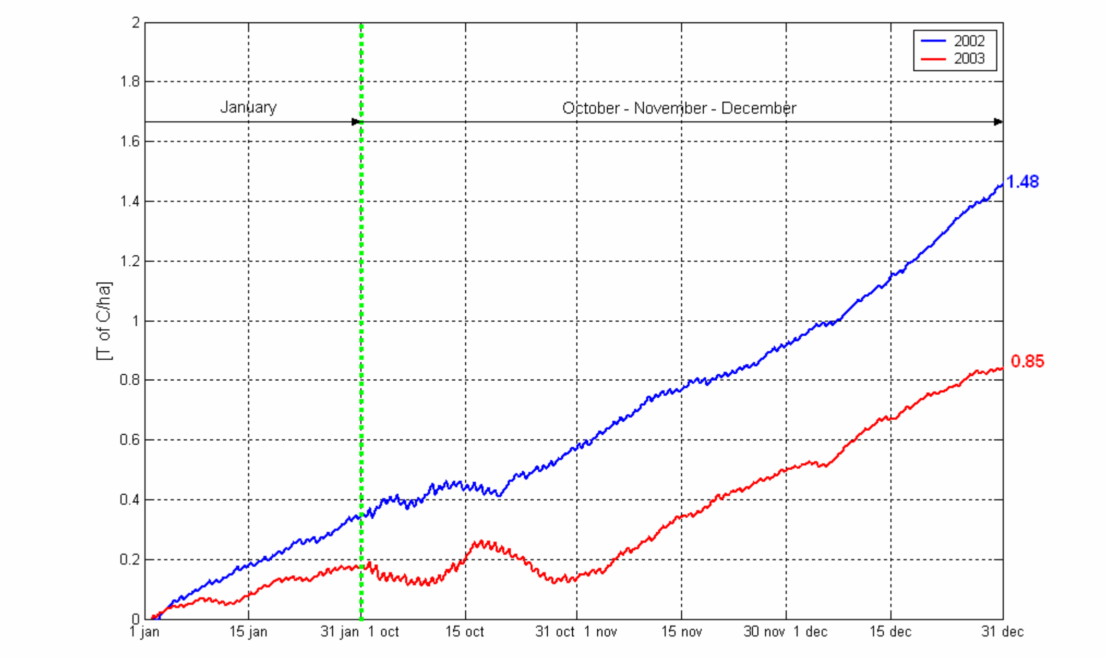

Figure 6.17: Cumulative uptake of carbon for the winter months (October, November, December and January) in T.C/ha for 2002 (blue) and 2003 (red).

6.3.4 Carbon balance

Carbon sequestration reflects the difference between two larger fluxes, respiratory efflux during the night and photosynthetic uptake during the day [*Lafleur et al.*, 2001]. Gross Primary Production (GPP) refers to the total amount of carbon (above ground and below ground) fixed in the process of photosynthesis by plants [*Kirschbaum et al.*, 2001].

In order to find out the range of GPP for 2002 and 2003 at Dripsey site we modelled respiration during the day. Here we define R as Ecosystem Respiration (autotrophic and heterotrophic) obtained from measured NEE during the nighttime (see Tables 6.4 and 6.5) and estimated for daytime using the equations:

$$F_{ni}^{2002} = 1.476 \times e^{(0.095 \times tsoil)} \qquad \text{for 2002} \tag{6.7}$$

$$F_{ni}^{2003} = 1.109 \times e^{(0.1221 \times tsoil)} \qquad \text{for 2003} \tag{6.8}$$

Using the NEE and modelled respiration GPP was calculated [*Kirschbaum et al.*, 2001]:

$$GPP = NEE + R \tag{6.9}$$

where GPP is Gross Primary Production, NEE is Net Ecosystem Exchange and R is ecosystem respiration (autotrophic and heterotrophic together).

Figure 6.18 shows cumulative NEE, R and GPP. Respiration (R) is 14.8T of C/ha and 14.6 T of C/ha for 2002 and 2003 respectively, hence difference in respiration between these two years is negligible (0.2T of C/ha/year). Gross primary production is 16.7T of C and 17.2T of C for 2002 and 2003 respectively which is in agreement with what was found by other researchers [e. g. *Kirschbaum et al*., 2001].

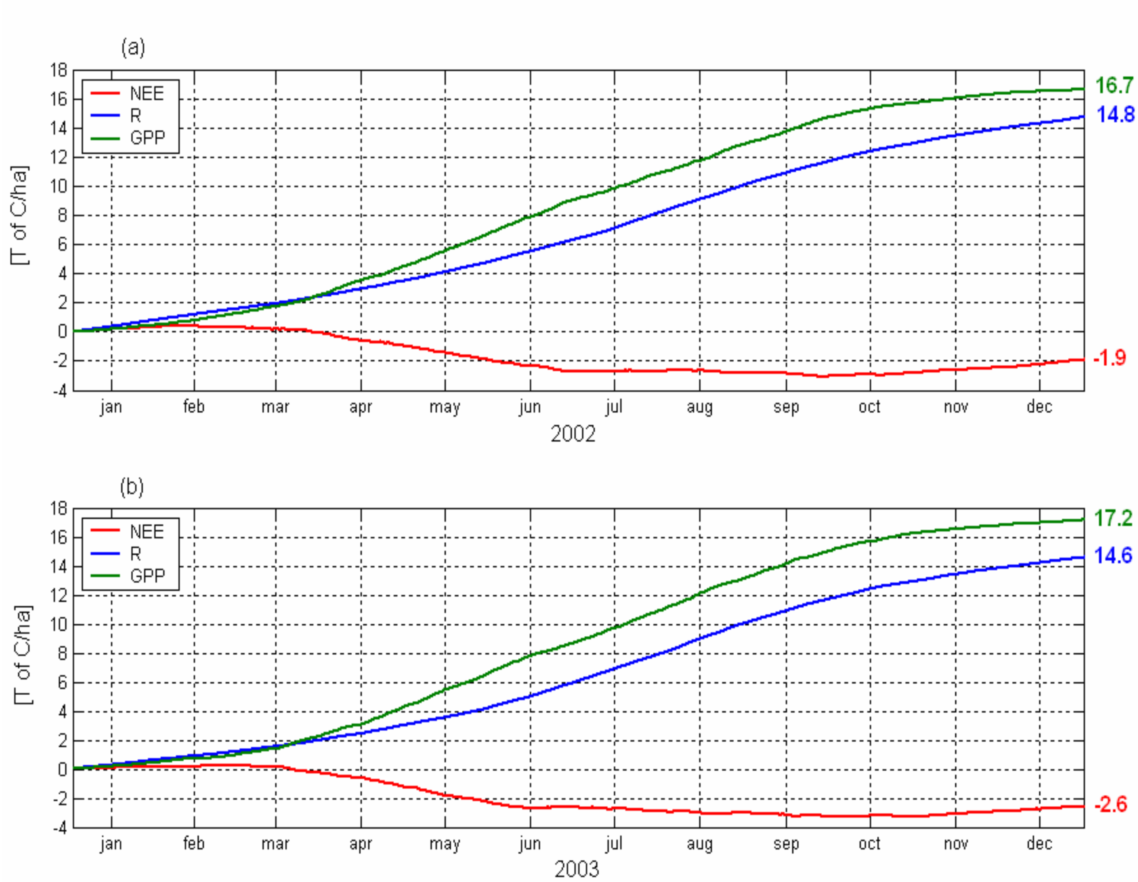

Figure 6.18: **Cumulative NEE (red), R (blue) and GPP (green) in T of C/ha: (a) for 2002 and (b) for 2003.**

Chapter 7

Modelling

Chapter 7 Modelling

7.1 Introduction

There are models that can then describe the main plant mechanisms involved in the CO_2 budget and their interactions; these models can be adjusted to fit each specific environment. On the other hand, they constitute a basis to compare and adjust variables in order to describe the observations and processes. With all the climatic issues at present, proper predictions are needed of the effect on an ecosystem of changes due to CO_2 increasing concentration, or any other variable (precipitation, air temperatures….).

In this study, modelling tools will be discussed in an effort to fit as well as possible the CO_2 fluxes during the year.

A wide range of models is nowadays available to estimate the exchange between leaves and the atmosphere in terms of CO_2. Biochemical models as proposed by Farquhar *et al.* [1980] consider the full biochemical components of photosynthetic carbon assimilation in plants and therefore require a large number of physiological parameters that are not trivial to determine for a wide variety of species and sites. On the opposite, empirical models for the stomata conductance calculation introduced by Jarvis [1976] require few parameters but ignore well-known mechanisms. Models proposed by Collatz *et al* [1991] and Jacobs [1994] are semi-empirical models combining the two approaches. Thus, they require relatively few parameters and retain the mechanisms of assimilation. After a brief presentation of the plant physiological background, those two models will be presented and applied to seasonal variation of CO_2 fluxes in our study.

7.1.1 Global processes

Photosynthesis

The photosynthesis of green plants is a highly complicated set of interactive reactions in which the energy of light is trapped and used to convert CO_2 into carbohydrates ($(CH_2O)_n$). Two groups of reactions can be distinguished: the light reactions and the dark reactions.

In the light reactions, solar energy is trapped and stored into carriers of chemical energy. Only the light in the visible wavelength range (400 nm to 700 nm) is utilized. Solar radiations in this part of the spectrum may be referred to as Photosynthetically active radiations (PAR).

During the dark reactions, the light trapped in the light reactions is converted from CO_2 to carbohydrates. The most important pathway of the dark reaction is the so-called Calvin cycle. The first step in this chain of reactions is the fixation of CO_2, which is catalysed by the enzyme rubilose 1,5 bi-phosphate carboxylase oxygenase, Rubisco [*Campbell and Norman*, 1998]. The subsequent steps result in the formation of the required carbohydrate products. The complete set of light reactions can be described by a general reaction:

$$CO_2 + H_2O + light_{PAR} \rightarrow CH_2O + O_2 \tag{7.1}$$

The ratio of the number of fixed CO_2 molecules (or O_2 produced) to the amount of photons used is called the quantum efficiency. The quantum efficiency near zero light intensity (the initial quantum use efficiency ε) is an important parameter in photosynthesis models because it determines the initial slope of the light response curve.

During photosynthesis, CO_2 passes trough the intercellular spaces and enters the chloroplasts in the leaf mesophyll cells (Figure 7.1) where the carboxylation (transformation into an organic carbon product) occurs.

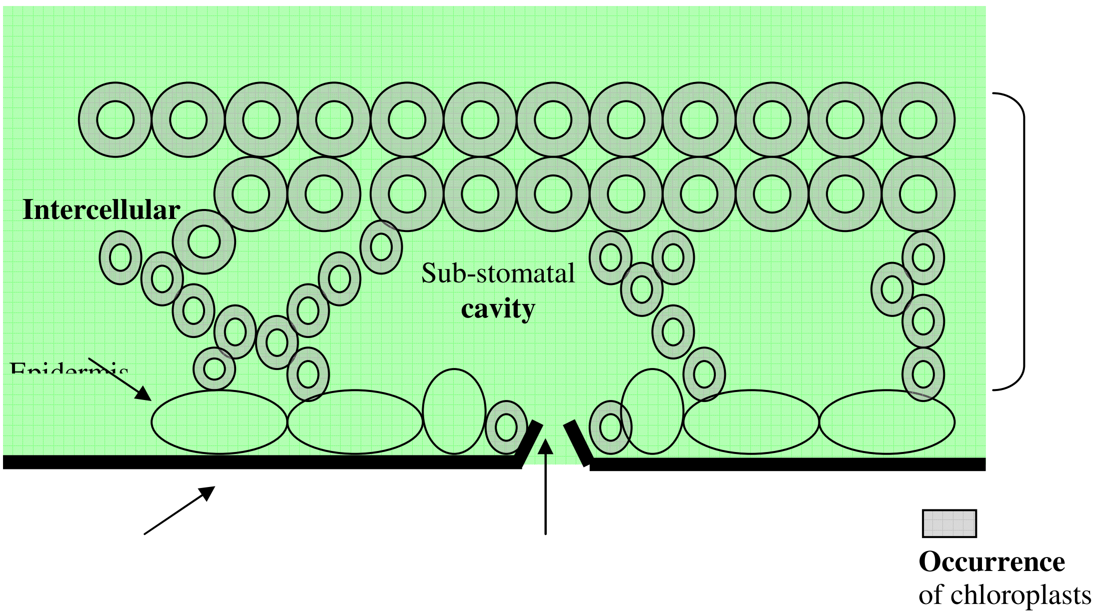

Figure 7.1: Structure of a leaf from Jacobs [1994]

Dark respiration

The fixed carbon is used as an energy source for plant processes and as a material to build structural dry matter. All these processes result in the release of CO_2. They are considered together under the name of dark respiration, because it takes place in the dark. There are indications that dark respiration in leaves is suppressed by light [*Graham*, 1979]. The equation is the counter reaction of photosynthesis.

Photorespiration

Because the carbon fixing enzyme of the Calvin cycle, Rubisco, is not only a carboxylase but also an oxidase, CO_2 and O_2 compete for the same active site of Rubisco. Therefore, photosynthesis will be inhibited in the presence of O_2. At the same time the oxidase activity of Rubisco will trigger a process that depends on the availability of light and ultimately results in the release of previously fixed CO_2. This process is called photorespiration. C_3 plants may loose up to 50 % of the newly fixed CO_2 by photorespiration. No clear function has been identified yet for this mechanism so that it is often considered as a waste of energy.

Soil respiration

This release of CO_2 corresponds to the plant root respiration and decomposition of organic matter by micro-organisms.

Plant categories

In our case, the metabolic pathway for carbon fixation is assumed to be a C_3 Cycle (see section 1.1.5).

Stomata

Stomata is a small opening on leaf surface through which plant communicate with environment. The full mechanisms which control stomata aperture remain unknown. However, it has been demonstrated that the stomata are sensitive to the intercellular concentration of CO_2, C_i, (and not to the concentration outside the leaf or inside stomatal pores) and is influenced by light, leaf temperature, air humidity and soil water content as well [*Campbell and Norman*, 1998]. Generally, stomata close in the darkness and open if exposed to light. Higher temperatures increase the speed of stomatal movements and the final aperture. Moreover, stomata tend to close if the vapour pressure deficit of the surrounding air increases, and in response to the drying of soil. In the latter case, closure starts only if the soil water potential drops down to rather low values.

7.1.2 Terminology

Regarding the CO_2 budget, fluxes have to be described separately for the plant and the ecosystem. Let P_p be the plant photosynthetic flux, R_p the plant respiration and R_s the soil respiration. Then R_e, the ecosystem respiration is defined as $R_e = R_s + R_p$. The net primary productivity (NPP) for the plant is the quantity of CO_2 absorbed when all processes have been taken into accounts:

$$NPP = P_p - R_p \tag{7.2}$$

At the scale of the whole ecosystem, the soil respiration must be added for the net ecosystem productivity (NEP):

$$NEP = NPP - R_s = P_p - R_p - R_s = P_p - R_e \tag{7.3}$$

The NPP for each part of the plant depends on the efficiency of growth.

At the leaf level, the net assimilation, A_n, is balanced between the amount of carbon fixed by photosynthesis (the gross assimilation rate A_g) and the losses due to the dark respiration R_d:

$$A_n = A_g - R_d \tag{7.4}$$

The compensation point, Γ, is defined as the CO_2 concentration at which no assimilation occurs [*Farquhar*, 1980]. In the absence of 'dark respiration', that means at light time, Γ increases linearly with the oxygen concentration in air (210000 µmol/mol), so that the light compensation point Γ^* can be written:

$$\Gamma^* = \frac{C_{oa}}{2\tau} \tag{7.5}$$

where C_{oa} is the oxygen concentration in the air and τ is the ratio describing the partitioning between carboxylase and oxygenase reactions of Rubisco.

The common way of expressing the total leaf area in a forest canopy or any other vegetation type is to use the leaf area index (LAI). It is the leaf surface per square meter ground surface. It is expressed in m^2/m^2 and allows the scaling up of leaf processes to a whole canopy.

Senescence is a productive form of aging leading to plant death. Plants age productively; as tissues senesce they produce enzymes necessary to recycle "expensive" materials and reroute the subunits to areas for use by active growth elsewhere, in the next season, or by the next generation. This process is responsible for the decrease in LAI in autumn.

7.2 Models presentation

7.2.1 Collatz's Model

Leaf-level assimilation model

According to Farquhar et al. [1980], and later modified by Collatz et al. [1991] and Campbell and Norman [1998], the gross photosynthetic rate at the leaf scale depends on light, CO_2 concentration, and leaf temperature. The light-limited assimilation can be computed from:

$$J_e = \frac{\alpha_{PAR} \times e_m \times Q_p \times \left(C_i - \Gamma^*\right)}{C_i + 2\Gamma^*} \tag{7.6}$$

where α_{PAR} is the leaf absorptivity for PAR, e_m is the maximum quantum efficiency for leaf CO_2 uptake (maximum number of CO_2 molecules fixed per quantum of radiation absorbed), Q_p is the PAR photon flux density incident on the leaf (μmol/m^2/s), C_i is the intercellular CO_2 concentration (see equation 7.15), and Γ^* is the light compensation point.

The Rubisco-limited assimilation rate is:

$$J_c = \frac{V_m \times \left(C_i - \Gamma^*\right)}{C_i + K_c \times \left(1 + \dfrac{C_{oa}}{K_o}\right)} \tag{7.7}$$

where V_m is the maximum Rubisco capacity per unit leaf area [μmol/m^2/s], K_c is the Michaelis constant for CO_2 fixation, and K_o is the Michaelis constant for oxygen inhibition.

Finally, the last rate is controlled by the export and use of products of photosynthesis. When sucrose builds up, the photosynthesis slows. It is considered as the most likely rate-limiting step. The sucrose-limited assimilation is assumed, by Collatz *et al.* [1991] to be just:

$$J_s = \frac{V_m}{2} \tag{7.8}$$

The gross assimilation rate then is the minimum of those limiting-rates:

$$A_g = \min[J_e, J_c, J_s] \qquad (7.9)$$

The net assimilation A_n is deduced from equation (7.9) minus the dark respiration.

$$A_n = A_g - R_d \qquad (7.10)$$

Temperature response

The dark respiration and some other parameters of the model need a temperature adjustment. Temperature dependence of kinetic variables is computed following the equation in Campbell and Norman [1998]. For K_c, K_o and τ the temperature dependence is an exponential relationship normalized with respect to 25°C (equation 7.11) whereas, for V_m and R_d, a high temperature cut-off is needed (equations 7.12 and 7.13).

$$X(T) = X(@\,25)e^{q\times(T-25)} \qquad (7.11)$$

where q is the temperature coefficient for the parameter X and X(@25) is its value at 25°C.

$$V_m = \frac{V_{m,25} \times e^{0.088\times(T-25)}}{1+e^{0.29\times(T-41)}} \qquad (7.12)$$

$$R_d = \frac{R_{d,25} \times e^{0.069\times(T-25)}}{1+e^{1.3\times(T-55)}} \qquad (7.13)$$

where $V_{m,25}$ and $R_{d,25}$ are values of V_m and R_d at 25°C, respectively [*Campbell and Norman*, 1998].

Stomatal conductance

The stomatal conductance is deduced using the empirical formula from Ball *et al.* [1987] when the net assimilation is known:

$$g_s = \frac{m \times A_n \times h_s}{C_s} + b_{gs} \qquad (7.14)$$

where m and b_{gs} are constants, h_s is the humidity at leaf surface (which is assumed to be air humidity) and C_s is the CO_2 concentration at leaf surface.

The third equation needed to solve the C_i/ A_n/ g_s system is the Fick's Law of diffusion applied to CO_2.

$$C_i = C_s - \frac{A_n}{g_s} \tag{7.15}$$

It has been assumed here that C_s is equal to the atmospheric CO_2 concentration C_a (380 ppm).

Equations (7.9), (7.14) and (7.15) constitute the core of the model as the description of interactions between the internal concentration of CO_2, the net assimilation and the stomatal conductance. Being interdependent, they need to be solved simultaneously.

In the light of those equations, this model has few inputs (PAR radiation, air temperature, and air humidity) but about fifteen parameters depending on the plant type. The full list of values chosen in our case is given in Appendix 5. However, considering the works done by Collatz *et al.* [1991], Ball *et al.* [1987] and Farquhar *et al.* [1980] as for C_3 grass, only few of those parameters have been estimated for the Dripsey site [*Le Bris*, 2002].

7.2.2 Jacobs or A-g_s Model

Based on the empirical model from Jarvis [1976] for the stomatal conductance, the A-g_s model uses the model from Goudriaan *et al.* [1985] to describe the photosynthesis part. Goudriaan's model describes most of the essential characteristics of photosynthesis. It is less detailed than Farquar's model and therefore needs less inputs parameters. This model is often linked to meteorological research [*Calvet et al.*, 1998; *Calvet et al.*, 2001].

A correct model for stomatal behaviour must be able to include the effect of short-term variations (light, temperature) as well as long-term changes (increase of atmospheric CO_2). The effects of those factors are combined, since it is known for instance that an increase of atmospheric CO_2 increases the plant sensitivity to light and temperature and possibly to other factors too [*Meidner and Mansfield*, 1968]. However, Jarvis's model, frequently used in meteorological research, does not take into account synergistic effects between different stimuli. The alternative used in A-g_s is based on the observed correlation between the photosynthetic rate A, and the stomatal conductance. At the cost of increased complexity, the responses to CO_2 are described including interactions between stimuli. Moreover, this model may be expected to be more generally applicable since it relies more on the nature of plants and less on statistics.

In Goudriaan *et al.* [1985] the photosynthetic rate does not only depend on the biochemical processes of photosynthesis. The diffusion process which controls the transport of CO_2 from the atmosphere to the carboxylation sites inside the leaf, sets a physical limit to the photosynthetic rate and is controlled by many conductances. Some of these conductances are physical in nature. Others are related to chemical processes and are called 'conductance' to allow a convenient comparison of limitations imposed by chemical and physical processes. See figure 7.1 for location of conductances described here:

- The stomatal conductance (g_{sc} for CO_2 and g_s for vapour water) describes the diffusion through stomata pores. The difference in diffusivity has to be accounted for so that $g_s = 1.6 \times g_{sc}$.

- The cuticular conductance describes the diffusion of water and CO_2 through the waxy cuticle. For convenience, g_c is usually assumed to be the same for water and CO_2. The total conductance through epidermis (see Figure 7.1) can be calculated as $g_{epidermis} = g_s + g_c$ for water and with g_{sc} instead of g_s for CO_2. When stomata are widely open $g_c \ll g_s$, whereas g_c may become larger than g_s when they are closed.

- The mesophyll conductance (g_m), describes the transport of CO_2 between the sub-stomatal cavity and the site of carboxylation. g_m includes a variety of conductances from physical or chemical processes. Since the values of those latter are not known for certain, g_m is treated as one residual resistance.

Assimilation

The modelling approach of A-g_s directly relies on conductances to describe the diffusion of CO_2 between the air and chloroplasts. It is based on the distinction between two different conditions:

- the light-limiting factor.
- the CO_2 limiting factor.

If light is the limiting factor, A_n can be written as:

$$A_n = \varepsilon \times I_a - R_d \tag{7.16}$$

where I_a is the amount of absorbed PAR radiation, R_d is the dark respiration and ε is the initial quantum use efficiency. The ε quantifies the slope of the light response curve and is affected by photorespiration. It can be calculated as [*Goudriaan et al.*, 1985]:

$$\varepsilon = \varepsilon_0 \times \frac{C_i - \Gamma}{C_i + 2\Gamma} \tag{7.17}$$

Γ is the compensation point [ppm], C_i is the internal concentration of CO_2 and ε_o is the maximum quantum use efficiency based on the theoretical efficiency of the Calvin cycle. Equation (7.17) is derived from biochemical considerations and is similar to the result obtained by Farquhar [1980].

In case that CO_2 is the only limiting factor, the photosynthetic rate at light saturation, A_m, is linearly related to the CO_2 concentration.

$$A_m = 0.001 \times g_m \times (C_i - \Gamma) \times \varphi_c \tag{7.18}$$

Putting together equations (7.16) and (7.18), the final expression for A_n including both the effect of limited light and CO_2 is:

$$A_n = (A_m + R_d) \times \left(1 - e^{\frac{-\varepsilon \times I_a}{A_m + R_d}}\right) - R_d \tag{7.19}$$

Here, the respiration rate R_d is simply defined as $R_d = \dfrac{A_m}{9}$. (7.20)

In order to bound the photosynthetic rate at high light intensities and high CO_2 concentrations, A_m must be limited to a maximum value $A_{m,max}$. A smooth transition between equation (7.18) and $A_{m,max}$ is provided with:

$$A_m = A_{m,\max} \times \left(1 - e^{\frac{-0.001 \times g_m \times (C_i - \Gamma) \times \varphi_c}{A_{m,\max}}}\right) \tag{7.20}$$

A_n and A_m are calculated here in [mg/m^2/s], g_m is in [mm/s] and the concentrations are in ppm [µmo/mol]. φ_c is a conversion factor transforming ppm to [mg/m^3].

$$\varphi_c = \frac{M_{CO2} \times \rho_{a,v}}{M_a} \tag{7.21}$$

where M_{CO2} and M_a are the molecular masses of CO_2 and air (44 and 28.9 g/mol respectively), and ρ_a is the density of air calculated thanks to the vapour content

$$\rho_{a,v} = \frac{P}{R_a \times T \times \left(1 + \left(\frac{R_v}{R_a} - 1\right) \times \frac{q}{1000}\right)} \tag{7.22}$$

where R_v and R_a are the gas constants for air and vapour pressure, P is the air pressure in Pa, T is the air temperature [K] and q is the specific air humidity [kg/kg].

Temperature response

As for Collatz *et al.* [1991], the temperature dependence of photosynthesis is accounted for through the temperature dependence of several parameters. The response of those parameters is based on a Q_{10} function, which is a proportional increase of a parameter for a 10°C increase in temperature [*Berry and Raison*, 1982]. For Γ, the equation (7.23) is used, whereas for g_m and $A_{m,max}$ the function is modified using an inhibition expression (equation (7.24)).

$$X(T) = X(@\,25) \times Q_{10}^{\frac{T-25}{10}} \tag{7.23}$$

X(T) is the value of any variable X at temperature T, with a reference value X(@25) at 25°C.

$$X(T) = \frac{X(@\,25) \times Q_{10}^{\frac{T-25}{10}}}{\left(1+e^{0.3(T_1-T)}\right) \times \left(1+e^{0.3(T_2-T)}\right)} \tag{7.24}$$

T_1 and T_2 denote reference temperatures, which can be adjusted to mimic species-specific features.

The reference values have been adapted from Jacobs [1994] and Bruse [2001]. The calibration process was done by Le Bris [2002] and the full list of parameters can be found in Appendix 5.

Stomatal conductance

The effect of humidity on the stomatal response and internal CO_2 concentration is parameterised using a factor f defined as:

$$f = f_0 \times \left(1 - \frac{D_s}{D_{\max}}\right) + f_{\min} \times \left(\frac{D_s}{D_{\max}}\right) \tag{7.25}$$

D_s is the vapour pressure deficit of air at the plant surface [g/kg] and D_{max} is its maximum value. The f_o is the value of f for D_s = 0 g/kg, and is around 0.85 for C_3 plants. The minimum f_{min} is calculated from equation (7.26).

$$f_{\min} = \frac{g_c}{g_c + g_m} \tag{7.26}$$

where g_c is the cuticular conductance and g_m is the mesophyll conductance.

The internal CO_2 concentration, C_i, is then obtained from f, and the value of CO_2 concentration at leaf surface:

$$C_i = f \times C_s + (1-f) \times \Gamma \tag{7.27}$$

Considering A_g the gross assimilation rate defined in equation (7.4) and $A_{m,g}$ the gross assimilation at light saturation, the stomatal conductance g_{sc} [m/s] of the leaf for CO_2 transfer can be calculated as

$$g_{sc} = \frac{A_n - A_{\min} \times \dfrac{D_s \times A_g}{D_{\max} \times A_{mg}} + R_d \times \left(1 - \dfrac{A_g}{A_{mg}}\right)}{(C_s - C_i) \times \varphi_c} \tag{7.28}$$

where A_{min} is the value of A_m for $C_i = C_{min}$ in equation (7.18) and C_{min} is given as:

$$C_{\min} = \frac{g_s \times C_s + g_m \times \Gamma}{g_c + g_m} \tag{7.29}$$

The total leaf stomatal conductance for vapour, including the cuticular conductivity can then be deduced from equation (7.30).

$$g_s = 1.6 \times 1000 \times g_{sc} + g_c \tag{7.30}$$

This model is closely linked up with micrometeorological research practice. The description remains simple, but effective in its simulation of most of the well-known features of photosynthesis. As well as for Collatz's model, few inputs are needed: PAR radiation, air temperature, air humidity, and atmospheric pressure. However, fewer parameters related to the plant type are needed for Jacobs's than for Collatz's model.

The full list of values chosen in our case is given in Appendix 5.

7.3 Parameters

The two sets of equations in the previous section (from equation (7.6) to equation (7.15) and from (7.16) to (7.30)) model photosynthesis processes at leaf scale. In order to find the parameters that best describe the vegetation and climate of the Dripsey site, we compared Collatz's and Jacobs' models to the observations. To do so we needed to work on the same scale for measured and modelled values. The scaling up from leaf to canopy for both models was obtained by a simple multiplication by the estimated LAI for the site.

The LAI has not been measured and consequently has been assumed for this study that it changes through seasons. In prediction of LAI cutting of the grass and grazing were taken in account. The assumed LAI values are given in the Table 7.1 and its behaviour during 2002 and 2003 is shown in Figure 7.

Table 7.1: **Estimated LAI for 2002 and 2003 at Dripsey grassland**

LAI	jan		feb		mar		apr		may		jun		jul		aug		sep		oct		nov		dec	
2002	1.0	1.1		1.2	1.5	1.6	1.8			1.7	1.5	1.3	1.0	1.3	1.4	1.5	1.6	1.7	1.2	1.3			1.0	0.8
2003	0.8	0.9	1.0	1.1	1.4	1.7	1.8	1.9	2.0	1.8	1.7	0.9	1.3	1.5			1.6	1.7		1.3		1.4	1.2	1.1

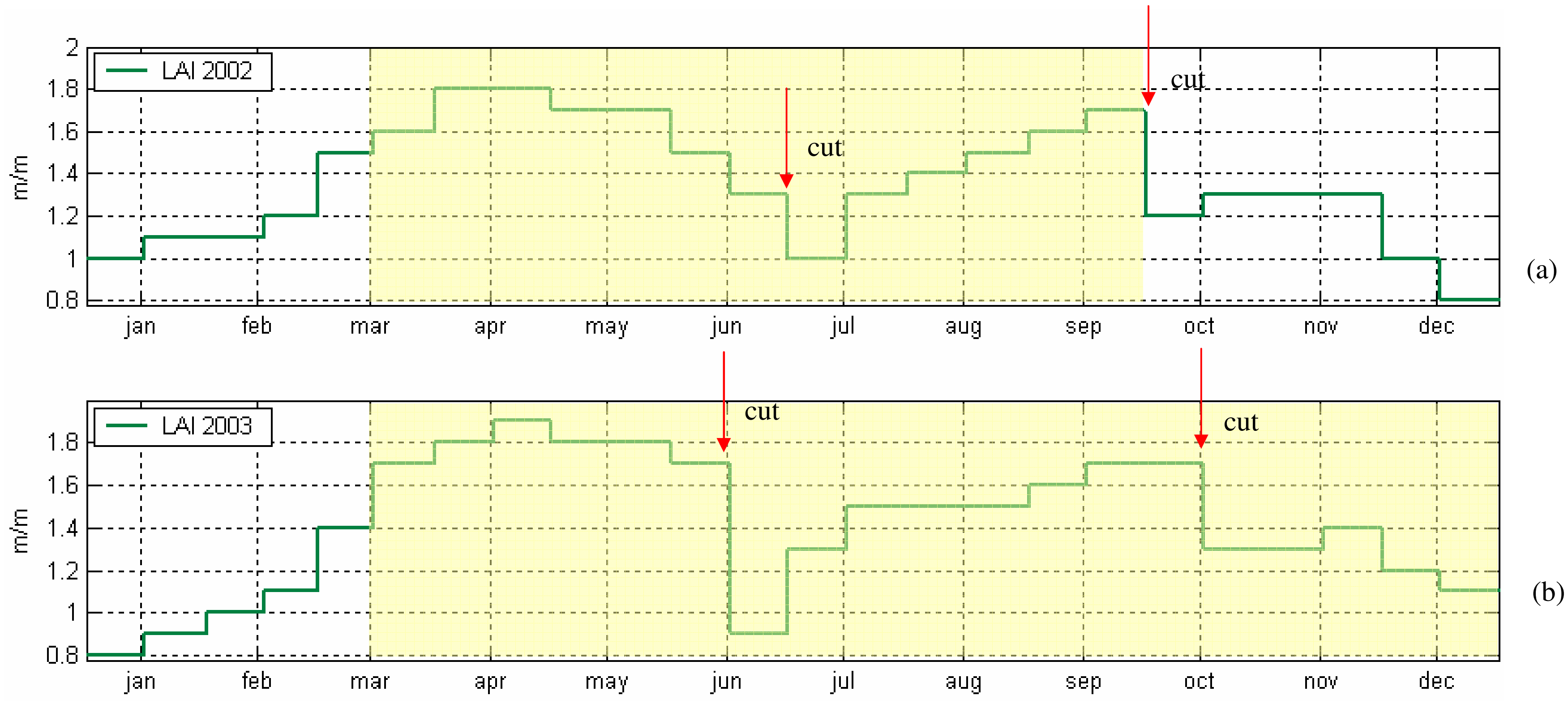

Figure 7.2: **Estimated LAI for (a) 2002 and (b) 2003. Periods of grazing are shadowed yellow.**

Moreover, the available light is not the same between the bottom and the top of the canopy. The radiation is attenuated as a function of the LAI, so that young grass near the ground receives a smaller photosynthetic photon flux. The rate of decrease is generally considered exponential (Figure 7.3).

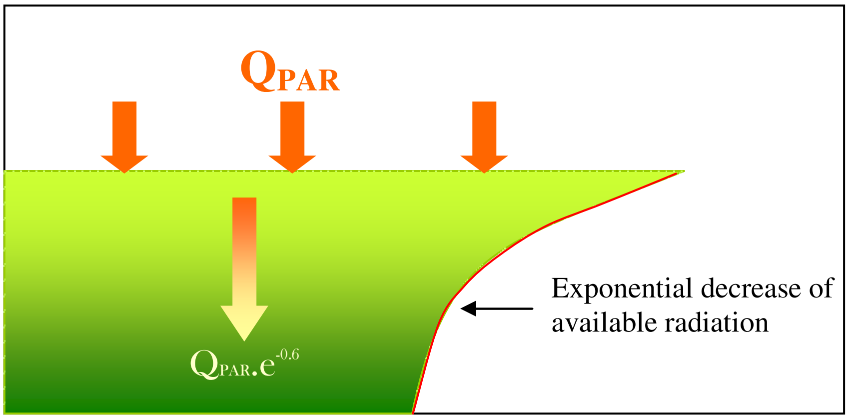

Figure 7.3: Light extinction in the canopy [*Le Bris*, 2002]

Considering the lower complexity of a grassland field in comparison with canopy system such as forests, an average value of the photon flux received at the top and at the bottom of the canopy has been applied uniformly. The PAR radiation input for modelling becomes:

$$Q = Q_{PAR} \times \frac{\left(1 + e^{(-0.4 \times LAI)}\right)}{2} \qquad \textbf{(7.31)}$$

where Q_{PAR} is the measured incoming photon flux in the PAR wavelength from the weather station (see section 4.6).

The calibration of each model for the most varying parameters for the Dripsey site was done by Le Bris [2002]. Those parameters are adopted in this thesis.

7.3.1 Collatz's model

This model has a great number of parameters. In order to reduce the computation time of the sensitivity analysis, most parameters were held at the value defined by Farquhar [1980] for C_3 grass (Appendix 5). Le Bris [2002] considered only parameters that were usually different from one site to another or from one type of grass to another (see values given by Collatz for C_4 grass and by Farquhar for C_3 grass in Appendix 5). The sensitivity analysis was done for: q_{Ko}, q_{Kc}, q_τ and m from the stomatal conductance equation (7.14) [*Le Bris*, 2002].

A more detailed analysis should be done when the values of the seasonal variability of the leaf area index (LAI) for the site will be known.
The adopted values for tested parameters are:

$q_{Ko} = 0.05$ $q_{Kc} = 0.07$ $q_\tau = -0.02$ $m = 6.75$

Those results are consistent with usual values for such coefficients and are used for the modelled CO_2 flux analysis.

7.3.2 Jacobs' model

Jacobs's model has fewer parameters than Collatz's model. Four parameters were tested by Le Bris [2002] and the other parameters were held at the value given by Jacobs [1994] for C_3 grass (Appendix 5). In this study we adopted parameter values determined by Le Bris [2002].
The adopted values for tested parameters are:

$f_o = 0.94$ $Q_{10}(\Gamma) = 1.2$ $Q_{10}(A_{m,max}) = 1.6$ $Q_{10}(g_m) = 1.6$

Those results are consistent with usual values for such coefficients and are used for the modelled CO_2 flux analysis.

7.4 Modelling results and comparisons

The following analysis examines the results of the Collatz's model and Jacobs's models for the study period. The daily, monthly fluxes were examined, and Collatz's and Jacobs's cumulative fluxes compared in terms of global uptake and photosynthesis.

7.4.1 Daily flux

Figure 7.4 (a) and (b) shows the daily CO_2 flux (F_d) for observed data and both models for 2002 and 2003. General trends for modelled F_d agree reasonably well with the observed flux.

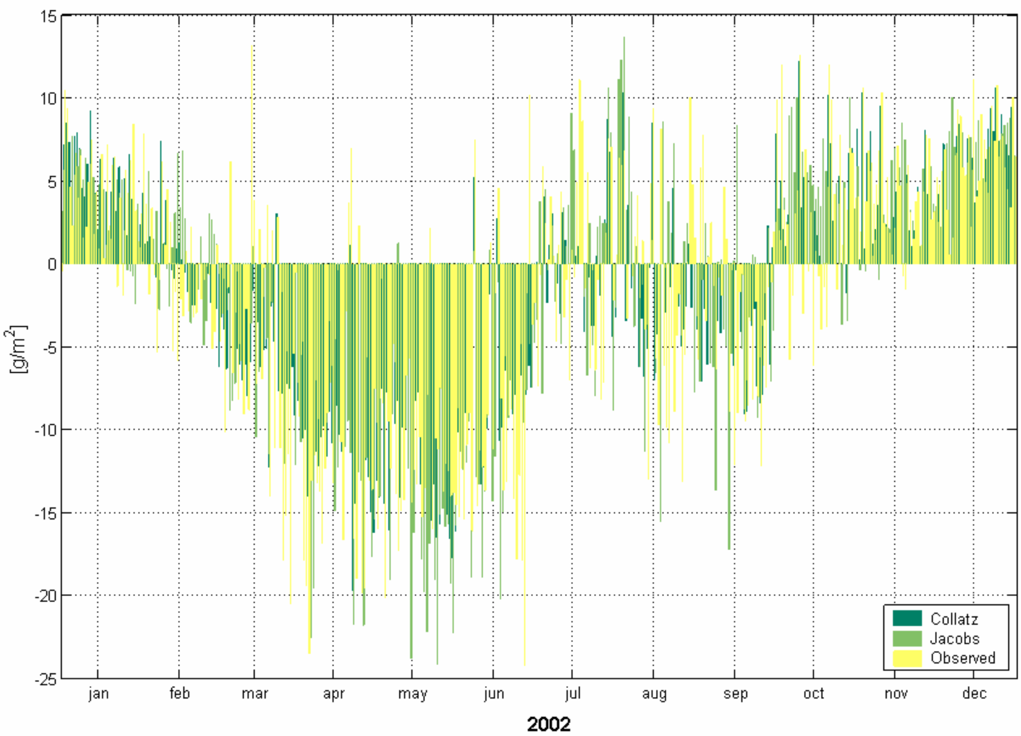

(a)

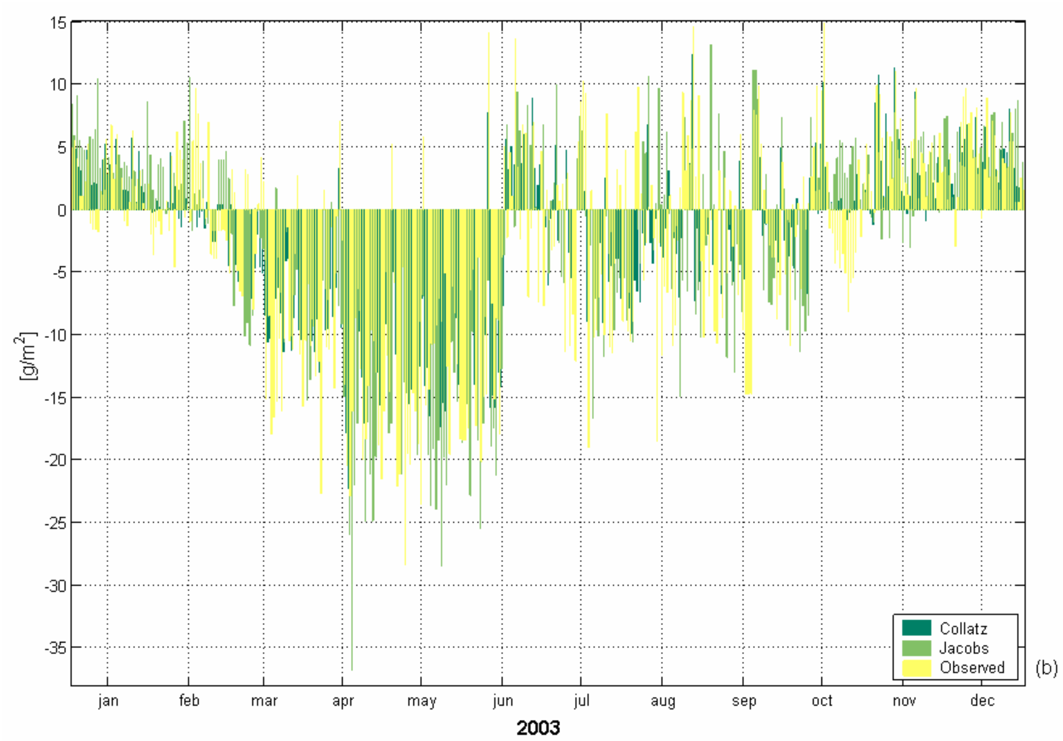

Figure 7.4: Daily CO_2 flux in g/m^2 for observed data, Collatz model and Jacobs model: (a) for 2002 and (b) for 2003

Figures 7.5 to 7.8 show daily observed and modelled CO_2 fluxes month by month for 2002 and 2003.

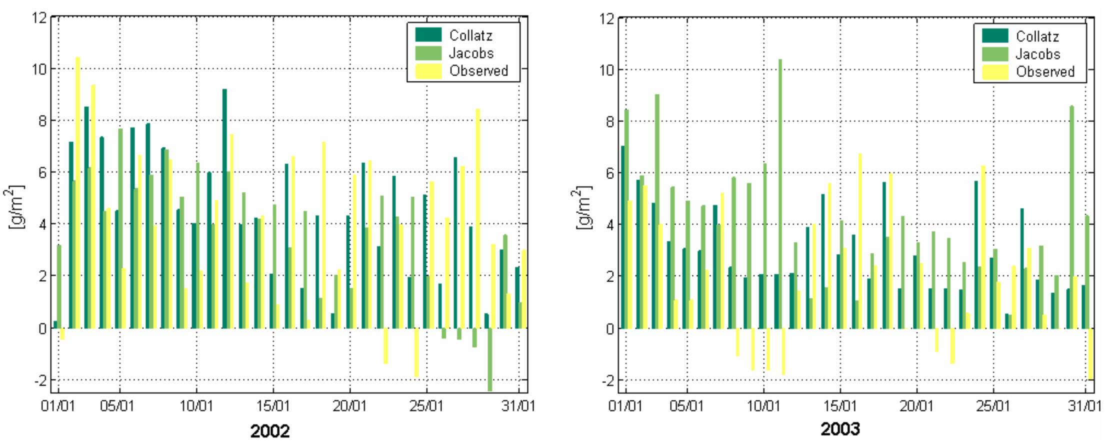

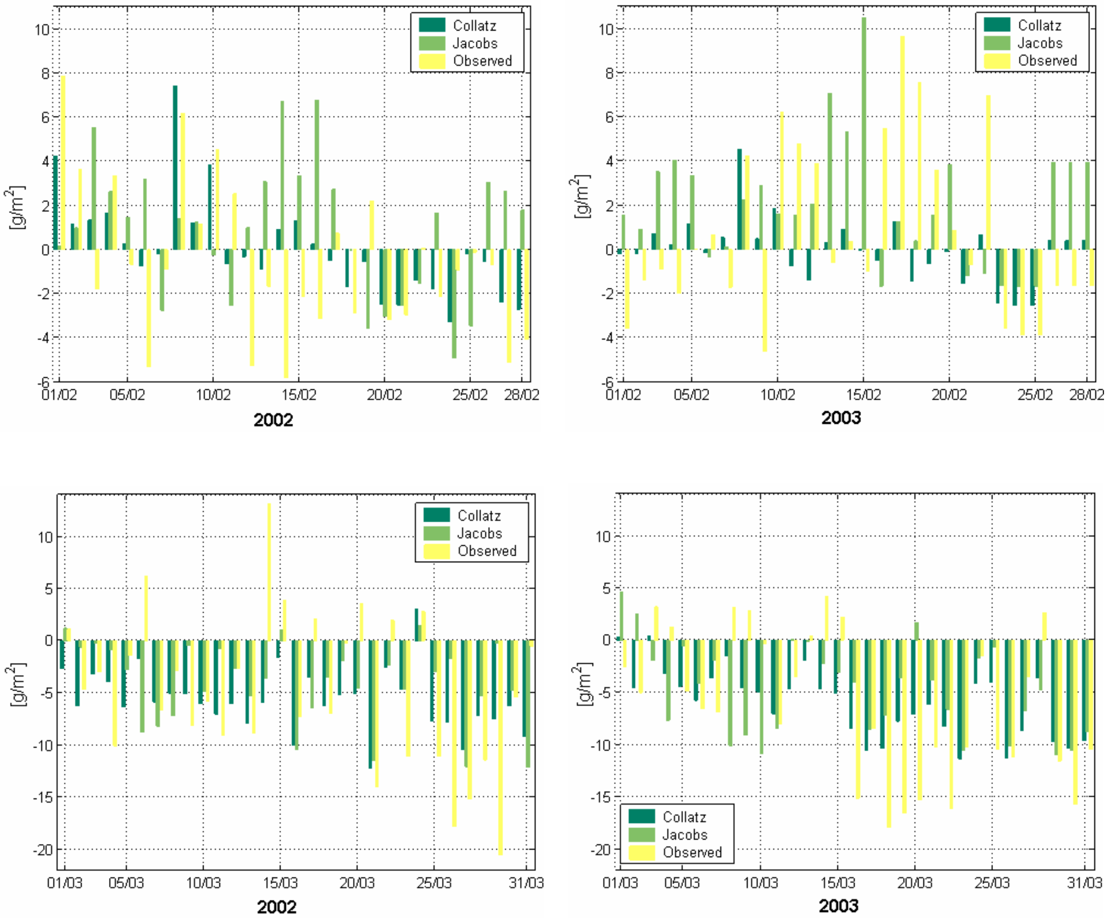

Figure 7.5: Daily CO_2 flux (observed and modelled) for January, February and March for 2002 (left) and 2003 (right)

The daily flux in January for both observed years shows good agreement between measured and modelled data most of the time. Exceptions are the periods around 10th and 22th January 2003 where measured flux gives uptake of CO_2 while models predict high respiration for those periods. Measured and modelled daily flux in February for both years shows poor agreement. Reasons for this can be switching grassland from being CO_2 source to sink and poor definition of LAI for this period. For March in both years modelled CO_2 flux follows the sign pattern of measured flux (the models predict that grassland is a sink for CO_2 for this period), but the magnitude of uptake is not predicted well by the models.

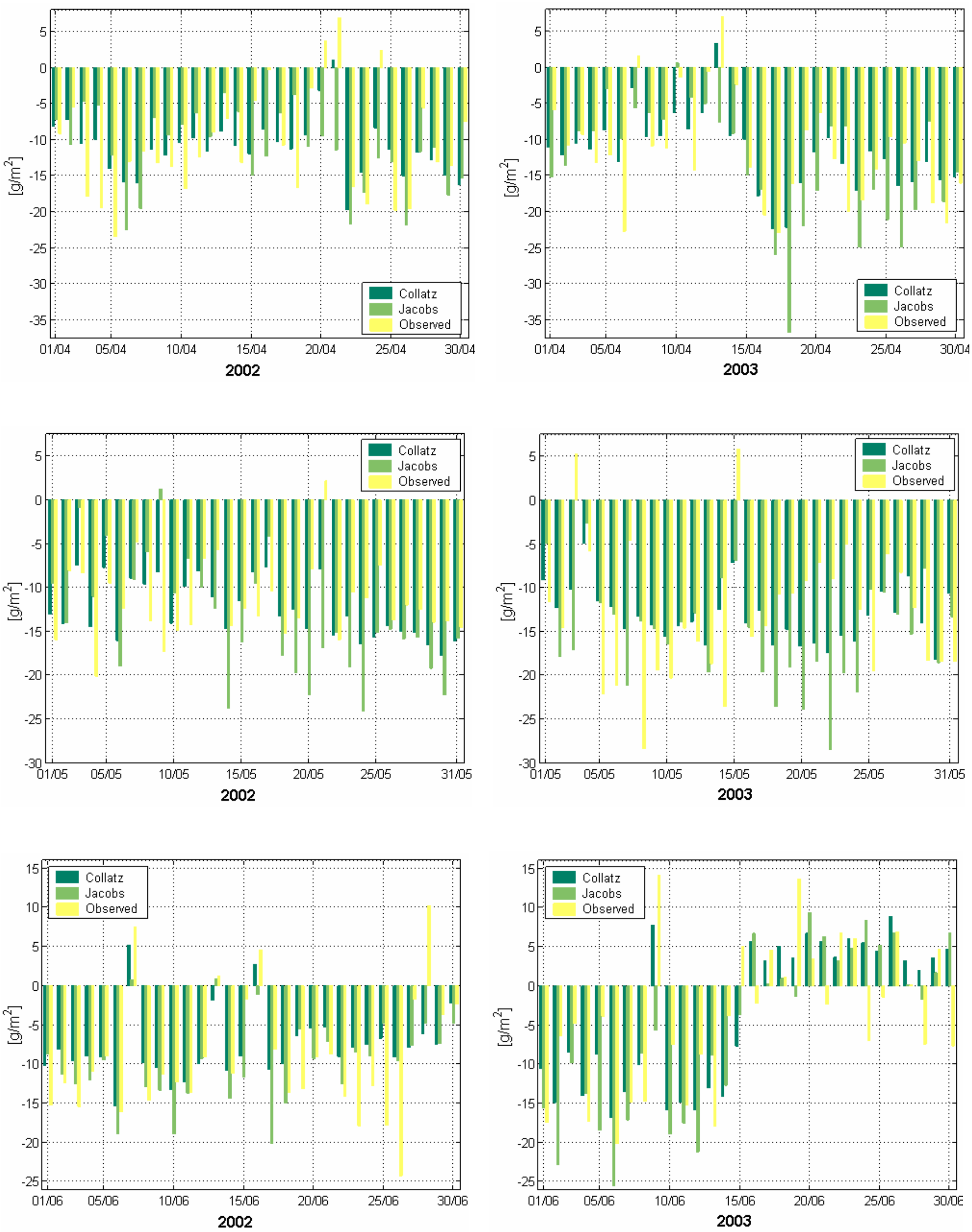

Figure 7.6: Daily CO_2 flux (observed and modelled) for April, May and June for 2002 (left) and 2003 (right)

Figure 7.6 shows good agreement between measured and modelled CO_2 flux for April May and June on a daily basis. In April and May it seems that both models are late in response. Notice that on 15th June 2003 the grass was cut, and models reflect that event well.

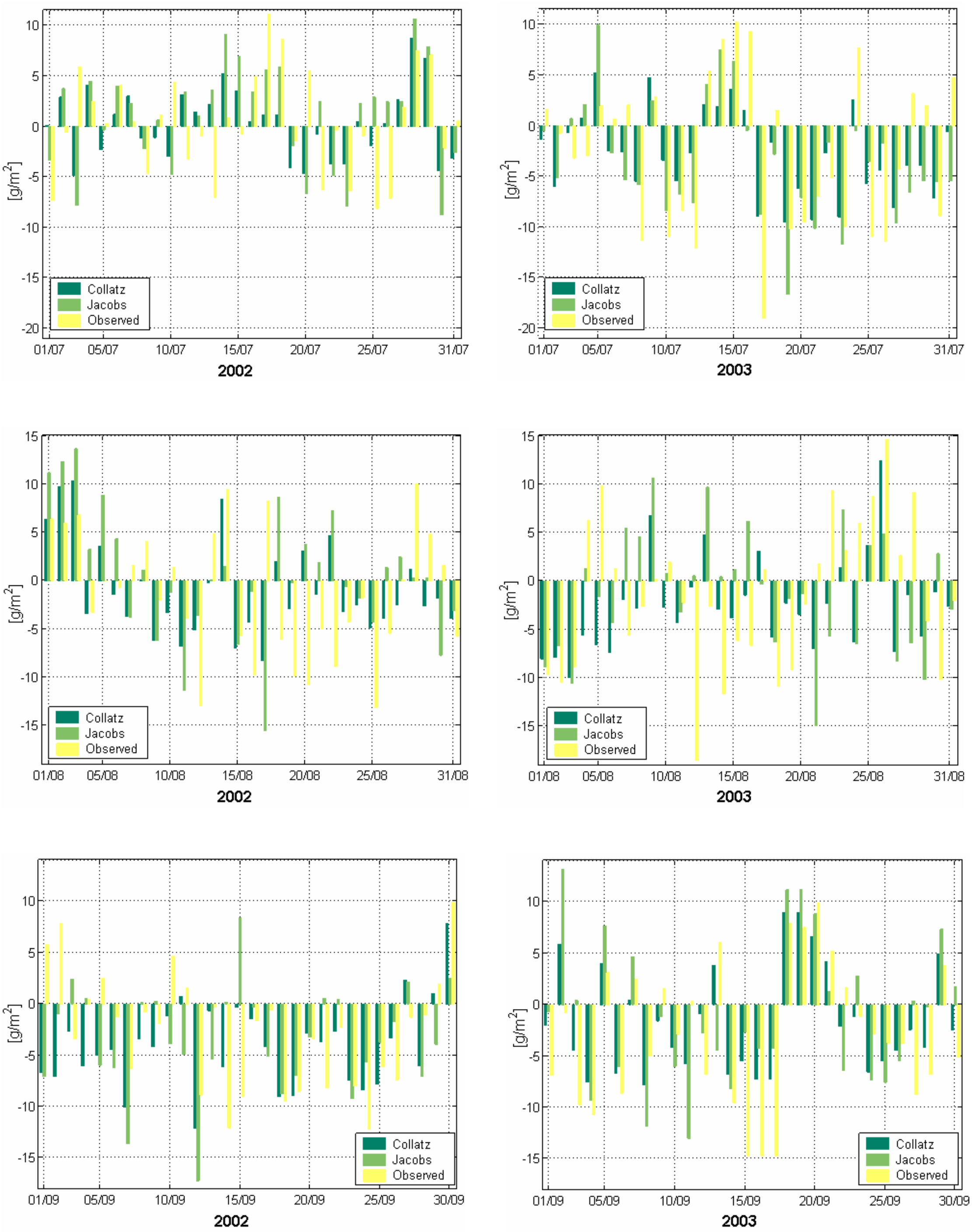

Figure 7.7: Daily CO_2 flux (observed and modelled) for July, August and September for 2002 (left) and 2003 (right)

Figure 7.7 shows generally good agreement between the sign of measured and modelled CO_2 flux, except for the period after 10th August for both years. This can be a consequence of poor definition of LAI for this period. We still notice good model agreement with decrease of LAI at the beginning of July 2002 and the end of September 2002 and at the mid of June 2003.

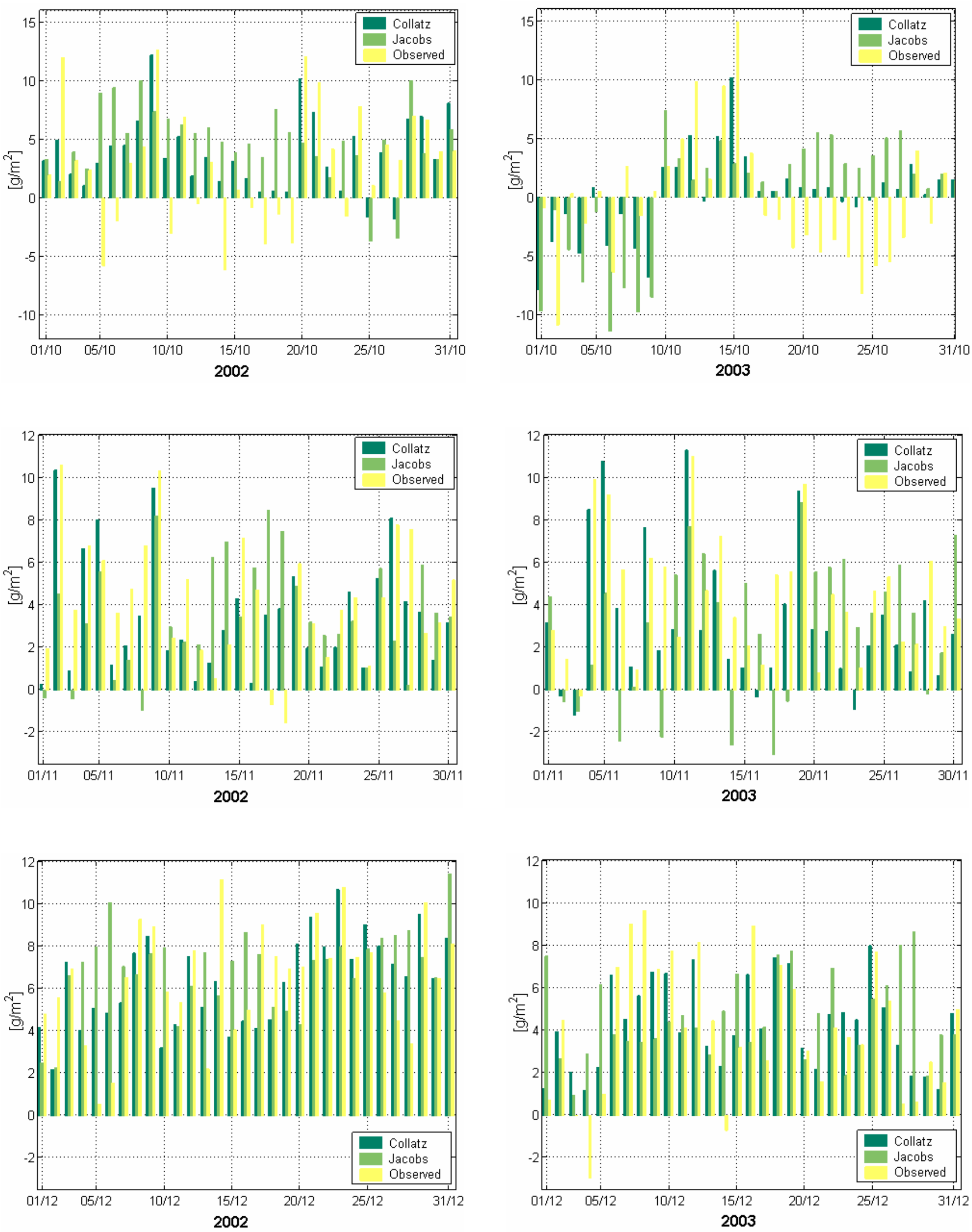

Figure 7.8: Daily CO_2 flux (observed and modelled) for October, November and December for 2002 (left) and 2003 (right)

Figure 7.8 shows that for daily CO_2 flux in October for both years there is disagreement between measured and modelled flux, especially for periods where measured flux shows uptake. For November and December of both years measured daily flux is in good agreement with the models.

As data for both models are generally close during the whole study period, we can infer that they are calibrated on the same physical and biological basis. The difference with the observed CO_2 flux is most likely linked with the LAI definition in the models.

7.4.2 Monthly flux

The monthly fluxes for Collatz's and Jacobs's models, and measured flux for 2002 and 2003 are presented in Table 7.2 and plotted in Figure 7.9.

On the monthly scale during 2002 both models show good agreement regarding the sink-source behaviour with measured flux for all months except February and August (see Figure 7.9 (a)). In February and August 2002 measured flux shows uptake of CO_2 while Jacobs's model shows release of CO_2.

On the monthly scale during 2003, both models show good agreement regarding sink-source behaviour with measured flux for all months except October (see Figure 7.9 (b)). In October measured flux shows uptake of CO_2 while both models show release of CO_2.

Both models show a quicker decrease in autumn than the observations and a slower increase in early spring. The shift between winter and spring is slower but longer in the modelling case.

Table 7.2: Monthly observed and modelled CO_2 flux in g/m^2 for 2002 and 2003

	CO_2 flux	jan	feb	mar	apr	may	jun	jul	aug	sep	oct	nov	dec
2002	observed	128	-15	-160	-322	-362	-276	9	-44	-80	86	127	200
	Colatz	142	1	-176	-334	-388	-231	10	-30	-124	115	105	197
	Jacobs	114	25	-126	-342	-418	-291	33	15	-103	146	106	215
2003	observed	63	17	-195	-348	-405	-114	-84	-48	-87	-8	131	126
	Colatz	94	0	-186	-356	-409	-98	-89	-79	-49	8	96	132
	Jacobs	132	57	-150	-401	-472	-162	-106	-40	-31	9	88	142

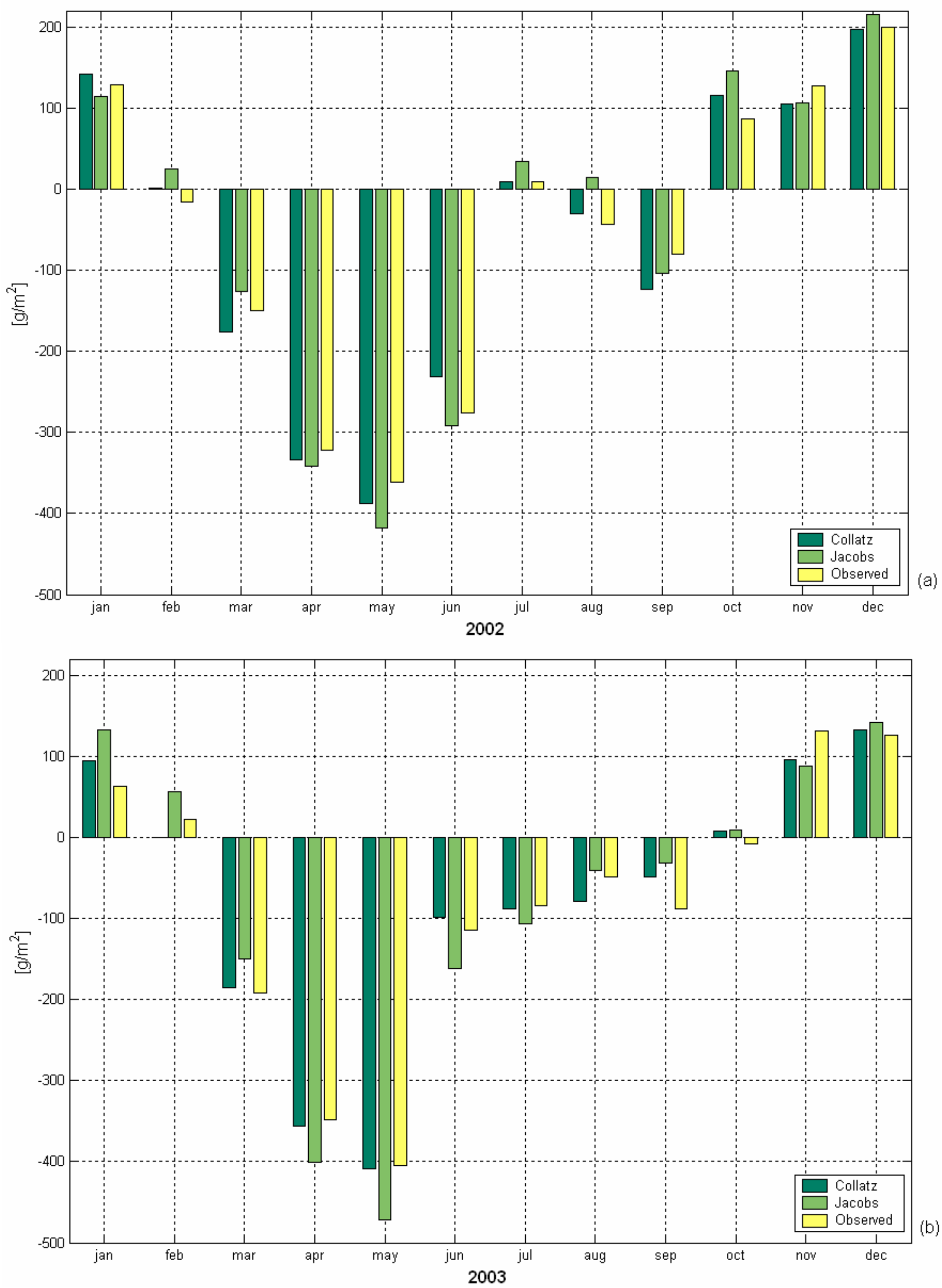

Figure 7.9: Monthly observed and modelled CO_2 flux for (a) for 2002 and (b) for 2003.

7.4.3 Cumulative photosynthesis and global uptake

The cumulative quantities are important as they represent in a striking way the main characteristics of a site and its capacity to act as a sink or a source of carbon. Having reasonably good results for the previous time scales, one can be confident of the cumulative fluxes be it the photosynthesis flux or the net uptake over the year of study.

Figures 7.10 and 711 depict the evolution of C and photosynthesis for Collatz's model and Jacobs's model in comparison with the observations.

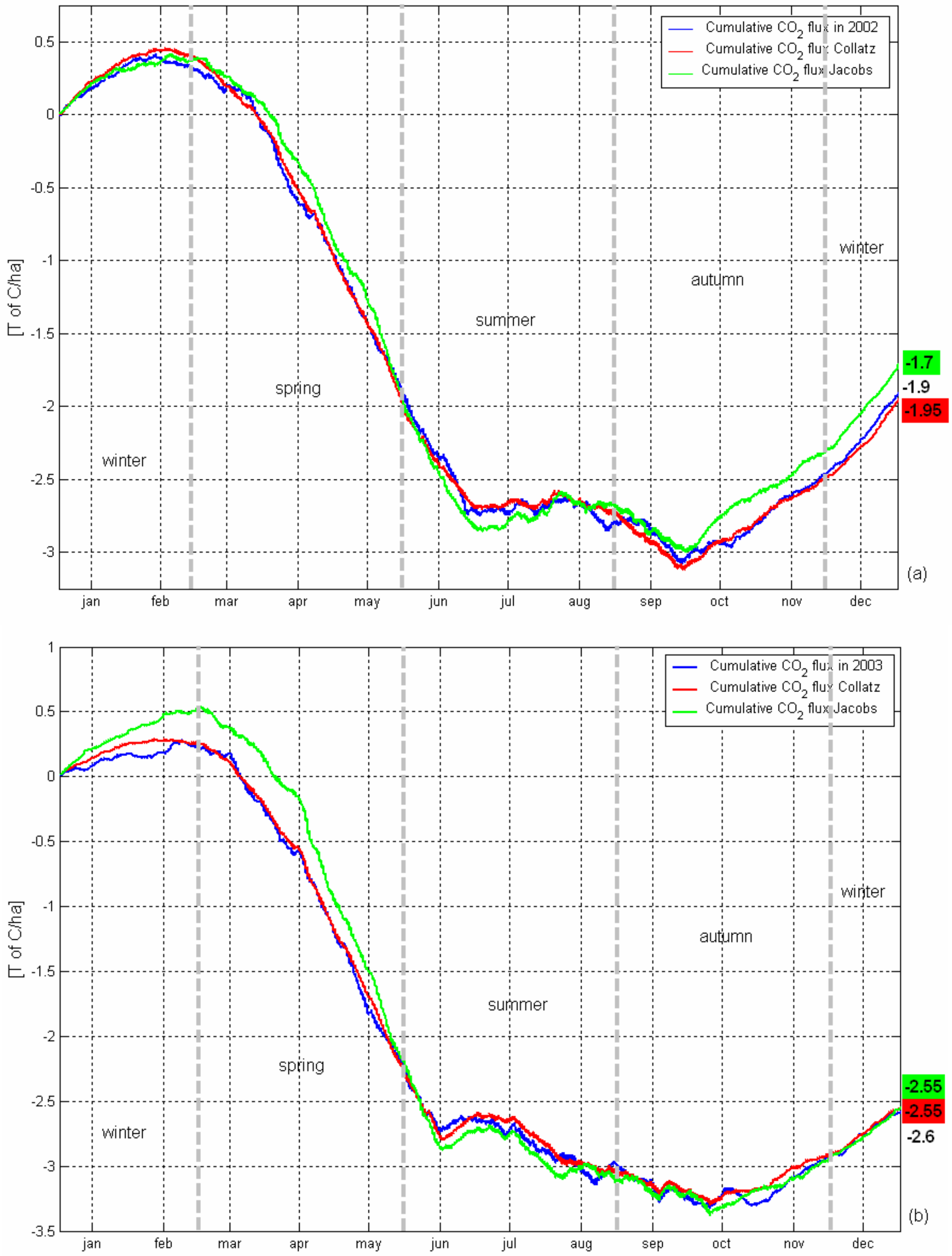

Figure 7.10: Comparison of the cumulative uptake of C between the observed data and the two models: (a) for 2002, and (b) for 2003

Regarding the observed and modelled cumulative curve for carbon in 2002, the models show good agreement with measured flux in the first half of the year (see Figure 7.10 (a)). From July to October 2002 it seems that models cannot predict very well the situation on the field regarding the decrease in LAI due to ununiform grazing and cutting. From October to the end of December Colatz's model shows similar behaviour to the measured flux, while Jacobs's model predicts larger release of carbon than measured. The cumulative uptake of carbon in 2002 was -1.9T of C/ha, Collatz's model gives -1.95T of C/ha, and Jacobs's model gives -1.7T of C/ha.

Cumulative carbon uptake in 2003 was -2.6T of C/ha and both models for 2003 give similar cumulative uptake of -2.55T of C/ha (see Figure 7.10 (b)). Still it seems that Colatz's model shows better performance, while Jacobs's model predicts higher respiration for the period January-May 2003 and higher uptake for the period June-October 2003.

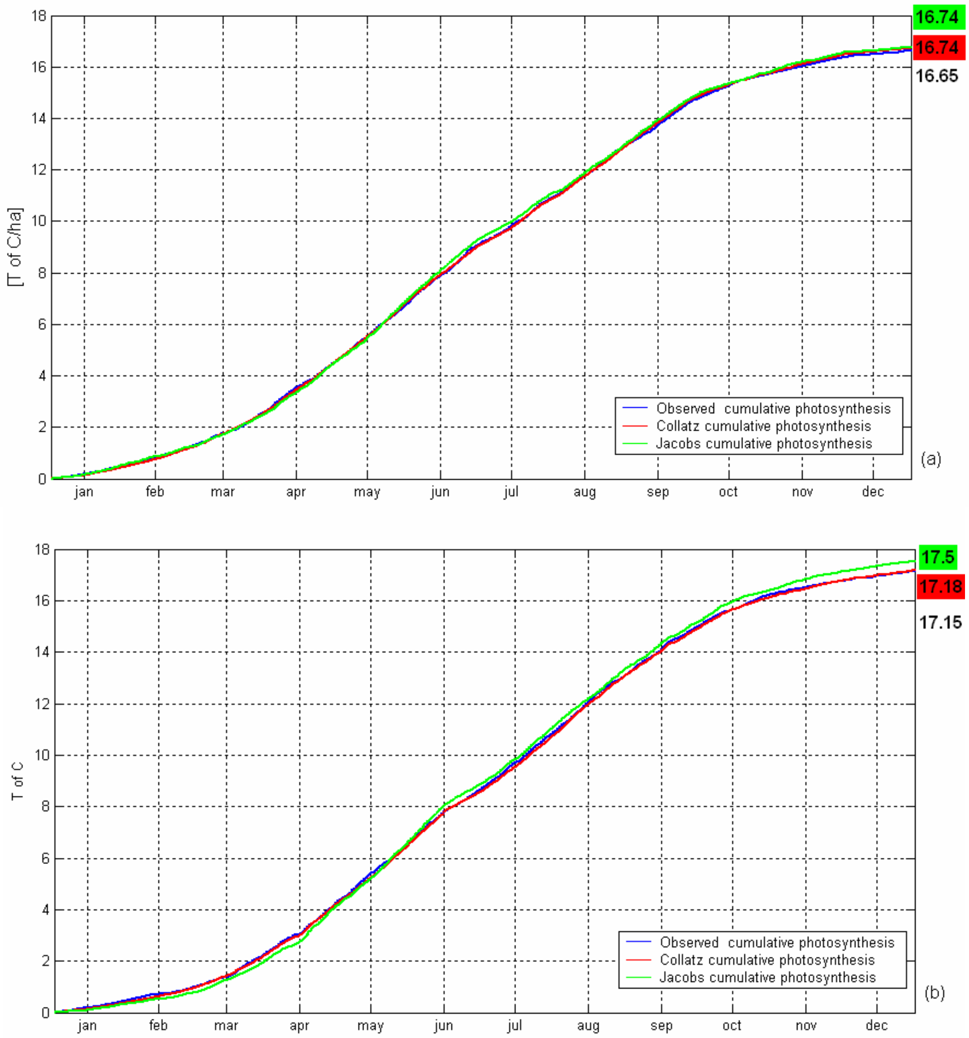

Figure 7.11: **Comparison of the cumulative photosynthesis over the year of study between the observed data and the two models: (a) for 2002, and (b) for 2003.**

The photosynthetic part of the flux for both Collatz's and Jacobs's models is in good agreement with observed data for 2002 (Figure 7.11 (a)). In 2003 the photosynthetic part of the flux is in good agreement with Collatz's model and to somewhat less extent with Jacobs's model. The difference between Jacobs's model and observed photosynthesis is from October to December where the modelled photosynthesis has to be reduced to fit the observations. The final cumulative uptakes (by the photosynthesis process only, i.e. GPP) agree well for both models and both studied years.

In conclusion, both Collatz's model and Jacobs' model give in general satisfactory results on the different time scales for both observed years. As for the senescence and growing transition in autumn and spring, they can be improved by a better definition of the variation of LAI during the year.

Chapter 8
Conclusion

Chapter 8 Conclusion

8.1 Conclusion

The eddy correlation flux measurements presented here cover two years of a planned long-term research programme of net ecosystem exchange of CO_2 begun in July 2001 at a humid temperate grassland ecosystem in southern Ireland. The experimental grassland encompasses eight small dairy farms (of size 10 to 40ha each) with approximately 2/3$^{rd's}$ of the area grazed for eight months of the year while in the other 1/3rd (which is off-limits for grazing from March to September) the grass is cut (harvested for winter feed) twice per year: June and September. The two cuts of silage during the study period may have affected the LAI and thus CO_2 flux at the beginning and also at the end of the study The two years are: 2002 which was a wet year (precipitation at 1785mm, 22% above average); and 2003 which was a dry year (precipitation at 1185mm, 15% below average). The climate being very temperate in Ireland, very few days are under 4°C, which is a critical temperature for the photosynthetic process and no snow occurred during the study period. Therefore, the leaf area index stays higher with a minimum value around 1. The farmland management practices in both years were similar, including nitrogen fertilisation rates (305kg.N/ha and 294kg.N/ha for 2002 and 2003 respectively). We found that the wet year of 2002 had a NEE of -1.9TC/ha compared to -2.6TC/ha for the dry year of 2003 (a 27% difference). We found that the cumulative NEE from February to September (Spring plus Summer) was the same in both years. The difference in NEE in the two years of 0.7 T.C/ha was concentrated in the winter months (October, November, December and January). The wet year winter had a cumulative NEE of +1.5 T.C/ha while for the corresponding NEE for the dry year was +0.8 T.C/ha. The precipitation of the wet winter (2002) was 903 mm while in the dry winter it was 435 mm. As the land use and land management practices were similar in both years, the main difference between the two years was in the magnitude of the winter rainfall. We conclude that the wetter winter of 2002 with its saturating effect on soil moisture had enhanced ecosystem respiration which was responsible for the lower annual NEE of 2002. Another issue that have been raised here is the use of the site by cattle and the effects of the silage cuts. They stimulated the growth as well by bringing more light to the most active and youngest grass situated near the ground. In the meantime the LAI is reduced and so is the photosynthetic flux. A better understanding of those processes and long time measurements are required.

8.2 Suggestion for further investigation

Many believe that grasslands may be missing carbon sink [*Ham & Knapp*, 1998; *Robert*, 2001; *Pacala et al.*, 2001; *Goodale and Davidson*, 2002]. In order to define the amount of carbon sequestered (i.e. fixed to the soil) at Dripsey experimental site it is very important to define the footprint of tower. Our findings suggest that during the stable and neutral conditions footprint can be larger (up to 7 km radius) than the area occupied by farms with known management. This estimation of footprint was done for the instruments positioned at 10 m height. As is described in section 3.4, size of footprint area depends on surface roughness, change in stability (i.e. from unstable to stable), and the instrument's height. It was suggested to decrease instrumentation height for CO_2 fluxes was reduced from 10 to 3m on December 22, 2003. This change will decrease the footprint area and better define the land management in the smaller footprint.

The carbon budget for the farm can be written:

$$NEE - (A + B + C + ...) = C_{soil/atm} \tag{8.1}$$

where NEE is Net ecosystem exchange [T of C/ha], A, B, C… is carbon leaving the farm (in milk, in meat, in enteric fermentation) and $C_{soil/atm}$ is a carbon fixed in the soil or lost in the atmosphere.

If we assume that new footprint area encompasses eight small dairy farms (of size 10 to 40ha each) with approximately $2/3^{rd's}$ of the area grazed for eight months of the year while in the other $1/3^{rd}$, the grass cut (harvested for winter feed) twice per year: June and September; carbon leaving the farm can be calculated:

A. Carbon in milk [T.C/ha.yr.]

average production 7500L/ha.

density $\varphi = 1.03$kg/L

carbon in milk = 4.5%

$$C_{milk} = 7500 \times 1.03 \times \frac{4.5}{100} \times 10^{-3} = 0.35 T.C/ha.yr \tag{8.2}$$

B. Carbon in meat [T.C/ha.yr.]

~18% of live weight

1LU = 520kg pasture dry matter per year

Stocking Density for Dripsey = 2.2LU/ha

Assume that 1/3 of animals leave farm for the meat factory

$$C_{meat} = 2.2 \times 520 \times \frac{18}{100} \times \frac{1}{3} \times 10^{-3} \approx 0.1 T.C/ha.yr \tag{8.3}$$

C. Carbon in CH_4 respired from animal and CH_4 from manure for full year

100kg CH_4 from animal
15kg CH_4 from manure
Stocking Density for Dripsey = 2.2LU/ha

$$C_{(CH_4)} = 115 \times 2.2 \times \frac{12}{16} \times 10^{-3} = 0.2 \text{T.C/ha.yr} \tag{8.4}$$

D. Carbon as CO_2 from respiring animal indoors for 4 months of year

Diet = 10kgDM/day/LU
DM = 45%Carbon
Assume 40% respire

$$C_{(CO_2)} = 10 \times 365 \times \frac{45}{100} \times 2.2 \times \frac{4}{12} \times \frac{40}{100} \times 10^{-3} = 0.45 \text{T.C/ha.yr} \tag{8.5}$$

It is of great importance to estimate new footprint and to check if there are changes in NEE. In order to calculate this long-term measurements (at least 6 months) are needed. That will open new research on carbon sequestration in this grassland ecosystem.

Thanks to the good collaboration with the farmers the application of nitrogen fertilizer and slurry for the farms is known. Some investigation should be done on grass root efficiency to uptake spread fertilizer on the field (i.e during the dry and wet weather) and contribution of fertilizer to the grass growth in different seasons in the year.

In the future, some measurements on the site of the leaf area index (LAI) should improve our knowledge of the growth of plants throughout seasons, highlight the effects of silage cuts on grass growth and give a good assessment of the amount of matter removed in summer. Such measurements are widely described in literature and could be either carried out by remote sensing measurements (from satellite data) or with manual measurements as it is usually done for sites of field scale size such as our catchment. This data could then be used to validate a model of growth to simulate a variable LAI during the year. The LAI found in this way could also be used for calculating actual evapotranspiration since bulk surface resistance (r_s) in Penman-Monteith equation depend on it.

Very important for future investigation of evapotranspiration and CO_2 canopy-atmosphere exchange is finding not only meteorological, but physiological explanations for interannual variability (e.g. canopy conductance (g_c), 'omega factor' (Ω) which is an index of relative importance of meteorological and physiological limitations to evapotranspiration).

In this study, only two components are considered in the CO_2 fluxes: the ecosystem respiration (nighttime CO_2 flux) and the photosynthesis (daytime CO_2 flux minus the daytime CO_2 respiration deduced from the nighttime measurements). However, soil surface carbon dioxide flux, the sum of plant root and microbial respiration, is an important part of the carbon cycle of terrestrial ecosystem too. In our case no device measured this component alone, so that it could not be separated from the plant respiration (they together compose the ecosystem respiration). Many papers report the method of close-chamber or open-chamber measurements, used to measure soil respiration, and the accuracy of such method. This could be an interesting part to add to the instruments present on this Irish grassland site to deepen the understanding of process of carbon cycle.

References

References

Aber, D. J., and C. A. Federer, A generalized, lumped-parameter model of photosynthesis, evapotranspiration and net primary production in temperate and boreal forest ecosystems, *Oecologia, 92*, 463-474, 1992.

Albertson, J. D., and G. Kiely, On the structure of soil moisture time series in the context of land surface models, *Journal of Hydrology, 243*, 101-119, 2001.

Aubinet, M., A. Grelle, A. Ibrom, U. Rannik, J. Moncrieff, T. Foken, A. S. Kowalski, P. H. Martin, P. Berbigier, C. H. Bernhofer, R. Clement, J. Elbers, A. Granier, T. Grunwald, K. Morgenstern, K. Pilegaard, C. Rebmann, W. Snijders, R. Valentini, and T. Vesala, Estimates of annual net carbon and water exchange of forests: the EUROFLUX methodology, *Adv. Ecol. Res., 30*, 114-175, 2000.

Baldocchi, D.D., Assessing the eddy covariance technique for evaluating carbon dioxide exchange rates of ecosystems: past, present and future, *Global Change Biol., 9*, 479-492, 2003.

Baldocchi, D., R Valentini, S. Runing, W. Oechel, and R. Dahlman, Strategies for measuring and modeling carbon dioxide and water vapour fluxes over terrestrial ecosystems, *Global Change Biol., 2*, 159-168, 1996.

Ball, J.T., I. E. Woodrow, and J. A. Berry, A model predicting stomatal conductance and its contribution to the control of Photosynthesis under different environmental conditions. *Progress in Photosynthesis Research. 4*, 221-224, 1987.

Batjes, H. N., Management options for reducing CO_2 – concentrations in the atmosphere by increasing carbon sequestration in the soil, *Report no. 410 200 031,* 114 pp., Dutch National Research Programme on Global Air Pollution and Climate Change, Netherlands, 1999.

Berbigier, P., J.-M. Bonnefond, and P. Mellmann , CO_2 and water vapour fluxes for 2 years above Euroflux forest site, *Agric. For. Meteorol., 108*, 183-197, 2001.

Berry, J. A., and J. K. Raison, Responses of Macrophytes to temperature. In: Lange, O.L., Nobel, P.S., Osmond, C.B., Ziegler, H., *Encyclopedia of Plant Physiology, New series, Vol. 12B*, Physiological Plant Ecology II. Springer Verlag, Berlin, 277-338, 1982.

Bruce, P. J., M. Frome, E. Haites, H. Joanne, L. Rattan, and K. Faustian, Carbon sequestration in soils, *J. Soil and Water cons.*, 382-389,1999.

Bruse, M., ENVI-met implementation of the Jacobs A-gs model to calculate the stomata conductance. Working paper, 2001. http://www.geographie.ruhr-uni-bochum.de/agklima/envimet/

References

Brutsaert, W., *Evaporation into the atmosphere*, edited by A. J. Davenport, B. B. Hicks, G. R. Hilst, R. E. Munn, J. D. Smith, Kluwer Academic Publishers, London, 1991.

Budyko, I. M., *Climate and Life*, Climatic factors of Photosynthesis, 497, Academic Press INC, London, 1974.

Calvet, J.C., J. Noilhan, J. L. Roujean, P. Bessemoulin, M. Cabelguenne, A. Olioso, and J. P. Wigneron, An interactive vegetation SVAT model tested against data from six contrasting sites. *Agric. For. Meteorol. 92*, 73-95, 1998.

Calvet, J. C., and J. F.Soussana, Modelling CO2 enrichment effects using an interactive vegetation SVAT scheme. *Agric. For. Meteorol. 108*, 129-152, 2001.

Campbell, S. G., and J. M. Norman, *An introduction to environmental Biophysics*, second edition, Springer-Verlag New York, 1998.

Campbell, Soil moisture, surface wetness and heat flux sensors, *Campbell Scientific, Ltd.* 1998. www.campellsci.co.uk

Campbell, Tipping bucket raingauges, ARG100, *Campbell Scientific, Ltd*. 2000. www.campellsci.co.uk

Campbell, PTB101B Barometric Pressure Sensor User Guide, *Campbell Scientific, Ltd*. 2001. www.campellsci.co.uk

Campbell, CS616 Water Content Reflectometer, *Campbell Scientific, Ltd*. 2002a. www.campellsci.co.uk/products/sensors/cs616.htm

Campbell, CR23X Micrologger, *Campbell Scientific, Inc*. 2002b. www.campellsci.co.uk/products/sensors/cs616.htm

Campbell, Model HMP45C temperature and relative humidity probe instruction manual, *Campbell Scientific, inc.* 2003a. www.campellsci.co.uk

Campbell, Model 107 & 107B temperature probes instruction manual, *Campbell Scientific, inc.* 2003b. www.campellsci.co.uk

Cava D., U. Giostra, M. Siqueira, and G. Katul, Organised Motion and Radiative Perturbations in the Nocturnal Canopy Sublayer above an Even-Aged Pine Forest, Boundary-Layer Meteorol, 112, No. 1, 129-157, 2004.

Collatz, G.J., J.T Ball, C Grivet, and J.A. Berry, Physiological and environmental regulation of stomatal conductance, photosynthesis and transpiration: a model that includes a laminar boundary layer. *Agric. For. Meteorol. 54*, 107-136, 1991.

References

Conant, T.R., K. Paustian, and E. T. Elliott, Grassland management and conversion into grassland: effects on soil carbon, *Ecol. Applications, 11*, No. 2, pp. 343-355, 2001.

Cruickshank, M.M., R.W. Tomlinson, P.M. Devine, and R. Milne, Carbon in the vegetation and soils of Northern Ireland, *Biology and Environment: Proceedings of the Royal Irish Academy, vol. 98B, No. 1,* 9-21, 1998.

Dabberdt, W. F., D. H. Lenschow, T. W. Horst, P. R. Zimmerman, S. P. Oncley, and A. C. Delany, Atmosphere-surface exchange measurements, *Science, 260*, 1472-1481, 1993.

Daly, K., An Environmentalappraisal of the phosphorous of the Irish grassland soils, PhD. Thesis, Trinity College Dublin, 1999.

Dingman, S. L., *Physical Hydrology*, editor Robert McConnin, Macmillan Publishing Company, New York, 1994.

Dugas, W.A., M.L. Heuer, and H.S. Mayeux, Carbon dioxide fluxes over a Bermuda grass, native prairie, and sorghum. *Agric. For. Meteorol. 93*,121-139, 1999.

Earlham College, http://www.earlham.edu/~biol/syllabi/ecobio02/notes.htm, 2002

EMS (Environmental Media Service), Pentagon Report Describes Global Warming Dangers, 2003. http://www.ems.org/climate/pentagon_climate_change.html#report

Encyclopedia Britannica, 20th Edition

EPA (Environmental Protection Agency-Ireland), *Ireland's environment*, chapter 4: Emissions to air, A Millennium Report, edited by Michael McGettigan, April 2000.

EPA (Environmental Protection Agency-Ireland), *National Inventory Report 2003*, Greenhouse gas emissions 1990-2001 reported to the United Nations framework convention on climate change, edited by Michael McGettigan and Paul Duffy, 2003.

Falge, E., D. Baldocchi, J. Tenhunen, M. Aubinet, P. Bakwin, P. Berbigier, C. Bernhofer, G. Burba, R. Clement, K. J. Davis, J. A. Elbers, A. H. Goldstein, A. Grelle, A. Granier, J. Guðmundsson, D. Hollinger, A. Kowalski, G. Katul, B. E. Law, Y. Malhi,T. Meyers, R. K. Monson, J. W. Munger, W. Oechel, K. Tha Paw U, K. Pilegaard, Ü. Rannik, C. Rebmann, A. Suyker, R. Valentini, K. Wilson, and S. Wofsy, Seasonality of ecosystem respiration and gross primary production as derived from FLUXNET measurements, *Agric. For. Meteorol., 113*, 53-74, 2002.

Falge, E., D. Baldocchi, R. Olson, P. Athoni, M. Aubinet, C. Bernhofer, G. Burba, R. Ceulemans, R. Clement, H. Dolman, A. Granier, P. Gross, T. Grünward, D. Hollinger, N-O. Jensen, G. Katul, P. Keronen, A. Kowalski, C. T. Lai, B. E. Law, T. Meyers, J. Moncrieff, E. Moors, J. W. Munger, K. Pilegaard, Ü. Rannik, C. Rebmann, A. Suyker, J.

Tenhunen, K. Tu, S. Verma, T. Vesala, K. Wilson, and S. Wofsy, Gap filling strategies for defensible annual sums of net ecosystem exchange, *Agric. For. Meteorol., 107*, 43-69, 2001.

FAO, Crop evapotranspiration – Guidelines for computing crop water requirements – *FAO Irrigation and drainage paper 56*, Food and Agriculture Organisation of the United Nations, Rome, 1998.

Farquhar, G.D., S von Caemmerer, and J. A. Berry, A biochemical model of photosynthetic CO_2 assimilation in leaves of C3 species. *Planta. 149*, 78-90, 1980.

Foken, Th., and B. Wichura, Tools for quality assessment of surface-based flux measurements, *Agric. For. Meteorol., 78*, 83-105, 1996.

Frank, B. A., and Dugas, A. W., Carbon dioxide fluxes over northern, semiarid, mixed-grass prairie, *Agric. For. Meteorol., 108*, 317-326, 2001.

Frank, B.A., P. L. Sims, J. A. Bratford, P. C. Milenick, W. A. Dugas, and H. S. Mayeux, Carbon dioxide fluxes over three great plains grasslands, *The Potential of U.S. Grazing Lands to Sequester Carbon and Mitigate the Greenhouse Effect,* edited by R. F. Follett, J. M. Kimble, and R. Lal, 167-187, Lewis Puplishers, New York, 2001.

Garatt, R. J., *The atmospheric boundary layer*, Edited by J. T. Houghton, M. J. Rycroft, A. J. Dessler, Cambridge University Press, 1992.

Gash, J. H. C., A note on estimating the effect of a limited fetch on on micrometeorological evaporation measurements. *Boundary-Layer Meteor., 35*, 409-413, 1986.

Gash, J. H. C., F. Valente, and J. S. David, Estimates and measurements of evaporation from wet, sparse pine forest in Portugal, *Agric. For. Meteorol., 94*, 149-158, 1999.

Gardiner, M. J., and T. Radford, Soil associations of Ireland and their land use potential, An Foras Taluntais, Sandymount Avenue, Dublin, Ireland, 1980.

Goodale, L. C., and E. A. Davidson, Uncertain sinks in the shrubs, *Nature, 418*, 593-594, 2002.

Goudriaan, J., H.H. van Laar, H. van Keulen, and W. Lovwerse, Photosynthesis, CO_2 and plant production. In: Day, W. Day & R.K. Atkin (Eds.), *Wheat growth and modelling*. NATO ASI Series, Series A, Vol. 86. Plenum Press, New York, 107-122, 1985.

Goulden, M.L., J.W., Munger, S.M., Fan, B.C., Daube, and S.C., Wofsy, Measurements of carbon sequestration by long-term eddy covariance: methods and critical evaluation of accuracy, *Global Change Biol., 2*, Pages 196-182, 1996.

References

Guenther, B. A., and A. J. Hills, Eddy covariance measurement of isoprene fluxes, *J. Geophysical Res., 103*, No. D11, 13,145-13,152, 1998.

Hall, O. D., J. M. O. Scurlock, D. S. Ojima, and W. J. Parton, Grasslands and the Global Carbon Cycle: Modeling the Effects of Climate Change, in *The Carbon Cycle*, edited by T.M.L. Wigley and D.S. Schimel, pp. 102-114,Cambridge Univ. Press, UK, 2000.

Ham, M. J., and A. K. Knapp, Fluxes of CO_2, water vapor, and energy from a prairie ecosystem during the seasonal transition from carbon sink to carbon source, *Agric. For. Meteorol., 89*, 1-14, 1998.

Horst, T. W., and J. C. Weil, How far is far enough? The fetch requirements for micrometeorological measurement of surface fluxes, *J.Atmos Oceanic Technol, 12*, 447, 1995.

Houghton, J., Global Climate change digest report, 1990.

Hsieh, C-I., G. G. Katul, J. Schieldge, J. T. Sigmon, and K. K. Knoerr, The Lagrangian stochastic model for fetch and latent heat flux estimation above uniform and nonuniform terrain, *Water Resources Res., 33*, No. 3, 427-438, 1997.

Hsieh, C-I., G. G. Katul, and T-W. Chi, An approximate analytical model for footprint estimation of scalar fluxes in thermally stratified atmospheric flows, *Advances in Water Resources, 23*, 765-772, 2000.

Humphreys, E. R., T. A. Black, G. J. Ethier, G. B. Drewitt, D. L. Spittlehouse, E.-M. Jork, Z. Nesic, N. J. Livingston, Annual and seasonal variability of sensible and latent heat fluxes above coastal Douglas-fir forest, British Columbia, Canada, *Agric. For. Meteorol., 115*, 109-125, 2003.

Hunt, E. J., F. M. Kelliher, T. M. McSeveny, and J. N. Byers, Evaporation and carbon dioxide exchange between the atmosphere and a tussock grassland during a summer drought, *Agric. For. Meteorol., 111*, 65-82, 2002.

IPCC (Intergovernmental Panel on Climate Change), *Revised 1996 Guidelines for National Greenhouse Gas Inventories*, OECD, Paris, 1997.

Jackson, B. R., J. L. Banner, E. G. Jobbágy, W. T. Pockman, and D. H. Wall, Ecosystem carbon loss with woody plant invasion of grasslands, *Nature, 418,* 623-626, 2002.

Jacobs, C.M.J., Direct impact of atmospheric CO_2 enrichment on regional transpiration. Ph.D. Thesis. Agricultural University, Wageningen, 1994.

Jarvis, P.G., The interpretation of leaf water potential and stomatal conductance found in canopies in the field. *Phil. Trans. R. Soc*. London B. *273*, 593-610, 1976.

Kiely, G., Global climate change-greenhouse gases, in *Environmental Engineering* , pp. 358-362,McGraw-Hill Publishing Company, UK, 1997.

References

Kipp & Zonen, CNR1 Net-Radiometer instruction manual, *Kipp & Zonen*, Delft, Netherlands 2000. http://www.campbellsci.ca/CampbellScientific/Catalogue/CNR1_Br.pdf

Kipp & Zonen, PAR LITE Sensor for photosynthetic photon flux, *Kipp & Zonen*, Delft, Netherlands 2001. http://www.campbellsci.ca/CampbellScientific/Catalogue/PAR_Lite_Br.pdf

Kirschbaum, U. F. M., The temperature dependence of soil organic matter decomposition, and the effect of global warming on soil organic C storage, *Soil Biol. Biochem, 27* (D6), 753-760, 1995.

Kirschbaum, M. U. F., D. Eamus, R. M. Gifford, S. H Roxburgh,. and P. J. Sands, Definitions of some ecological terms commonly used in carbon accounting. *Net Ecosystem Exchange*, edited by Kirschbaum, M.U.F. and Mueller, R, Cooperative Research Centre for Greenhouse Accounting, Canberra, pp. 2-5, 2001. http://www.ffp.csiro.au/nfm/staff/kirschbaum/definitions.pdf

Knapp, K. A., P. A. Fay, J. M. Blair, S. L. Collins, M. D. Smith, J. D. Carlisle, C. W. Harper, B. T. Danner, M. S. Lett, and J. K. McCarron, Rainfall variability, carbon cycling, and plant species diversity in a mesic grassland, *Science, 298*, 2202-2205, 2002.

Kozaki, A., and G. Takeba, Photorespiration protects C3 plants from photooxidation, *Nature 384*, 557 – 560, 1996; doi:10.1038/384557a0

Kramm, G., R. Dlugi, and D. H. Lenschow, A re-evaluation of the Webb correction using density-weighted averages, *Journal of Hydrology, 166*, 283-292, 1995.

Kyoto Protocol, the text of the Kyoto Protocol is available at: www.unfccc.de

Lafleur, P. M., N. T. Roulet, and S. W. Admiral, Annual cycle of CO_2 exchange at a bog peatland, *J. Geophysical Res., 106*, No. D3, 3071-3081, 2001.

Lai, C.-T., G. Katul, J. Butnor, D. Ellsworth, and R. Oren, Modelling night-time ecosystem respiration by a constrained source optimization method, *Global Change Biol., 8*, 124-141, 2002.

Law, E. B., E. Falge, L. Gu, D. D. Baldocchi, P. Bakwin, P. Berbigier, K. Davis, A. J. Dolman, M. Falk, J. D. Fuentes, A. Goldstein, A. Granier, A. Grelle, D. Hollinger, I. A. Janssens, P. Jarvis, N. O. Jansen, G. Katul, Y. Mahli, G. Matteucci, T. Meyers, R. Monson, W. Munger, W. Oechel, R. Olson, K. Pilegaard, K. T. Paw U, H. Thorgeirsson, R. Valentini, S. Verma, T. Vesala, K. Wilson, and S. Wofsy, Environmental controls over carbon dioxide and water vapor exchange of terrestrial vegetation, *Agric. For. Meteorol., 113*, 97-120, 2002.

References

Le Bris, C., Observations and modelling of carbon dioxide flux from an Irish Grassland for a one year campaign, *A Master thesis submitted to the National University of Ireland*, Department of Civil Engineering, UCC, Oct. 2002.

Leclerc, M. Y., and G. W. Thurtell, Footprint prediction of scalar fluxes using a Markovian analysis, *Boundary-Layer Meteorology, 52*, 247-258, 1990.

Lewis, C., Phosphorus, Nitrogen and Suspended Sediment loss from Soil to Water from Agricultural Grassland, *A Master thesis submitted to the National University of Ireland*, Department of Civil Engineering, UCC, Oct. 2003.

LI-COR, LI-7500 Product Information, *LI-COR, inc.*, 2001. www.licor.com.

Lloyd, J., and J.A Taylor, On the temperature dependence of soil respiration. *Funct. Ecol. 8*, 315–323, 1994.

McGettigan, M., and Duffy P., Emissions to air in Ireland 1990-1998, *Environmental Protection Agency*, Wexford, 2000.

McMillen, R. T., An eddy correlation technique with extended applicability to non-simple terrain, *Boundary Layer Meteorology, 43*, 231-245, 1988.

Michaelis, L., and M. L. Menten, Die Kinetik der Invertinwirkung, *Biochem. Z. 49*, 333, 1913.

Meidner, H., and T. A Mansfield, Physiology of Stomata, McGraw-Hill, London, 1968.

Mizutani, K., K. Yamanoi, T. Ikeda, T. Watanabe, Applicability of eddy correlation method to measure sensible heat transfer to forest under rainfall conditions, *Agric. For. Meteorol., 86*, 193-203, 1997.

Moncrieff, J.B., J. M. Massheder, H. de Bruin, J. Elbers, T. Friborg, B. Heusinkveld, P. Kabat, S. Scott, H. Soegaard, and A. Verhoef, A system to measure surface fluxes of momentum, sensible heat, water vapour and carbon dioxide, *J. Hydrol., 188-189*, 589-611, 1997.

Moncrieff, J.B., Y. Mahli, and R. Leuning, The propagation oferrors in long term measurements of land atmosphere fluxes of carbon and water. *Global Change Biol. 2*, 231-240, 1996.

Monteith, J., Climate and the efficiency of crop production in Britain, *Phil. Tans. Res. Soc., 281*, 277-329, London, 1965.

Nederhoff, E., How to use RH and other humidity measures, Humidity in Greenhouses, *Hot Research Publication*, 2004. http://www.hortnet.co.nz/publications/science/n/neder/humid02.htm

References

Novick, K.A., P. C. Stoy, G. G. Katul, D. S. Ellsworth, M. B. S. Siqueira, J. Juang, R. Oren, , Carbon dioxide and water vapor exchange in a warm temperate grassland, *Oecologia, 138*: 259–274, 2004.

Ortega-Farias, O. S., R. H. Cuenca, and M. Ek, Daytime variation of sensible heat flux estimated by the bulc aerodynamic method over a grass canopy, *Agric. For. Meterol., 81*, 131-143, 1996.

Pacala, W. S., G. C. Hurtt, D. Baker, P. Peylin, R. A. Houghton, R. A. Birdsey, L. Heath, E. T. Sundquist, R. F. Stallard, P. Ciais, P. Moorcroft, J. P. Caspersen, E. Shevliakova, B. Moore, G. Kohlmaier, E. Holland, M. Gloor, M. E. Harmon, S. -M. Fan, J. L. Sarmiento, C. L. Goodale, D. Schimel, and C. B. Field, Consistent Land- and Atmosphere-Based U.S. Carbon Sink Estimates, *Science, 292,* 2316-2319, 2001.

Pattey E., I. B. Strachan, R. L. Desjardins, and J. Massheder, Measuring nightime CO_2 flux over terrestrial ecosystems using eddy covariance and nocturnal boundary layer methods, *Agric. For. Meteorol., 113*, 145-158, 2002.

Pidwirny, M., *Fundamentals of physical geography*, chapter8: Introduction to the Hydrosphere, 2004. http://www.physicalgeography.net/fundamentals/8j.html

Post, M. W., T-H. Peng, W. R. Emanuel, A. W. King, V. H. Dale, and D. L. DeAngelis, The Global Carbon Cycle, *Amer. Sci., 78,* 310-326. 1990.

Priestley, C. H. B., and R. J. Taylor, On the assessment of surface heat flux and evaporation using large scale parameters, *Mon. Weath. Rev*., *100*, 81-92, 1972.

Radford University, Temperate Grasslands, Oct. 2000. http://www.runet.edu/~swoodwar/CLASSES/GEOG235/biomes/tempgrass/tempgras.html

Reynolds, O., On the dynamical theory of incompressible viscous fluids and the determination of criterion, *Phil. Trans. Of Royal Soc. Of London, A174*, 935-982.

Rind, D., C. Rosenzweig, and M. Stieglitz, The role of moisture transport between ground and atmosphere in global change, *Annu. Rev. Energy Environ, 22*, 47-74, 1997.

Robert, M., Soil Carbon Sequestration for improved land management, *World Soil Resources Report 96*, 58 pp., FAO (Food and Agriculture Organization of UN), Rome, 2001.

Royer, L. D., S. L. Wing, D. J. Beerling, D. W. Jolley, P. L. Koch, L. J. Hickey and R. A. Berner, Paleobotanical evidence for near present-day levels of atmospheric CO_2 during part of the tertiary, *Science, 292*, 2310-2313, 2001.

References

Ruimy, A., P. G. Jarvis, D. D. Baldocchi, and B. Saugier, CO_2 fluxes over plant canopies and solar radiation: a review, *Adv. Ecol. Res. 26*, 1-63, 1995.

Saigusa, N., T. Oikawa, and S. Liu, Seasonal variations of the exchange of CO_2 and H_2O between a grassland and the atmosphere: An experimental study, *Agric. For. Meteorol., 89*, 131-139, 1998.

Sarmiento, L. J., and N. Gruber, Sinks for anthropogenic carbon, *Phisics Today*, 30-36, 2002.

Scanlon, M. T., G. Kiely, and Q. Xie, A nested catchment approach for defining the hydrological controls on non-point phosphorus transport, *Journal of Hydrology, xx*, xxx-xxx, 2004.

Schimel, D., I. G. Enting M. Heimann, T. M. L. Wigley, D. Raynaud, D. Alves, and U. Siegenthaler, CO_2 and the Carbon cycle (Extracted from the Intergovernmental Panel on climate change (IPCC) Report "Climate Change, 1994"), in *The Carbon Cycle*, edited by T.M.L. Wigley and D.S. Schimel, pp. 7-36,Cambridge Univ. Press, UK, 2000a.

Schimel, D., D. Alves, I. Enting M. Heimann,F. Joos, D. Raynaud, and T. Wigley, CO_2 and the Carbon cycle (Extracted from the 1995 Intergovernmental Panel on climate change (IPCC) "Second Assessment Report," Climate Change 1995 The science of Climate Change), in *The Carbon Cycle*, edited by T.M.L. Wigley and D.S. Schimel, pp. 37-49,Cambridge Univ. Press, UK, 2000b.

Schmid, P.H., Footprint modelling for vegetation atmosphere exchange studies: a review and perspective, *Agric. For. Meteorol., 113*, 159-183, 2002.

Schmid, H.P., C.S.B. Grimmond, F. Cropley, B. Offerle, and H.B. Su, Measurements of CO_2 and energy fluxes over a mixed hardwood forest in the mid-western United States. *Agric. For. Meteorol. 103*, 357-374, 2000.

Sims, P.L., and J. A. Bradford, Carbon dioxide fluxes in a southern plains prairie. *Agric.For. Meteorol. 109*, 117-134, 2001.

Smith, E., Limiting factors in photosynthesis: light and carbon dioxide, *Gen. Physiol. 22*, 21–35, 1938.

Soussana, J.-F., P. Loiseau, N. Vuichard, E. Ceschia, J. Balesdent, T. Chevallier, and D. Arrouays, Carbon cycling and sequestration opportunities in temperate grasslands, *Soil Use and Management,* in press, 2003.

Suyker, E. A., S. B. Verma, and G. G. Burba, Interannual variability in net CO_2 exchange of a native tallgrass prairie, *Global Change Biol., 9*, 255-265, 2003.

References

Twine, T. E., W. P. Kustas, J. M. Norman, D. R. Cook, P. R. Houser, T. P. Meyers, J. H. Prueger, P. J. Starks, and M. L. Weseley, Correcting eddy-covariance flux underestimates over a grassland, *Agric. For. Meterol., 103*, 279-300, 2000.

UC Berkeley, Grasslands, *This page was created by the Biomes Group of the Fall 96 Biology 1B class, section 115*, Oct. 2000 http://www.ucmp.berkeley.edu/glossary/gloss5/biome/grasslan.html

UMIST, Atmospheric Physics Research Group, Introduction to the eddy covariance method, Manchester, UK, 2002. http://cloudbase.phy.umist.ac.uk/people/dorsey/Edco.htm

Valentini, R., G. Matteucci, A. J. Dolman, E.-D. Schulze, C. Rebmann, E. J. Moors, A. Granier, P. Gross, N. O. Jensen, K. Pilegaard, A. Lindroth, A. Grelle, C. Bernhofer, T. Grünwald, M. Aubinet, R. Ceulemans, A.S. Kowalski, T. Vesala, Ü. Rannik, P. Berbigier, D. Loustau, J. Guðmundsson, H. Thorgeirsson, A. Ibrom, K. Morgenstern, R. Clement, J. Moncrieff, L. Montagnani, S. Minerbi, and P. G. Jarvis, Respiration as the main determinant of carbon balance in European forests, *Nature, 404, 861-865*, 2000.

Van der Tol, C., J. H. C. Gash, S. J. Grant, D. D. McNeil, M. Robinson, Average wet conopy evaporation for Sitka spruce forest derived using the eddy correlation-energy balance technique, *Journal of Hydrology, 276*, 12-19, 2003.

Vourlitis, L. G., and W. C. Oechel, Eddy covariance measurements of CO_2 and energy fluxes of an Alaskan tussock tundra ecosystem, *Ecology, 80(2)*, 686-701, 1999.

WCRP/SCOR, Working Group on AirSea Fluxes, Direct flux observations, *The Working Group Report*, 55-63, 2000. http://www.soc.soton.ac.uk/JRD/MET/WGASF/get_chapters.html

Webb, E.K., G. I. Pearman, and R. Leuning, Correction of flux measurements for density effects due to heat and water vapor transfer, *Quart. J. R. Meteorol. Soc. 106*, 85-100, 1980.

Wever, A. L., L.B. Flanagan, and P. J. Carlson, Seasonal and interannual variation in evapotranspiration, energy balance and surface conductance in northern temperate grassland, *Agric. For. Meteorol., 112*, 31-49, 2002.

Wilkinson, J., and M. Janssen, BIOME3, National Emissions Inventory Workshop, Denver, Colorado, May 1-3, 2001.

Wilson, B. K., P. J. Hanson, and D. D. Baldocchi, Factors controlling evaporation and energy partitioning beneath a deciduous forest over an annual cycle, *Agric. For. Meteorol., 102*, 83-103, 2000.

References

Young, Model 81000 Ultrasonic anemometer, manual PN 81000-90, *RM Young Company*, Michigan, USA, 2001. http://www.youngusa.com/81000.pdf

Appendix 1

Hsieh’s model

matlab codes

matlab codes

```
% ======================================================================
%                          Hsieh's model
%       * Calculating fetch requirement and maximum footprint location*
% ======================================================================

% Reference: Hsieh, C-I., G. G. Katul, and T-W. Chi,
%       An approximate analytical model for footprint estimation of scalar fluxes in thermally
%       stratified atmospheric flows, Advances in Water Resources, 23, 765-772, 2000.

% The code is available at
%               http://www.env.duke.edu/faculty/katul/Matlab_footprint.html.

% ------------------------------------------Constants------------------------------------------

zo = 0.03;                    % surface roughness  [m]
k = 0.4;                      % von Karman constant
d = 1.2;                      % air density[kg/m^3]
Cp = 1005;                    % specific heat for dry air [J/(kgK)]
g = 9.81;                     % gravity  [m/s^2]
zm = 10;                      % height of eddy covariance set [m]
z2 = 3;                       % height of air temperature probe [m]

% -----------------------------------------Variables-------------------------------------------

% ustar                       - friction velocity [m/s]
% TaC                         - sonic temperature at zm=10m [degC]
% ta1                         - air temperature at z2=3m [degC]
% ta2 = ta1+273.15            - air temperature at z2=3m [K]
% L                           - Monin-Obukhov length [m]
% h                           - sensible heat flux [w/m^2]
% xp                          - peak distance from measuring point to
%                           the maximum contributing source area [m]
%xf                           - fetch [m]

% ----------------------------------------Footprint model--------------------------------------

function [xp,xf,L,unstable,neutral,stable]=footprint_hsieh1(ustar1,h1,ta1,zm,zo)
stable=0;
neutral=0;
unstable=0;
k=0.4;
d=0;
p=0;
L=-1*1.2*1005*ustar1.^3./(0.4*9.8/(273.15+ta1)*h1);
zu=zm*(log(zm/zo)-1.+zo/zm);

if abs(zu/L) <= 0.04    % neutral conditions
        d=0.97;
        p=1;
        neutral=1
```

```
 elseif (zu/L) > 0.04     % stable conditions
          d=2.44;
          p=1.33;
          stable=1;
 else                     % unstable conditions
          d=0.28;
          p=0.59;
          unstable=1;
end
xf=d/(0.105*k*k)*(abs(L).^(1-p))*(zu^p);
xp=d/(2.*k*k)*(abs(L).^(1.-p))*(zu^p);

%==========================================================
```

Appendix 2.1:

Penman-Monteith equation

matlab codes

```
%=============================================================
%                              Penman-Monteith equation
%=============================================================
% -----------------------------------------Constants-----------------------------------------

zm =10;                % [m] height of wind measurements
zh =3;                 % [m] height of humidity measurements
h = 0.12;              % [m] height of crop
d1 = 2/3*h;            % [m] zero plane displacement height
zom = 0.123*h;         % [m] roughtness length governing momentum transfer
zoh = 0.1*zom;         % [m] roughtness length governing transfer of heat and vapour
cp = 1013;             % [J/(kg*degC)]   specific heat of moist air
epsilon = 0.622;       % [-] ratio molecular weight of water vapour/dry air
rho = 1.29;            % [kg/m^3] the mean air density
a1 = log((zm-d1)/zom);
a2 = log((zh-d1)/zoh);
rs = 70;               % [s/m] grass surface resistance
k = 0.4                % [-] von Karmans constant

% ----------------------------------------Variables------------------------------------------

% % u2                   - [m/s] wind speed at 2m height
% % Ubar_filt            - [m/s] resultant of wind speed at 10m
% % ra                   - [s/m] aerodynamic resistance
% % lambda               - [kJ/kg] latent heat of vaporization
% % ta1                  - [degC] air temperature
% % gamma                - [kPa/degC] psychrometric konstant
% % patm                 - [kPa] atmospheric pressure
% % es                   - [kPa] saturation vapour pressure
% % ea                   - [kPa] air vapour pressure
% % rh                   - [%/100] relative humidity of air
% % delta                - [kPa/degC] slope of saturation vapoure pressure curve
% % Rn                   - [W/m^2] Net radiation
% % G                    - [W/m^2] ground heat flux (corrected)

% ------------------------------- Penman-Monteith equation ---------------------------------

   u2= Ubar_filt.*(4.87/log(67.8*zm-5.42));
   ra = a1.*a2./(k*k*u2);                          % [s/m] aerodynamic resistance
   lambda = (2.501-(2.361/1000)*ta1)*1000;         % [kJ/kg]
   gamma = cp.*(patm./10)/(epsilon.*lambda.*1000);
   es = 0.6108*exp(17.27*ta1./(ta1+237.3));
   ea = rh.*es./100;
   delta = 4098*es./(ta1+237.3)^2;
   Rn = Rn;  G = Gavg;
   A = delta.*(Rn-G) + rho.*cp*(es-ea)/ra;
   B1 = delta+gamma*(1+rs./ra);
   B2 = delta+gamma;
   PET1= A./B1./lambda./1000000*1000*30*60;
   PET2 = A./B2./lambda./1000000*1000*30*60;
```

Appendix 2.2:
Priestley-Taylor equation matlab codes

```
%=======================================================================
%                                Priestley-Taylor equation
%=======================================================================
% -------------------------------------------Constants-------------------------------------------

k = 0.4;                                        % [-] von Karmans constant
ae = 1.26;                                      % [-] Priestley-Taylor factor
r = 0.67;                                       % [kPa/degC] psychrometric constant
smlim=0.48;                                     % transpiration to cease
smwilt=0.08;                                    % vegetation to wilt

% -------------------------------------------Variables-------------------------------------------

% % ta1                    % [degC] air temperature at 3m
% % sm5,10,25,50           % volumetric soil moisture at 5, 10, 25, 50 cm
% % es                     % [kPa] saturation vapour pressure
% % de                     % [kPa/degC] slope of saturation vapoure pressure curve
% % beta                   % soil moisture reduction factor
% % Rn                     % [W/m^2] Net radiation
% % G                      % [W/m^2] ground heat flux (corrected)

% ------------------------------- Priestley-Taylor equation------------------------------------

  for i=1:35040                                 % for two years data
      tr(i)=1.-(373.15/(ta1(i)+273.15));        % Wilfried Brutsaert p.42;215
        es(i)=1013.25*exp(13.3185*(tr(i))-1.9760*((tr(i))^2)-0.6445*((tr(i))^3)-

  0.1299*((tr(i))^4));


        de(i)=373.15*(es(i))/(((ta1(i))+273.15)^2)*(13.3185-3.952*(tr(i))-

  1.9335*((tr(i))^2)-0.5196*((tr(i))^3));


      smm(i)=(sm5(i)+sm10(i)+sm25(i))/3.;
      smlim=0.48;
      smwilt=0.08;
      if (smm(i) >= smlim)
       beta(i)=1.;
       elseif (smm(i) > smwilt)
       beta(i)=(smm(i)-smwilt)/(smlim-smwilt);
       else
       beta(i)=0.;
      end
   lept(i)=beta(i)*ae*(de(i)/(de(i)+r))*(Rn(i) - Gavg(i));
 end


%=======================================================================
```

Appendix 3

Contribution of Webb correction to CO_2 flux

Contribution of Webb correction to CO_2 flux in 2002

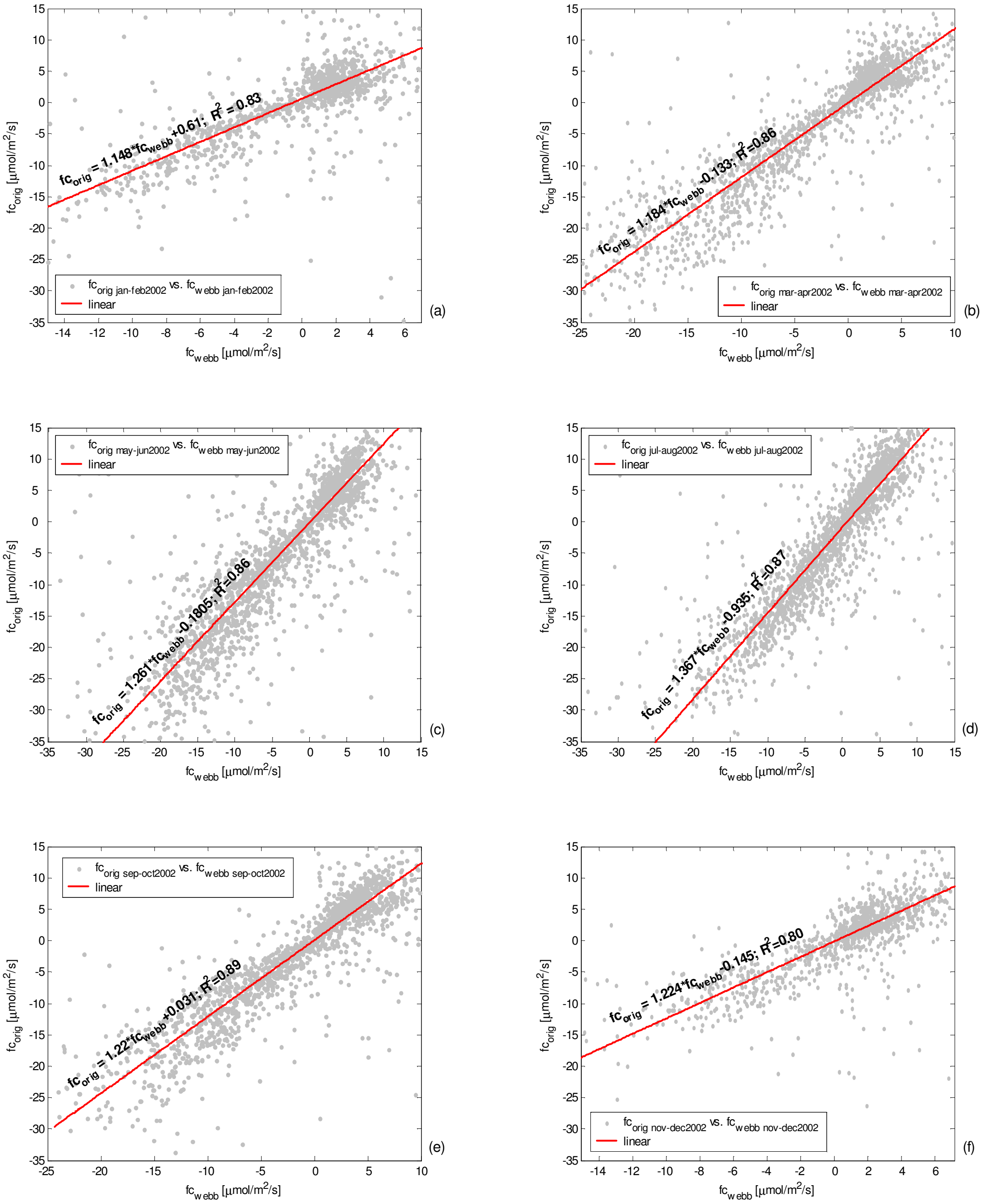

Figure A3.1: Contributions of Webb correction to final CO_2 flux two by two months in 2002 for: (a) January-February; (b) March-April; (c) May-June; (d) July-August; (e) September-October; (f) November-December

Contribution of Webb correction to CO_2 flux in 2003

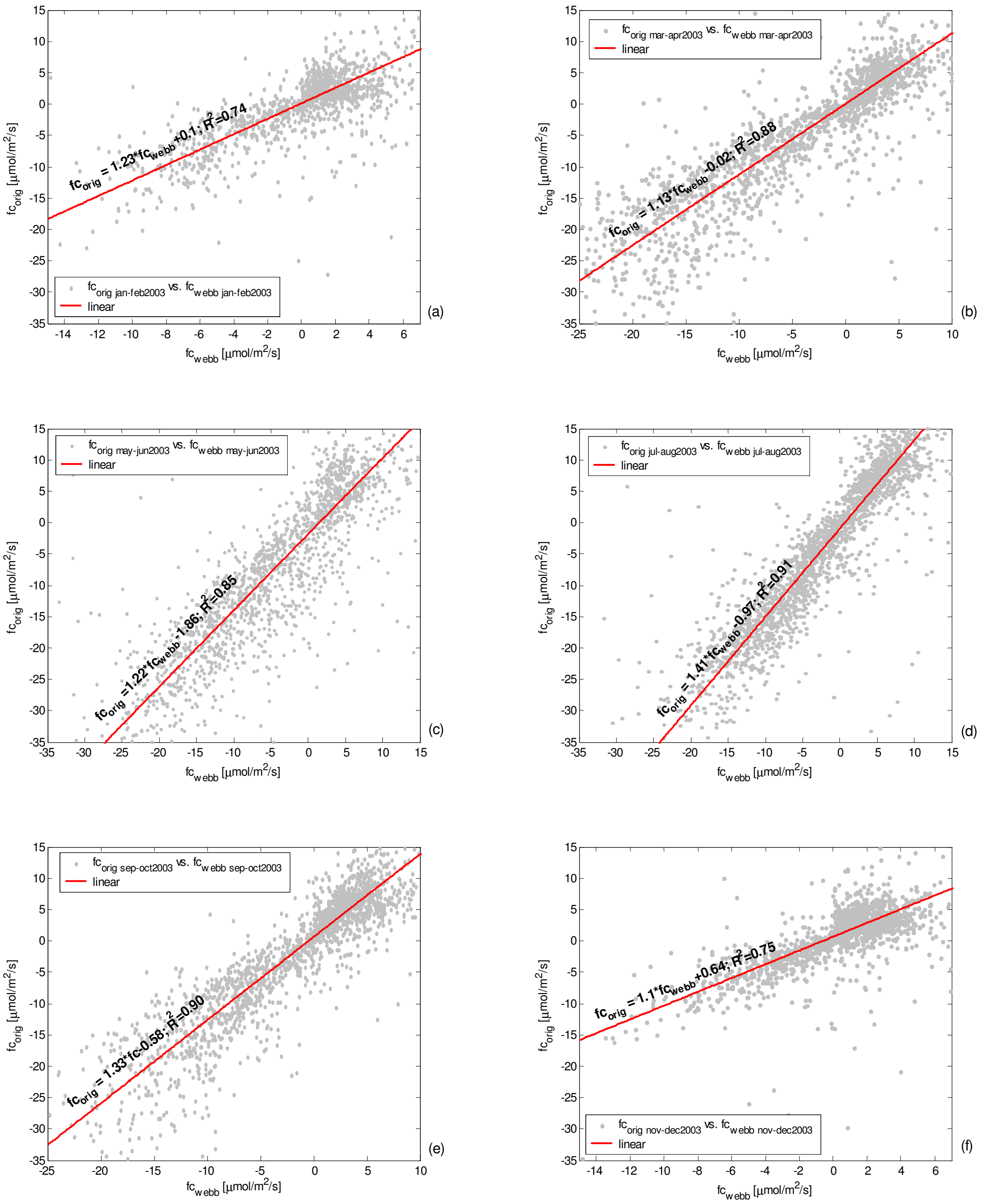

Figure A3.2: Contributions of Webb correction to final CO_2 flux two by two months in 2003 for: (a) January-February; (b) March-April; (c) May-June; (d) July-August; (e) September-October; (f) November-December

Appendix 4.1

Daytime fitting for 2002

❖ January - February 2002

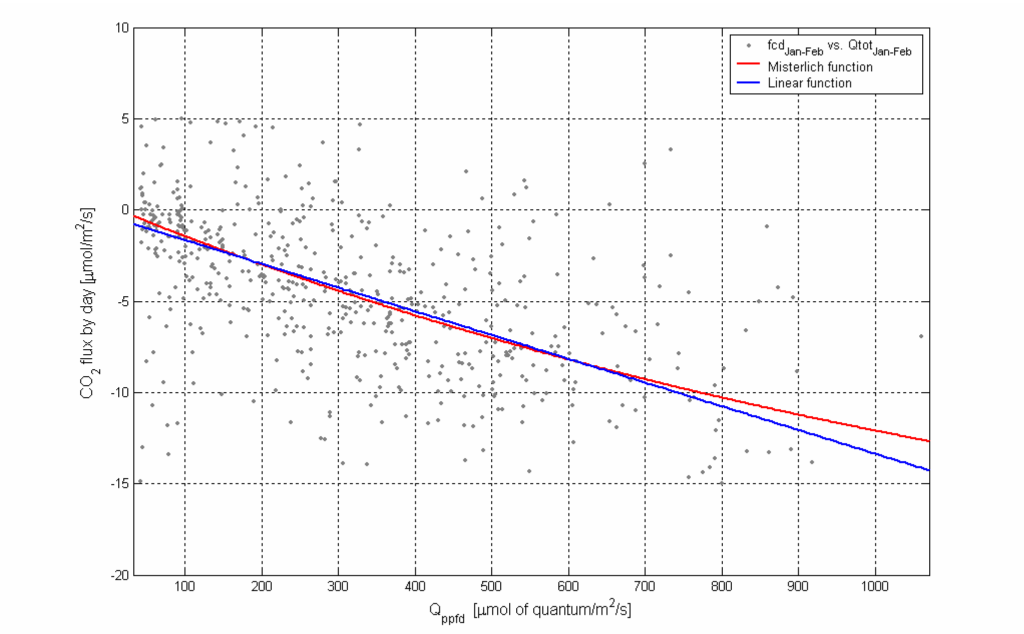

Figure A4.1.1: Best daytime fitting curves for January and February 2002

Table A4.1.1: Fitting function for daytime for January and February 2002

	Equation	Coefficients	SEE	R^2	Ad. R^2	RMSE
Ruimy func.	$F_d = \frac{\alpha\times Q_{par}\times\beta}{(\alpha\times Q_{par}+\beta)}+\gamma$	α = -50.23 ± 6.5e8 β = 0.174 ± 1.1e6 γ = -4.76 ± 1.1e6	6608	9.53e-7	-0.0042	3.746
Michaelis function	$F_d = \frac{\alpha\times Q_{par}}{\left(1-\frac{Q_{par}}{2000}+\frac{\alpha\times Q_{par}}{\beta}\right)}+\gamma$	α = -5.686 ± 7.5e7 β = -0.08 ± 5.5e5 γ = -4.498 ± 5.5e5	6608	1.94e-6	-0.0042	3.746
Smith func.	$F_d = \frac{\alpha\times\beta\times Q_{par}}{\sqrt{\beta^2+(\alpha\times Q_{par})^2}}+\gamma$	α = 0.006 ± 0.017 β = -1.64 ± 1.42 γ = -3.038 ± 1.64	5851	0.115	0.1108	3.525
Linear func.	$F_d = \alpha\times Q_{par}+\beta$	α = -0.013 ± 0.001 β = -0.367 ± 0.45	3312	0.499	0.4978	2.649
Misterlich function	$F_d = -24\times\left(1-e^{\left(\frac{\alpha\times Q_{par}}{-24}\right)}\right)+\gamma$	α = 0.0173 ± 0.002 γ = 0.217 ± 0.54	3252	0.508	0.5069	2.625

❖ March - April 2002

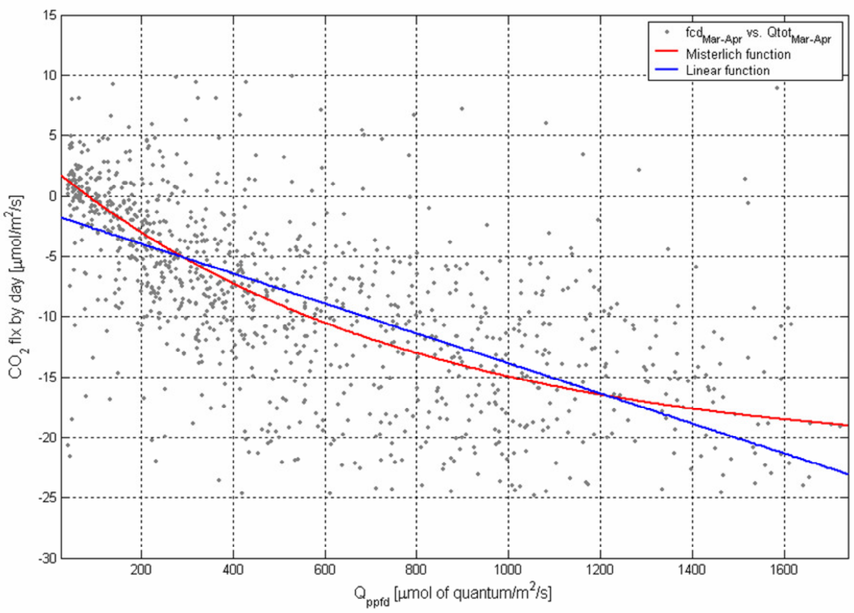

Figure A4.1.2: Best daytime fitting curves for March and April 2002

Table A4.1.2: Fitting function for daytime for March and April 2002

	Equation	Coefficients	SEE	R^2	Ad. R^2	RMSE
Ruimy func.	$F_d = \frac{\alpha\times Q_{par}\times\beta}{(\alpha\times Q_{par}+\beta)}+\gamma$	α = -3886 ±1.6e10 β = 16.24 ± 3.4e7 γ = -24.7 ± 3.4e7	5.0e4	5.28e-5	-0.002	7.155
Michaelis function	$F_d = \frac{\alpha\times Q_{par}}{\left(1-\frac{Q_{par}}{2000}+\frac{\alpha\times Q_{par}}{\beta}\right)}+\gamma$	α = -1.3e4 ± 5.8e9 β = 159.9 ± 3.6e7 c = -168.4 ± 3.6e7	5.0e4	0.0015	-0.0005	7.15
Smith func.	$F_d = \frac{\alpha\times\beta\times Q_{par}}{\sqrt{\beta^2+(\alpha\times Q_{par})^2}}+\gamma$	α = -1.97 ± 9.97e6 β = -2.72 ± 9.2e6 γ = -11.18 ± 9.2e6	5.0e4	-3.0e-5	-0.0021	7.156
Linear func.	$F_d = \alpha\times Q_{par}+\beta$	α =-0.012±0.0008 β = -1.486 ± 0.54	2.5e4	0.4986	0.4981	5.064
Misterlich function	$F_d = -24\times\left(1-e^{\left(\frac{\alpha\times Q_{par}}{-24}\right)}\right)+\gamma$	α = 0.031 ±0.004 γ = 2.525 ± 0.95	2.2e4	0.5529	0.5524	4.782

❖ **May - June 2002**

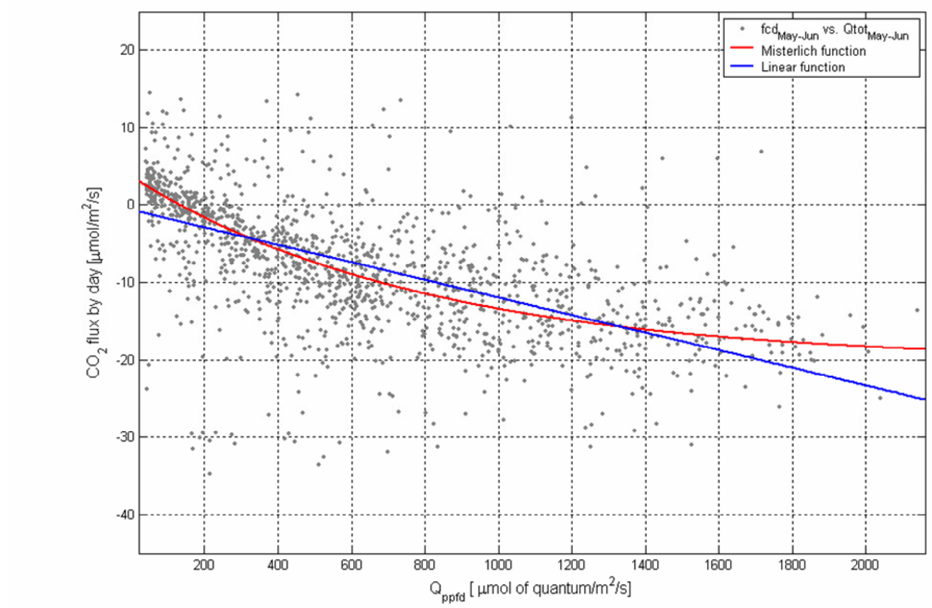

Figure A4.1.3: Best daytime fitting curves for May and June 2002

Table A4.1.3: Fitting function for daytime for May and June 2002

	Equation	Coefficients	SEE	R^2	Ad. R^2	RMSE
Ruimy func.	$F_d = \frac{\alpha\times Q_{par}\times\beta}{(\alpha\times Q_{par}+\beta)}+\gamma$	α = -3308 ±1.8e10 β = 13.2 ± 3.7e7 γ = -21.24± 3.7e7	7.1e4	3.8e-5	-0.0015	7.449
Michaelis function	$F_d = \frac{\alpha\times Q_{par}}{\left(1-\frac{Q_{par}}{2000}+\frac{\alpha\times Q_{par}}{\beta}\right)}+\gamma$	α = -1.0e4±1.7e10 β = 44.37 ± 3.7e7 γ = -52.42 ± 3.7e7	7.1e4	0.0001	-0.0014	7.448
Smith func.	$F_d = \frac{\alpha\times\beta\times Q_{par}}{\sqrt{\beta^2+(\alpha\times Q_{par})^2}}+\gamma$	α = 82.56 ± 1.8e8 β = -21.64± 2.1e7 γ = -13.59± 3.1e7	7.1e4	7.88e-6	-0.0016	7.449
Linear func.	$F_d = \alpha\times Q_{par}+\beta$	α =-0.011±0.0006 β = -0.630 ± 0.50	3.5e4	0.4965	0.4965	5.281

Misterlich function	$F_d = -24\times\left(1-e^{\left(\frac{\alpha\times Q_{par}}{-24}\right)}\right)+\gamma$	α = 0.030 ±0.004 γ = 3.703 ± 0.88	3.1e4	0.5541	0.5537	4.972

- **July - August 2002**

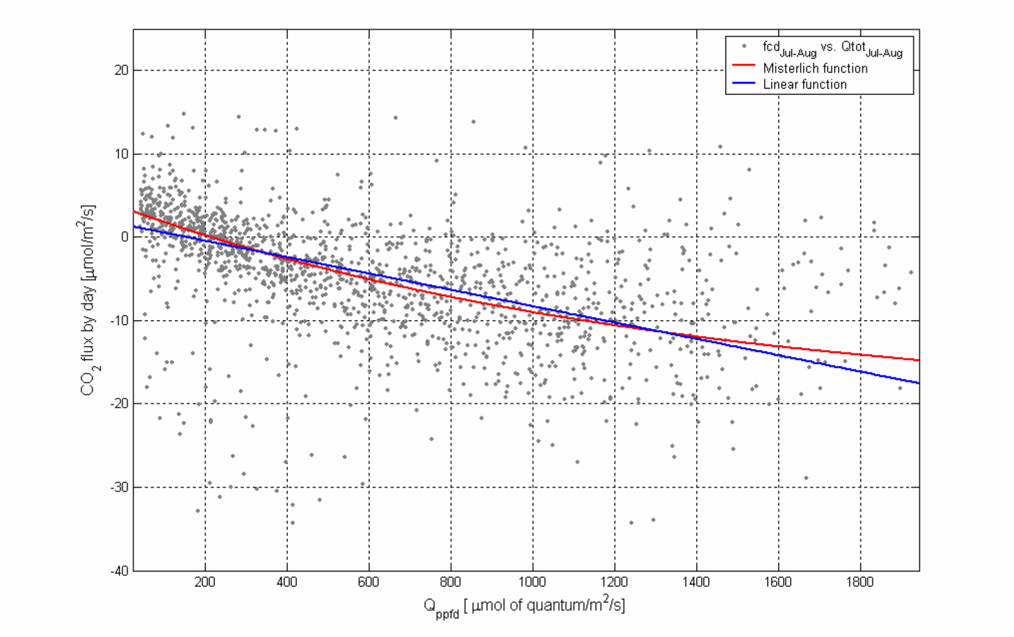

Figure A4.1.4: Best daytime fitting curves for July and August 2002

Table A4.1.4: Fitting function for daytime for July and August 2002

	Equation	Coefficients	SEE	R^2	Ad. R^2	RMSE
Ruimy func.	$F_d = \frac{\alpha\times Q_{par}\times\beta}{(\alpha\times Q_{par}+\beta)}+\gamma$	α = -50.21 ±4.4e8 β = 0.156 ± 6.8e5 γ = -4.661± 6.8e5	4.9e4	3.85e-7	-1.5e-3	6.01
Michaelis function	$F_d = \frac{\alpha\times Q_{par}}{\left(1-\frac{Q_{par}}{2000}+\frac{\alpha\times Q_{par}}{\beta}\right)}+\gamma$	α = -1.3e4±1.5e10 β = 48.62 ± 3.0e7 γ = -53.13± 3.0e7	4.9e4	1.51e-4	1.32e-3	6.01
Smith func.	$F_d = \frac{\alpha\times\beta\times Q_{par}}{\sqrt{\beta^2+(\alpha\times Q_{par})^2}}+\gamma$	α = 29.38 ± 2.0e8 β = -3.636± 1.7e7 γ = -0.87± 1.67e7	4.9e4	2.93e-7	-1.5e-3	6.01

Linear func.	$F_d = \alpha \times Q_{par} + \beta$	α =-0.01±0.0005 β = 1.495 ± 0.40	2.5e4	0.4811	0.481	4.328
Misterlich function	$F_d = -24 \times \left(1 - e^{\left(\frac{\alpha \times Q_{par}}{-24}\right)}\right) + \gamma$	α = 0.018 ±0.001 γ = 3.501 ± 0.55	2.3e4	0.5215	0.521	4.156

❖ **September - October 2002**

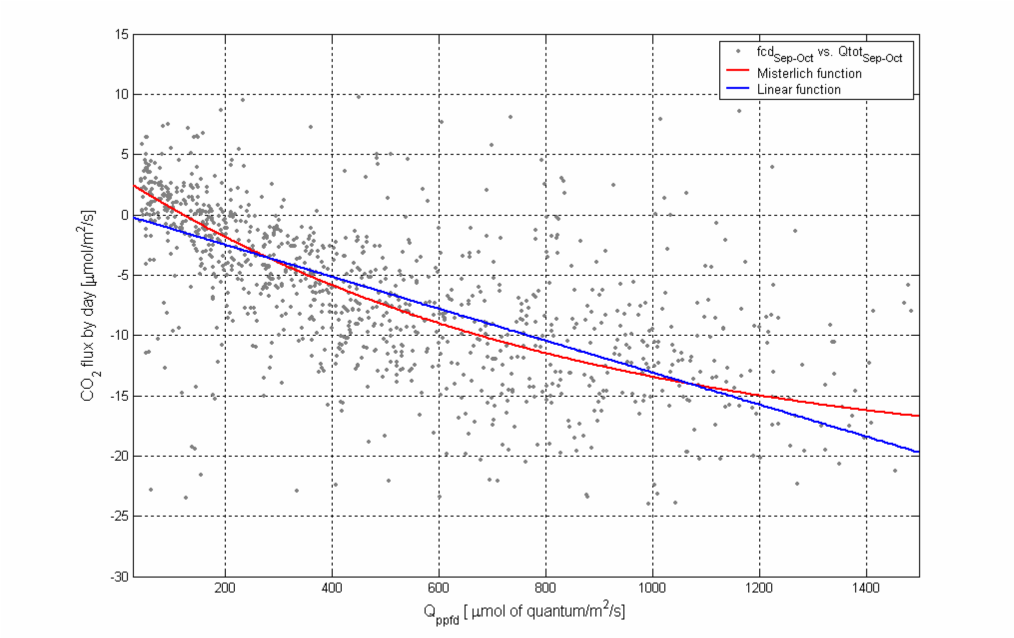

Figure A4.1.5: Best daytime fitting curves for September and October 2002

Table A4.1.5: Fitting function for daytime for September and October 2002

	Equation	Coefficients	SEE	R^2	Ad. R^2	RMSE
Ruimy func.	$F_d = \frac{\alpha \times Q_{par} \times \beta}{(\alpha \times Q_{par} + \beta)} + \gamma$	α = -5531 ±1.6e10 β = 26.36 ±3.84e7 γ = -32.86±3.84e7	3.7e4	1.18e4	-1.9e-3	6.17
Michaelis function	$F_d = \frac{\alpha \times Q_{par}}{\left(1 - \frac{Q_{par}}{2000} + \frac{\alpha \times Q_{par}}{\beta}\right)} + \gamma$	α = -31.24±1.55e8 β = 0.504 ±2.86e6 γ = -7.0 ± 2.86e6	3.7e4	7.60e-6	-2.1e-3	6.171

	Equation	Coefficients	SEE	R^2	Ad. R^2	RMSE
Smith func.	$F_d = \frac{\alpha\times\beta\times Q_{par}}{\sqrt{\beta^2+(\alpha\times Q_{par})^2}}+\gamma$	α = -9.37 ± 5.79e7 β = -2.06 ±8.48e6 γ = -8.56 ± 8.48e6	3.7e4	-6.7e-7	-2.1e-3	6.171
Linear func.	$F_d = \alpha\times Q_{par}+\beta$	α =-0.013±0.0008 β = 0.14 ± 0.462	1.7e4	0.5454	0.5449	4.158
Misterlich function	$F_d = -24\times\left(1-e^{\left(\frac{\alpha\times Q_{par}}{-24}\right)}\right)+\gamma$	α = 0.029 ±0.003 γ = 3.24 ± 0.717	1.5e4	0.661	0.6005	3.896

❖ **November - December 2002**

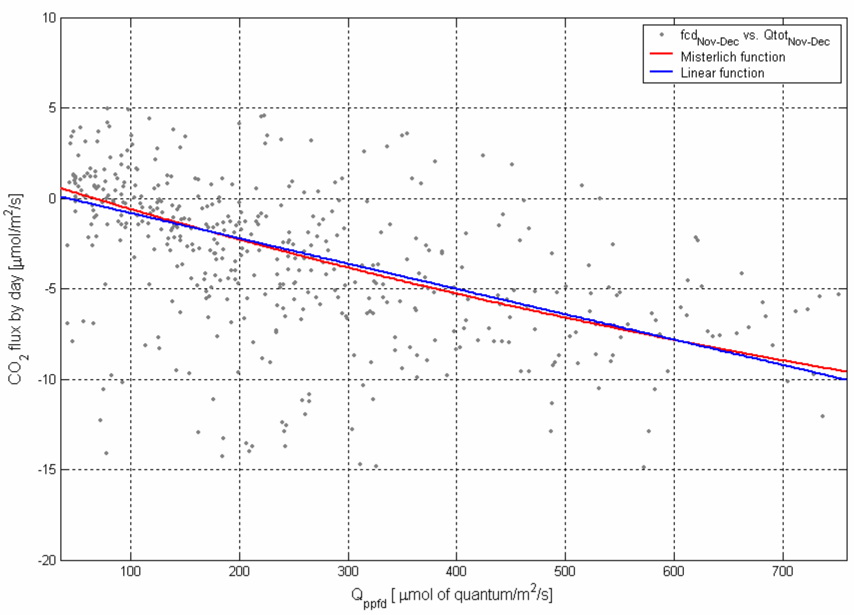

Figure A4.1.6: Best daytime fitting curves for November and December 2002

Table A4.1.6: Fitting function for daytime for November and December 2002

	Equation	Coefficients	SEE	R^2	Ad. R^2	RMSE
Ruimy func.	$F_d = \frac{\alpha\times Q_{par}\times\beta}{(\alpha\times Q_{par}+\beta)}+\gamma$	α = 38.21 ± 4.2e8 β = 1.05 ± 5.71e6 γ = -4.121± 5.7e6	4514	-5.6e-5	-0.0052	3.407

Appendix 4.1 Daytime

fitting for 2002

Michaelis function	$F_d = \frac{\alpha \times Q_{par}}{\left(1 - \frac{Q_{par}}{2000} + \frac{\alpha \times Q_{par}}{\beta}\right)} + \gamma$	α = 27.8 ± 2.45e8 β = 1.18 ± 5.19e6 γ = -4.2 ± 5.2e6	4515	-9.7e-5	-0.0052	3.407
Smith func.	$F_d = \frac{\alpha \times \beta \times Q_{par}}{\sqrt{\beta^2 + (\alpha \times Q_{par})^2}} + \gamma$	α = 24.73 ± 3.5e8 β = -1.3 ± 1.21e7 γ = -1.77 ± 1.21e7	4514	6.0e-8	-0.0051	3.407
Linear func.	$F_d = \alpha \times Q_{par} + \beta$	α =-0.014±0.0014 β = 0.571 ± 0.436	2270	0.497	0.4958	2.413
Misterlich function	$F_d = -24 \times \left(1 - e^{\left(\frac{\alpha \times Q_{par}}{-24}\right)}\right) + \gamma$	α = 0.019 ± 0.002 γ = 1.212 ± 0.514	2171	0.519	0.5179	2.359

Appendix 4.2

Daytime fitting for 2003

❖ January - February 2003

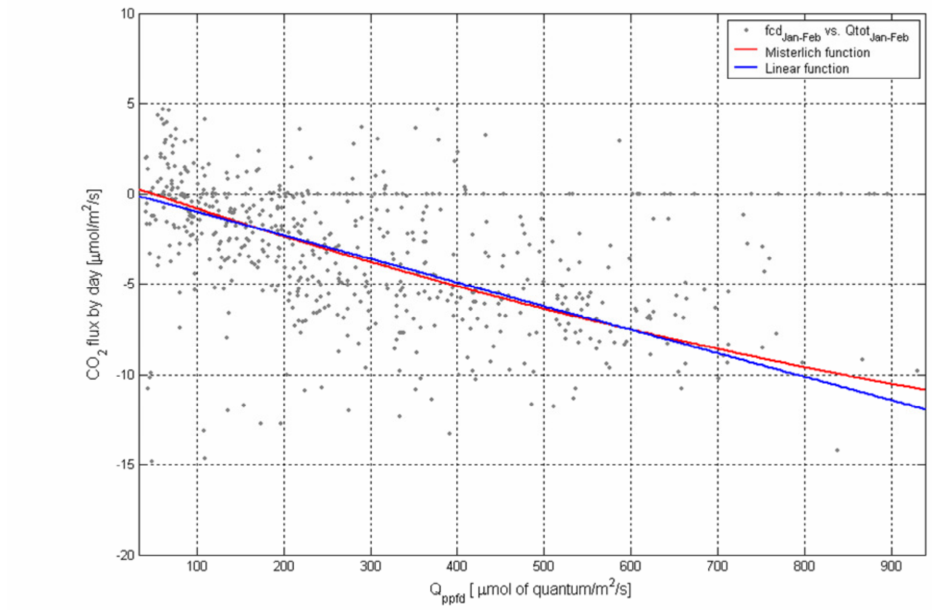

Figure A4.2.1: Best daytime fitting curves for January and February 2003

Table A4.2.1: Fitting function for daytime for January and February 2003

	Equation	Coefficients	SEE	R^2	Ad. R^2	RMSE
Ruimy func.	$F_d = \frac{\alpha \times Q_{par} \times \beta}{(\alpha \times Q_{par} + \beta)} + \gamma$	α = 51.27 ± 6.1e8 β = 0.889 ± 5.2e6 γ = -4.31 ± 5.2e6	6329	-2.7e-5	-0.0036	3.377
Michaelis function	$F_d = \frac{\alpha \times Q_{par}}{\left(1 - \frac{Q_{par}}{2000} + \frac{\alpha \times Q_{par}}{\beta}\right)} + \gamma$	α = 72.09 ± 6.7e8 β = 1.54 ± 7.14e6 γ = -4.97 ± 7.14e6	6329	-5.8e-5	-0.0037	3.377
Smith func.	$F_d = \frac{\alpha \times \beta \times Q_{par}}{\sqrt{\beta^2 + (\alpha \times Q_{par})^2}} + \gamma$	α = 11.44 ± 8.3e7 β = -4.08 ± 2.0e7 γ = 0.646 ± 2.0e7	6329	7.50e-6	-0.0036	3.377
Linear func.	$F_d = \alpha \times Q_{par} + \beta$	α = -0.013 ±0.011 β = -0.279 ± 0.37	3146	0.503	0.5021	2.379
Misterlich function	$F_d = -24 \times \left(1 - e^{\left(\frac{\alpha \times Q_{par}}{-24}\right)}\right) + \gamma$	α = 0.0171 ±0.002 γ = 0.809 ± 0.431	3069	0.5151	0.5143	2.349

❖ March - April 2003

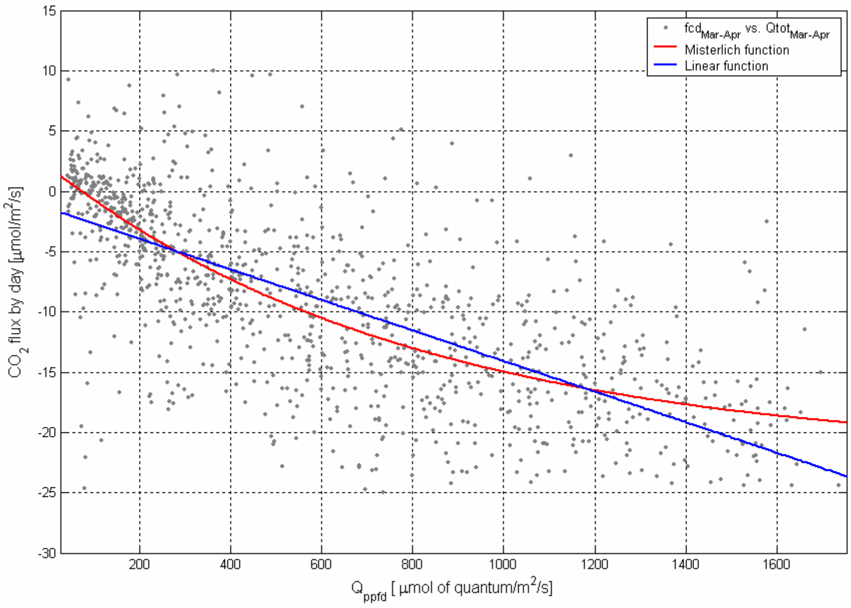

Figure A4.2.2: Best daytime fitting curves for March and April 2003

Table A4.2.2: Fitting function for daytime for March and April 2003

	Equation	Coefficients	SEE	R^2	Ad. R^2	RMSE
Ruimy func.	$F_d = \frac{\alpha\times Q_{par}\times\beta}{(\alpha\times Q_{par}+\beta)}+\gamma$	α = -5426 ±1.1e10 β = 33.10 ± 3.3e7 γ = -42.2 ± 3.3e7	5.6e4	1.35e4	-0.0018	7.384
Michaelis function	$F_d = \frac{\alpha\times Q_{par}}{\left(1-\frac{Q_{par}}{2000}+\frac{\alpha\times Q_{par}}{\beta}\right)}+\gamma$	α = -1.4e4±1.3e10 β = 89.01 ± 4.1e7 γ = -98.07 ± 4.1e7	5.6e4	3.70e4	-0.0016	7.383
Smith func.	$F_d = \frac{\alpha\times\beta\times Q_{par}}{\sqrt{\beta^2+(\alpha\times Q_{par})^2}}+\gamma$	α = 6.992 ± 3.6e7 β = -4.12 ± 1.4e7 γ = -4.94 ± 1.4e7	5.6e4	6.09e-6	-0.0019	7.384
Linear func.	$F_d = \alpha\times Q_{par}+\beta$	α =-0.013±0.0007 β = -1.422 ± 0.53	2.6e4	0.5381	0.5377	5.016
Misterlich function	$F_d = -24\times\left(1-e^{\left(\frac{\alpha\times Q_{par}}{-24}\right)}\right)+\gamma$	α = 0.0298 ±0.004 γ = 2.088 ± 0.93	2.4e4	0.5781	0.5776	4.794

❖ May - June 2003

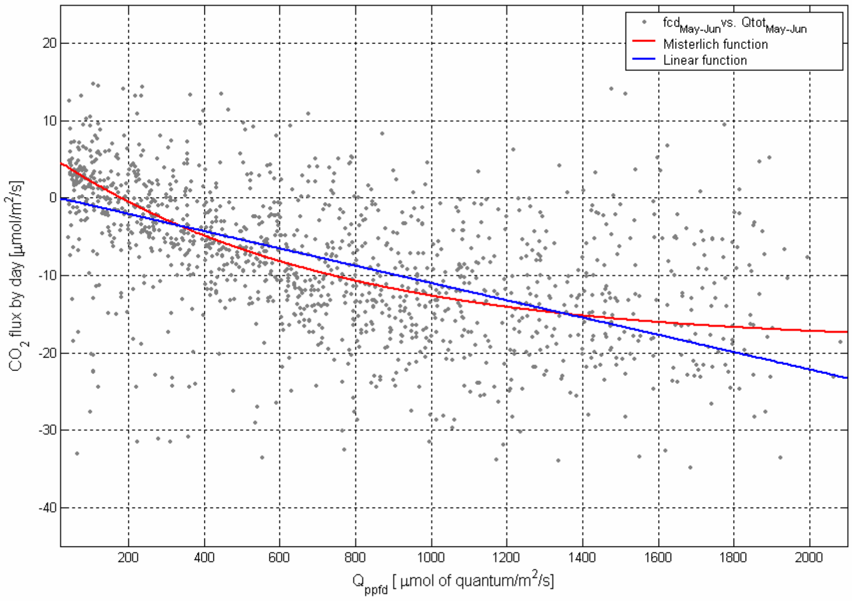

Figure A4.2.3: Best daytime fitting curves for May and June 2003

Table A4.2.3: Fitting function for daytime for May and June 2003

	Equation	Coefficients	SEE	R^2	Ad. R^2	RMSE
Ruimy func.	$F_d = \frac{\alpha \times Q_{par} \times \beta}{(\alpha \times Q_{par} + \beta)} + \gamma$	α = -5233 ±2.2e10 β = 17.9 ± 3.7e7 γ = -26.2± 3.7e7	8.4e4	3.26e-5	-0.0016	8.388
Michaelis function	$F_d = \frac{\alpha \times Q_{par}}{\left(1 - \frac{Q_{par}}{2000} + \frac{\alpha \times Q_{par}}{\beta}\right)} + \gamma$	α = -7927±1.6e10 β = 38.87 ± 4.0e7 γ = -47.12 ± 4.0e7	8.4e4	0.0001	-0.0016	8.388
Smith func.	$F_d = \frac{\alpha \times \beta \times Q_{par}}{\sqrt{\beta^2 + (\alpha \times Q_{par})^2}} + \gamma$	α = -2.35 ± 1.1e7 β = -2.804± 8.9e6 γ = -11.06± 8.9e6	8.4e4	-1.4e-5	-0.0017	8.388
Linear func.	$F_d = \alpha \times Q_{par} + \beta$	α =-0.011±0.0007 β = 0.1594 ± 0.65	4.7e4	0.4376	0.4371	6.288

Misterlich function	$F_d = -24\times\left(1-e^{\left(\frac{\alpha\times Q_{par}}{-24}\right)}\right)+\gamma$	α = 0.033 ±0.005 γ = 5.243 ± 1.19	4.3e4	0.4938	0.4934	5.965

❖ July - August 2003

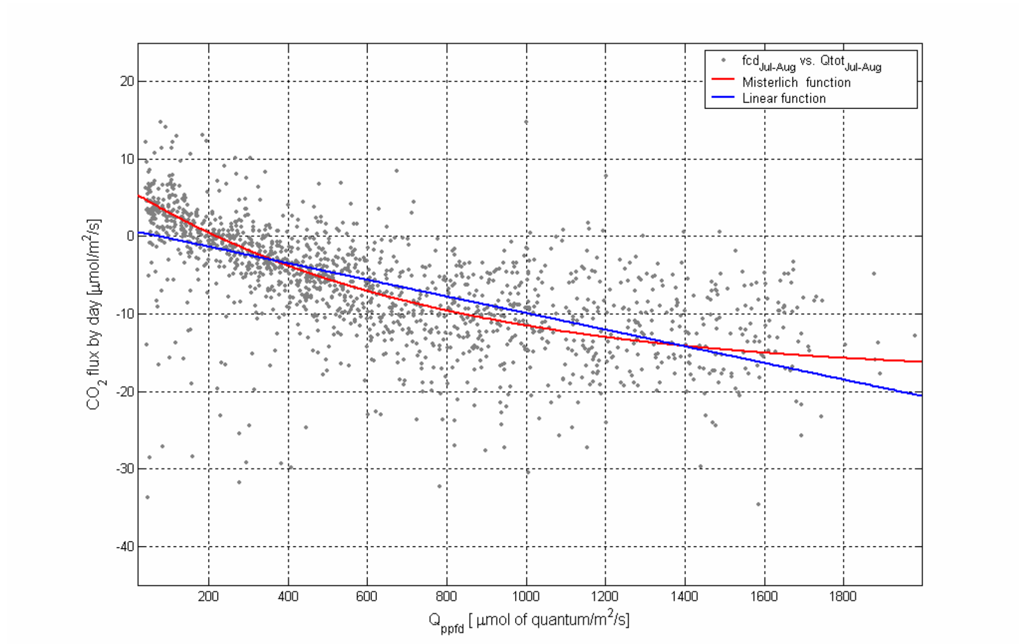

Figure A4.2.4: Best daytime fitting curves for July and August 2003

Table A4.2.4: Fitting function for daytime for July and August 2003

	Equation	Coefficients	SEE	R^2	Ad. R^2	RMSE
Ruimy func.	$F_d = \frac{\alpha\times Q_{par}\times\beta}{(\alpha\times Q_{par}+\beta)}+\gamma$	α = -1.09e4±6.6e9 β = 98.48 ± 3.0e7 γ = -104.8 ± 3.0e7	6.3e4	6.4e-4	-0.0008	6.758
Michaelis function	$F_d = \frac{\alpha\times Q_{par}}{\left(1-\frac{Q_{par}}{2000}+\frac{\alpha\times Q_{par}}{\beta}\right)}+\gamma$	α = -6432 ±2.0e10 β = 20.85 ± 3.2e7 γ = -27.19± 3.2e7	6.3e4	4.9e-5	-0.0014	6.76
Smith func.	$F_d = \frac{\alpha\times\beta\times Q_{par}}{\sqrt{\beta^2+(\alpha\times Q_{par})^2}}+\gamma$	α = 4.043 ± 3.8e7 β = -1.13 ± 7.1e6 γ = -5.21 ± 7.1e6	6.3e4	4.2e-7	-0.0015	6.76

Linear func.	$F_d = \alpha \times Q_{par} + \beta$	α =-0.01 ± 0.0006 β = 0.811 ± 0.448	3.1e4	0.5065	0.5061	4.747
Misterlich function	$F_d = -24 \times \left(1 - e^{\left(\frac{\alpha \times Q_{par}}{-24}\right)}\right) + \gamma$	α = 0.032 ±0.004 γ = 6.039 ± 0.827	2.6e4	0.5792	0.5789	4.383

❖ **September - October 2003**

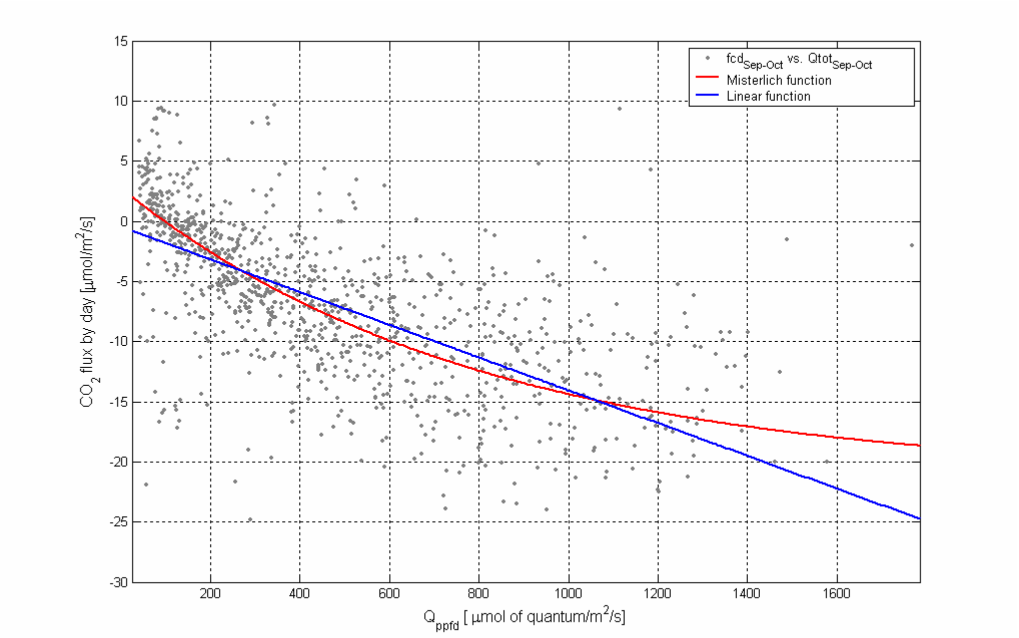

Figure A4.2.5: Best daytime fitting curves for September and October 2003

Table A4.2.5: Fitting function for daytime for September and October 2003

	Equation	Coefficients	SEE	R^2	Ad. R^2	RMSE
Ruimy func.	$F_d = \frac{\alpha \times Q_{par} \times \beta}{(\alpha \times Q_{par} + \beta)} + \gamma$	α = -2537 ±1.6e10 β = 9.46 ± 3.04e7 γ = -16.52±3.04e7	4.1e4	3.14e-5	-0.0019	6.325
Michaelis function	$F_d = \frac{\alpha \times Q_{par}}{\left(1 - \frac{Q_{par}}{2000} + \frac{\alpha \times Q_{par}}{\beta}\right)} + \gamma$	α = -6131 ±1.9e10 β = 21.76 ± 3.4e7 γ = -28.82 ± 3.4e7	4.1e4	6.87e-5	-0.0019	6.325

Smith func.	$F_d = \frac{\alpha\times\beta\times Q_{par}}{\sqrt{\beta^2+(\alpha\times Q_{par})^2}}+\gamma$	α =-1.6e-3±6.5e-3 β =0.761 ± 1.493 γ = -6.29 ± 1.561	3.9e4	0.0440	0.0422	6.185
Linear func.	$F_d = \alpha\times Q_{par}+\beta$	α =-0.014±0.0008 β = -0.458 ± 0.45	1.9e4	0.5397	0.5393	4.289
Misterlich function	$F_d = -24\times\left(1-e^{\left(\frac{\alpha\times Q_{par}}{-24}\right)}\right)+\gamma$	α = 0.030 ±0.003 γ = 2.788 ± 0.736	1.7e4	0.5938	0.5934	4.029

❖ **November - December 2003**

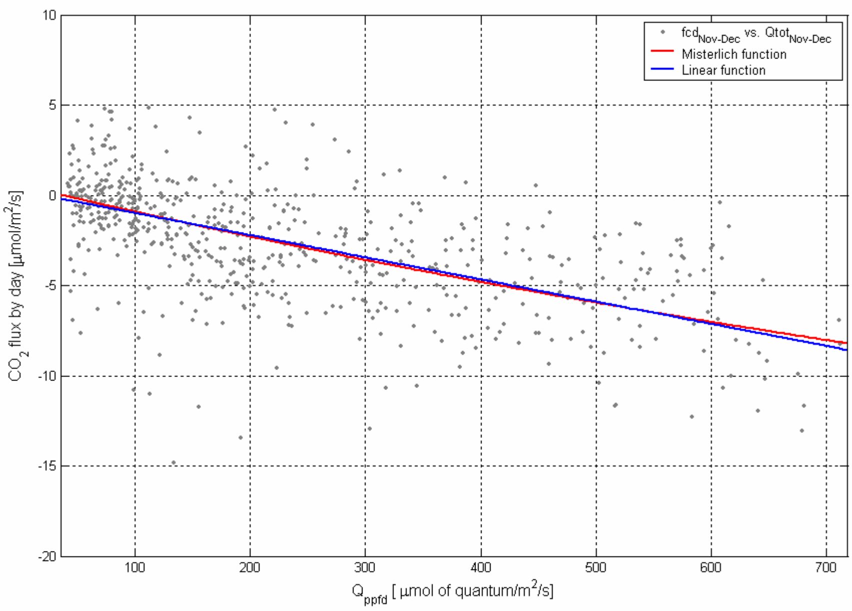

Figure A4.2.6: Best daytime fitting curves for November and December 2003

Table A4.2.6: Fitting function for daytime for November and December 2003

	Equation	Coefficients	SEE	R^2	Ad. R^2	RMSE
Ruimy func.	$F_d = \frac{\alpha\times Q_{par}\times\beta}{(\alpha\times Q_{par}+\beta)}+\gamma$	α = 33.27 ± 1.8e8 β = 1.34 ± 3.63e6 γ = -4.04± 3.63e6	4729	-1.3e-4	-0.0038	2.935

fitting for 2003

Michaelis function	$F_d = \dfrac{\alpha \times Q_{par}}{\left(1 - \dfrac{Q_{par}}{2000} + \dfrac{\alpha \times Q_{par}}{\beta}\right)} + \gamma$	α = 27.86 ± 8.9e7 β = 1.52 ± 2.43e6 γ = -4.22 ± 2.43e6	4730	-2.1e-4	-0.0039	2.935
Smith func.	$F_d = \dfrac{\alpha \times \beta \times Q_{par}}{\sqrt{\beta^2 + (\alpha \times Q_{par})^2}} + \gamma$	α = 9.59 ± 7.72e7 β = -1.46 ± 7.8e6 γ = -1.24 ± 7.8e6	4729	7.43e-7	-0.0036	2.935
Linear func.	$F_d = \alpha \times Q_{par} + \beta$	α =-0.012±0.0012 β = 0.230 ± 0.298	2344	0.5043	0.5034	2.064
Misterlich function	$F_d = -24 \times \left(1 - e^{\left(\frac{\alpha \times Q_{par}}{-24}\right)}\right) + \gamma$	α = 0.015 ± 0.002 γ = 0.544 ± 0.334	2298	0.514	0.5131	2.044

Appendix 5

Parameters for CO_2 flux modelling

Table A5.1: Parameters for Jacob's and Collatz's models [Le Bris, 2002] (pp 163-166)

Notation	Description	Value	Units	Source
A_g	gross assimilation rate	Equ(4.9) Equ(4.4)	µmol/m^2/s	Collatz Jacobs
A_m	the photosynthetic rate at light saturation	Equ(4.20)	mg/m^2/s	
A_{m_max}(@25)	maximum value for Am @ 25 °C	2.4	mg/m^2/s	
A_n	Net assimilation	Equ(4.10) Equ(4.19)	µmol/m^2/s	Collatz Jacobs
b_gs	intercept in B-B model	0.003	mol/m^2/s	Ball-Berry
Ca	ambient CO_2 conc	380	ppm	
Ci_{min}	minimum Ci when stomata are closed from water stress	190	ppm	Farquhar
Co	oxygen concentration in air	210000 air	µmol/mol	
Cp		1005	J/kg air/C	
D_{max}	maximum vapor pressure deficit	45	g/kg	Jacobs
Ds	vapor pressure deficit	1000(q_{asat}. -q_a.)	g/kg	Jacobs
e_m	maximum moles CO_2 fixed per quantum PAR	0.08	mol/quantum	Farquhar
f_o	f factor value for Ds=0g/k	0.85 0.94	unit less	Jacobs This case
g_c	cuticular conductance	0.25	mm/s	
g_m(@25)	mesophyll conductance @ 25°C	7.0	mm/s	

Notation	Description	Value	Units	Source
g_s	Stomatal conductance for water vapor	Equ(4.14) Equ(4.30)	$mol/m^2/s$ mm/s	Collatz Jacobs
g_{sc}	Stomatal conductance for CO_2	Equ(4.28)	mm/s	
hs	humidity @ leaf surface		decimal fraction	
Jc	Rubisco-limited rate	Equ(4.7)	$\mu mol/m^2/s$	Collatz
Je	Light-limited rate	Equ(4.6)	$\mu mol/m^2/s$	Collatz
J_{max}**(@25)**	light saturated potential rate of electron @ 25 ° C	210	$\mu Eq/m^2/s$	Farquhar
Js	Sucrose-limited rate	Equ(4.8)	$\mu mol/m^2/s$	Collatz
k	stefan boltzmann constant	5.67e-8		
Kc(@25)	Michaelis constant for CO_2 fixation at @ 25°C	460	µmol/mol	Farquhar
Ko(@25)	Michaelis constant for O_2 fixation at @ 25°C	330000	µmol/mol	Farquhar
lai	Leaf area index	1.5		This case
Lv		2450	J/gH_2O	
m	Ball-Berry constant	5.6 6.75		Ball-Berry This case
m_{air}	molecular weight of air	28.97	g/mol	
m_c	molecular weight of carbon dioxide	44.0098	g/mol	
Mc	molecular weight of carbon	12	g/mol	
m_v	molecular weight of water	18.02	g/mol	
P	atmospheric pressure	1013	mb	

Notation	Description	Value	Units	Source
$q(\tau)$	temperature coefficient for τ	-0.041 -0.056 -0.02	unit less	Farquhar Collatz (C_4grass) Thid case
$q(J_{max})$	temperature coefficient for Jmax	0.0524	unit less	Farquhar
$q(K_c)$	temperature coefficient for K_c	0.084 0.074 0.07	unit less	Farquhar Collatz (C_4grass) This case
$q(K_o)$	temperature coefficient for K_o	0.051 0.018 0.05	unit less	Farquhar Collatz (C_4grass) This case
$q(R_d)$	temp coeff for Rd	0.094	unit less	Farquhar
$Q10(\Gamma)$	Q_{10} coefficient for Γ	1.5 1.2	unit less	Jacobs This case
$Q10(A_{m,max})$	Q_{10} coefficient for $A_{m,max}$	2 1.6	unit less	Jacobs This case
$Q10(g_m)$	Q_{10} coefficient for g_m	2 1.6	unit less	Jacobs This case
qa	specific air humidity		kg/kg	
$R_{\_gas}$	universal gas constant	8.314	J/mol/K	
R_a	gas constant for air	287.05	J/kg/K	
Rd(@25)	0.015*Vm(@25)	1.1	$\mu mol/m^2/s$	Farquhar
R_v	gas constant for vapour pressure	461.51	J/kg/K	
V_m(@25)	maximum carboxylation velocity at @ 25°C	98	$\mu mol/m^2/s$	Farquhar
α_{PAR}	leaf absorptivity	0.8		Farquhar

Notation	Description	Value	Units	Source
Γ(@25)	compensation point @ 25°C	45	ppm	Jacobs
ε_o	maximum quantum use efficiency	0.017	mg/J	Jacobs
ρ	superficial density of chlorophyll	0.45	g/m^2	
ρ_a	density of air		kg/kg	
ρ_g	molar density of any gases	44.6	mol/m^3	
ρ_v	density of water	1e6	g/m^3	
τ(@25)	Ratio of partitioning between carboxylase and oxigenase reactions of Rubisco	3416		Farquhar
φ_c	conversion factor transforming [CO2]	Equ(4.21)	from ppm into mg/m^3	Jacobs

Appendix 6

Wexford grassland

Appendix 6

Table of Contents

A6.1 Introduction

A6.1.1 Methods

The Wexford flux site, Southwest Ireland, is a perennial ryegrass (C3 category) pasture, very typical of the vegetation of this part of the country. The flux tower monitoring CO_2, water vapour and energy was established in October/November 2002 and we have continuous data since then. We present the results and analysis for CO_2 for the year 2003.

The climate is cool maritime with a small range of temperature changes during the year and abundant precipitation. Several methods can be used to measure CO_2 fluxes. Here, CO_2 and H_2O fluxes between the ecosystem and the atmosphere as well as other meteorological data were recorded continuously at 30 minutes intervals. No device has been set up to measure specific soil respiration or LAI (Leaf Area Index). Once collected, data were filtered and filled when found inadequate or suspect, as it is generally the case with tower-based flux measurements.

This work is part of a five-year (2002-2006) research project funded by the Irish Environmental Protection Agency.

A6.1.2 Objectives

The objective of the project was to determine the energy and CO_2 fluxes over a year (2003) using an eddy covariance (EC) system to measure CO_2 and water vapour fluxes in a humid temperate grassland ecosystem in Ireland. Central to this objective is the investigation of seasonal and annual variation in terrestrial (grassland ecosystem) CO_2 and energy fluxes and to determine possible meteorological and biological controls on net CO_2 and energy exchange. Long-term measurements of this kind are essential for examining the seasonal and interannual variability of carbon fluxes [*Goulden et al.*, 1996; *Baldocchi*, 2003].

A6.2 Data collection

A6.2.1 Site description

A6.2.1.1 Location

The Wexford experimental grassland is located at Johnstown Castle near the town of Wexford, in South East Ireland, (52º 30' North latitude, 6º 40' West longitude), see Figure A6.2.1.

Figure A6.2.1: Location of the site area

The site location is within the National Agriculture Research Station lands (Co-ordinates of CO_2 tower: 117289.525 N; 302396.928 E).

The Wexford grassland is situated at an elevation about 50 m above sea level (see Figure A6.2.2 (a)). Soils at Johnstown Castle estate are shown in figure A6.2.2 (b). The types of soils within footprint (see section A6.4.2.1) are A1 (brown earth), A2 (gley), C1 (brown earth), and C2 (gley).

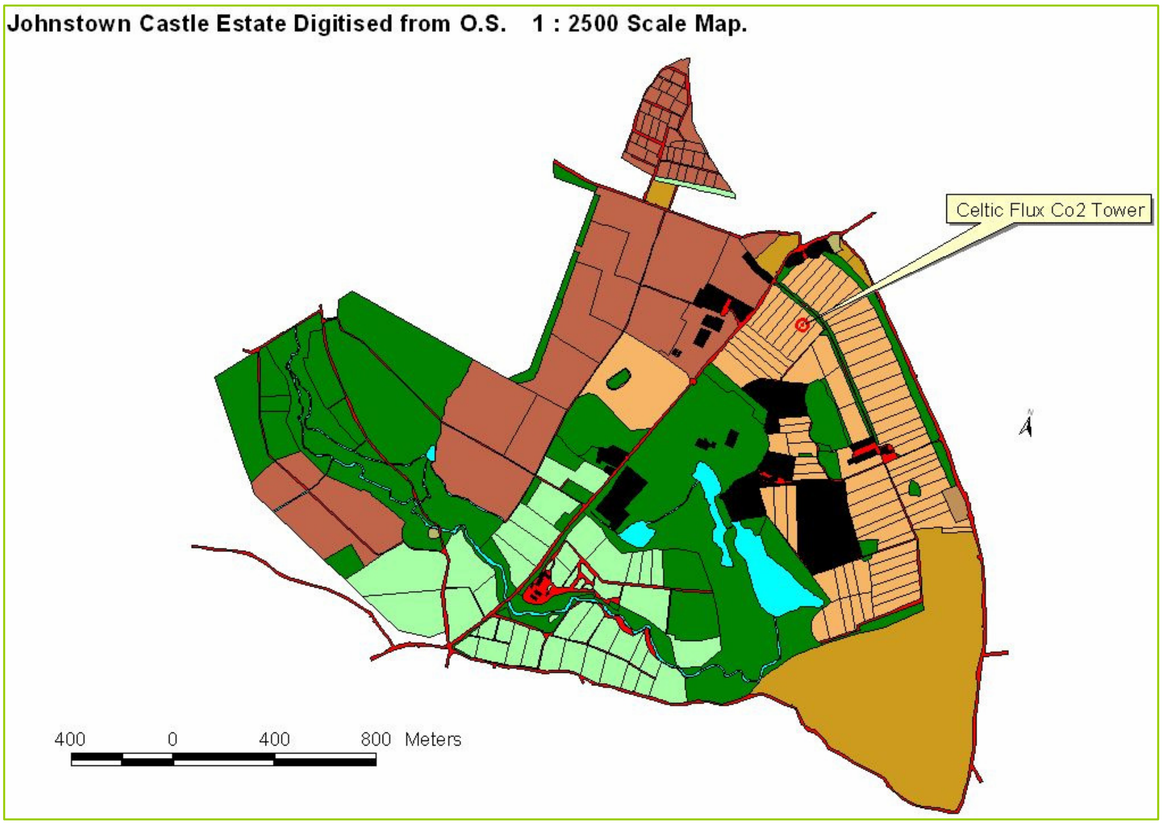

Figure A6.2.2 (a): Map of Johnstown Castle estate with the flux tower

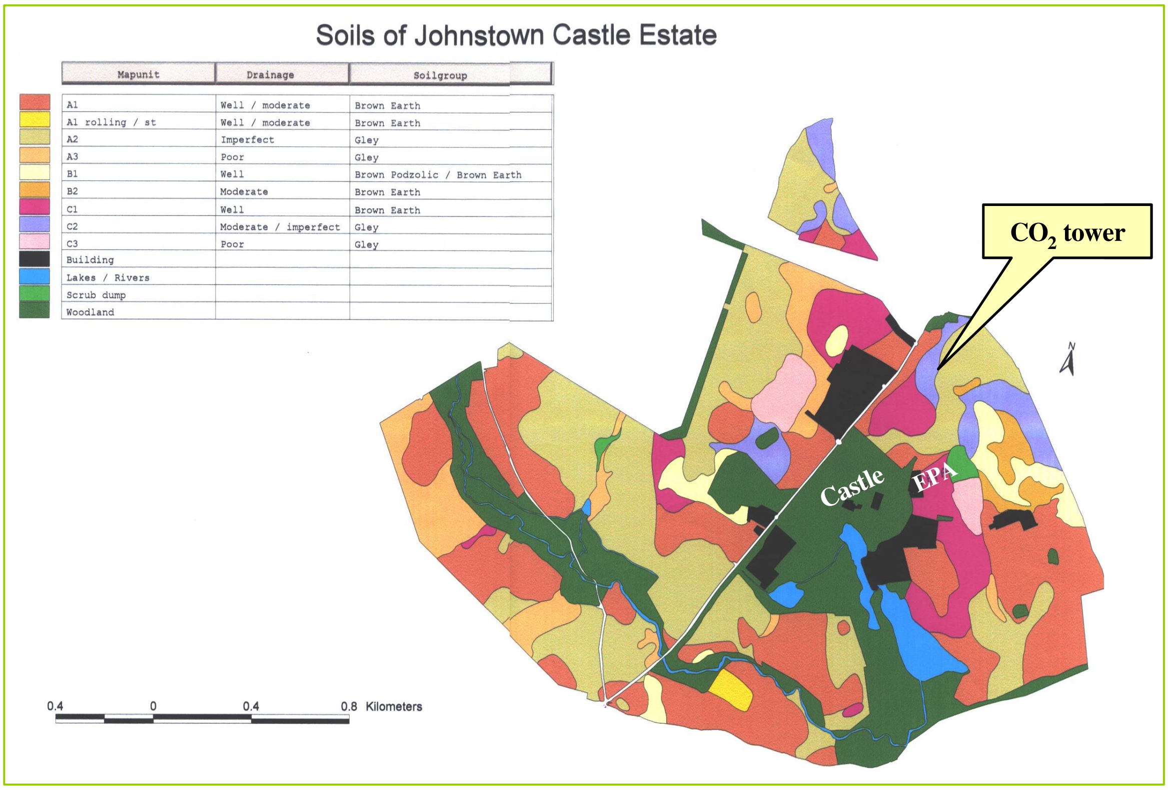

Figure A6.2.2 (b): Soils of Johnstown Castle estate

A6.2.1.2 Field history and Grassland management

The site is agricultural grassland, typical of the land use and vegetation in this part of the country. The vegetation cover is grassland of moderately high quality pasture and meadow, whereas the dominant plant species is perennial ryegrass. Considering the environmental conditions, warm but not hot temperatures and high humidity with very good airflow and the latitude of Ireland, the metabolic pathway for carbon fixation is assumed to be a Calvin-Benson Cycle (C3 grass).

The grassland is part of Johnstown Castle Agriculture Research Institute (Teagasc) property and is managed by that institution. The land use is a mixture of paddocks for cattle grazing and fields for cutting (silage harvesting). The map of the fields with soil classification within the footprint (see section A6.4.2.1) is given in figure A6.2.2 (c).

Figure A6.2.2 (c): The map of the fields with soil classification within the footprint. Fields within footprint are (1PH, 2PH, 3PH, 1PL, 2PL, 3PL, 4PL, 1C, 2C, 3C, 4C, 5C)

In 2003 the grass was harvested first on 27/05/2003 (fields: 1PL, 3PL, 1PH, and 4C) and a second time on 5/08/2003 (fields: 1PL, 3PL, and 1PH) [G. Kiely, O. Carton and D. Fay, personal communication], and exported as silage from the pastureland for winter feed. In a dry meter (DM) after first cut it is exported in an average 126 g/kg and after the second one 157 g/kg of dry meter from each field.

Cattle grazing began in February (21/02/2003) and ended in November (21/11/2003) [G. Kiely, O. Carton and D. Fay, personal communication]. Cattle removes from the fields for cutting 5 weeks before harvest and put beck in the field once the grass grow again.

Livestock density at the site varies through the year. Before the first silage cut it was 4.6 LU/ha, between first and second cut it was 3.44 LU/ha, and after the last cut it was 2.5 LU/ha [G. Kiely, O. Carton and D. Fay, personal communication]. In average trough the year livestock density at the site is 3.5 LU/ha.

Due to the mild climatic conditions the field stays green all year. No measurements of the biomass or Leaf Area Index (LAI) of grass have been made on this site during 2003.

The amount of fertiliser used in each individual paddock is controlled. Nitrogen in chemical fertilizer was applied at the rate of 176 kg of N/ha, urea at the rate of 125 kg of N/ha. Slurry was applied at the rate of 61.5 m^3/ha, where first application took place on 31st March (in average 28.5 m^3/ha) and second on 3rd June (in average 33 m^3/ha) [G. Kiely, O. Carton and D. Fay, personal communication].

The monthly rates of chemical fertilizer and urea are given in Figure A6.2.3, while exact values in kg.N/ha.month are given in Table A6.2.1.

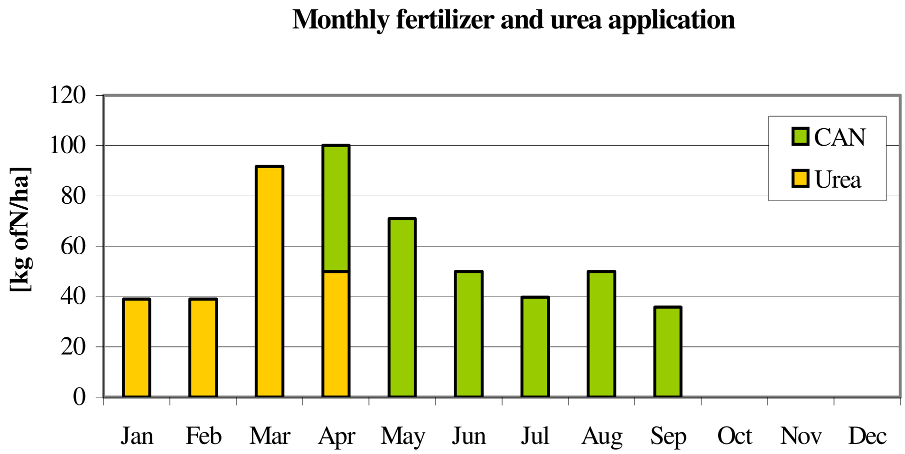

Figure A6.2.3: Monthly application of nitrogen fertilizer (green) and urea (yellow) for year 2003 at Wexford site

Table A6.2.1: Monthly application of nitrogen fertilizer, urea in [kg/ha] and slurry in [m^3/ha]

Month	Fertiliser CAN [kg/ha]	Urea [kg/ha]	SUM [kg/ha]	Slurry [m^3/ha]
January		39	39	
February		39	39	
March		91.7	91.7	28.5
April	50	50	100	
May	71		71	
June	50		50	33
July	39.7		39.7	
August	50		50	
September	35.7		35.7	
October				
November				
December				
SUM	296.4	219.7	516.1	61.5

A6.2.1.3 Climate

The climate is temperate and humid (from the influence of warm Gulf Stream in the North East Atlantic Ocean) with mean annual precipitation in the Wexford region of about 1002 mm [Ryan, 1998]. The rainfall regime is characterized by long duration events of low intensity (values up to 5 mm/day). Short duration events of high intensity are more seldom and occur in summer.

Daily air temperatures have a very small range of variation during the year, going from a maximum of 24ºC to a minimum of -2ºC, with an average of 15ºC in summer and 6ºC in winter. The mean wind velocity is 4 m/s at the site with peaks up to 13 m/s. The main wind comes from the southwest.

A6.3 General meteorological data

A6.3.1 Data collection

The experimental system used in this study is composed of a 2.5 m high tower which supports different types of sensors connected to a datalogger. The datalogger controls the measurements, data processing and digital storage of the sensor outputs. A secured perimeter has been defined with a wire fence to protect the tower sensors, as well as to define a setting up area for the soil devices (see Figure A6.3.1).

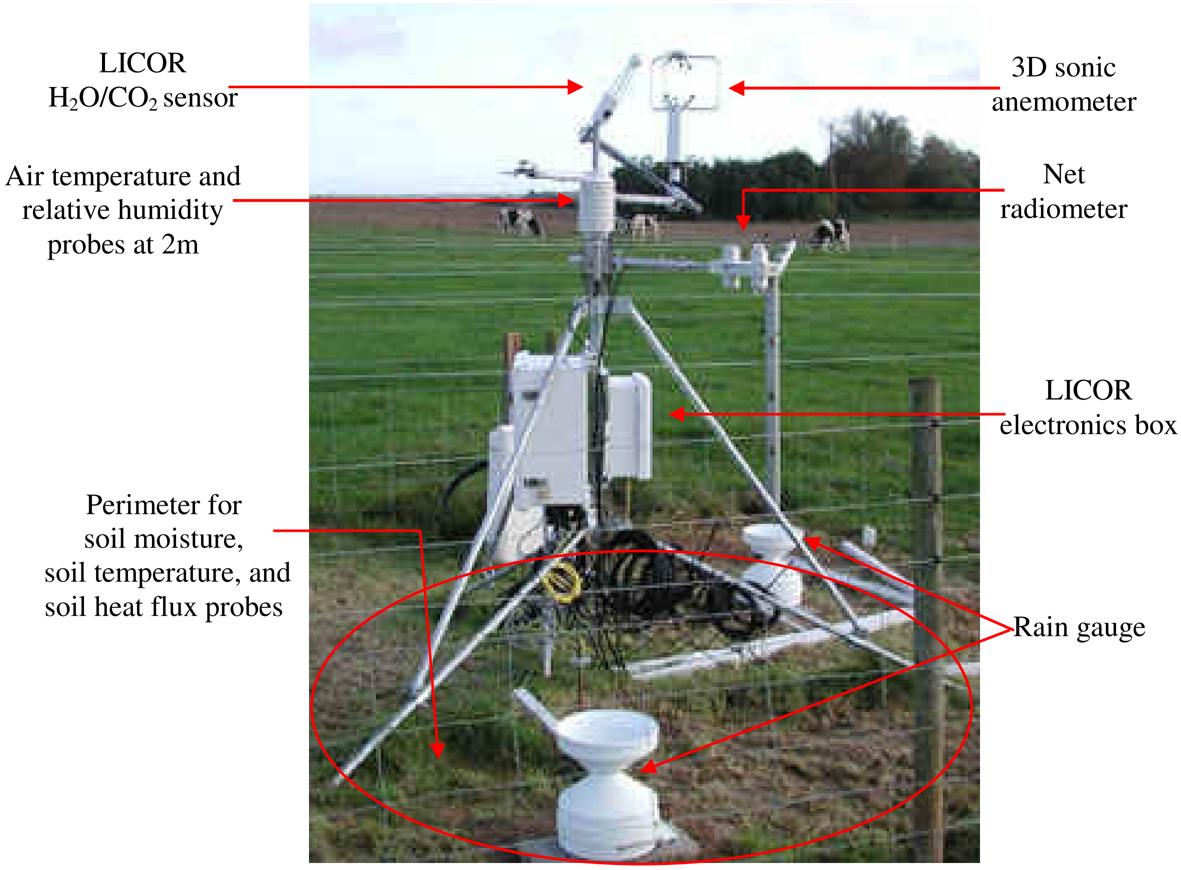

Figure A6.3.1: Tower at Wexford site
(http://www.ucc.ie/hydromet/Projects/johnstown.htm)

Meteorological data were monitored since November 2002 and we have continuous data since then. In this report the whole year data set for 2003 was analysed. Precipitation and meteorological measurements were read each one minute intervals and recorded at 30-minute intervals.

A gap in the data set appears due to the electricity failure for certain days in July and August (2003). Meteorological data for those periods were filled as follows:

- Data from 15/07/03 (from 17:30 to 22:30) were used to fill missing data for 16/07/03 (from 17:30 to 22:30),
- Data from 21/07/03 (from 01:30 to 11:30) were used to fill missing data for 20/07/03 (from 01:30 to 11:30),
- Data from 22/07/03 (from 08:30 to 23:30) were used to fill missing data for 23/07/03 (from 08:30 to 23:30),
- Data from 25/08/03 (from 04:30 to 07:30) were used to fill missing data for 26/08/03 (from 04:30 to 07:30).

Precipitation for this period was filled up with data from a nearby rain gauge.
All meteorological data was transferred from site to office by telemetry.

A6.3.2 Precipitation

A6.3.2.1 Annual precipitation

The long-term annual average rainfall for Wexford site is 1002 mm [Ryan, 1998]. In 2003 annual rainfall was 1078 mm (~ 7% above mean annual precipitation). The cumulative precipitation for 2003 is shown in Figure A6.3.2. It should be noted that there was no snow during the study period.

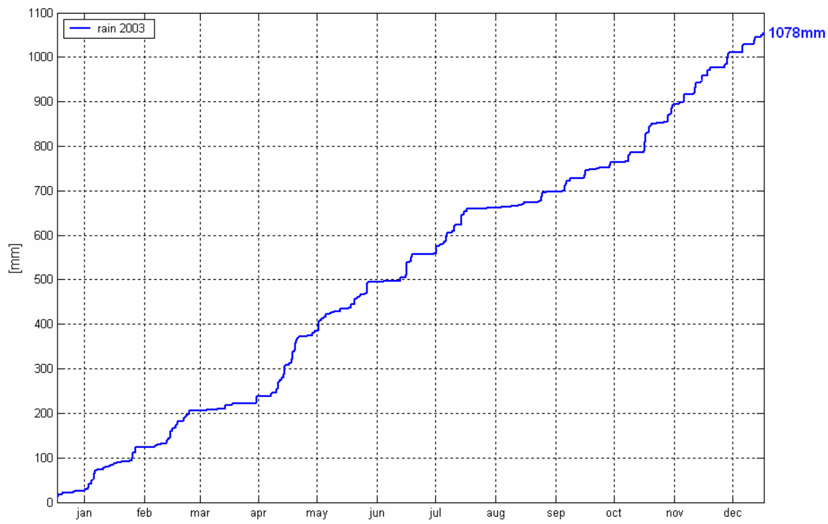

Figure A6.3.2: Cumulative precipitation in mm for 2003.

A6.3.2.2 Monthly precipitation

There is no clear seasonality in precipitation in 2003. Monthly precipitation (Figure A6.3.3) shows that November was the wettest month with 129 mm/month and August was the driest month with 14 mm/month. The average spring monthly rainfall was 92 mm while the average monthly summer rainfall was 79 mm (Table A6.3.1).

Table A6.3.1: Monthly precipitation in mm

[mm]	jan	feb	mar	apr	may	jun	jul	aug	sep	oct	nov	dec
2003	89	71	58	97	121	103	121	14	73	83	129	119

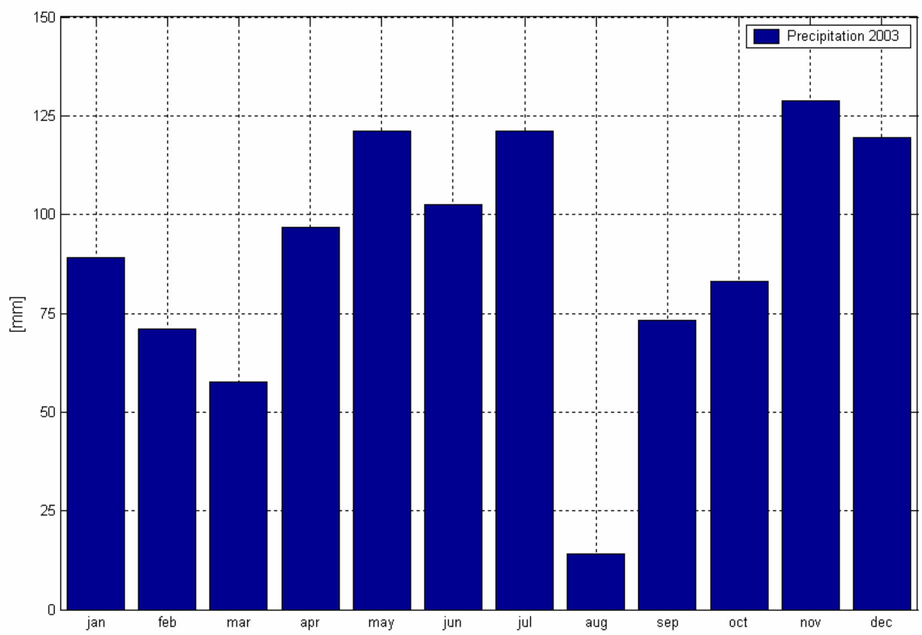

Figure A6. 3.3: **Monthly precipitation in mm for 2003**

A6.3.2.3 Daily precipitation

Figure A6.3.4 shows daily precipitation. It can be seen that maximum daily precipitation was 24 mm/day (May and December). We note that the spring and summer months have continuous periods of more days with no rain at all. The rainfall regime for the winter in both years is characterized by long duration events of low intensity. Short duration events of high intensity are more seldom and occur in summer. Summer rains are more intermittent and intense but no dry season is evident.

Rains are usually of small intensity with rainfalls below 0.2 mm per 30 minutes 91% of the time. Rains are more likely to occur in the morning, with a lower frequency after mid-afternoon.

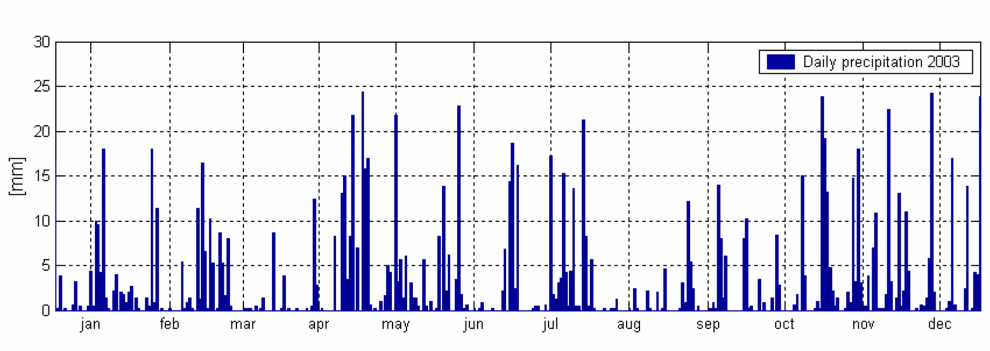

Figure A6.3.4: Daily precipitation in mm for 2003

A6.3.3 Soil moisture

The volumetric soil water content (m^3/m^3) was measured at depths of 5, 10, 25, and 50 cm with CS615 time domain reflectometer (Campbell Scientific USA, or CSI) set horizontally. Two other CS615's were installed vertically, from 0 cm to 30 cm, and from 30 cm to 60 cm depth.

The volumetric soil moisture in the topsoil at 5 cm and in root zone at 30 cm (Figure. A6.3.5 (b)) shows that during the period November to February levels are at approximately 0.48 m^3/m^3 and 0.47 m^3/m^3, respectively.

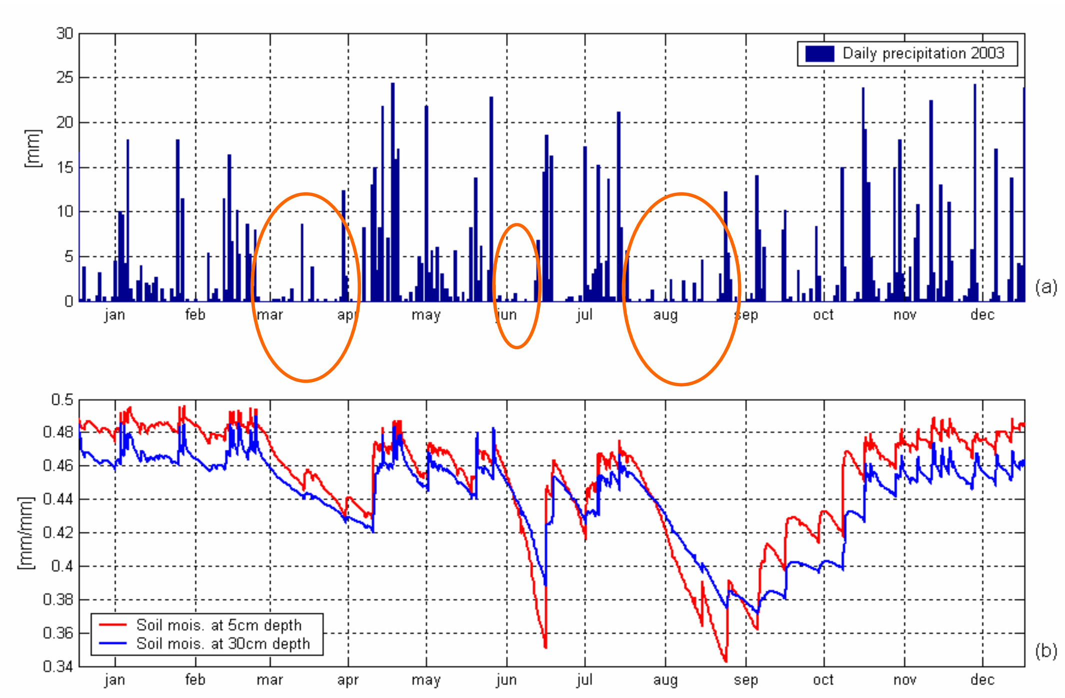

Figure A6.3.5: Soil moisture dependence on precipitation: (a) daily precipitation in mm (b) soil moisture in mm/mm at 5cm depth (30min interval) in red and soil moisture in mm/mm at 30cm depth (30min interval) in blue.

There are three periods in the year (Figure A6.3.5 (a)) when soil moisture drops due to low precipitation. In the second half of March and first half of April soil moisture was 0.43 m^3/m^3 (at 5 cm) and 0.42 m^3/m^3 (at 30 cm). Drought in second half of June caused soil moisture to drop to 0.35 m^3/m^3 (at 5 cm) and 0.39 m^3/m^3 (at 30 cm). The long period of low precipitation from mid July to mid September lead soil moisture to drop to its lowest level of 0.34 m^3/m^3 (at 5 cm) and 0.37 m^3/m^3 (at 30 cm).

Near surface soil moisture shows a strong relationship with precipitation, and has a fast response to rain events. The soil moisture at root zone also shows relationship with precipitation, still there is delay in its response.

The lowest record of soil moisture is ~ 34% and the state at which soil moisture becomes limiting and eventually causes vegetation to wilt (θ_{wilt}) is ~ 8% [*Albertson and Kiely*, 2001]. Therefore, the system was not water limited during the study period and its growth/production was not water limited.

A6.3.4 Relative air humidity and atmospheric pressure

The barometric pressure was measured with a PTB101B (CSI) and humidity was measured with a HMP45A sensor (CSI) at the height of 2 m.

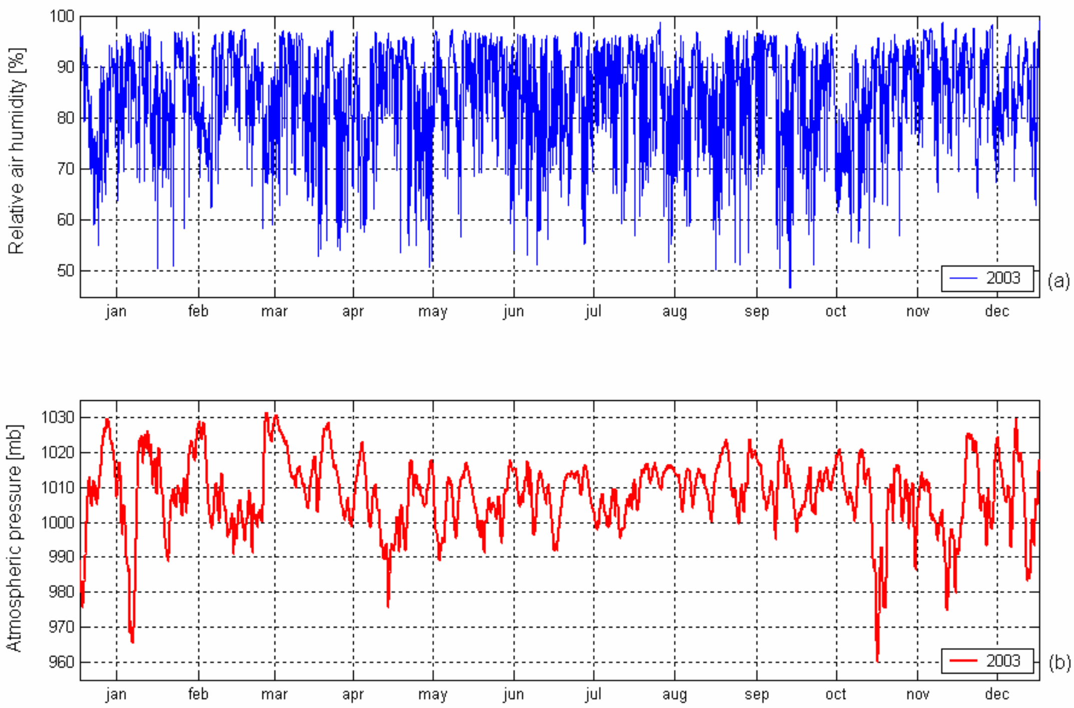

Figure A6.3.6: **30 minute (a) Relative air humidity in %; and (b) Atmospheric pressure in mbar**

The relative air humidity (Figure A6.3.6 (a)) stays high throughout the year, and fluctuates a lot on a daily basis. The relative air humidity ranges from 47% to 99%. The drier points in measured half hour relative air humidity correspond to lows in the precipitation and soil moisture curves.

Atmospheric pressure (Figure A6.3.6 (b)) fluctuates a lot on a daily basis, and those fluctuations are more pronounced during the winter period. In wintertime atmospheric pressure ranges from 960 to 1030 mb, and in summertime from 990 to 1020 mb. The mean atmospheric pressure was 1008 mb.

A6.3.5 Air and soil temperature

The air temperature was measured with a HMP45A sensor (CSI) at the height of 2 m. Soil temperatures were measured with three 107 temperature probes (CSI), at the depths of 2.5, 5, and 7.5 cm.

The half hour air temperatures have a small range of variation during the year, going from a maximum of 24ºC (August) to a minimum of -2ºC (January). The average half hour temperature is 15º C in summer and 6º C in winter.

The daily air temperatures (Figure A6.3.7(a)) range from a maximum of 20ºC (August) to minimum of 1ºC (January).

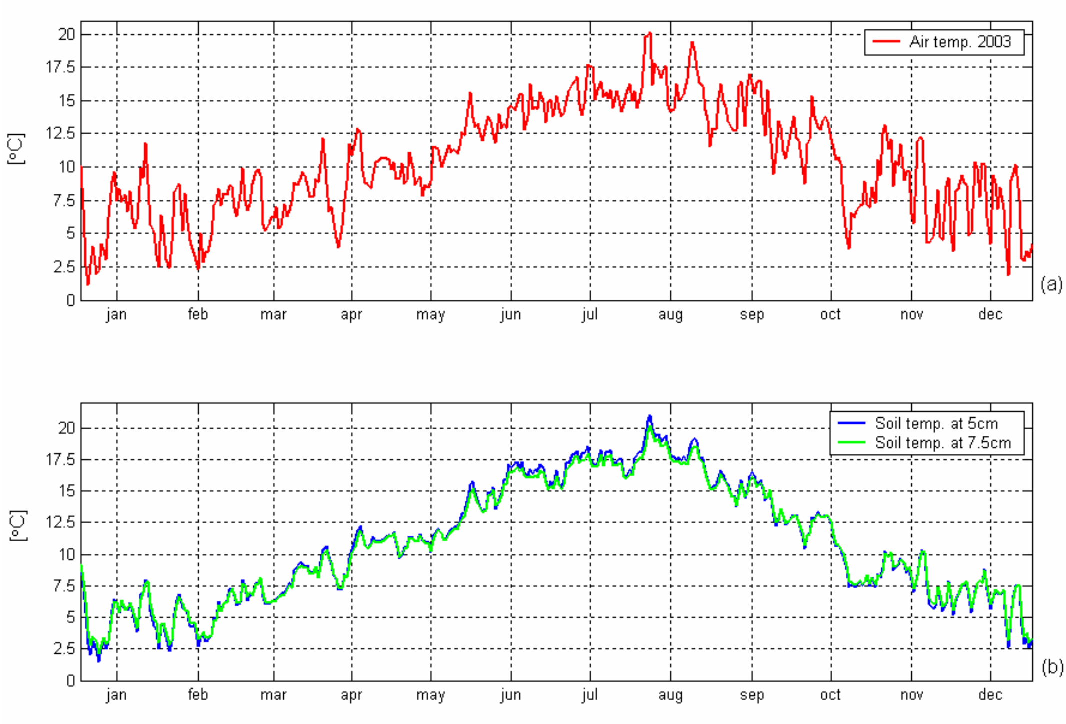

Figure A6.3.7: Daily average over 30min in °C: (a) air temperature; and (b) soil temperature at 5 cm depth (blue) and soil temperature at 7.5 cm depth (green)

The local climate is humid temperate, with very few days with temperature under 4°C (the lower threshold temperature for the photosynthetic process). No frost has been noticed during the study period.

The soil temperature at 5 cm and 7.5 cm depth follows the same annual pattern as air temperature, except for the night data where, as expected, the soil does not cool down as quickly as the air (Figure A6.3.7(b)). The soil temperature at 5 cm depth was used for the nighttime fitting function in the case of bad CO_2 flux data.

Figure A6.3.8 shows monthly mean temperatures of air and soil (at 5 cm and 7.5 cm) with standard deviations. The mean air temperature in the winter months is 1°C to 2 °C higher compared with mean soil temperature. In summer months mean soil temperature is approximately 1°C higher than the air temperature.

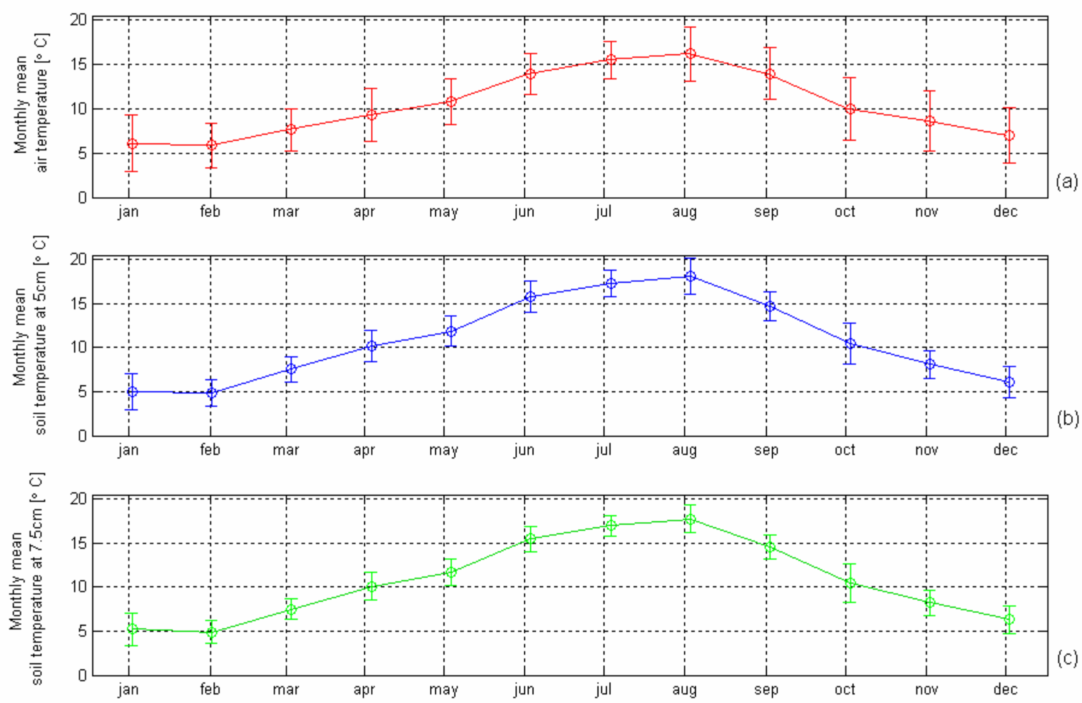

Figure A6.3.8: Monthly mean and standard deviation of: (a) air temperature; (b) soil temperature at 5 cm depth; (c) soil temperature at 7.5 cm depth

The values of mean air temperature and soil temperatures at 5 cm and 7.5 cm depth are given in Table A6.3.2.

Table A6.3.2: Monthly mean air temperature, and soil temperature at 5 cm and 7.5 cm depths

[°C]	jan	feb	mar	apr	may	jun	jul	aug	sep	oct	nov	dec
t_{air}	6	6	8	9	11	14	15	16	14	10	9	7
t_{soil} (5cm)	5	5	8	10	12	16	17	18	15	10	8	6
t_{soil} (7.5cm)	5	5	7	10	12	15	17	18	15	10	8	6

A6.3.6 Photosynthetic photon flux (Q_{par})

The photosynthetic photon flux was measured with a PAR LITE sensor (Kipp & Zonen).

The photosynthetic photon flux density Q_{par} shows the clear annual pattern with 30 minute values (Figure A6.3.9(a)) reaching the maximum in summer months and minimum over the winter period. Those values were used for finding the function for CO_2 flux at daytime during the periods with bad CO_2 flux data.

The 30 minute Q_{par} averaged over one day is shown in Figure A6.3.9(b).

The 30 minute Q_{par} averaged over one month (Figure A6.3.9(c) and Table A6.3.3) shows difference in monthly distribution within the year.. It can be noticed that average Q_{par} values for January and December are below 200 μmol of quantum/m^2/s; for all other months values are above that value. The average Q_{par} in July is 493 μmol of quantum/m^2/s, which is lower than in June (~19%) and August (~18%). We suspect that the reason for reduction in Q_{par} during July is cloudiness (high precipitation in July, see section A6.3.2.2).

Cumulative Q_{par} for 2003 was 4674 μmol of quantum/m^2/s.

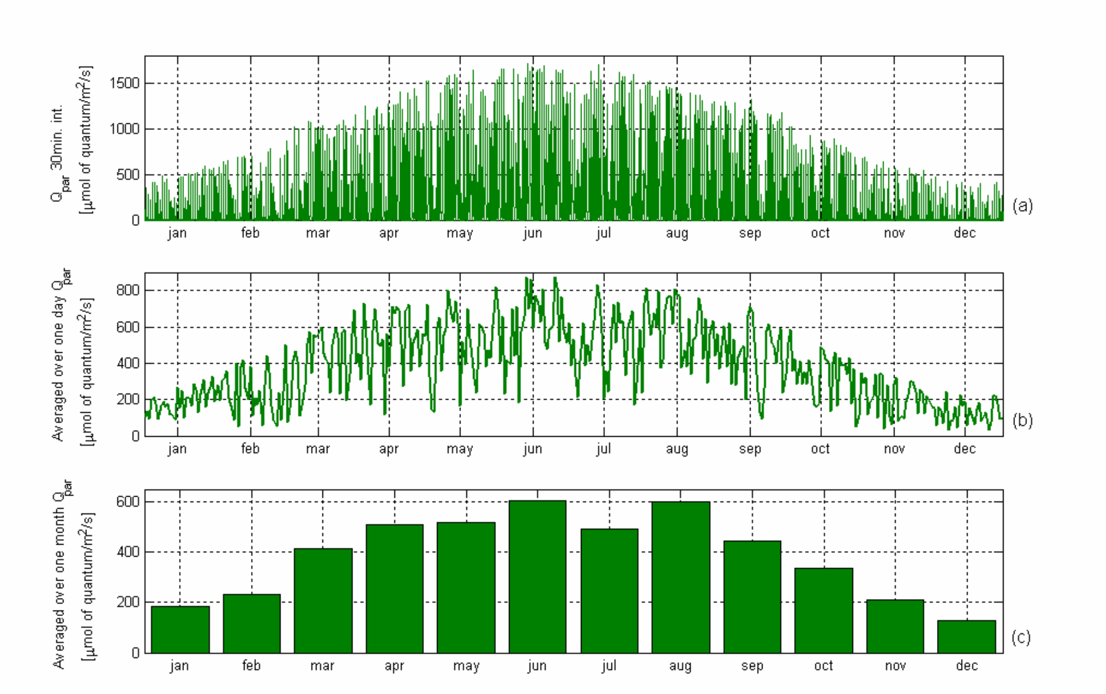

Figure A6.3.9: Photosynthetic photon flux during 30 minute intervals in μmol of quantum/m^2/s: (a) row data (b); averaged over one day; and (c) averaged over one month

Table A6.3.3: **Daily Q_{par} averaged over one month in μmol of quantum/m^2/s**

	jan	feb	mar	apr	may	jun	jul	aug	sep	oct	nov	dec
2003	186	232	414	510	517	606	493	598	444	336	212	126

A6.3.7 Wind velocity

The wind velocity in three different directions was measured at 10 Hz with an RM Young Model 81000 3-D sonic anemometer positioned at the top of the 2.5 m tower.

Thirty-minute averages of wind direction were from the southwest most of the time (see section A6.4.2.1.). The mean wind velocity in m/s is derived as resultant of the wind speed in two horizontal directions, u and v, measured with sonic anemometer:

$$U = \sqrt{u^2 + v^2} \qquad (3.1)$$

The mean wind velocity at 2.5 m is approximately 4.0 m/s with peaks in wintertime up to 13 m/s (Figure A6.3.10).

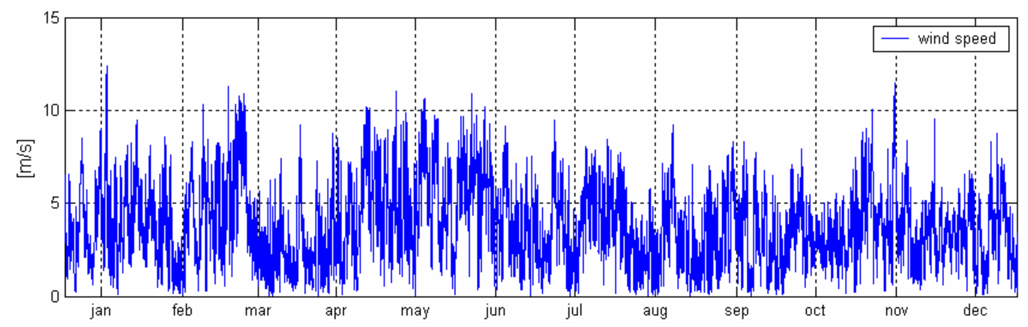

Figure A6.3.10: Wind speed in m/s in 30 min intervals

A6.3.8 Cloudiness

Clouds are important in the climate system because they reflect a significant amount of radiation back in the space, which acts as cooling mechanism. However, clouds also absorb outgoing long wave radiation, which is a heating mechanism. Hence clouds can reduce photosynthetic photon flux, which is necessary for the process of photosynthesis, and thereby reduce carbon dioxide uptake of the plants during the day.

The climate in Ireland is such that we cannot overlook the cloud effects.

We do not measure clouds or cloud cover directly but we can use the photosynthetic photon flux density (Q_{par}) data as an indirect measure of clouds.

A6.4 The Eddy Covariance Method

A6.4.1 Accuracy of Eddy Covariance measurements

There are a number of diagnostic test statistics, which illustrate the correct functioning of individual components of an eddy covariance technique [*Gash et al.*, 1999; *Moncrieff et al.,* 1997]. Two useful statistics are the ratio of the standard deviation of vertical wind speed (σ_w) to the friction velocity (u_*) and the ratio of standard deviation of a scalar concentration (σ_c) to the relevant scalar concentration (c_*) [*Moncrieff et al.*, 1997].

In order to test the performance of the anemometer that was used in this experiment we plot the standard deviation of the vertical velocity fluctuations (σ_w) against the friction velocity or momentum flux (u_*) [*Gash, et al.* 1999; *Van der Tol, et al.*, 2003]. The resultant mean values of σ_w/u_* are 1.13 for dry periods (Figure. A6.4.1(a)) and 1.21 for wet periods (Figure. A6.4.1(b)), which is in agreement with the Monin-Obukhov similarity theory where σ_w/u_* in neutral conditions is a universal constant. Observed values for σ_w/u_* are typically about 1.25 [*Garatt*, 1992; *Gash, et al.*, 1999; *van der Tol, et al.*, 2003].

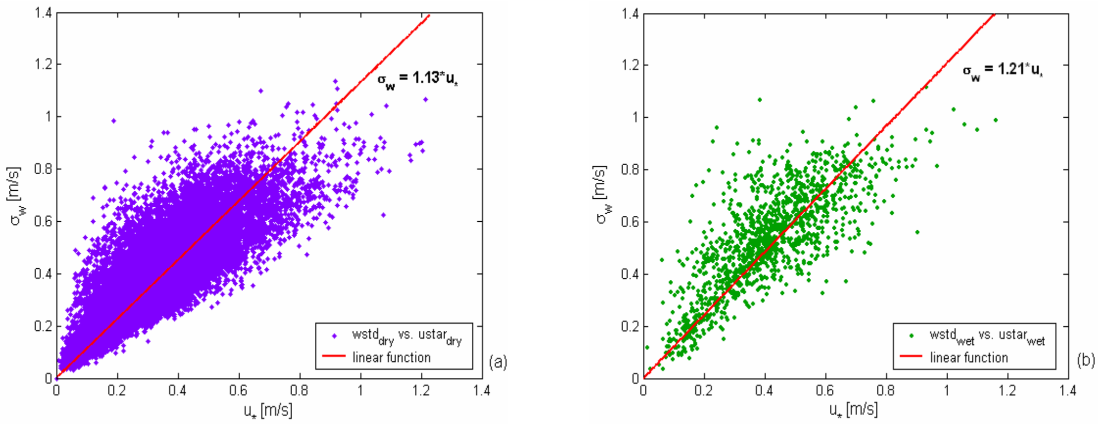

Figure A6.4.1: Scatter diagram of the standard deviation of the vertical velocity fluctuations (σ_w) with friction velocity (u_*) - half an hour data: (a) dry and (b) rainy conditions

Since the test described above is a sensitive indicator of the anemometer's performance and the ability of the instrument to measure σ_w/u_* in both wet and dry conditions, one can conclude that performance of the sonic anemometer during the study period was satisfactory.

A6.4.2 Footprint and fetch

A6.4.2.1 Footprint estimation

Numerous models have been developed to investigate the relationship between scalar flux and its source areas, e.g. Eulerian analytical model [*Gash*, 1986; *Horst and Weil*, 1995], Lagrangian stochastic dispersion model [*Hsieh et al*., 1997].

To interpret the eddy correlation measured scalar flux and understand the fetch requirement and contributing source areas for these measurements, the flux footprint model developed by Hsieh et al. [2000] was adopted. The model describes the relationship between footprint, atmospheric stability, observation height, and surface roughness.

Figure A6.4.2. shows the scatter plots of xf (the fetch requirement) and xp (the peak source distance) versus wind directions. Table A6.4.1 shows percentage of the measurements during the neutral, unstable and stable atmospheric condition.

Table A6.4.1: Atmospheric conditions occurrence in %

Atmospheric condition	[%]
Neutral	43
Unstable	24
Stable	32

In Figure A6.4.2 the fetch requirements for unstable (and neutral) conditions (67% of time), is less than 500 m and the strongest source areas are within 25 m from the tower. For stable conditions (32% of time), xf and xp are within 1km and 50 m, respectively, except for some (~18%) very stable cases. Also, it is noted that 90% of the xf and xp values are less than 1 km and 50 m, respectively, for the whole year 2003.

With this footprint analysis, it can be interpreted that most of the time (~ 90%) the eddy-correlation scalar flux measurements (i.e., sensible heat, latent heat, and CO_2 fluxes) represent the space averaged fluxes resulted from the circle area 1 km in radius from the tower, and the strongest source area is just 50 m away. Also, from the information given by the wind direction histogram shown in Figure A6.4.3, it is clear that the eddy correlation measured fluxes are mainly from the southwest part of the field. This suggests that the footprint is changeable during the time and it is not within a circle around the tower, but it shaped according to the wind direction and wind speed (the plot is more scattered in directions other than S-W in Figure A6.4.2).

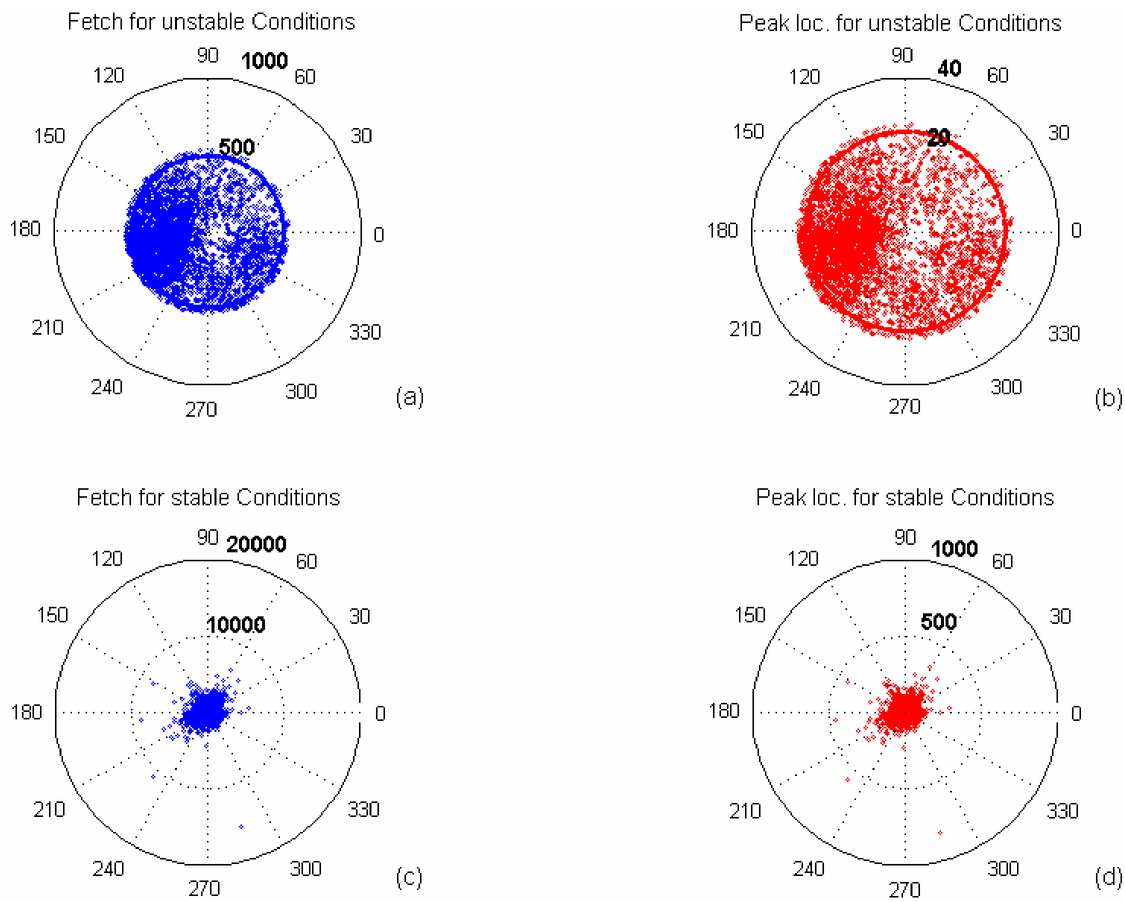

Figure A6.4.2: Fetch requirement: (a) fetch and (b) peak locations for unstable conditions; (c) fetch and (d) peak locations for stable conditions

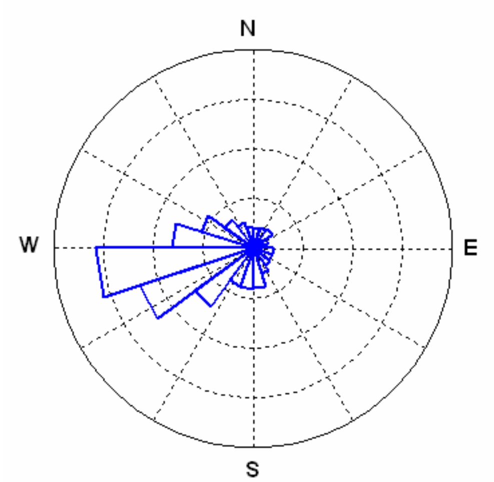

Figure A6.4.3: **Wind direction**

Leclerc and Thurtell [1990] applied a Lagrangian particle trajectory model to examine 'rule of thumb' fetch requirement and found that the 100 to 1 fetch to height ratio underestimates fetch requirements when observations are carried out above smooth surfaces, in stable conditions, or at high observation level. Hsieh et al. [2000] found that height to fetch ratio is about 1:100, 1:250, and 1:300 for unstable, neutral, and stable conditions, respectively.

Applying 1:200 height (here 2.5m) to fetch ratio, combined with information from the probability density function of the wind direction [*Hsieh et al*., 2000], on our case we found that footprint for unstable condition can be reduced to the dimensions of the study site. The map of the tower with footprint is shown in figure A6.4.4 (a) and (b).

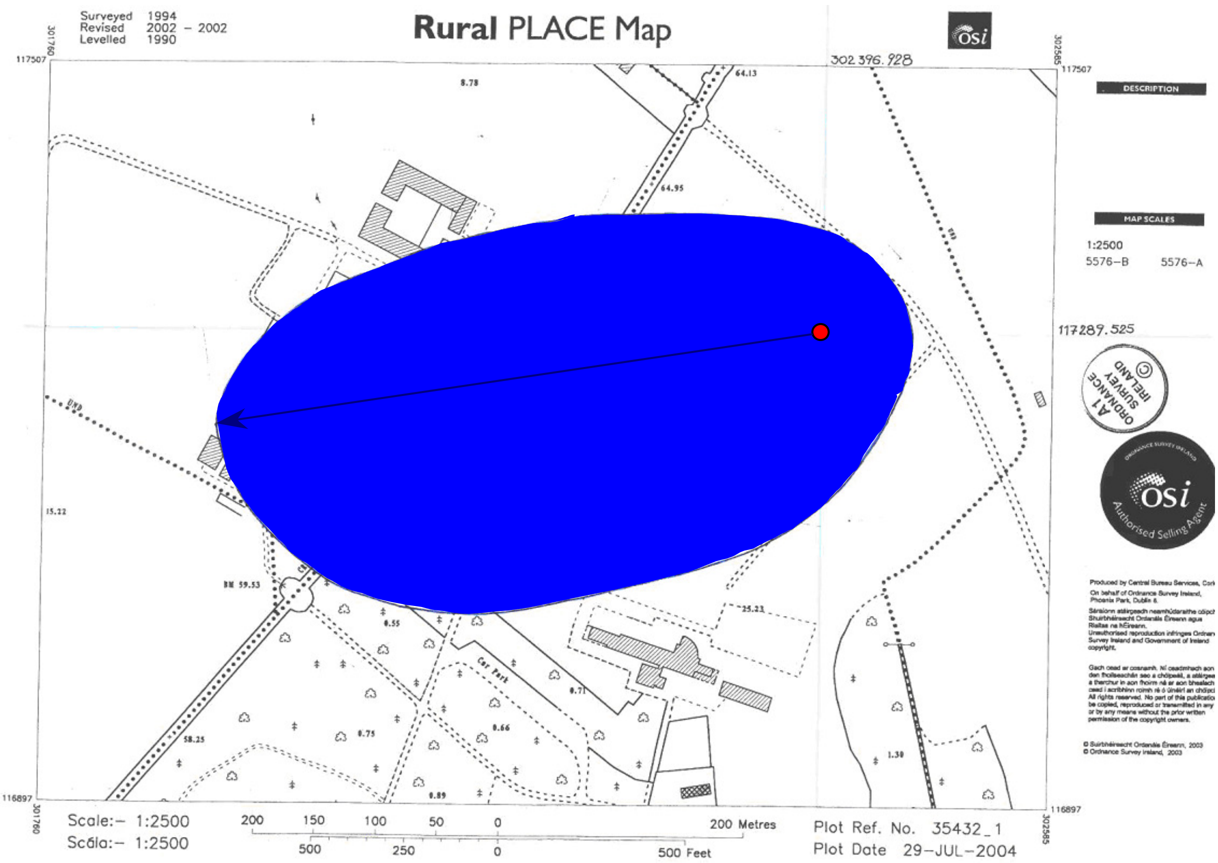

Figure A6.4.4 (a): Map of the grassland catchment with eddy covariance tower location and the shaded area indicative of the flux footprint. The prevailing wind direction is from the south-west.

Figure A6.4.4 (b): Map of the grassland catchment with eddy covariance tower location and the shaded fields indicative of the flux footprint. The fields in the footprint are 1PH, 2PH, 3PH, 1PL, 2PL, 3PL, 4PL, 1C, 2C, 3C, 4C, and 5C. The dominant type of soil within footprint is brown earth (A2 and C1).

A6.5 Energy balance

A6.5.1 Energy balance

A6.5.1.1 Energy balance closure

Energy balance closure is used to assess the performance of eddy covariance flux system. Under perfect closure, the sum of the sensible and latent heat flux (H+λE) measured by eddy covariance is equal to the difference between net radiation and ground (soil) heat flux (Rn-G) measured independently from the meteorological sensors (see Chapter 2) [*McMillen*, 1988].

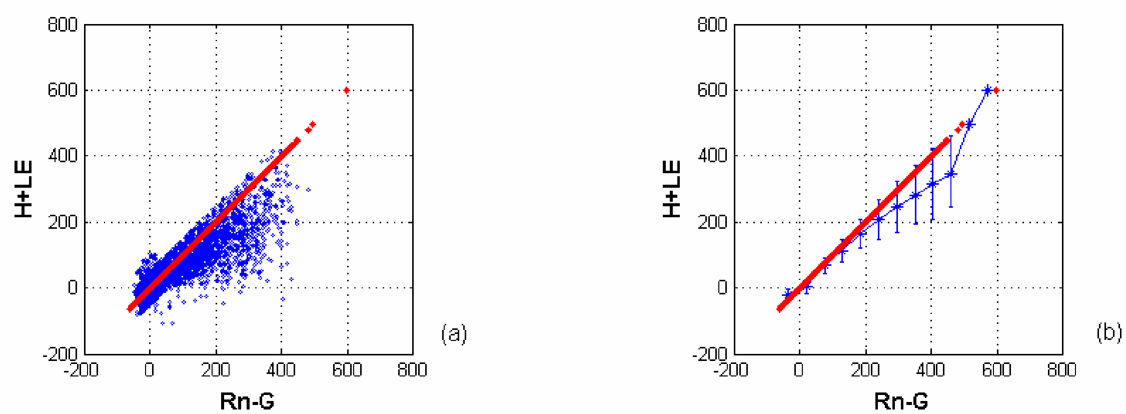

Figure A6.5.1: Relationships between (Rn-G) and (H+ λE): (a) 30 minute data; (b) average with standard deviation. The solid line (in red) represents the case of perfect energy balance closure, i.e. H+λE=Rn-G.

The slope 0.9 of the relationships between (Rn-G) and (H+λE) in Figure A6.5.1 indicates that the eddy covariance measurements underestimated sensible and/or latent heat fluxes (or (Rn-G) was overestimated). A portion of the discrepancy may relate to the different locations of the footprints for the measurements of net radiation and soil heat flux, which are close to the instrument tower, while the footprints for the latent and sensible heat fluxes are larger and upwind of the tower. This may in part be due to the heterogeneity of soil moisture status in the near surface and root zone.

Figure A6.5.2 shows monthly difference between net radiation and soil heat flux (Rn-G) and monthly sum of sensible and latent heat fluxes (H+λE). Observing the figure A6.5.2, it can be seen that there is agreement in energy balance during the winter months. Difference between (Rn-G) and (H+λE) becomes greater going from spring to summer, when it reaches maximum, and than again becomes small as autumn comes (see Table A6.5.1 for the values). The underestimation of energy fluxes occurs during the spring-summer time.

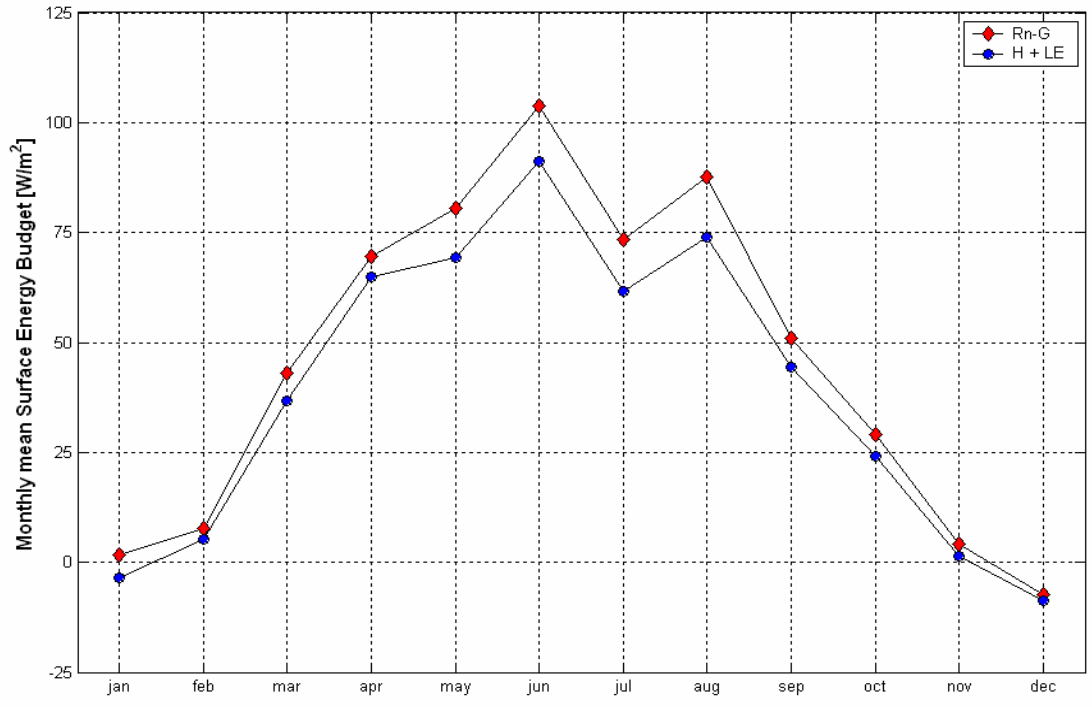

Figure A6.5.2: Monthly averaged (a) difference between net radiation and soil heat flux (Rn-G); (b) sum of sensible and latent heat flux (H+λE)

Table A6.5.1: Monthly averaged (a) (Rn-G); (b) (H+λE)

[W/m^2]	jan	feb	mar	apr	may	jun	jul	aug	sep	oct	nov	dec
Rn-G	2	8	43	70	81	104	73	88	51	29	4	-7
LE+H	-4	5	37	65	69	91	62	74	44	24	1	-9

A6.5.1.2 Annual energy fluxes

Cumulative energy fluxes for Wexford site during 2003 are shown in figure A6.5.3. Cumulative fluxes in W/m^2 are: Rn = 8.1 x 10^5; LE = 4.9 x 10^5; H = 1.8 x 10^5; G = 1.1 x 10^5. That means that at the end of the year latent heat flux is 60 %, sensible heat flux is 22%, and ground heat flux is 14% of all net radiation for 2003. The difference of 4% may be due to the heat storage in the grass canopy and discrepancies due to different measurement techniques (i.e. latent and sensible heat flux were measured with the EC technique, fetch is greater, while net radiation and ground heat flux use meteorological measurement with instruments sampling near the tower).

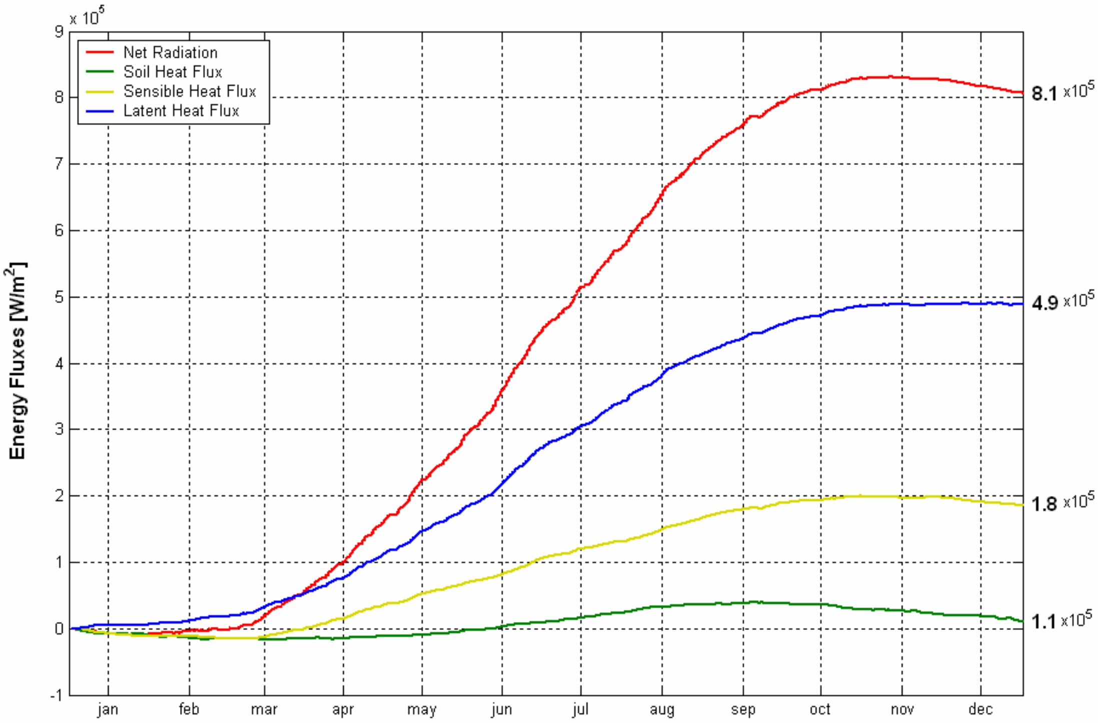

Figure A6.5.3: Cumulative net radiation (Rn), latent heat flux (λE), sensible heat flux (H) and soil heat flux (G) for 2003

A6.5.1.3 Monthly energy fluxes

The average monthly distribution of net radiation and energy fluxes is shown in Figure A6.5.4, and their values in Table A6.5.2. There is a clear seasonality in distribution of net radiation with maximum values reached in the summer. Notice that averaged net radiation in July is 83 W/m^2 while for June and August it is 113 and 96 W/m^2, respectively. The reason for lower average net radiation during the month of July might be more precipitation (i.e. cloudiness) during this month compared with June and August.

Table A6.5.2: Average monthly Rn, LE, H and G in [W/m^2]

[W/m^2]	jan	feb	mar	apr	may	jun	jul	aug	sep	oct	nov	dec
Rn	-6	4	42	72	86	113	83	96	52	23	-1	-14
LE	5	7	24	40	45	64	45	49	29	18	1	~ 0
H	-10	-4	11	24	20	26	16	25	15	6	-1	-9
G	-7	-3	~ 0	2	7	9	10	8	1	-6	-5	-6

Latent heat flux is small during the winter and it increases during spring-summer period. Sensible heat flux is negative during the winter months, as the air is warmer than the earth's surface. In the spring, air above the ground becomes warmer and sensible heat flux changes its sign. Soil heat flux is positive from March to September and in that period heat was absorbed by the soil, as the surface was warmer than subsurface. In the partitioning of the water balance, the biggest part of the radiation is in latent heat flux.

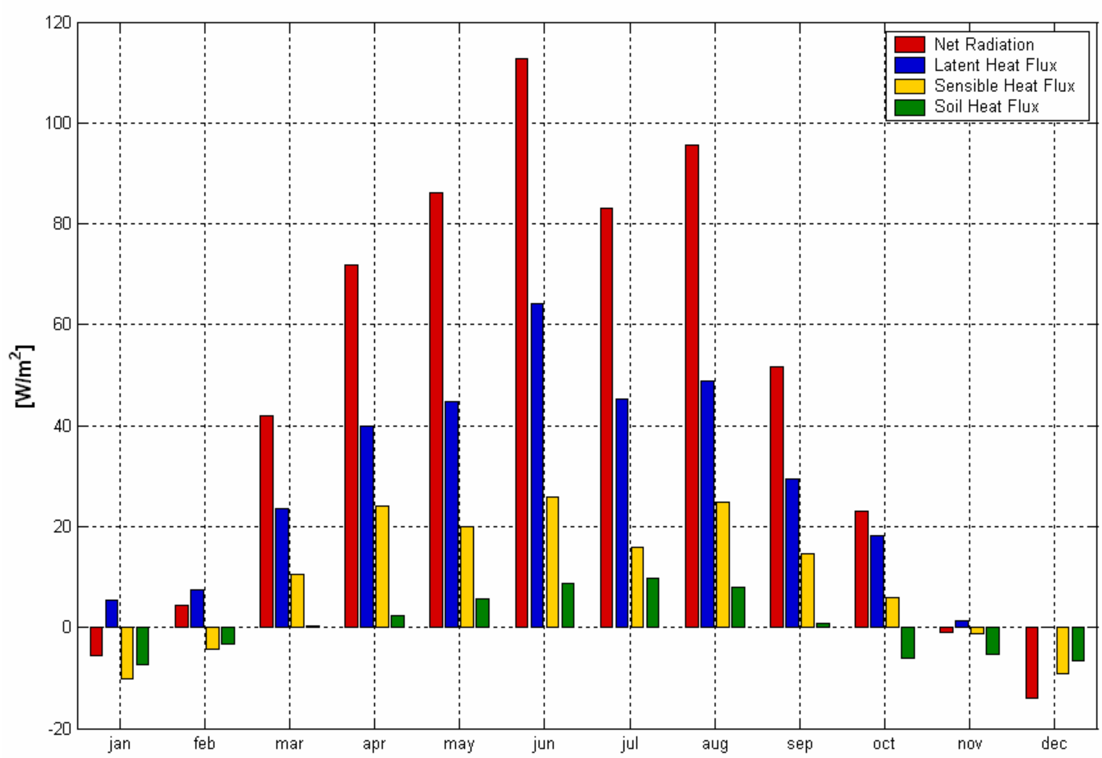

Figure A6.5.4: Average monthly distribution of Rn (red), LE (blue), H (yellow) and G (green)

A6.5.1.4 Daily energy fluxes

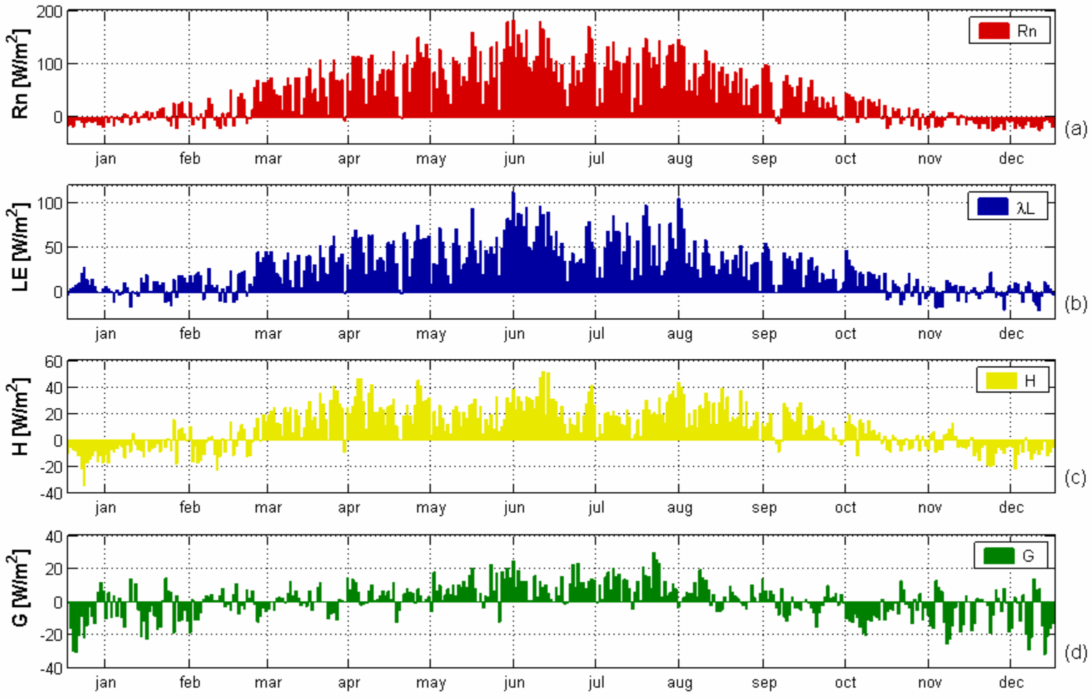

Figure A6.5.5: Average daily distribution of: (a) Rn; (b) LE; (c) H; and (d) G

A6.5.1.5 Bowen ratio

Seasonal variation of Bowen ratio is presented in figure A6.5.6 and the values are in Table A6.5.3.

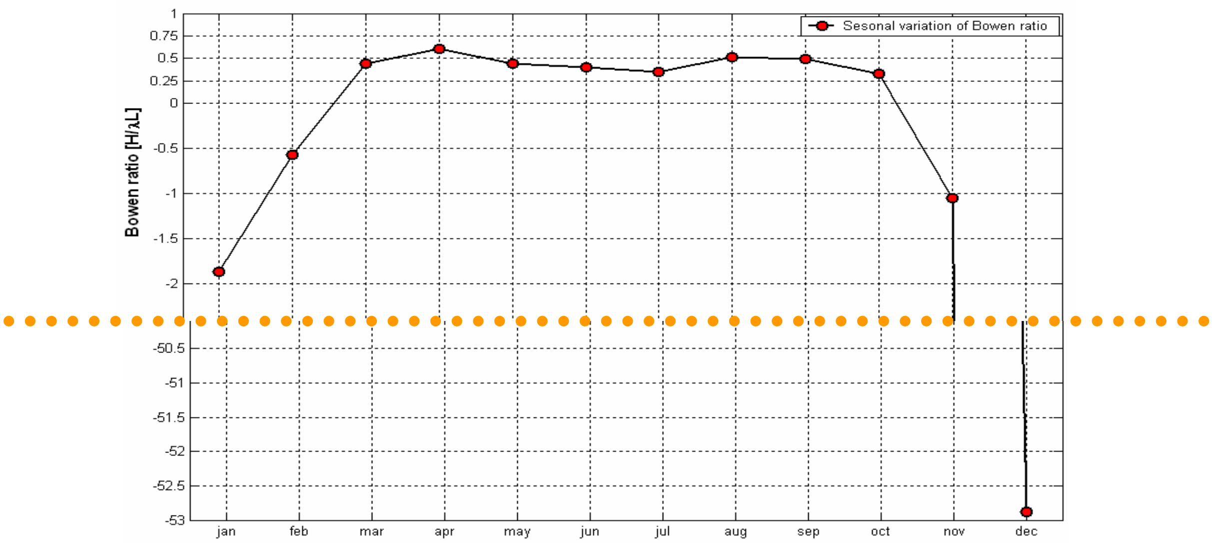

Figure A6.5.6: **Seasonal variation of Bowen ratio**

Table A6.5.3: **Values of monthly variation of Bowen ratio**

[W/m^2]	jan	feb	mar	apr	may	jun	jul	aug	sep	oct	nov	dec
H/λE	-1.87	-0.57	0.44	0.61	0.45	0.41	0.35	0.51	0.49	0.33	-1.05	-52.8

Negative values for Bowen ratio usually occur only when sensible heat (H) is low, around sunrise, sunset and occasionally at night [*Brutsaert*, 1991]. This situation does occur more often in cold weather [*Garratt*, 1992].

The Bowen ratio is negative during the winter season and positive from March to October. The wet canopy tends to act as a sink for sensible heat flux (H was directed downwards, supplying the energy for evaporation of intercepted rainfall), especially throughout the winter months, resulting in the negative Bowen ratio. This contrasts dramatically with March to October turbulent exchange, which was usually dominated by upward sensible heat flux.

A6.5.2 Evapotranspiration

A6.5.2.1 Annual evapotranspiration

Evapotranspiration was obtained when corrected measured latent heat flux was divided by λ = 2.45 MJ/kg [*Garratt*, 1992; *FAO*, 1998].

Figure A6.5.7 shows the cumulative precipitation, potential evapotranspiration (obtained form the Penman-Monteith equation for reference grassland) and actual (measured) evapotranspiration. Cumulative precipitation was 1078 mm, potential evapotranspiration (PET) was 471 mm (~ 44% of total precipitation) and actual evapotranspiration (AET) was 353 mm (~ 33% of cumulative precipitation). We can assume that more precipitation must have gone down to the groundwater (stored as soil moisture or exported to the streams). Evaporation shows a flat part when radiation is lower in winter.

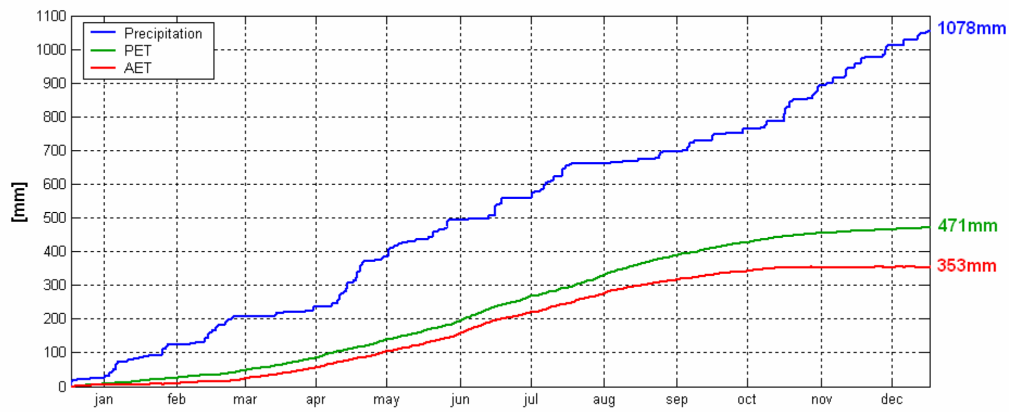

Figure A6.5.7: Cumulative: precipitation; potential evapotranspiration (PET) and actual evapotranspiration (AET).

A6.5.2.2 Monthly evapotranspiration

Figure A6.5.8 shows monthly mean air temperature with standard deviation, monthly precipitation and evapotranspiration. The monthly evapotranspiration shows a clear seasonal pattern with maximum values reached during the summer months and minimum values in winter time (see Table A6.5.4).

Table A6.5.4: Monthly temperature, precipitation and evapotranspiration

months	jan	feb	mar	apr	may	jun	jul	aug	sep	oct	nov	dec
t_{air} [°C]	6	6	8	9	11	14	15	16	14	10	9	7
prec [mm]	89	71	58	97	121	103	121	14	73	83	129	119
AET [mm]	6	7	26	42	49	68	50	53	31	20	1	~ 0

In summer, almost all of the precipitation is evaporated with hardly anything going to groundwater. A shift happens in October when more precipitation is lost via the runoff phenomenon. There is almost nothing to evaporate when radiation is lower in winter.

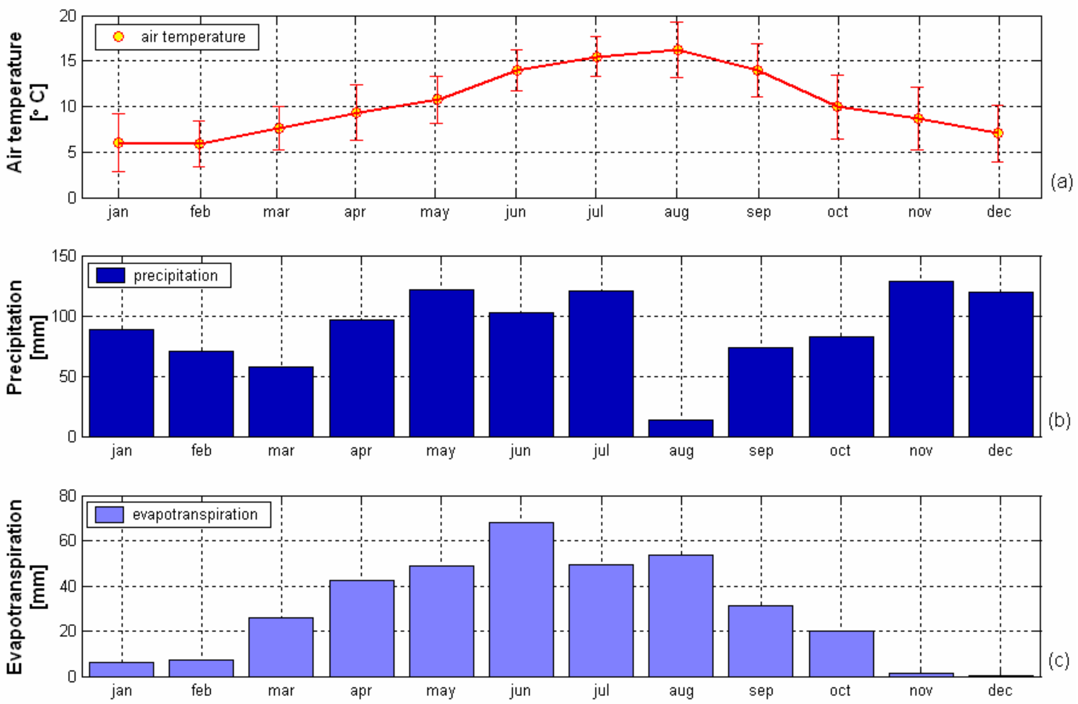

Figure A6.5.8: Monthly: (a) air temperature with standard deviations; (b) precipitation; and evapotranspiration

Two main meteorological factors driving the evapotranspiration are Radiation and vapour pressure deficit (VPD) [*Campell and Norman*, 1998], the increase of both enhancing evapotranspiration. The beginning of the year was very wet, and evapotranspiration is low due to the low air temperature, low VPD (see Figure A6.5.9 (a)) and the short height of grass (LAI is low). From March to June air temperature rises, average precipitation is above 100 mm per month and evapotranspiration reaches the highest level in June (68 mm). August is dryer and although the temperature reaches its maximum in August, the rate of evapotranspiration is smaller compared with June. The decrease in LAI caused by grass cutting in August also contributes to the decrease of evapotranspiration. The end of the year is wet, and because of low temperatures and low LAI evapotranspiratinon is low.

A6.5.2.3 Measured and modelled evapotranspiration

The Penman-Monteith equation for reference grassland was used to compare actual evapotraspiration with potential evapotraspiration. Their monthly values are given in the Table A6.5.5. The actual evapotranspiration was estimated as 75% of potential.

Figure A6.5.9 shows monthly vapour pressure deficit, evapotranspiration from the reference grassland, and measured evapotranspiration. The higher vapour pressure deficit, the more space in the air for accepting the water vapour. The high humidity and low potential for evaporation of the region is evidenced by low VPD's with a maximum of 0.36 kPa in August and as low as 0.14 kPa in the winter months. Potential evapotraspiration closely follows this pattern and for that reason is higher than measured evapotraspiration. Namely, measured evapotraspiration mostly follows the vapour pressure deficit pattern. Examining August (Table A6.5.5) we note that the actual evapotranspiration was 53 mm, while the potential was 72 mm. This confirms that the evapotranspiration was water limited in August. Differences between reference and measured evapotranspiration is also high for winter months that might be due to low LAI and net radiation.

Table A6.5.5: Actual and potential evapotranspiration in [mm] and water pressure deficit in [kPa]

months	jan	feb	mar	apr	may	jun	jul	aug	sep	oct	nov	dec
VPD [kPa]	0.15	0.14	0.17	0.23	0.21	0.27	0.26	0.36	0.26	0.25	0.15	0.14
AET (353mm)	6	7	26	42	49	68	50	53	31	20	1	~ 0
PET (471mm)	17	16	32	48	54	71	56	72	45	34	17	10
Δ (AET/PET)*100 (%)	35	44	81	88	91	96	89	74	69	59	6	± ∞

PET/AET	2.8	2.3	1.2	1.1	1.1	1.0	1.1	1.4	1.4	1.7	17	± ∞

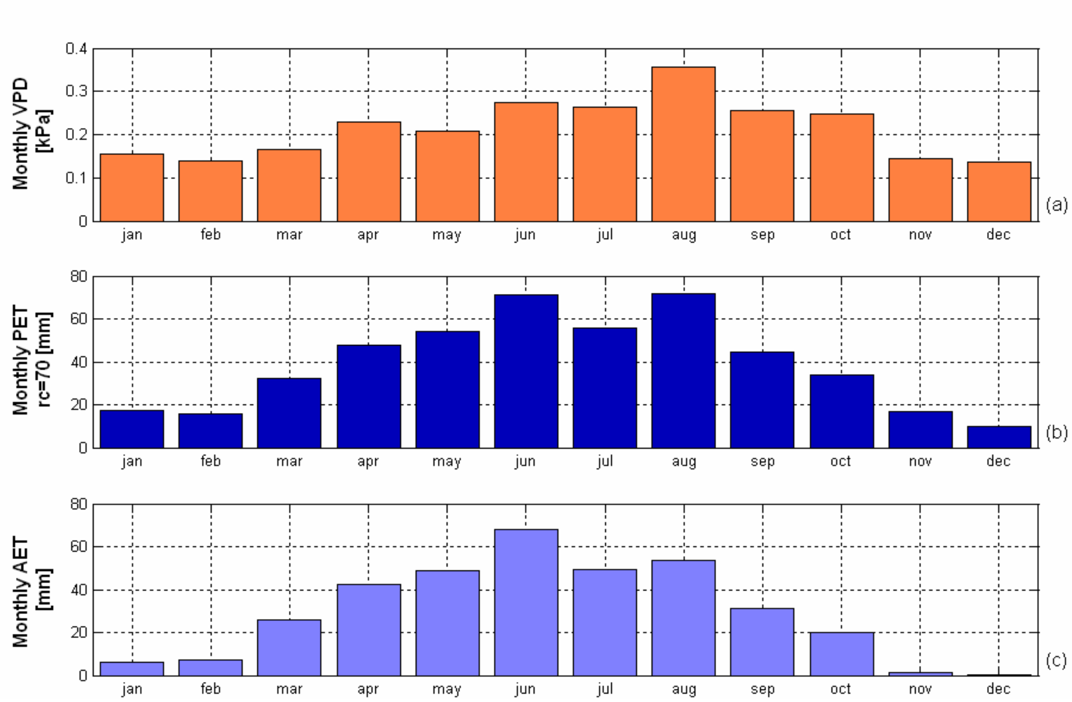

Figure A6. 5.9: Monthly (a) averaged water pressure deficit [kPa]; (b) evapotranspiration from reference grassland (r_c = 70s/m); and (c) measured evapotranspiration.

A6.6 Carbon dioxide flux

A6.6.1 Data analysis

A6.6.1.1 Precipitation filter

It was found that 6% of day data and 8% of night data were rejected after the application of precipitation filter (see Chart A6.6.1).

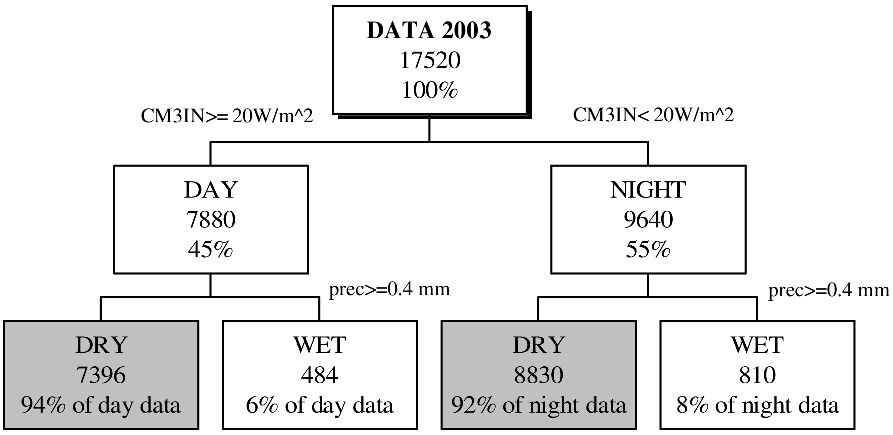

Chart A6.6.1: Day and Night data and percentage of their goodness regarding the precipitation filter

A6.6.1.2 Momentum flux filter

Observing the night time Webb corrected flux during the dry periods and corresponding values for friction velocity (Figure A6.6.1), we estimate the threshold for friction velocity as 0.15 m/s. Therefore we filtered CO_2 fluxes at night when $u_* < 0.15$ m/s [*Pattey et al.*, 2002; *Baldocchi et al.*, 2003].

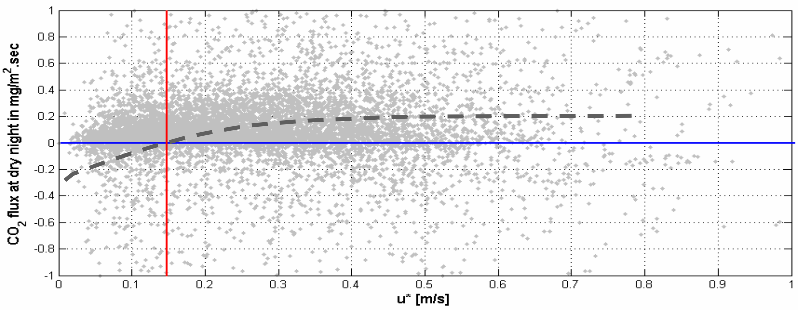

Figure A6.6.1: CO_2 flux during the dry nights in [mg/m^2/sec] versus friction velocity during the dry nights in [m/s]

It can be seen from the frequency histogram (Figure A6.6.2) of the friction velocity for dry nights that values below 0.15 m/s occur approximately 22.7% of dry nighttime. This value is consistent with the average data retrieved during a year for eddy covariance systems in the literature.

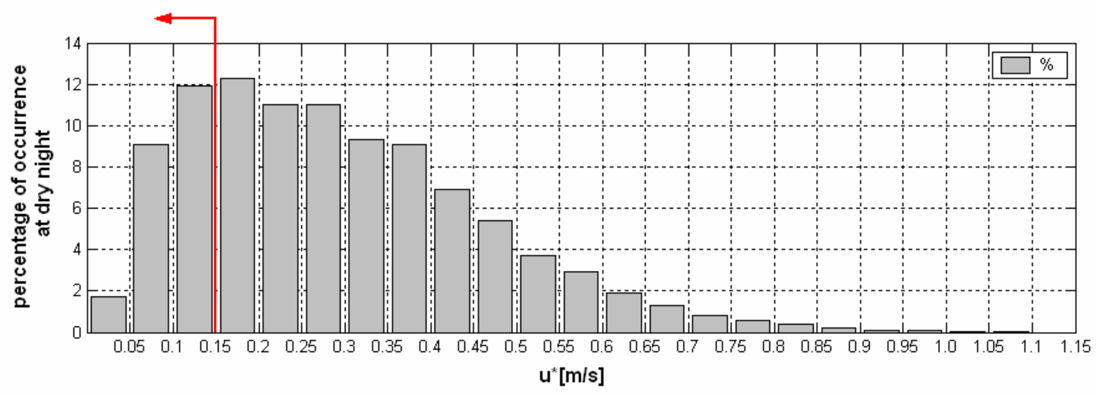

Figure A6.6.2: Frequency histogram of friction velocity during the nighttime without precipitation

A6.6.1.3 CO_2 filter for nighttime

We filtered nighttime fluxes when respiration exceeded predetermined threshold values for the season (see Table A6.6.1) and when the friction velocity was less than 0.15 m/s.

Table A6.6.1: CO_2 filter for nighttime and data goodness

(u*>=0.15 m/s)	NEE limit [μmol/m^2/s]	2003		
		good	**bad**	**sum**
Jan – Feb	up to 7	947	1017	1964
		48%	52%	
Mar – Apr	up to 10	667	826	1493
		45%	55%	
May – Jun	up to 15	565	580	1145
		49%	51%	
Jul – Aug	up to 15	552	685	1237
		45%	55%	
Sep – Oct	up to 10	587	1072	1659
		35%	65%	
Nov – Dec	up to 7	713	1429	2142
		33%	67%	
		4031	**5609**	**9640**

	42%	58%	

For instance, the night time summer fluxes were accepted if $u_* \geq 0.15$ m/s, $f_c > 0$ μmol/m^{2}s (there is no photosynthesis) and $f_c < 15$ μmol/m^{2}s. The nighttime data were binned in two-month increments according to Falge et al., [2001]. After filtering of nighttime CO_2 flux data it was found that 42% of night data were good.

A6.6.1.4 CO_2 filter for daytime

No physical environmental conditions were applied to filter CO_2 flux at day times. We filtered daytime fluxes when respiration and uptake exceeded predetermined threshold values for the season (see Table A6.6.2).

The daytime data was binned in two-month increments according to Falge et al., [2001]. For instance, the daytime summer fluxes were accepted if $f_c > -35$ μmol/m^{2}s and $f_c < 15$ μmol/m^{2}s. Daytime data were good in 85% of all cases.

Table A6.6.2: CO_2 filter for daytime and data goodness

	NEE [μmol/m^2/s]	NEE [μmol/m^2/s]	2003		
			good	**bad**	**sum**
Jan – Feb	-15	5	768	148	916
			84%	16%	
Mar – Apr	-25	10	1170	217	1387
			84%	16%	
May – Jun	-35	15	1494	289	1783
			84%	16%	
Jul – Aug	-35	15	1523	216	1739
			88%	12%	
Sep – Oct	-25	10	1100	169	1269
			87%	13%	
Nov – Dec	-15	5	621	165	786
			79%	21%	
			6676	**1204**	**7880**
			85%	**15%**	

A6.6.1.5 Quality of data

After post-processing and filtering of spurious data, 61% of the CO_2 flux data were suitable for analysis. The percentage of usable data reported by other studies is approximately 65% [*Falge et al.*, 2001; *Law et al.*, 2002]. The remaining data (39%) were rejected when found to be out of range or during periods of low nighttime friction velocity or due to water drops on the LI-7500 during the rain and within hour after the rain.

A6.6.1.6 Contribution of Webb correction

After the Webb correction and filtering it was important to find out how big Webb correction contribution is to the CO_2 flux. We plotted measured CO_2 flux against Webb corrected and filtered CO_2 flux for all good daytime and good night time data (Figure A6.6.3).

According to correlation found between these two fluxes (see Figure A6.6.3), average reduction of the flux after Webb correction is 5.2%.

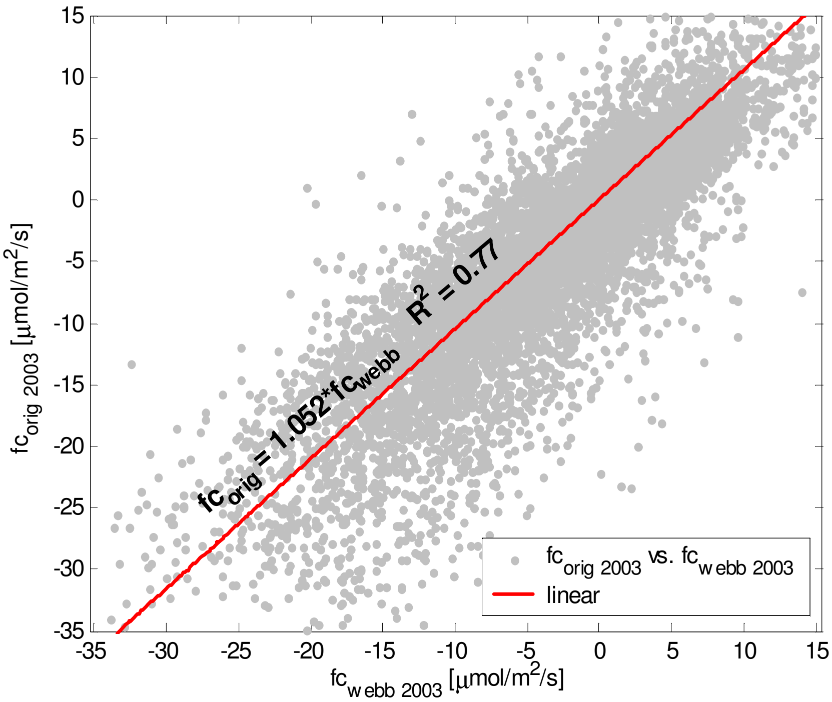

Figure A6.6.3: Correlation between measured and Webb corrected CO_2 flux for 2003

Plots of correlation between measured and Webb corrected flux for each two month period are shown in Figure A6.6.4. The Webb correction reduces the magnitude of the fluxes in both day and night periods. The greatest reduction of the flux in average is for period March-April, when it is 31%.

It is important to note for some particular cases 30 minute and daily CO_2 flux reduction by Webb correction may be much greater/smaller than the average reduction for the whole year or two month periods.

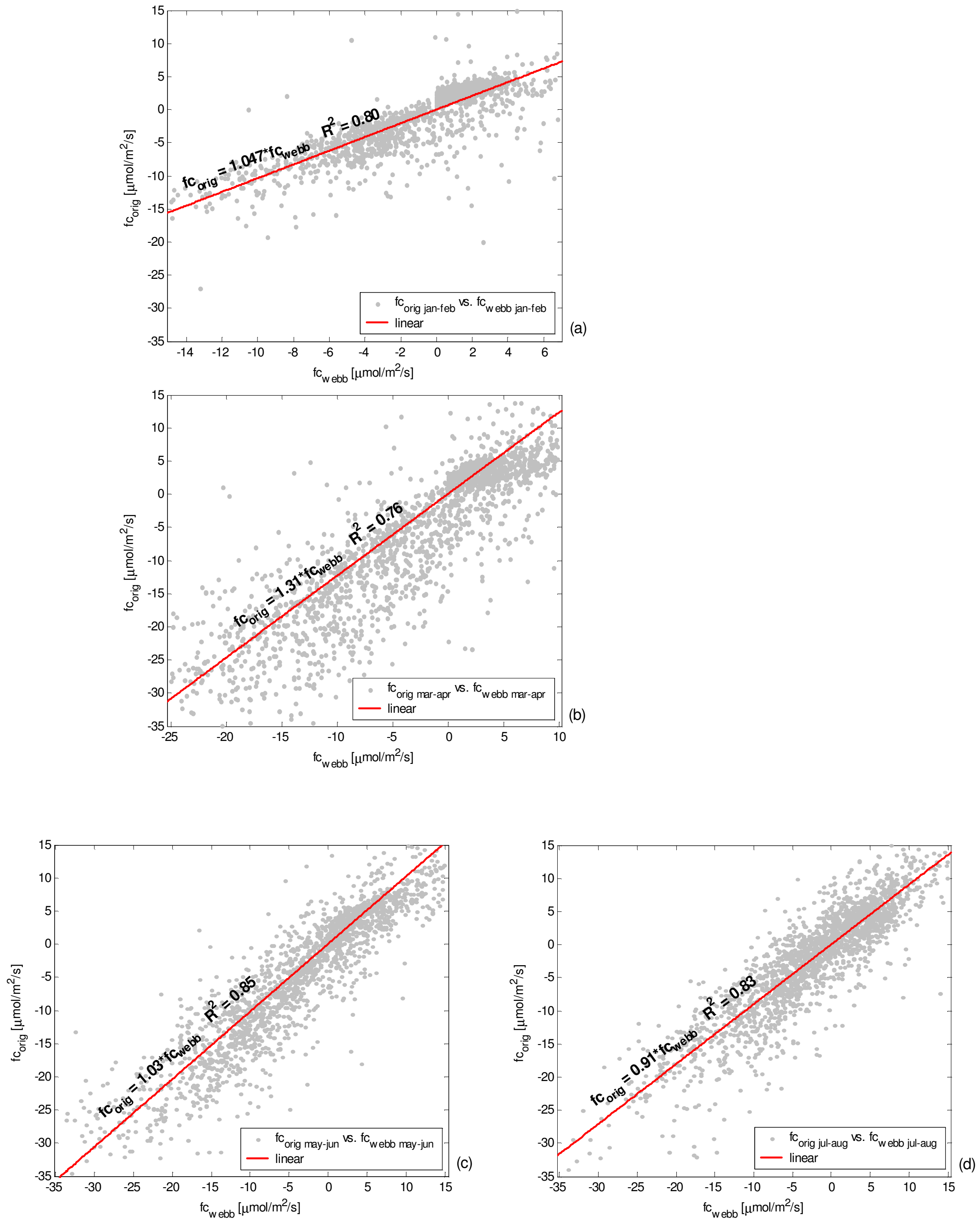
fc_orig = 1.047*fc_webb R^2 = 0.80
fc_orig jan-feb vs. fc_webb jan-feb
linear
(a)
fc_orig [µmol/m^2/s]
fc_webb [µmol/m^2/s]
fc_orig = 1.31*fc_webb R^2 = 0.76
fc_orig mar-apr vs. fc_webb mar-apr
linear
(b)
fc_orig = 1.03*fc_webb R^2 = 0.85
fc_orig may-jun vs. fc_webb may-jun
linear
(c)
fc_orig = 0.91*fc_webb R^2 = 0.83
fc_orig jul-aug vs. fc_webb jul-aug
linear
(d)

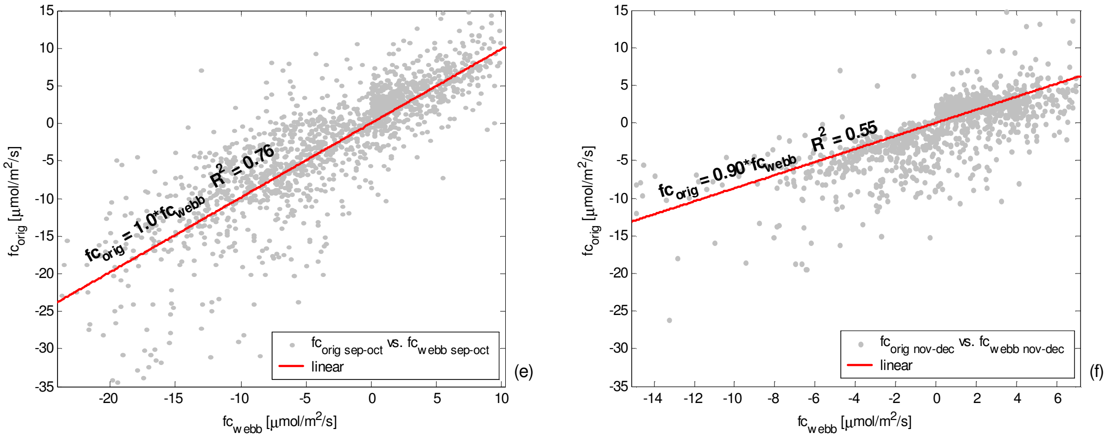

Figure A6.6.4: Contributions of Webb correction to final CO_2 flux two by two months for: (a) January-February; (b) March-April; (c) May-June; (d) July-August; (e) September-October; (f) November-December

A6.6.2 Gap filling

A6.6.2.1 Nighttime gap filling

For nighttime data, the ecosystem respiration is known to be linked to the soil temperature [*Lloyd and Taylor*, 1994; *Kirschbaum*, 1995] and to a lesser extent to soil moisture (consistent with the analysis of Novick et al. [2004] for warm temperate grassland). Different temperature response functions were tested (Table A6.6.3) and parameterised statistically. The Matlab curve fitting toolbox was used to determine parameterisation of those functions, as well as the goodness of each fit in terms of SSE (Sum of Squares Error), R^2 (Root-Square), adjusted-R^2 (adjusted Root Square), and RMSE (Root Mean Squared Error).

The best fit for nighttime was obtained for the quadratic polynomial function defined as:

$$F_{ni} = p_1 \times t_{soil}^2 + p_2 \times t_{soil} + p_3 \tag{6.1}$$

where t_{soil} is the soil temperature at 5 cm depth in ºC, p_1 = 0.0055, p_2 = 0.328 and p_3 = -0.323.

Table A6.6.3: Fitting functions for nighttime

	Equation	Coefficients	SSE	R^2	Ad. R^2	RMSE
Arrhenius function	$F_{ni} = a \times e^{\left(b - \frac{c}{t_{soil}}\right)}$	a = 0.661 ± 2.065e6 b = 2.693 ± 3.112e6 c = 8.936 ± 0.453	1.1e4	0.5166	0.5164	1.76
Q_{10} func. 25°C	$F_{ni} = a \times b^{\left(\frac{t_{soil} - 25}{10}\right)}$	a = 17.42 ± 0.79 b = 3.094 ± 0.116	1.05e4	0.5359	0.5358	1.724
Exp. fitting	$F_{ni} = a \times e^{(b \times t_{soil})}$	a = 1.0.35 ± 0.055 b = 0.113 ± 0.004	1.05e4	0.5359	0.5358	1.724
Linear fitting	$F_{ni} = a \times t_{soil} + b$	a = 0.439 ± 0.01128 b = -0.774 ± 0.131	1.0e4	0.5593	0.5592	1.68
Quadratic poly func.	$F_{ni} = p_1 \times t_{soil}^2 + p_2 \times t_{soil} + p_3$	p_1 = 0.0055 ± 2.8e-3 p_2 = 0.328 ± 0.0588 p_3 = -0.323 ± 0.2682	9968	0.5611	0.5608	1.677

Figure A6.6.5 shows that the regression of nighttime CO_2 fluxes against soil temperature is a very scattered plot. This is likely linked to the different respiration sources, leaf and soil. They have not been separated in this study but their contribution changes over time and in response to different developmental factors. However, this separation is not possible without independent measurements of soil and vegetation respiration.

In using t_{soil} at one location near the tower, this does not represent the t_{soil} in the total footprint. Akin to the debate about energy balance closure where Rn and G are measured at one point and may not represent the flux footprint.

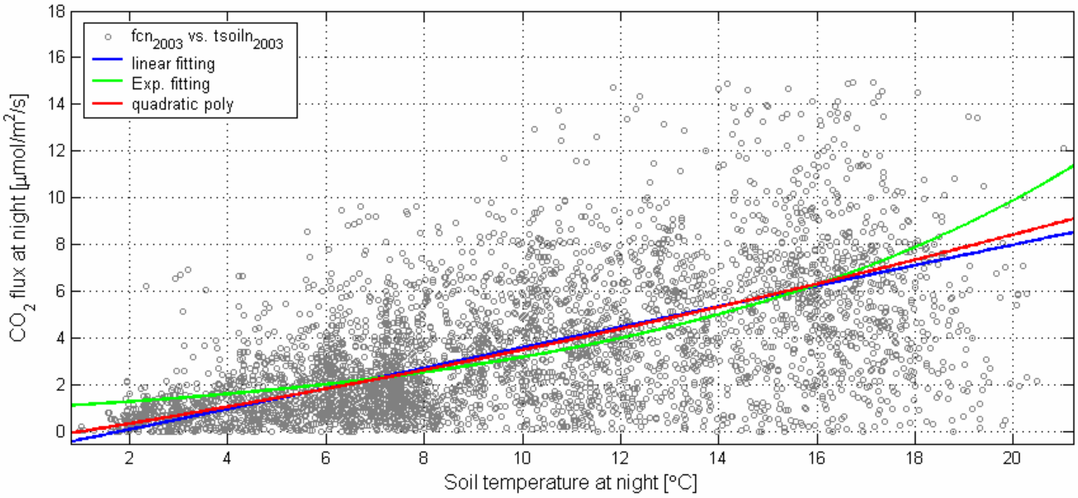

Figure A6.6.5: **Nighttime fitting functions**

The nighttime CO_2 flux for bad night data points was found using equation 6.1 with coefficients in Table A6.6.3 and the soil temperature for those data points.

A6.6.2.2 Daytime gap filling

For daytime, the net ecosystem exchange of CO_2 is linked to the photosynthetic photon flux density Q_{ppfd} (photosynthetic active radiation Q_{par}) in μmol of quantum/m^2/s [e.g., *Michaelis and Menten*, 1913; *Smith*, 1938; *Goulden et. al.*, 1996]. The Matlab curve fitting toolbox was used to parameterise different light response functions, and determine goodness of each fit (see Tables from A6.6.4 to A6.6.9). Since Q_{par} varies seasonally, data were analysed for and the function was fitted to two-month data bins. For periods of two months two best fits are shown in figures from A6.6.6 to A6.6.11.

Table A6.6.4: Fitting function for daytime for January and February

January February	Equation	Coefficients	SEE	R^2	Ad. R^2	RMSE
Ruimy func.	$F_d = \frac{\alpha\times Q_{par}\times\beta}{(\alpha\times Q_{par}+\beta)}+\gamma$	α = -1.191 ± 1.757e+9 β = 188.5 ± 1.391e+7 γ = -192.4 ± 1.391e7	5436	0.0069	0.0037	2.961
Michaelis function	$F_d = \frac{\alpha\times Q_{par}}{\left(1-\frac{Q_{par}}{2000}+\frac{\alpha\times Q_{par}}{\beta}\right)}+\gamma$	α = -5416 ± 1.185e10 β = 16.22 ± 1.775e7 γ = -20.08± 1.775e7	5473	0.0001	-0.0031	2.971
Smith func.	$F_d = \frac{\alpha\times\beta\times Q_{par}}{\sqrt{\beta^2+(\alpha\times Q_{par})^2}}+\gamma$	α = 22.92 ± 1.161e8 β = 3.292 ± 1.111e7 γ = -7.149 ± 1.111e7	5474	-1.6e-6	-0.0032	2.971
Linear func.	$F_d = \alpha\times Q_{par}+\beta$	α = -0.012 ± 0.001 β = -0.11 ± 0.32	3272	0.4022	0.4013	2.295
Misterlich function	$F_d = -24\times\left(1-e^{\left(\frac{\alpha\times Q_{par}}{-24}\right)}\right)+\gamma$	α = 0.0142 ± 0.002 γ = -0.798 ± 0.359	3218	0.4121	0.4111	2.276

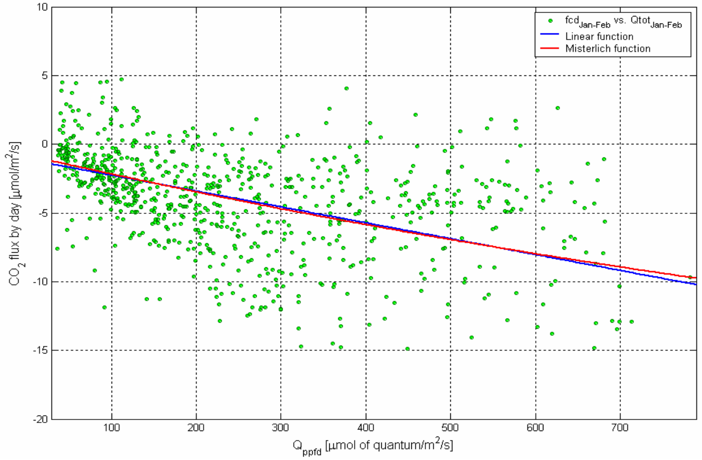

Figure A6.6.6: **Best daytime fitting curves for Jan. and Feb.**

Table A6.6.5: Fitting function for daytime for March and April

March April	Equation	Coefficients	SEE	R^2	Ad. R^2	RMSE
Ruimy func.	$F_d = \frac{\alpha\times Q_{par}\times\beta}{(\alpha\times Q_{par}+\beta)}+\gamma$	α = -1.206e4 ± 4.03e7 β = 1054 ± 1.76e6 γ = -1062 ± 1.76e6	4.55e4	0.0694	0.06752	6.798
Michaelis function	$F_d = \frac{\alpha\times Q_{par}}{\left(1-\frac{Q_{par}}{2000}+\frac{\alpha\times Q_{par}}{\beta}\right)}+\gamma$	α = -1.714e4 ± 7.81e9 β = 164.3 ± 3.747e7 γ = -172.3 ± 3.747e7	4.89e4	0.0012	-0.0008	7.043
Smith func.	$F_d = \frac{\alpha\times\beta\times Q_{par}}{\sqrt{\beta^2+(\alpha\times Q_{par})^2}}+\gamma$	α = 2.096 ± 2.557e7 β = -0.728 ± 5.922e6 γ = -7.249 ± 5.922e6	4.89e4	5.22e-7	-0.0020	7.047
Linear func.	$F_d = \alpha\times Q_{par}+\beta$	α = -0.0155 ± 0.0008 β = -0.517 ± 0.539	2.08e4	0.5744	0.5739	4.595
Misterlich function	$F_d = -24\times\left(1-e^{\left(\frac{\alpha\times Q_{par}}{-24}\right)}\right)+\gamma$	α = 0.0368 ± 0.00485 γ = 4.249 ± 0.963	1.85e4	0.6207	0.6204	4.338

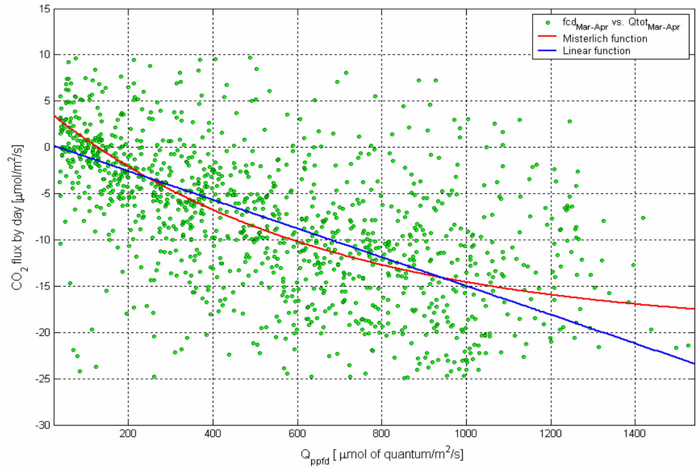

Figure A6.6.7: **Best daytime fitting curves for Mar. and Apr.**

Table A6.6.6: Fitting function for daytime for May and June

May June	**Equation**	**Coefficients**	**SEE**	**R^2**	**Ad. R^2**	**RMSE**
Ruimy func.	$F_d = \frac{\alpha \times Q_{par} \times \beta}{(\alpha \times Q_{par} + \beta)} + \gamma$	α = -1.173e4 ± 5.62e6 β = 1894 ± 4.54e5 γ = -1902 ± 4.54e5	4.79e4	0.1879	0.1866	6.321
Michaelis function	$F_d = \frac{\alpha \times Q_{par}}{\left(1 - \frac{Q_{par}}{2000} + \frac{\alpha \times Q_{par}}{\beta}\right)} + \gamma$	α = -8719 ± 1.397e10 β = 46.71 ± 3.742e7 γ = -53.91± 3.742e7	5.90e4	1.81e-4	-0.0015	7.014
Smith func.	$F_d = \frac{\alpha \times \beta \times Q_{par}}{\sqrt{\beta^2 + (\alpha \times Q_{par})^2}} + \gamma$	α = 26.99 ± 2.566e8 β = -2.405 ± 1.524e7 γ = -4.793 ± 1.524e7	5.90e4	1.0e-7	-0.0017	7.015
Linear func.	$F_d = \alpha \times Q_{par} + \beta$	α = -0.011 ± 6.7e-4 β = -0.0376 ± 0.5325	3.22e4	0.454	0.4536	5.181
Misterlich function	$F_d = -24 \times \left(1 - e^{\left(\frac{\alpha \times Q_{par}}{-24}\right)}\right) + \gamma$	α = 0.0252 ± 0.003 γ = -3.681 ± 0.852	2.89e4	0.510	0.5092	4.91

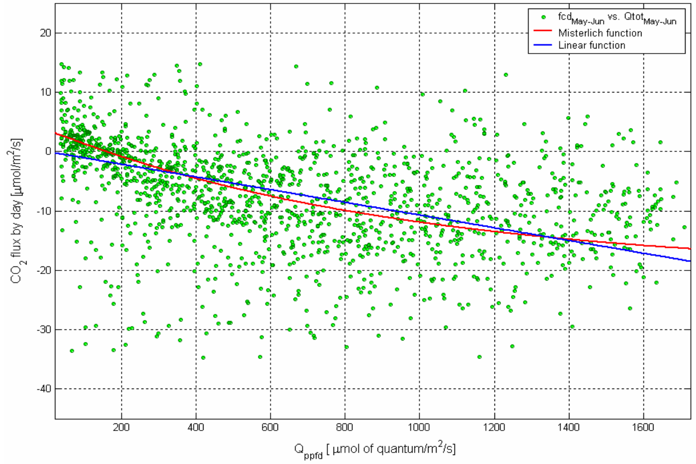

Figure A6.6.8: **Best daytime fitting curves for May. and Jun.**

Table A6.6.7: Fitting function for daytime for July and August

July August	**Equation**	**Coefficients**	**SEE**	**R^2**	**Ad. R^2**	**RMSE**
Ruimy func.	$F_d = \frac{\alpha \times Q_{par} \times \beta}{(\alpha \times Q_{par} + \beta)} + \gamma$	α = -7621 ± 4.981e5 β = 2455 ± 7.68e4 γ = -2464 ± 8.172e4	2.43e4	0.3435	0.3423	4.693
Michaelis function	$F_d = \frac{\alpha \times Q_{par}}{\left(1 - \frac{Q_{par}}{2000} + \frac{\alpha \times Q_{par}}{\beta}\right)} + \gamma$	α = -130.8 ± 1.469e9 β = 0.717 ± 4.025e6 γ = -6.214 ± 4.025e6	3.7e4	3.66e-6	-0.0018	5.73
Smith func.	$F_d = \frac{\alpha \times \beta \times Q_{par}}{\sqrt{\beta^2 + (\alpha \times Q_{par})^2}} + \gamma$	α = -0.208 ± 8.993e6 β = -0.0658 ± 1.893e6 γ = -5.563 ± 1.893e6	3.7e4	-4.7e-8	-0.0018	5.73
Linear func.	$F_d = \alpha \times Q_{par} + \beta$	α = -0.009 ± 5.9e-4 β = 0.0189 ± 0.446	2.09e4	0.434	0.4334	4.309
Misterlich function	$F_d = -24 \times \left(1 - e^{\left(\frac{\alpha \times Q_{par}}{-24}\right)}\right) + \gamma$	α = 0.015 ± 0.0014 γ = 1.597 ± 0.566	1.96e4	0.470	0.4697	4.169

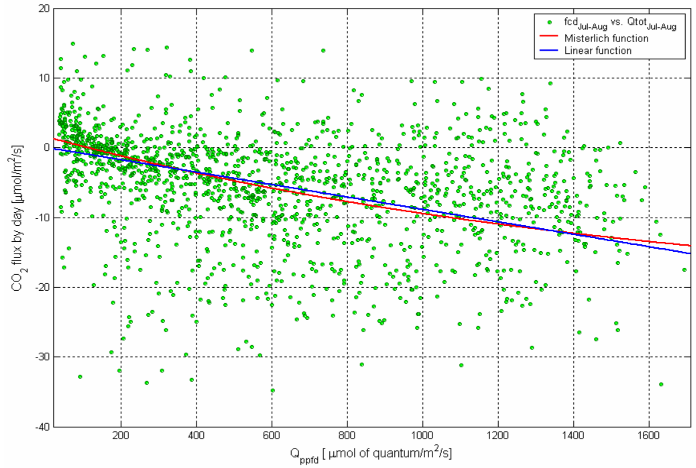

Figure A6.6.9: **Best daytime fitting curves for Jul. and Aug.**

September October	Equation	Coefficients	SEE	R^2	Ad. R^2	RMSE
Ruimy func.	$F_d = \frac{\alpha\times Q_{par}\times\beta}{(\alpha\times Q_{par}+\beta)}+\gamma$	α = -1.201e4 ± 2.08e7 β = 1211 ± 1.05e6 γ = -1219 ± 1.05e6	3.82e4	0.0667	0.065	5.899
Michaelis function	$F_d = \frac{\alpha\times Q_{par}}{\left(1-\frac{Q_{par}}{2000}+\frac{\alpha\times Q_{par}}{\beta}\right)}+\gamma$	α = -1.805e4 ± 4.99e8 β = 620.7 ± 8.58e6 γ = -627.2 ± 8.58e6	2.08e4	0.0227	0.0204	4.911
Smith func.	$F_d = \frac{\alpha\times\beta\times Q_{par}}{\sqrt{\beta^2+(\alpha\times Q_{par})^2}}+\gamma$	α = -0.672 ± 1.637e8 β = -0.008 ± 1.25e7 γ = -6.497 ± 1.25e7	2.13e4	-1e-13	-0.0023	4.968
Linear func.	$F_d = \alpha\times Q_{par}+\beta$	α = -0.011 ± 7.7e-4 β = -1.297 ± 0.441	1.13e4	0.4685	0.4678	3.62
Misterlich function	$F_d = -24\times\left(1-e^{\left(\frac{\alpha\times Q_{par}}{-24}\right)}\right)+\gamma$	α = 0.0169 ± 0.0017 γ = -0.0208 ± 0.5612	1.07e4	0.4964	0.4958	3.524

Table A6.6.8: Fitting function for daytime for September and October

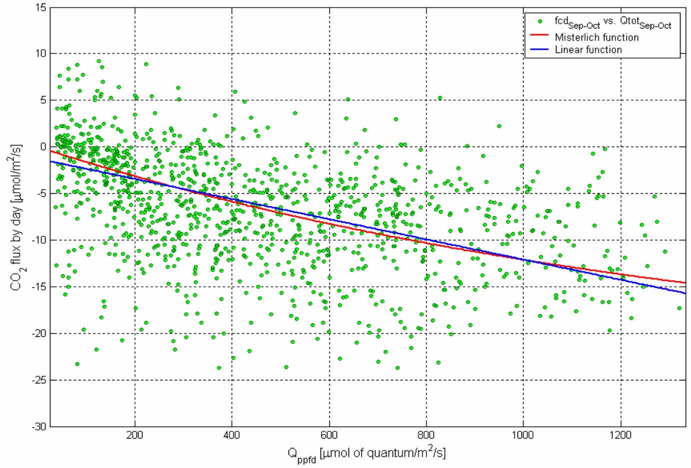

Figure A6.6.10: Best daytime fitting curves for Sep. and Oct.

November December	Equation	Coefficients	SEE	R^2	Ad. R^2	RMSE
Rui[illegible]	$\frac{\alpha\times Q_{par}\times\beta}{[illegible]}$	α = 308.2 ± 3.502e6 [illegible]	[illegible]	[illegible]	[illegible]	[illegible]
Misterlich function	$F_d = -24\times\left(1-e^{\left(\frac{\alpha\times Q_{par}}{-24}\right)}\right)+\gamma$	α = 0.0137 ± 0.0016 γ = 0.383 ± 0.304	904	0.4836	0.4823	1.488
[illegible] function	$\left(1-\frac{Q_{par}}{2000}+\frac{\alpha\times Q_{par}}{\beta}\right)$	β = 1.063 ± 1.816e6 γ = -3.19 ± 1.816e6	1751	-0.0002	-0.0051	2.074
Smith func.	$F_d = \frac{\alpha\times\beta\times Q_{par}}{\sqrt{\beta^2+(\alpha\times Q_{par})^2}}+\gamma$	α = 7.763 ± 4.437e7 β = 2.634 ± 1.004e7 γ = -4.762 ± 1.004e7	1750	-1.2e-5	-0.0049	2.074
Linear func.	$F_d = \alpha\times Q_{par}+\beta$	α = -0.0117 ± 0.0012 β = 0.184 ± 0.278	921	0.4738	0.4725	1.502

Table A6.6.9: Fitting function for daytime for November and December

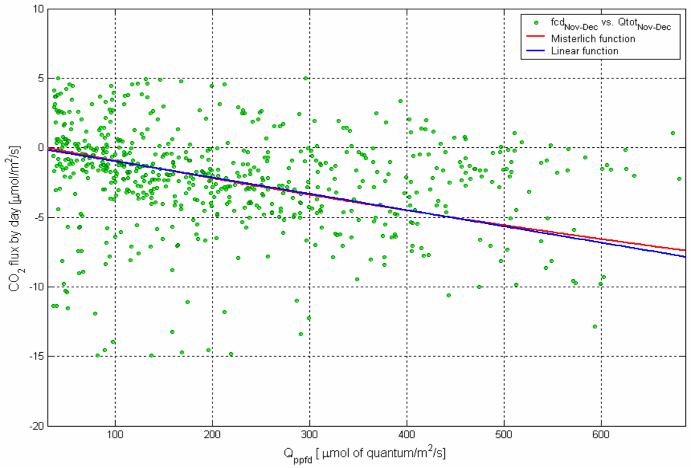

Figure A6.6.11: **Best daytime fitting curves for Nov. and Dec.**

The best fit was obtained with the Misterlich formula defined as:

$$F_{day} = -24 \times \left(1 - e^{\left(\frac{\alpha \times Q_{par}}{-24}\right)}\right) + \gamma \tag{6.2}$$

where $Q_{par} \equiv Q_{ppfd}$ is the photosynthetic photon flux density in µmol of quantum/m^2/s. Table A6.6.10 gives coefficients α and γ for adopted Misterlich function:

Table A6.6.10: Coefficients α and γ for Misterlich function for 2002 and 2003

2003	Jan-Feb	Mar-Apr	May-Jun	Jul-Aug	Sep-Oct	Nov-Dec
α	0.0142	0.0368	0.0252	0.015	0.0169	0.0137
γ	-0.798	4.249	-3.681	1.597	-0.0208	0.383

A6.6.3 Results and discussion

A6.6.3.1 Daily flux

Figure A6.6.12 shows the daily uptake of CO_2 and the daily maximum temperature during 2003.

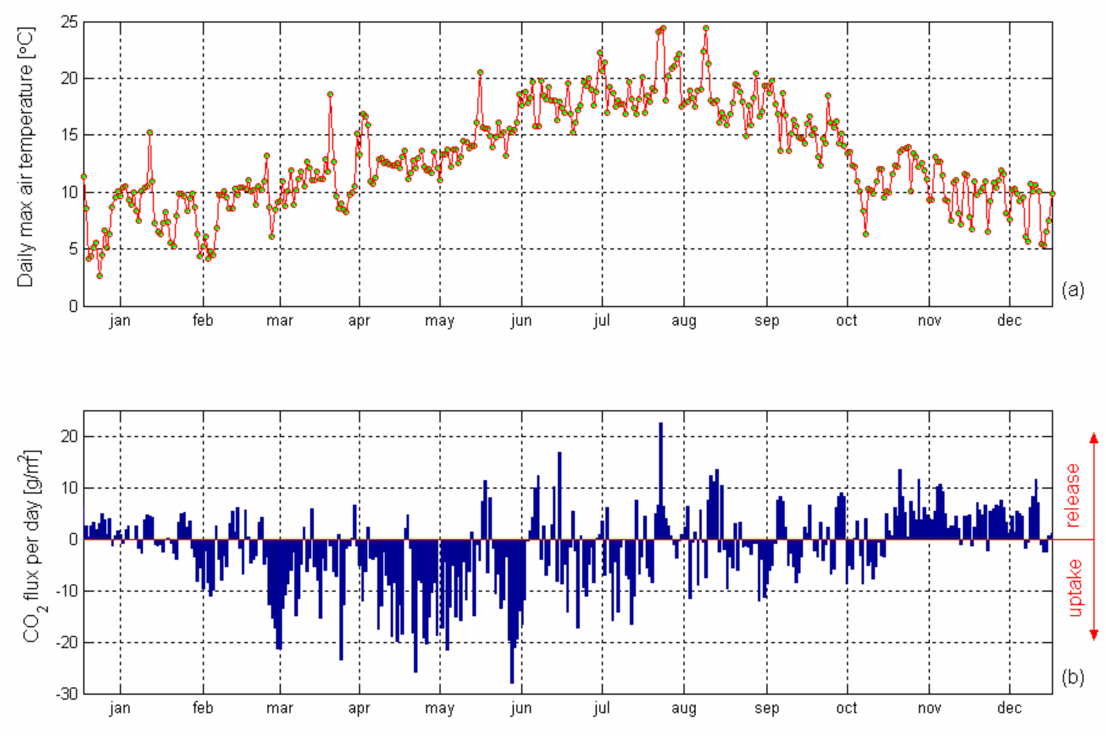

Figure A6.6.12: (a) daily maximum air temperature; and (b) daily CO_2 flux

The maximum daily uptake is –28g of $CO_2/m^2/d$ and occurs on 11th June when the maximum daily temperature was 15°C. The maximum daily emission is 22g of $CO_2/m^2/d$ and occurs on 6th August when the maximum daily temperature was 24°C. Those values are consistent with data from other grassland sites [e. g. *Saigusa et al.*, 1998; *Dugas et al.*, 1999; *Frank and Dugas*, 2001; *Sims and Bradford*, 2001]. Both days were with no rain, but cutting the grass on the 5th August caused this release of CO_2 flux, while the grass that was cut on 27th May was then emerging growth in June.

A6.6.3.2 Monthly flux

Examining the monthly uptake of CO_2 shown (Figure A6.6.13) and its values (Table A6.6.11), the seasonal trend is clear. The part of the year for which the site behaves as a sink of carbon is from February to October and period that it behaves as a source of carbon is from November to January. If we convert those data in average daily uptake during a month, we obtain for May (the month with the maximum sink), -9.7 g of $CO_2/m^2/d$ and for December (the month with the maximum source) average daily release of 5.3 g of $CO_2/m^2/d$.

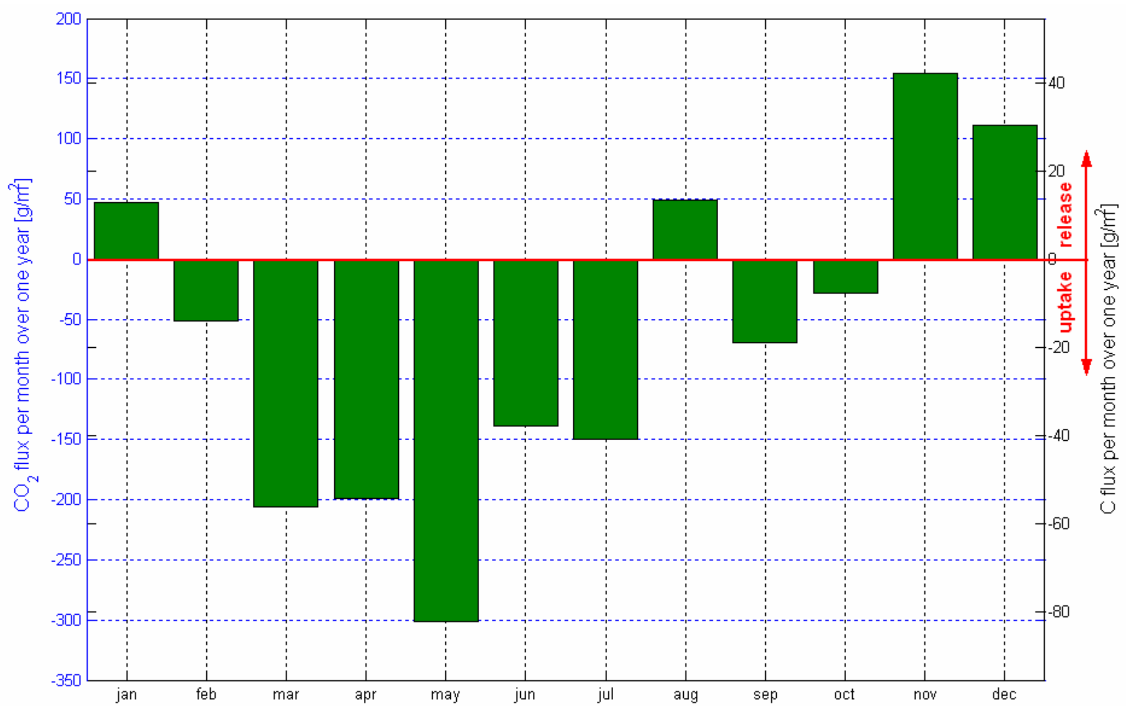

Figure A6.6.13: **Monthly CO_2 (C) flux in g/m^2**

Table A6.6.11: **Monthly CO_2 (C) flux in $[g/m^2]$**

$[g/m^2]$	jan	feb	mar	apr	may	jun	jul	aug	sep	oct	nov	dec
f_{CO2}	47	-51	-206	-199	-301	-139	-150	49	-69	-28	154	111
f_C	13	-14	-56	-54	-82	-38	-41	13	-19	-8	42	30

The monthly uptake of CO_2 in June is -139 g/m^2, which is less about 50% than in May. The reason for this is cutting the grass on 27th May and thus reduction of the LAI.

Also, notice that there is release of 49 g of CO_2/m^2 during August. The reasonsfor the release was twofold: first, the part of the grassland in the footprint was cut (on 5th August); and second, August was dry with 14 mm of rainfall (average temperature was 21°C) and the soil moisture consequently dropped from 0.46m^3/m^3 to 0.36m^3/m^3 (see Figure A6.3.5). It has been shown [*Frank and Dugas*, 2001] that short-term droughts during the growing season reduce CO_2 fluxes to near zero (photosynthesis balances respiration). Also, the timing and magnitude of precipitation events influence the total growing season flux and induce a considerable day-to-day variability in CO_2 fluxes. Decreases in LAI (Leaf Area Index) caused by the grass (silage) harvesting, reduce gross primary productivity (GPP) [*Budyko*, 1974].

Figures A6.6.14 and A6.6.15 show the mean daily courses of NEE with standard deviations month by month.

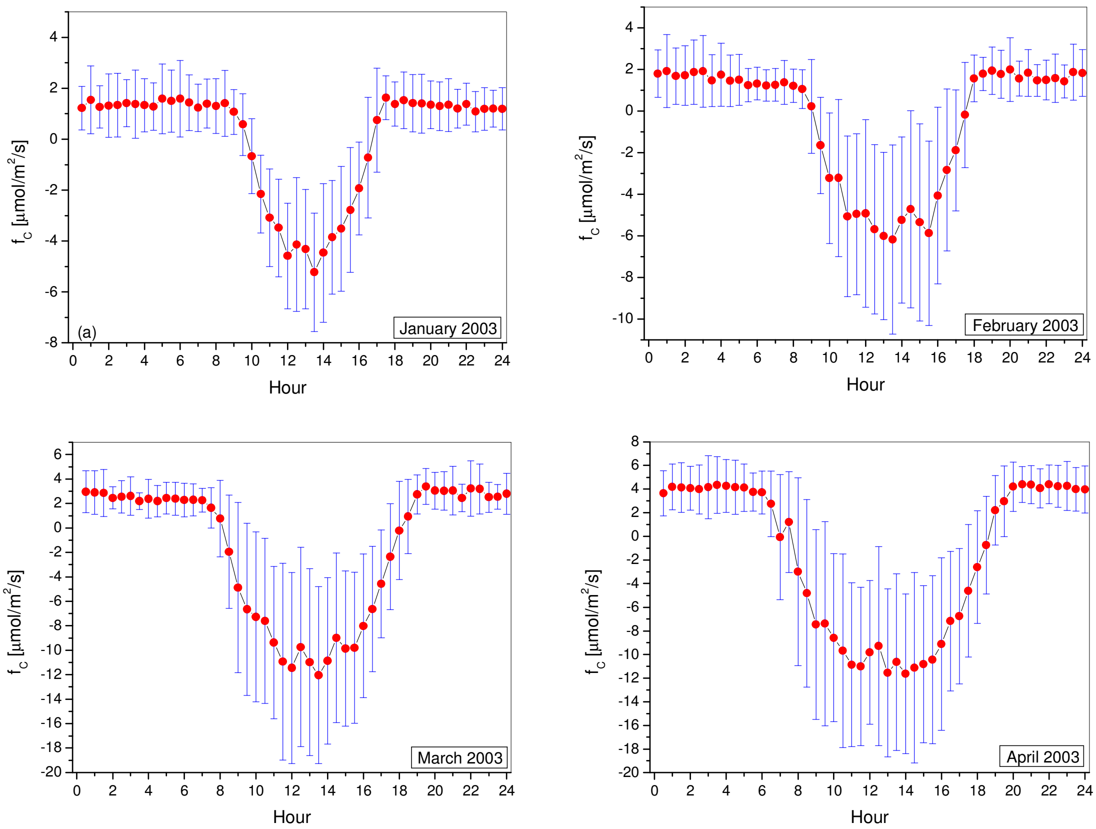

Figure A6.6.14: Mean daily courses of NEE with standard deviations for January, February, March and April

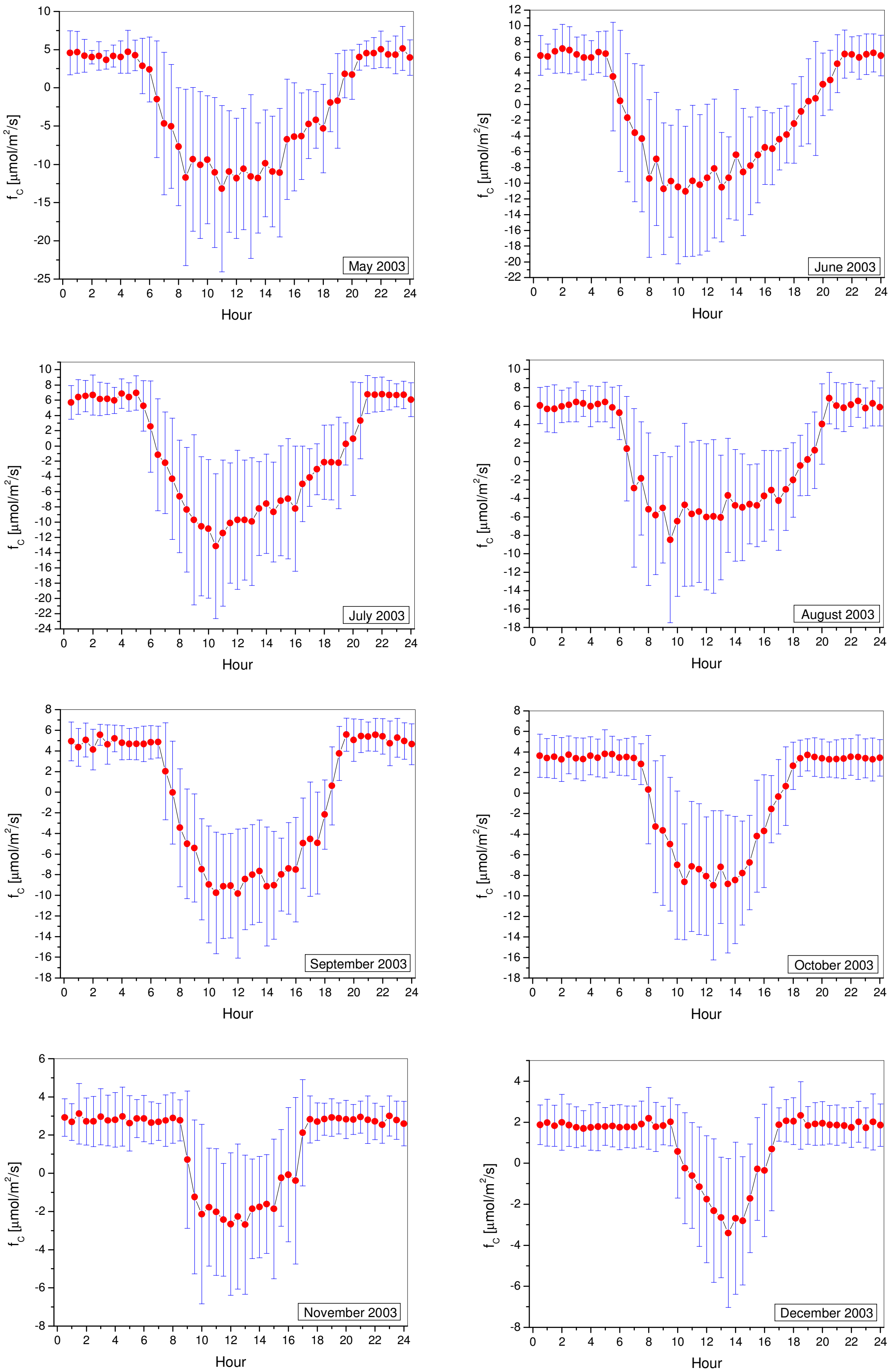

Figure A6.6.15: Mean daily courses of NEE with standard deviations for May, June, July, August, September, October, November, and December

A general observation is that the uptake of CO_2 is smaller during winter and autumn months and higher during spring and summer months. The variation in duration of the day during which there is a CO_2 uptake (i.e. photosynthesis process takes part) is clearly visible – it is the shortest during winter months (in January from 8:30am to 5:00pm) and the longest during summer months (in July from 4:30am to 8:30pm). Variation of the flux between the days in the month is more pronounced for daytime than for nighttime.

Table A6.6.12 summarises some relevant parameters measured month by month.

Table A6.6.12: Monthly precipitation, PAR, Ta (Ts_5) (Ts_{30}), VPD, ET, PET, θ_5 (θ_{30}), LAI and f_{CO2} (f_c)

parameter	units	Jan	Feb	Mar	Apr	May	Jun	Jul	Aug	Sep	Oct	Nov	Dec	Sum
precip	[mm]	89	71	58	97	121	103	121	14	73	83	129	119	1078
PAR	[W/m^2]	186	232	414	510	517	606	493	598	444	336	212	126	
Ta **(Ts_5)** **(Ts_{30})**	[°C]	6 (5) (5)	6 (5) (5)	8 (8) (7)	9 (10) (10)	11 (12) (12)	14 (16) (15)	15 (17) (17)	16 (18) (18)	14 (15) (15)	10 (10) (10)	9 (8) (8)	7 (6) (6)	
VPD	[kPa]	0.15	0.14	0.17	0.23	0.21	0.27	0.26	0.36	0.26	0.25	0.15	0.14	
ET	[mm]	6	7	26	42	49	68	50	53	31	20	1	~ 0	353
PET	[mm]	17	16	32	48	54	71	56	72	45	34	17	10	471
θ_5 **(θ_{30})**	[mm/mm]	0.484 (0.467)	0.483 (0.465)	0.469 (0.457)	0.448 (0.438)	0.464 (0.456)	0.435 (0.438)	0.453 (0.445)	0.414 (0.425)	0.384 (0.382)	0.438 (0.411)	0.473 (0.454)	0.478 (0.457)	
LAI			21/02/03 grazing starts			27/05/03 1st cut			05/08/03 2nd cut			21/11/03 grazing ends		
f_{CO2} **(f_C)**	[g/m^2]	47 (13)	-51 (-14)	-206 (-56)	-199 (-54)	-301 (-82)	-139 (-38)	-150 (-41)	49 (13)	-69 (-19)	-28 (-8)	154 (42)	111 (30)	-782 (-214)

PAR – photosynthetic active radiation
Ta (Ts) – air (soil) temperature
VPD – water pressure deficit
ET – actual (measured) evapotranspiration
PET – potential (Penman-Monteith) evapotranspiration
θ_5 (θ_{30}) – soil moisture at 5 cm (30 cm) depth
LAI – leaf area index
f_{CO2} (f_c) – carbon dioxide (carbon) flux

A6.6.3.3 Annual flux

The cumulative NEE, expressed in Tonnes of carbon per hectare (T.C/ha) is shown in Figure A6.6.16. The NEE for 2003 was –2.1T.C/ha (-7.8 T.CO_2/ha).

From the beginning of January to 12th February (42 days) the grassland was a source of 0.16 T.C/ha. From 12th to 26th February (14 days) the uptake was -0.1 T.C/ha. The site is in equilibrium regarding the carbon from 26th February to 10th March (11 days). From 10th March site behaves as sink for carbon. Up to 16th June the uptake was –2.4 T.C/ha and up to 1st November it was –2.9 T.C/ha. From 1st November to 31st December site was a source of 0.8 T.C/ha.

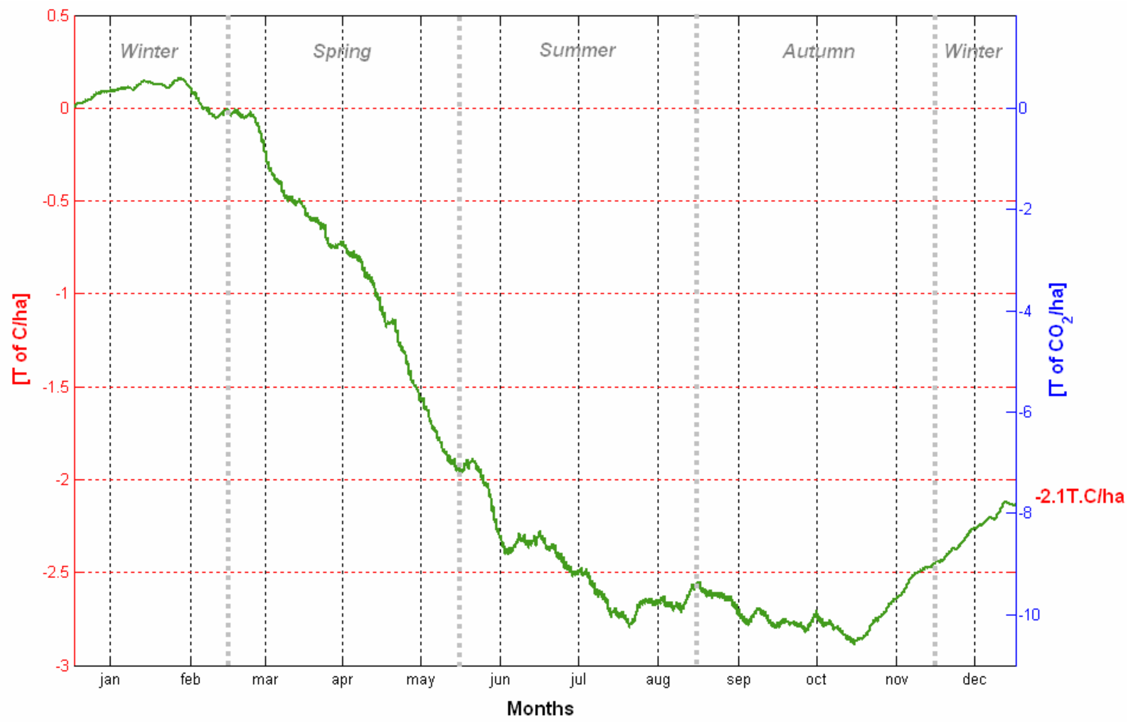

Figure A6.6.16: **Cumulative uptake of carbon (C) and carbon dioxide (CO_2) in T/ha**

The Wexford grassland is managed, thus the two cuts of silage during the study period may have affected the LAI and hence CO_2 flux at the beginning and also at the end of the study. The site was intensively grazed and Nitrogen fertilized. The latter is likely to have increased the plant growth and the annual cumulative uptake.

A6.6.3.4 Carbon balance

In order to find out the range of GPP (Gross Primary Production) for 2003 at Wexford site we modelled respiration during the day. Here we define R as Ecosystem Respiration (autotrophic and heterotrophic) obtained from measured NEE (Net ecosystem exchange) during nighttime (see Table A6.6.3) and estimated for daytime using the equation:

$$F_{ni} = 0.0055 \times t_{soil}^{2} + 0.328 \times t_{soil} - 0.323 \qquad \text{for 2003} \qquad (6.3)$$

where, t_{soil} is soil temperature at 5 cm depth.

Using the NEE and modelled respiration GPP was calculated [*Kirschbaum et al*., 2001]:

$$\text{GPP} = \text{NEE} + \text{R} \qquad (6.4)$$

Figure A6.6.17 shows cumulative NEE, R and GPP. Respiration is 15.0T of C/ha. Gross primary production is 17.1T of C, which is in agreement with what was found by other researchers [e. g. *Kirschbaum et al*., 2001].

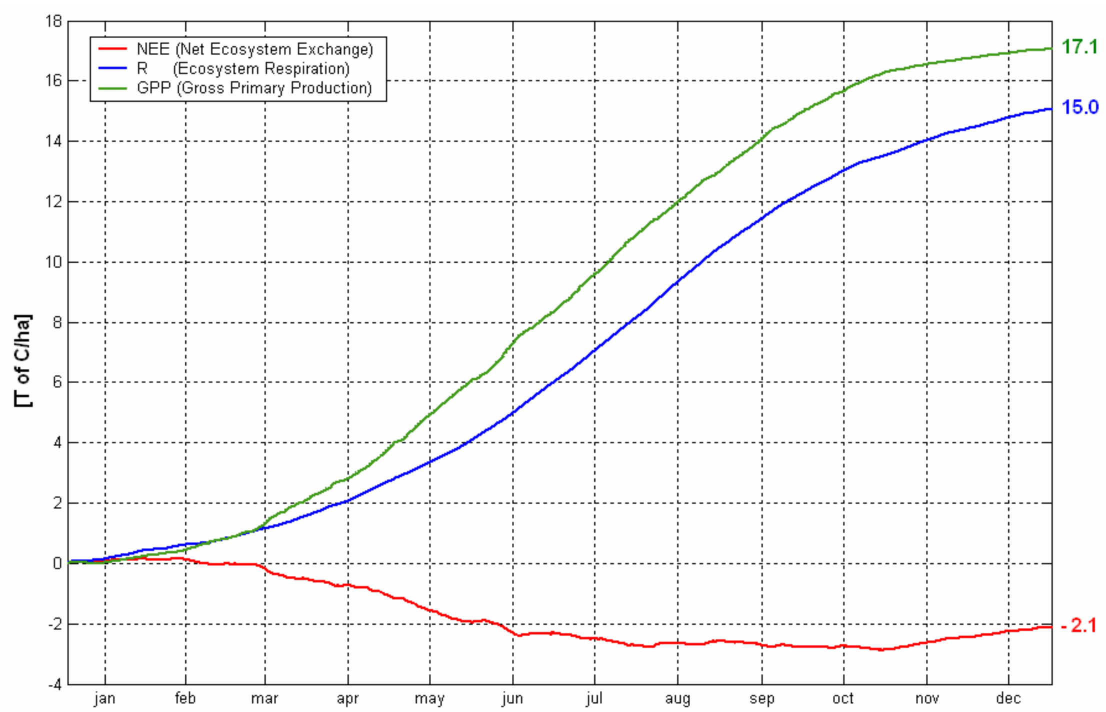

Figure A6.6.17: **Cumulative NEE (red), R (blue) and GPP (green) in T of C/ha**

A6. References

Albertson, J. D., and G. Kiely, On the structure of soil moisture time series in the context of land surface models, *Journal of Hydrology, 243*, 101-119, 2001.

Baldocchi, D.D., Assessing the eddy covariance technique for evaluating carbon dioxide exchange rates of ecosystems: past, present and future, *Global Change Biol., 9*, 479-492, 2003.

Brutsaert, W., *Evaporation into the atmosphere*, edited by A. J. Davenport, B. B. Hicks, G. R. Hilst, R. E. Munn, J. D. Smith, Kluwer Academic Publishers, London, 1991.

Budyko, I. M., *Climate and Life*, Climatic factors of Photosynthesis, 497, Academic Press INC, London, 1974.

Campbell, S. G., and J. M. Norman, *An introduction to environmental Biophysics*, second edition, Springer-Verlag New York, 1998.

Dugas, W.A., M.L. Heuer, and H.S. Mayeux, Carbon dioxide fluxes over a Bermuda grass, native prairie, and sorghum. *Agric. For. Meteorol. 93*,121-139, 1999.

FAO, Crop evapotranspiration – Guidelines for computing crop water requirements – *FAO Irrigation and drainage paper 56*, Food and Agriculture Organisation of the United Nations, Rome, 1998.

Falge, E., D. Baldocchi, R. Olson, P. Athoni, M. Aubinet, C. Bernhofer, G. Burba, R. Ceulemans, R. Clement, H. Dolman, A. Granier, P. Gross, T. Grünward, D. Hollinger, N-O. Jensen, G. Katul, P. Keronen, A. Kowalski, C. T. Lai, B. E. Law, T. Meyers, J. Moncrieff, E. Moors, J. W. Munger, K. Pilegaard, Ü. Rannik, C. Rebmann, A. Suyker, J. Tenhunen, K. Tu, S. Verma, T. Vesala, K. Wilson, and S. Wofsy, Gap filling strategies for defensible annual sums of net ecosystem exchange, *Agric. For. Meteorol., 107*, 43-69, 2001.

Frank, B. A., and Dugas, A. W., Carbon dioxide fluxes over northern, semiarid, mixed-grass prairie, *Agric. For. Meteorol., 108*, 317-326, 2001.

Garatt, R. J., *The atmospheric boundary layer*, Edited by J. T. Houghton, M. J. Rycroft, A. J. Dessler, Cambridge University Press, 1992.

Gash, J. H. C., A note on estimating the effect of a limited fetch on on micrometeorological evaporation measurements. *Boundary-Layer Meteor., 35*, 409-413, 1986.

Gash, J. H. C., F. Valente, and J. S. David, Estimates and measurements of evaporation from wet, sparse pine forest in Portugal, *Agric. For. Meteorol., 94*, 149-158, 1999.

Goulden, M.L., J.W., Munger, S.M., Fan, B.C., Daube, and S.C., Wofsy, Measurements of carbon sequestration by long-term eddy covariance: methods and critical evaluation of accuracy, *Global Change Biol., 2*, Pages 196-182, 1996.

Horst, T. W., and J. C. Weil, How far is far enough? The fetch requirements for micrometeorological measurement of surface fluxes, *J.Atmos Oceanic Technol, 12*, 447, 1995.

Hsieh, C-I., G. G. Katul, J. Schieldge, J. T. Sigmon, and K. K. Knoerr, The Lagrangian stochastic model for fetch and latent heat flux estimation above uniform and nonuniform terrain, *Water Resources Res., 33*, No. 3, 427-438, 1997.

Hsieh, C-I., G. G. Katul, and T-W. Chi, An approximate analytical model for footprint estimation of scalar fluxes in thermally stratified atmospheric flows, *Advances in Water Resources, 23*, 765-772, 2000.

Kirschbaum, U. F. M., The temperature dependence of soil organic matter decomposition, and the effect of global warming on soil organic C storage, *Soil Biol. Biochem, 27* (D6), 753-760, 1995.

Kirschbaum, M. U. F., D. Eamus, R. M. Gifford, S. H Roxburgh,. and P. J. Sands, Definitions of some ecological terms commonly used in carbon accounting. *Net Ecosystem Exchange*, edited by Kirschbaum, M.U.F. and Mueller, R, Cooperative Research Centre for Greenhouse Accounting, Canberra, pp. 2-5, 2001. http://www.ffp.csiro.au/nfm/staff/kirschbaum/definitions.pdf

Law, E. B., E. Falge, L. Gu, D. D. Baldocchi, P. Bakwin, P. Berbigier, K. Davis, A. J. Dolman, M. Falk, J. D. Fuentes, A. Goldstein, A. Granier, A. Grelle, D. Hollinger, I. A. Janssens, P. Jarvis, N. O. Jansen, G. Katul, Y. Mahli, G. Matteucci, T. Meyers, R. Monson, W. Munger, W. Oechel, R. Olson, K. Pilegaard, K. T. Paw U, H. Thorgeirsson, R. Valentini, S. Verma, T. Vesala, K. Wilson, and S. Wofsy, Environmental controls over carbon dioxide and water vapor exchange of terrestrial vegetation, *Agric. For. Meteorol., 113*, 97-120, 2002.

Leclerc, M. Y., and G. W. Thurtell, Footprint prediction of scalar fluxes using a Markovian analysis, *Boundary-Layer Meteorology, 52*, 247-258, 1990.

Lloyd, J., and J.A Taylor, On the temperature dependence of soil respiration. *Funct. Ecol. 8*, 315–323, 1994.

McMillen, R. T., An eddy correlation technique with extended applicability to non-simple terrain, *Boundary Layer Meteorology, 43*, 231-245, 1988.

Michaelis, L., and M. L. Menten, Die Kinetik der Invertinwirkung, *Biochem. Z. 49*, 333, 1913.

Moncrieff, J.B., J. M. Massheder, H. de Bruin, J. Elbers, T. Friborg, B. Heusinkveld, P. Kabat, S. Scott, H. Soegaard, and A. Verhoef, A system to measure surface fluxes of momentum, sensible heat, water vapour and carbon dioxide, *J. Hydrol., 188-189*, 589-611, 1997.

Novick, K.A., P. C. Stoy, G. G. Katul, D. S. Ellsworth, M. B. S. Siqueira, J. Juang, R. Oren, , Carbon dioxide and water vapor exchange in a warm temperate grassland, *Oecologia, 138*: 259–274, 2004.

Pattey E., I. B. Strachan, R. L. Desjardins, and J. Massheder, Measuring nightime CO_2 flux over terrestrial ecosystems using eddy covariance and nocturnal boundary layer methods, *Agric. For. Meteorol., 113*, 145-158, 2002.

Ryan, M., Water movement in a structured soil in the south-east of Ireland: preliminary evidence for preferential flow, *Irish Geography, vol.31(2)*, 124-137, 1998.

Saigusa, N., T. Oikawa, and S. Liu, Seasonal variations of the exchange of CO_2 and H_2O between a grassland and the atmosphere: An experimental study, *Agric. For. Meteorol., 89*, 131-139, 1998.

Sims, P.L., and J. A. Bradford, Carbon dioxide fluxes in a southern plains prairie. *Agric.For. Meteorol. 109*, 117-134, 2001.

Sims, P.L., and J. A. Bradford, Carbon dioxide fluxes in a southern plains prairie. *Agric.For. Meteorol. 109*, 117-134, 2001.

Smith, E., Limiting factors in photosynthesis: light and carbon dioxide, *Gen. Physiol. 22*, 21–35, 1938.

Van der Tol, C., J. H. C. Gash, S. J. Grant, D. D. McNeil, M. Robinson, Average wet conopy evaporation for Sitka spruce forest derived using the eddy correlation-energy balance technique, *Journal of Hydrology, 276*, 12-19, 2003.

Appendix 7

Complementary Production

EGS – AGU – EUG Joint Assembly

Nice, France, 06 – 11 April 2003

At the occasion of the EGS (European Geophysical Society), AGU (American Geophisical Union) and EUG (European Union of Geosciences) conference 2003 in Nice, a poster has been elaborated. Carbon dioxide flux for 2002 at Dripsey site has been analysed. Notice that NEE differ from results presented in this thesis the reasons for that are:

1) using the uniform filters for whole year day data and night data

- Nighttime CO_2 fluxes are filtered when:
  The momentum flux u* < 0.2 m/s
  The CO_2 flux fc < 0 μmol/m^2/s
  The CO_2 flux fc > 10 μmol/m^2/s

- Daytime CO_2 fluxes are filtered when:
  The CO_2 flux fc > 7.5 μmol/m^2/s
  The CO_2 flux fc < -30 μmol/m^2/s

2) using the one fitting function for all day and all night data.

$$Fc_{ni} = a \times b^{\left(\frac{t_{soil}-10}{10}\right)}; \qquad a=3.972;\ b=1.87 \qquad (A6.1)$$

$$Fc_{day} = -24 \times \left(1 - e^{\left(\frac{\alpha \times Q_{par}}{-24}\right)}\right) + \gamma; \qquad \alpha=0.01963;\ \gamma=1.314 \qquad (A6.2)$$

Hereunder are joined the submitted abstract as well as the complete poster.

Abstract:

Carbon Dioxide Flux For One Year Above a Temperate Grazed Grassland

Vesna Jaksic[1], Gerard Kiely[1], John Albertson[2], Gabriel Katul[3] and Todd Scanlon[1]

[1] Dept. of Civil and Environmental Engineering, University College Cork, Ireland
[2] Dept. of Civil and Environmental Engineering, Duke University, NC, USA
[3] Nicholas School of the Environment and Earth Science, Duke University, NC, USA

The Dripsey flux site in Cork, Ireland is a perennial ryegrass (C3 category) pasture and is grazed for approximately 8 to 10 months of the year. The lands are fertilised with approximately 200kg/ha/year of nitrogen. The flux tower monitoring CO_2, water vapour and energy was established in June 2001 and we have continuous data since then. The site also includes streamflow hydrology and stream water chemistry. We present the results and analysis for CO_2 for the year 2002. The Net Ecosystem Exchange (NEE) is estimated to be 3.0 T.C/ha/year. This work is part of a five-year (2002-2006) research project funded by the Irish Environmental Protection Agency.

Poster: (see end of the thesis)

NDP – EPA conference

Dublin, Ireland, 15 – 16 May 2003

Funded under the Environmental RTDI Programme 2000-2006, financed by the Irish Government under the National Development Plan and administered on behalf of the Department of the Environment and Local Government by the Environmental Protection Agency.

The Environmental Protection Agency (EPA) was hosting a conference to showcase the research work being carried out under the Environmental Research Technological Development and Innovation (ERTDI) programme. For the conference entitled **PATHWAYS to a sustainable future** a poster has been elaborated. Carbon dioxide flux for 2002 at Dripsey site has been analysed. Notice that NEE differ from results presented on Nice conference and in this thesis the reasons for that are:

1) using the uniform filters for whole year day data and night data

- Nighttime CO_2 fluxes are filtered when:
  The momentum flux u* < 0.2 m/s
  The CO_2 flux fc < 0 μmol/m^2/s
  The CO_2 flux fc > 10 μmol/m^2/s
- Daytime CO_2 fluxes are filtered when:
  The CO_2 flux fc > 7.5 μmol/m^2/s
  The CO_2 flux fc < -30 μmol/m^2/s

2) using the two month fitting functions for day and night data.

$$Fc_{ni} = a \times b^{\left(\frac{t_{soil}-10}{10}\right)}; \qquad \text{(A6.3)}$$

Table A6.1: Night time coefficients for 2002 and 2003.

	Jan-Feb	Mar-Apr	May-Jun	Jul-Aug	Sep-Oct	Nov-Dec
a	3.986	3.236	4.212	3.575	2.983	3.818
b	3.149	1.215	2.332	2.085	6.539	2.44

$$Fc_{day} = -24 \times \left(1 - e^{\left(\frac{\alpha \times Q_{par}}{-24}\right)}\right) + \gamma; \qquad \text{(A6.4)}$$

Table A6.1: Daytime coefficients for 2002 and 2003.

	Jan-Feb	Mar-Apr	May-Jun	Jul-Aug	Sep-Oct	Nov-Dec
α	0.01969	0.03251	0.02749	0.01981	0.02881	0.02032
γ	1.219	2.501	3.311	3.862	3.311	1.589

Hereunder are joined the submitted abstract as well as the complete poster.

Abstract:

Carbon Dioxide Flux For One Year Above a Temperate Grazed Grassland

Vesna Jaksic[1], Gerard Kiely[1], John Albertson[2], Gabriel Katul[3] and Todd Scanlon[1]

[1] Dept. of Civil and Environmental Engineering, University College Cork, Ireland
[2] Dept. of Civil and Environmental Engineering, Duke University, NC, USA
[3] Nicholas School of the Environment and Earth Science, Duke University, NC, USA

The Dripsey flux site in Cork, Ireland is a perennial ryegrass (C3 category) pasture and is grazed for approximately 8 to 10 months of the year. The lands are fertilised with approximately 200kg/ha/year of nitrogen. The flux tower monitoring CO_2, water vapour and energy was established in June 2001 and we have continuous data since then. The site also includes streamflow hydrology and stream water chemistry. We present the results and analysis for CO_2 for the year 2002. The Net Ecosystem Exchange (NEE) is estimated to be 3.25 T.C./ha/year. This work is part of a five-year (2002-2006) research project funded by the Irish Environmental Protection Agency.

Poster: (see end of the thesis)

Walsh Fellowships Seminar

Dublin, Ireland, 11 November 2003

At the occasion of the annual Teagasc Walsh Fellowships Seminar presentation was given on work in progress. NEE has been analysed and possibilities for carbon sequestration has been considered for Dripsey and Wexford site.

Abstract:

Opportunities of Carbon Sequestration in Irish Grasslands

Vesna Jaksic[1]
Supervisors: Ger Kiely[1], Owen Carton[2] and Deirdre Fay[2]

[1]Dept. of Civil and Environmental Engineering, University College Cork, Ireland
[2]Environment and Land Use Department, Research Centre Johnstown Castle, Wexford, Ireland

The Dripsey catchment in North Cork has a dominant land cover of perennial ryegrass (C3 category) and a land use of pasture and silage fields. A 10m high flux tower for carbon measurements is located at the head of the catchment at an elevation of 200masl. The fertiliser applications are approximately 190kgN/ha in chemical fertiliser and approximately 80kgN/ha in the form of slurry/manure. The farms are grazed for approximately 8 months of the year. The Wexford grassland site (20masl), also a perennial ryegrass (C3) pasture, is fertilized with about 300kgN/ha.year and grazed for about 8 months of the year. At both sites we continuously monitor CO_2 flux measurements using the eddy covariance technique. The Cork site is operational since July 2001, and the Wexford site since November 2002. The aim of this research is to measure and model the CO_2 flux at the two grassland ecosystems. Central to this objective is the investigation of seasonal, annual and interannual fluxes with the aim of estimating the carbon budget for the two sites. For the first year at the Cork site, the Net Ecosystem exchange (NEE) was 3.7T of C/ha and for the second year 2.2T of C/ha. The interannual variability is significant. The carbon uptake or NEE at the Wexford site was 2.5T of C/ha for the year (November 1, 2002 to October 30, 2003). In accounting for the various exports of carbon (e.g. off-farm carbon in meat and meat) we estimate the carbon sequestration (i.e. the carbon fixed to the soil or carbon sink) for the year 2002 at the Cork site to be 1.2T of C/ha. These preliminary results suggest that the Cork site is a sink for carbon. However, due to interannual variability this may change from year to year.

Net Ecosystem Exchange of a Fertilised Grassland: How Significant is the Variability between a Wet and a Dry Year?

Vesna Jaksic[1], Gerard Kiely[1*], John Albertson[2,3], Gabriel Katul[2,3], Ram Oren[3]

[1] Department of Civil and Environmental Eng., University College Cork, Ireland

[2] Department of Civil and Environmental Eng., Duke University, NC. USA

[3] Nicholas School of the Environment and Earth Sciences, Duke University, NC. USA

[*]Corresponding author: g.kiely@ucc.ie

ph.353-21-4902965 fax 353-21-4276648

Submitted to: *Geophysical Research Letters*

April, 2004.

Abstract

An eddy covariance (EC) system for CO_2 fluxes was used for two years (2002 and 2003) to study the variability of the net ecosystem exchange (NEE) at a humid grassland site in southern Ireland. Over 90% of Irish agricultural land is under grassland suggesting the importance of quantifying the carbon fluxes in this ecosystem type. Some of the grassland fields within the EC footprint were grazed by dairy cattle while other fields were harvested twice per year, (June and September). The area averaged nitrogen fertilisation rate was ~300 kg.N/ha per year. 2002 was wet (precipitation at 1785mm, 24% above average) and 2003 was dry (precipitation at 1185mm, 18% below average). We use the meteorological sign convention that, minus is uptake and plus is respiration. The wet year had a NEE of -193 g.C/m^2 compared to -260 g.C/m^2 for the dry year. One impact of 2002 being wet was that the first cut of silage was two weeks late (July 1) by comparison with the more normal date of June 15 for 2003. The NEE for June (July) 2002 was -75 (+2) g.C/m^2 and for June (July) 2003 was -31 (-23) g.C/m^2. The sum of the NEE for the eight months (February to September) was -340 g.C/m^2 for 2002 and -345 g.C/m^2 for 2003. The difference in NEE between the years was in the winter months (October to January) with 2002 having an NEE of +148 g.C/m^2 and 2003 with an NEE of + 85 g.C/m^2 .The rainfall in these four months was 903mm in 2002 and 435mm in 2003. The rainfall of 2002 caused the soil moisture status to be more frequently saturated than in 2003. This resulted in a wetter soil environment that respired more. We conclude that the wetter winter of 2002 with its saturating effect on soil moisture caused enhanced ecosystem respiration which was responsible for the lower NEE of 2002.

1. Introduction

The earth's vegetative cover is a key component in the global carbon cycle due to its dynamic response to photosynthetic and respirative processes. Oceanic and forestry ecosystems have been studied in much detail because of their significant carbon sink attributes [e.g., *Post et al.,* 1990; *Cruickshank et al.,* 1998; *Valentini et al.,* 2000; *Berbigier et al.,* 2001; *Falge et al.,* 2002]. Studies of carbon fluxes in temperate grassland have been overlooked due to the perception that this ecosystem is carbon neutral [*Hall et al*., 2000; *Ham and Knapp*, 1998; *Hunt et al*., 2002]. Representing approximately 40 % of earth's natural vegetation, carbon fluxes of grasslands are now being revisited [*Saigusa et al*., 1998; *Frank and Dugas*, 2001; *Hunt et al*., 2002; *Jackson et al*., 2002; Novick et al., 2004] and may yet play a role in the missing global carbon sink [*Ham & Knapp*, 1998; *Robert*, 2001; *Pacala et al.*, 2001; *Goodale and Davidson*, 2002]. Grassland is the dominant ecosystem in Ireland, representing 90% of agricultural land [*Gardiner and Radford, 1980*]. Several short-term studies have shown that grassland ecosystems can sequester atmospheric CO_2 [e.g. *Bruce et al*., 1999; *Batjes et al,* 1999; *Conant et al*., 2001; *Soussana et al.*, 2003] but few multi-annual data sets are available [*Frank et al*., 2001; *Frank and Dugas,* 2001; *Falge et al*., 2002; *Knapp et al*., 2002; Novick et al., 2004, Verburg et al, 2004]. To quantify the source-sink potential of grasslands in different climatic zones, long-term surface flux measurements are required [*Goulden et al*., 1996; *Ham and Knapp*, 1998; *Knapp et al*., 2002; *Baldocchi*, 2003] to build and test models that represent the biological and physical processes at the land surface interface. Such models (e.g. BIOME3, Pnet, PaSim, Canveg) [*Aber and Federer*, 1992; *Wilkinson and Janssen*, 2001; *Soussana et al*., 2003, Reido et al, 1998] can be used to examine scenarios of variation in land use and management as well as climate change. While it is known that most forest ecosystems are sinks for carbon, it is not at all so well defined for grasslands. The literature (summarised by Novick et al., 2004) shows that the wide annual range of NEE for grasslands varies from an uptake of -800g.C/m^2 to an emission of +521 g.C/m^2 with most grassland ecosystems in the range ±100 g.C/m^2. In this paper, we present the eddy covariance measured CO_2 fluxes for two years (2002 and 2003) in a humid temperate grassland ecosystem in Ireland. Long-term measurements are essential for examining the seasonal and interannual variability of carbon fluxes, particularly in humid temperate climates where grasslands are the largest ecosystem [*Goulden et al*., 1996; *Baldocchi*, 2003]. Our aim is to examine the processes involved in the variability of the net ecosystem exchange (NEE) between a wet year and a dry year.

2. Site Description and Methods

The experimental grassland, at 220 m above sea level is located in South West Ireland, 25 km northwest of Cork city (52º North latitude, 8º30' West longitude). The climate is temperate (summer average 15º C, winter average 5º C) and humid (mean annual precipitation 1470mm). The soil is classified as brown-grey podzols and the topsoil is rich in organic matter to a depth of about 15cm (about 12% organic matter, [*Daly*, 1999]), overlying a dark brown B-horizon of sand texture. A yellowish brown B-horizon of sand texture progressively changes to a brown, gravely sand which constitutes the parent material at a depth of approximately 0.3m and the underlying bedrock is old red sandstone [*Scanlon et al*., 2004]. Depth averaged over the top 30cm the volumetric soil porosity was 0.49 (m^3/m^3), the saturation moisture level was 0.45, the field capacity was 0.32, the wilting point was 0.12, and the air dried moisture was 0.02. The grassland type is moderately high quality pasture and meadow, with perennial ryegrass the dominant plant species (C_3 grass). The land use is a mixture, 2/3^{rds} of fields for cattle grazing and 1/3rd of fields for cutting (silage harvesting). Cattle grazing begins in March and ends in October. The rotational paddock grazing periods lasts approximately one week in four. Grass productivity is enhanced with applications of ~ 300kg of nitrogen in fertiliser and slurry, spread at intervals of approximately six weeks between February and September. In the harvested fields the grass is cut in the summer, firstly in June and secondly in September. The grass height in the grazing fields varies from 0.1m to 0.2m. The grass height in the silage fields reaches a maximum of ~ 0.45m prior to harvesting. The annual yield of silage in the region has been 8 to 12 Tonnes of dry matter per hectare per year depending on the weather (precipitation) and nitrogen application. The dry matter of silage is 46% carbon.The footprint area of the flux tower (Fig. 1) was estimated on a fetch to sensor height ratio of 100:1, combined with information from the probability density function of the wind direction [*Hsieh et al*., 2000]. The prevailing wind direction is from the south-west (Fig. 1).

Precipitation and meteorological measurements were sampled at one minute and recorded at 30 minute intervals. The barometric pressure was measured with a PTB101B and the air temperature and humidity were measured with a HMP45A sensor (Campbell Scientific USA, (CSI)) at the height of 3m. Soil temperatures were measured with three 107 temperature probes (CSI), at 2.5 cm, 5cm and 7.5 cm deep. The volumetric soil water content (m^3/m^3) was measured at depths of 5, 10, 25, and 50 cm with CS615 time domain reflectometry (CSI) set horizontally. Two other CS615's were installed vertically, from 0 cm to 30 cm, and from 30 cm to 60 cm depth. The datalogger was a CR23X (CSI). Net radiation was measured with a CNRI net radiometer (Kipp & Zonen) and the photosynthetic photon flux was measured with a PAR LITE sensor (Kipp & Zonen). All meteorological data was transferred from site to office by telemetry.

The 3D wind velocity and virtual potential temperature were measured at 10 Hz with an RM Young Model 81000 3-D sonic anemometer positioned at the top of the 10 m tower. Water vapour and CO_2 densities were measured at 10 Hz with an LI-7500 open path infrared gas analyser (LICOR Inc. USA) placed within 20 cm of the centre of the anemometer air volume. The 30 minute eddy covariance CO_2 fluxes are defined as:

$$F_c \cong -\overline{w'\rho_c'} \tag{1}$$

where w' is the vertical wind velocity fluctuations [m/s] and ρ_c' the CO_2 density fluctuations [mol/m^3]. We adopt the micrometeorological convention in which fluxes from the biosphere to the atmosphere are positive. The CO_2 flux data was firstly adjusted for the Webb correction [*Kramm et al.*, 1995; *Webb et al.*, 1980; *Baldocchi*, 2003]. This correction is important for CO_2 fluxes for which the density fluctuations range is comparable to the mean density value.

The F_c best represents the surface flux for steady-state, planar homogeneous, and well developed turbulent flow [e.g., *Goulden, et al.*, 1996; *Moncrieff et al.*, 1997; *Falge et al.*, 2001]. During calm climatic conditions the measured fluxes are underestimated: 1) as the fluctuations in the vertical wind speed are too small to be resolved by sonic anemometry [*Goulden, et al.*, 1996], and 2) for nocturnal and very stable conditions, the flow statistics may be dominated by transient phenomena or even the lack of turbulence (e.g. canopy waves). Cava et al. (2004) found that when canopy waves dominate night-time runs, the local CO_2 production from ecosystem respiration and observed mean fluxes above the canopy are, to a first order, de-coupled presumably through a storage term. What is important here is that when canopy waves dominate, there is “gross” mass and heat exchange between the canopy and the atmosphere; however, the net exchange over the lifecycle of the wave is negligible. Occasionally, these waves are under-sampled because of a short flux-averaging period leading to an apparent and spurious “photosynthesis” (or canopy C uptake) values at night in the case of CO_2. Correcting night-time fluxes with runs collected under high u_* (or more precisely for near-neutral to slightly stable conditions) ensures that the turbulent regime is fully-developed. Another reason why runs with high u_* (or near-neutral conditions) are preferred for night-time flux corrections is a much smaller (and perhaps the more realistic) footprint [Novick et al, 2003].

Uncertainties in night-time fluxes have been examined by many researchers and remains a challenge because a minor underestimation of night-time CO_2 fluxes (respiration) imply overestimations of the annual carbon uptake [*Falge et al.*, 2001; *Pattey et. al.*, 2002; *Baldocchi et al.*, 2003]. To compare with other long-term studies from various ecosystems, we use a friction velocity (u_*) to filter transients and weak turbulence conditions [e.g., *Goulden, et al.*, 1996; *Moncrieff et al.*, 1996; *Falge et al.*, 2001; *Pattey et al.*, 2002]. Specifically, we filtered CO_2 fluxes at night when $u_* < 0.2$ m/s [*Pattey et al.*, 2002; *Baldocchi et al.*, 2003]. After the Webb correction, double rotation and u_* filtering, we further filtered fluxes that exceeded predetermined threshold values for the season. For instance, the summer day-time fluxes were accepted if >-30 μmol/m^{2}s and <0 μmol/m^{2}s. The night-time summer fluxes were accepted if >0 μmol/m^{2}s and <15 μmol/m^{2}s. The daytime data was binned in two-month increments according to Falge et al., (2001).

After post-processing and filtering of spurious data, 54 % of the CO_2 flux data for 2002 and 58 % for 2003 were suitable for analysis. The percentage of usable data reported by other studies is approximately 65 % [*Falge et al.*, 2001; *Law et al.*, 2002]. About 13 % of the 2002 data and 8 % of the 2003 data were rejected due to water drops on the LI-7500 during rain and within two hours after rain. The rest of the non-usable data (33% for 2002, and 34% for 2003) were rejected when found to be out of range or during periods of low night-time friction velocity.

The gap filling functions tested were non-linear regressions [see *Goulden et al.*, 1996; *Falge et al.*, 2001; *Lai et al.*, 2002]. For night-time data, the ecosystem respiration is known to be linked to the soil temperature [*Lloyd and Taylor*, 1994; *Kirschbaum*, 1995] and to a lesser extent to soil moisture. The correlation with different temperatures (air, surface, different soil depths) showed best correlation with soil temperature at 5 cm depth, whereas the data set was less well correlated to soil moisture (consistent with the analysis of Novick et al. 2004, for a warm temperate grassland). Different temperature response functions were tested and parameterised statistically (Sum of Squares Error (SSE), Root-Square (R^2), adjusted Root Square (adjusted-R^2), and Root Mean Squared Error (RMSE)). A linear relationship, an exponential relationship, the Arrhenius function and a Q_{10} relation were first considered. The best fit (for night-time) was obtained for the exponential function defined as:

$$F_{ni} = a \times e^{(b \times t_{soil})} \qquad (2)$$

where t_{soil} is the soil temperature at 5 cm depth in ºC. The coefficient a = 1.476 and 1.109 for 2002 and 2003 respectively. The coefficient b = 0.095

and 0.122 for 2002 and 2003 respectively. This function was applied to the data for the full year (separately for 2002 and 2003) because the range of night-time soil temperature throughout the year was small (2 to 18º C).

For daytime, the net ecosystem exchange of CO_2 is linked to the photosynthetic photon flux density Q in µmol of quantum/m^2/s [e.g., *Michaelis and Menten*, 1913; *Smith*, 1938; *Goulden et. al.*, 1996]. Different light response functions tested included: a linear relationship, Smith formula [*Smith*, 1938; *Falge* et al., 2001], Michaelis-Menten formula (rectangular hyperbola), [*Michaelis & Menten*, 1913; *Falge et al.*, 2001], Misterlich formula [*Falge et al.*, 2001], and Ruimy formula [*Ruimy et al.*, 1995; *Lai et al.*, 2002]. The best fit was achieved with the Misterlich formula defined as:

$$F_{day} = -24 \times \left(1 - e^{\left(\frac{a \times Q_{ppfd}}{-24}\right)}\right) + c \tag{3}$$

where Q_{ppfd} is the photosynthetic photon flux density (or PAR) in µmol of quantum/m^2/s. As PAR varies seasonally, the values of the coefficients in two monthly bins are listed in Table 1.

3. Results and Discussion

As evidenced from Figure 2a, (and Table 2) 2002 was wet year, with an annual rainfall of 1785mm and 2003 was dry, with an annual rainfall of 1185mm (compared to the long-term average rainfall of 1470mm). No snow fell in either year. The monthly average vapour pressure deficit (VPD) is shown in Fig.2b. (and Table2). The high humidity and low potential for evaporation of the region is evidenced by the low VPD's with a maximum of 0.36 kPa in August 2003 and as low as 0.1 kPa in the winter months. The annual evapotranspiration measured using EC techniques [Brutsaert, 1982], (Fig.2c) was 372 and 368mm for 2002 and 2003 respectively with little differences in the monthly ET between the two years. This evapotranspiration was 21% and 31% of annual precipitation in 2002 and 2003 respectively. The corresponding potential evapotranspiration (PET, no water limitation) estimated using the Penman-Monteith equation (Fig.2d) was 422 and 455mm for 2002 and 2003 respectively. The actual evapotranspiration was 88% and 81% of potential in 2002 and 2003 respectively. We note from Fig.2a (VPD) and Fig.2c (PET) that the PET mimics the VPD. For instance, examining August (Table 2) we note that the actual evapotranspiration was 49 mm and 48 mm in 2002 and 2003 respectively, while the potential was 60 and 75 mm in 2002 and 2003 respectively. This confirms that the evapotranspiration was water limited in both Augusts but more so in 2003. The volumetric soil moisture (m^3/m^3), depth averaged over the top 30cm (Fig. 2e) is shown in both years to vary from highs of 0.45 (note that saturation is ~ 0.45) to lows of 0.21 (note that the wilting point is ~0.12 and field capacity is ~0.32). Examining Fig.2e (and Table 2) we see that the root zone (0 to 30cm depth) soil moisture was much drier in 2003 particularly during the months of June to October. In addition, the winter months, October to January were much drier in 2003 (see Table 2).

The photosynthetic photon flux density (Fig.3a, PAR in $\mu mol/m^2.s$) show that there is approximately 5% more PAR radiation in 2003 than in 2002. The mean annual air temperature was 9.63 ºC and 9.64 ºC in 2002 and 2003 respectively. The daily air temperatures (Fig. 3b) has a small range of variation during the year, going from a maximum of 21º C (in August) to a minimum of 0º C (January), with an average value of 15º C in summer and 5º C in winter verifying the temperate nature of the local climate. The local climate is humid temperate, with mild winters where very few daytime temperatures drop below 4 °C, (the lower air threshold temperature for the photosynthetic process). The soil temperature (at 5cm depth, Fig.3c) mimics the air temperature.

In Fig.4 we show the monthly net ecosystem exchange (NEE) for both years. There is net uptake (carbon sink) in the seven months, March to September and net respiration (carbon source) in the months, October to January. In February the ecosystem is close to equilibrium. The monthly NEE varies between the same months in the two years.

The net uptake of C in May 2002 of -99 $g.C/m^2$ is similar to -110 $g.C/m^2$ in 2003. The net uptake of C in June, 2002 of -75 $g.C/m^2$ was more than double the -31 $g.C/m^2$ of June, 2003. The reasons for the differences in NEE in June was twofold. Firstly, on June 15, 2003 part of the grassland in the footprint was cut (harvested to within 5cm of the bare soil). So, the first half of June 2003 had a strong uptake while the second half of June was net respiration with the net effect for June being a low uptake of -31 $g.C/m^2$. Secondly, On July 1, 2002 part of the grassland in the footprint was cut. So, all of June 2002 had the benefit of a maximum uptake of -75 g.C/m^2. The reason for the delay in harvesting in 2002 was that farm equipment could not access the fields due to the elevated soil moisture (see Fig.2e). The second half of June 2003 was much drier that that of the second half of June 2002. It has been shown [Frank and Dugas, 2001] that short-term droughts during the growing season reduce CO_2 fluxes to near zero (photosynthesis balances respiration). Decreases in LAI (Leaf Area Index) caused by the grass (silage) harvesting, reduces gross primary productivity (GPP), [Budyko, 1974].

In the spring months (March, April and May), there was a little more uptake in 2003 than there was in 2002. This may be explained by higher radiation and slightly drier soils. The NEE (uptake) in August and September 2002 was the same as August and September 2003. This occurred in spite of much drier soil moisture status in August and September 2003.

The sum of the NEE for the eight months (February to September) was -340 g.C/m^2 for 2002 and -345 g.C/m^2 for 2003. The difference in NEE between the years was in the winter months (October to January) with 2002 having an NEE of +148 g.C/m^2 and 2003 with an NEE of + 85 g.C/m^2 .The rainfall in these four months was 903mm in 2002 and 435mm in 2003. The rainfall of 2002 caused the soil moisture status to be more frequently saturated than in 2003. This resulted in a wetter soil environment that respired more. In addition, in the drier year (2003), cattle grazed the fields (during the daytime) during the parts of the months of October to January. By contrast, in the wet winter (2002) cattle did not graze the fields because to do so, they would have damaged the soil surface to an unacceptable level. So in the winter of 2002, there was a greater standing biomass (than in 2003), which enhanced the respiration. This suggests that the wetter winter of 2002 with its saturating effect on soil moisture, it's higher standing biomass and enhanced ecosystem respiration was responsible for the lower NEE of 2002.

The cumulative NEE, expressed in Tonnes of carbon per hectare (TC/ha) for both years is shown in Fig. 5. The NEE for 2002 was -1.9 TC/ha while for 2003 it was -2.6 TC/ha. The cumulative uptake to from January 1 to July 1, 2002 was -2.7 T.C/ha. The cumulative uptake from January 1 to June 15, 2003 was also -2.7 TC/ha. The uptake period that continued longer by two weeks in 2002, was due to the delay in cutting (because of wet weather). In Fig.6 we show the cumulative NEE for both years, for the months October, November, December and January. The NEE for these four months was +1.5 T.C./ha (respiration) for 2002 and +0.8 T.C/ha for 2003. The difference in the NEE between the two years was differences in these four winter months. Precipitation leading to near saturation soil moisture (as in 2002 but not in 2003), enhances the release of C, because of its effect on soil aeration and CO_2 transport within the soil profile [*Suyker, et al*., 2003].

4. Summary

The EC flux measurements presented here cover two years of a planned long-term research programme of net ecosystem exchange (of CO_2) begun in July 2001 at a humid temperate grassland ecosystem in southern Ireland. The grassland footprint encompasses eight small dairy farms (of size 10 to 40ha each) with approximately 2/3$^{rd's}$ of the area grazed for eight months of the year (March to October) while in the other 1/3rd (which is off-limits for grazing from March to September) the grass is cut (harvested for winter feed) twice per year: June and September. The two years are: 2002 which was a wet year (precipitation at 1785mm, 24% above average); and 2003 which was a dry year (precipitation at 1185mm, 18% below average). The farmland management practices in both years were similar, including nitrogen fertilisation rates (305 and 294 kg.N/ha for 2002 and 2003 respectively). We found that the wet year of 2002 had a NEE of -1.9 TC/ha compared to -2.6 TC/ha for the dry year of 2003 (a 27% difference). We found that the cumulative NEE from February to September (Spring plus Summer) was the same in both years. The difference in NEE in the two years of 0.7 T.C/ha was concentrated in the winter months (October, November, December and January). The wet year winter had a cumulative NEE of +1.5 T.C/ha while for the corresponding NEE for the dry year was +0.8 T.C/ha (see Fig.6). The precipitation of the wet winter (2002) was 903 mm while in the dry winter it was 435 mm. As the land use and land management practices were similar in both years, the main difference between the two years was in the magnitude of the winter rainfall. We conclude that the wetter winter of 2002 with its saturating effect on soil moisture had enhanced ecosystem respiration which was responsible for the lower annual NEE of 2002.

5. Acknowledgments

This work has been prepared as part of the Environmental Research Technological Development which is managed by the Environmental Protection Agency and financed by the Irish Government under the National Development Plan 2000-2006 (CELTICFLUX, Grant No. 2001-CC/CD-(5/7)). The Walsh Scholarship administered by Teagasc funds the first author. We appreciate the support of Dr.Owen Carton and Dr.Deidre Fay of Teagasc. We especially appreciate the experimental support by Mr. Adrian Birkby of the Civil and Environmental Engineering Department at University College Cork. We appreciate the co-operation of the landowners.

List of Figures

References

Aber, D. J., and C. A. Federer, A generalized, lumped-parameter model of photosynthesis, evapotranspiration and net primary production in temperate and boreal forest ecosystems, *Oecologia, 92*, 463-474, 1992.

Baldocchi, D.D., Assessing the eddy covariance technique for evaluating carbon dioxide exchange rates of ecosystems: past, present and future, *Global Change Biol., 9*, 479-492, 2003.

Batjes, H. N., Management options for reducing CO_2 – concentrations in the atmosphere by increasing carbon sequestration in the soil, *Report no. 410 200 031,* 114 pp., Dutch National Research Programme on Global Air Pollution and Climate Change, Netherlands, 1999.

Berbigier, P., J.-M. Bonnefond, and P. Mellmann , CO_2 and water vapour fluxes for 2 years above Euroflux forest site, *Agric. For. Meteorol., 108*, 183-197, 2001.

Bruce, P. J., M. Frome, E. Haites, H. Joanne, L. Rattan, and K. Faustian, Carbon sequestration in soils, *J. Soil and Water cons.*, 382-389,1999.

Brutaert WH. (1982). Evaporation into the Atmosphere. "Environmental Fluid Mechanics", D.Reidel, Dordrecht, Holland.

Budyko, I. M., *Climate and Life*, Climatic factors of Photosynthesis, 497, Academic Press INC, London, 1974.

Conant, T.R., K. Paustian, and E. T. Elliott, Grassland management and conversion into grassland: effects on soil carbon, *Ecol. Applications, 11*, No. 2, pp. 343-355, 2001.

Cruickshank, M.M., R.W. Tomlinson, P.M. Devine, and R. Milne, Carbon in the vegetation and soils of Northern Ireland, *Biology and Environment: Proceedings of the Royal Irish Academy, vol. 98B, No. 1,* 9-21, 1998.

Daly K 1999. An environmental appraisal of the phosphorous of the Irish grassland soils. Ph.D Thesis.Trinity College Dublin,Ireland.

Falge, E., D. Baldocchi, R. Olson, P. Athoni, M. Aubinet, C. Bernhofer, G. Burba, R. Ceulemans, R. Clement, H. Dolman, A. Granier, P. Gross, T. Grünward, D. Hollinger, N-O. Jensen, G. Katul, P. Keronen, A. Kowalski, C. T. Lai, B. E. Law, T. Meyers, J. Moncrieff, E. Moors, J. W. Munger, K. Pilegaard, Ü. Rannik, C. Rebmann, A. Suyker, J. Tenhunen, K. Tu, S. Verma, T. Vesala, K. Wilson, and S. Wofsy, Gap filling strategies for defensible annual sums of net ecosystem exchange, *Agric. For. Meteorol., 107*, 43-69, 2001.

Falge, E., D. Baldocchi, J. Tenhunen, M. Aubinet, P. Bakwin, P. Berbigier, C. Bernhofer, G. Burba, R. Clement, K. J. Davis, J. A. Elbers, A. H. Goldstein, A. Grelle, A. Granier, J. Guðmundsson, D. Hollinger, A. Kowalski, G. Katul, B. E. Law, Y. Malhi,T. Meyers, R. K. Monson, J. W. Munger, W. Oechel, K. Tha Paw U, K. Pilegaard, Ü. Rannik, C. Rebmann, A. Suyker, R. Valentini, K. Wilson, and S. Wofsy, Seasonality of ecosystem respiration and gross primary production as derived from FLUXNET measurements, *Agric. For. Meteorol., 113*, 53-74, 2002.

Flanagan LB, Wever LA, Carlson PJ (2002) Seasonal and interannual variation in carbon dioxide exchange and carbon balance in a northern temperate grassland. *Glob Change Biol* 8:599–615

Frank, B. A., and Dugas, A. W., Carbon dioxide fluxes over northern, semiarid, mixed-grass prairie, *Agric. For. Meteorol., 108*, 317-326, 2001.

Frank, B.A., P. L. Sims, J. A. Bratford, P. C. Milenick, W. A. Dugas, and H. S. Mayeux, Carbon dioxide fluxes over three great plains grasslands, *The Potential of U.S. Grazing Lands to Sequester Carbon and Mitigate the Greenhouse Effect,* edited by R. F. Follett, J. M. Kimble, and R. Lal, 167-187, Lewis Puplishers, New York, 2001.

Gardiner MJ., T., Radford, (1980). Soil Associations if Ireland and their Land Use Potential. An Foras Talúntais. Dublin, Ireland.

Goodale, L. C., and E. A. Davidson, Uncertain sinks in the shrubs, *Nature, 418*, 593-594, 2002.

Goulden, M.L., J.W., Munger, S.M., Fan, B.C., Daube, and S.C., Wofsy, Measurements of carbon sequestration by long-term eddy covariance: methods and critical evaluation of accuracy, *Global Change Biol., 2*, Pages 196-182, 1996.

Hall, O. D., J. M. O. Scurlock, D. S. Ojima, and W. J. Parton, Grasslands and the Global Carbon Cycle: Modeling the Effects of Climate Change, in *The Carbon Cycle*, edited by T.M.L. Wigley and D.S. Schimel, pp. 102-114,Cambridge Univ. Press, UK, 2000.

Ham, M. J., and A. K. Knapp, Fluxes of CO_2, water vapor, and energy from a prairie ecosystem during the seasonal transition from carbon sink to carbon source, *Agric. For. Meteorol., 89*, 1-14, 1998.

Hsieh, C-I., G. Katul, and T. Chi, An approximate analytical model for footprint estimation of scalar fluxes in thermally stratified atmospheric flows, *Advances in Water Res. 23*, 765-772, 2000.

Hunt, E. J., F. M. Kelliher, T. M. McSeveny, and J. N. Byers, Evaporation and carbon dioxide exchange between the atmosphere and a tussock grassland during a summer drought, *Agric. For. Meteorol., 111*, 65-82, 2002.

Jackson, B. R., J. L. Banner, E. G. Jobbágy, W. T. Pockman, and D. H. Wall, Ecosystem carbon loss with woody plant invasion of grasslands, *Nature, 418,* 623-626, 2002.

Kirschbaum, U. F. M., The temperature dependence of soil organic matter decomposition, and the effect of global warming on soil organic C storage, *Soil Biol. Biochem, 27* (D6), 753-760, 1995.

Knapp, K. A., P. A. Fay, J. M. Blair, S. L. Collins, M. D. Smith, J. D. Carlisle, C. W. Harper, B. T. Danner, M. S. Lett, and J. K. McCarron, Rainfall variability, carbon cycling, and plant species diversity in a mesic grassland, *Science, 298*, 2202-2205, 2002.

Kramm, G., R. Dlugi, and D. H. Lenschow, A re-evaluation of the Webb correction using density-weighted averages, *Journal of Hydrology, 166*, 283-292, 1995.

Lai, C.-T., G. Katul, J. Butnor, D. Ellsworth, and R. Oren, Modelling night-time ecosystem respiration by a constrained source optimization method, *Global Change Biol., 8*, 124-141, 2002.

Law, E. B., E. Falge, L. Gu, D. D. Baldocchi, P. Bakwin, P. Berbigier, K. Davis, A. J. Dolman, M. Falk, J. D. Fuentes, A. Goldstein, A. Granier, A. Grelle, D. Hollinger, I. A. Janssens, P. Jarvis, N. O. Jansen, G. Katul, Y. Mahli, G. Matteucci, T. Meyers, R. Monson, W. Munger, W. Oechel, R. Olson, K. Pilegaard, K. T. Paw U, H. Thorgeirsson, R. Valentini, S. Verma, T. Vesala, K. Wilson, and S. Wofsy, Environmental controls over carbon dioxide and water vapor exchange of terrestrial vegetation, *Agric. For. Meteorol., 113*, 97-120, 2002.

Liukang X, and DD.Baldocchi. Seasonal variation in carbon dioxide exchanges over a Mediterranean annual grassland in California. In press. Ag & Forest Met 2004.

Lloyd, J., and J.A Taylor, On the temperature dependence of soil respiration. *Funct. Ecol. 8*, 315–323, 1994.

Michaelis, L., and M. L. Menten, Die Kinetik der Invertinwirkung, *Biochem. Z. 49*, 333, 1913.

Moncrieff, J.B., Y. Mahli, and R. Leuning, The propagation of errors in long term measurements of land atmosphere fluxes of carbon and water. *Global Change Biol. 2*, 231-240, 1996.

Moncrieff, J.B., J. M. Massheder, H. de Bruin, J. Elbers, T. Friborg, B. Heusinkveld, P. Kabat, S. Scott, H. Soegaard, and A. Verhoef, A system to measure surface fluxes of momentum, sensible heat, water vapour and carbon dioxide, *J. Hydrol., 188-189*, 589-611, 1997.

Novick, K.A., P. C. Stoy, G. G. Katul, D. S. Ellsworth, M. B. S. Siqueira, J. Juang, and R. Oren, Carbon dioxide and water vapor exchange in a warm temperate grassland, *Oecologia*, 138: 259–274, 2004.

Pacala, W. S., G. C. Hurtt, D. Baker, P. Peylin, R. A. Houghton, R. A. Birdsey, L. Heath, E. T. Sundquist, R. F. Stallard, P. Ciais, P. Moorcroft, J. P. Caspersen, E. Shevliakova, B. Moore, G. Kohlmaier, E. Holland, M. Gloor, M. E. Harmon, S. -M. Fan, J. L. Sarmiento, C. L. Goodale, D. Schimel, and C. B. Field, Consistent Land- and Atmosphere-Based U.S. Carbon Sink Estimates, *Science, 292,* 2316-2319, 2001.

Pattey E., I. B. Strachan, R. L. Desjardins, and J. Massheder, Measuring nightime CO_2 flux over terrestrial ecosystems using eddy covariance and nocturnal boundary layer methods, *Agric. For. Meteorol., 113*, 145-158, 2002.

Post, M. W., T-H. Peng, W. R. Emanuel, A. W. King, V. H. Dale, and D. L. DeAngelis, The Global Carbon Cycle, *Amer. Sci., 78,* 310-326. 1990.

Reido M, A.Grub, M.Rosset, J.Fuhrer. A pasture simulation model for dry matter production, and fluxes of carbon, nitrogen and water. *Ecological Modelling* 105 (1998), 141-183.

Robert, M., Soil Carbon Sequestration for improved land management, *World Soil Resources Report 96*, 58 pp., FAO (Food and Agriculture Organization of UN), Rome, 2001.

Ruimy, A., P. G. Jarvis, D. D. Baldocchi, and B. Saugier, CO_2 fluxes over plant canopies and solar radiation: a review, *Adv. Ecol. Res. 26*, 1-63, 1995.

Saigusa, N., T. Oikawa, and S. Liu, Seasonal variations of the exchange of CO_2 and H_2O between a grassland and the atmosphere: An experimental study, *Agric. For. Meteorol., 89*, 131-139, 1998.

Scanlon T.M., G.Kiely, X.Quishi (2004). A nested catchment approach for defining the hydrological controls of non-point source pollution. In press. *J. of Hydrology.*

Smith, E., Limiting factors in photosynthesis: light and carbon dioxide, *Gen. Physiol. 22*, 21–35, 1938.

Suyker, E. A., S. B. Verma, and G. G. Burba, Interannual variability in net CO_2 exchange of a native tallgrass prairie, *Global Change Biol., 9*, 255-265, 2003.

Soussana, J.-F., P. Loiseau, N. Vuichard, E. Ceschia, J. Balesdent, T. Chevallier, and D. Arrouays, Carbon cycling and sequestration opportunities in temperate grasslands, *Soil Use and Management,* in press, 2003.

Valentini, R., G. Matteucci, A. J. Dolman, E.-D. Schulze, C. Rebmann, E. J. Moors, A. Granier, P. Gross, N. O. Jensen, K. Pilegaard, A. Lindroth, A. Grelle, C. Bernhofer, T. Grünwald, M. Aubinet, R. Ceulemans, A.S. Kowalski, T. Vesala, Ü. Rannik, P.

Berbigier, D. Loustau, J. Guðmundsson, H. Thorgeirsson, A. Ibrom, K. Morgenstern, R. Clement, J. Moncrieff, L. Montagnani, S. Minerbi, and P. G. Jarvis, Respiration as the main determinant of carbon balance in European forests, *Nature, 404, 861-865,* 2000.

Verburg, P.S., J.A.Arnone, D.Obrist,D.Schorran, R.D.Evans, D.Lerroux-Swarthout, D.W.Johnson, Y.Luo and J.S.Coleman. Net Ecosystem carbon exchange in two experimental grassland ecosystems. *Global Change Biology.* Vol.10.Issue 4, pp 498. April 2004.

Webb, E.K., G. I. Pearman, and R. Leuning, Correction of flux measurements for density effects due to heat and water vapor transfer, *Quart. J. R. Meteorol. Soc. 106,* 85-100, 1980.

Wilkinson, J., and M. Janssen, BIOME3, National Emissions Inventory Workshop, Denver, Colorado, May 1-3, 2001.

Figure 1

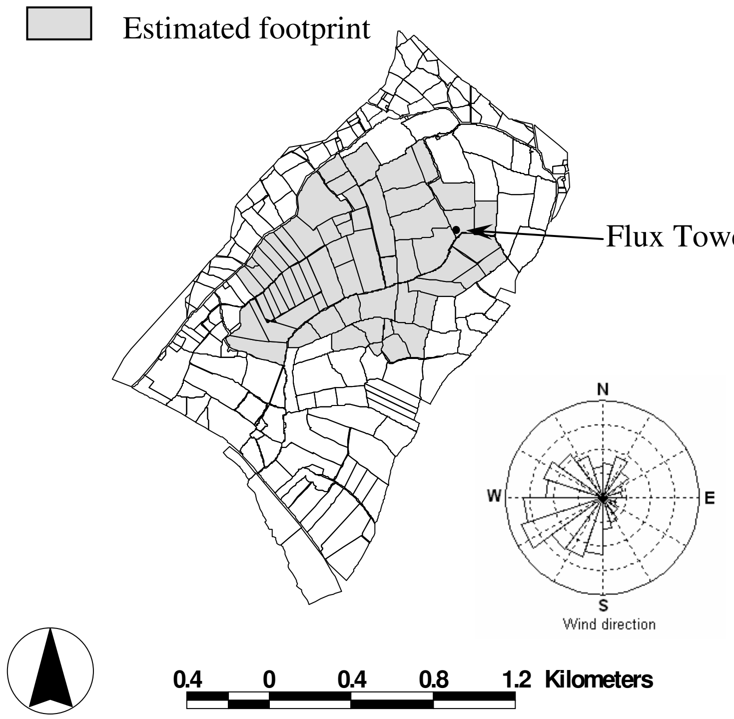
Estimated footprint
Flux Tower
N
W
E
S
Wind direction
0.4 0 0.4 0.8 1.2 Kilometers

Figure 2

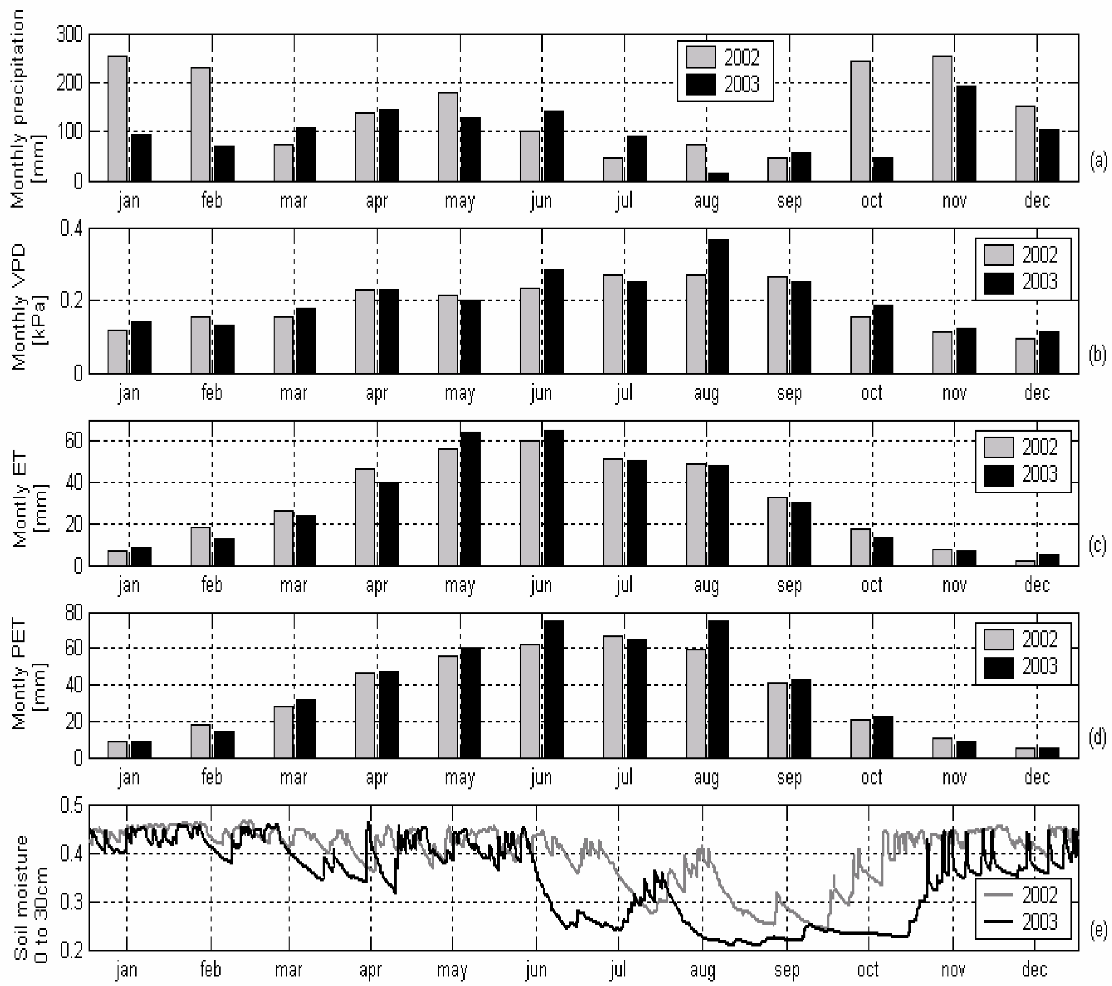
Monthly precipitation [mm]
300
200
100
0
2002
2003
(a)
jan
feb
mar
apr
may
jun
jul
aug
sep
oct
nov
dec
Monthly VPD [kPa]
0.4
0.2
0
(b)
Montly ET [mm]
60
40
20
0
(c)
Montly PET [mm]
80
60
40
20
0
(d)
Soil moisture 0 to 30cm
0.5
0.4
0.3
0.2
(e)

Figure 3.

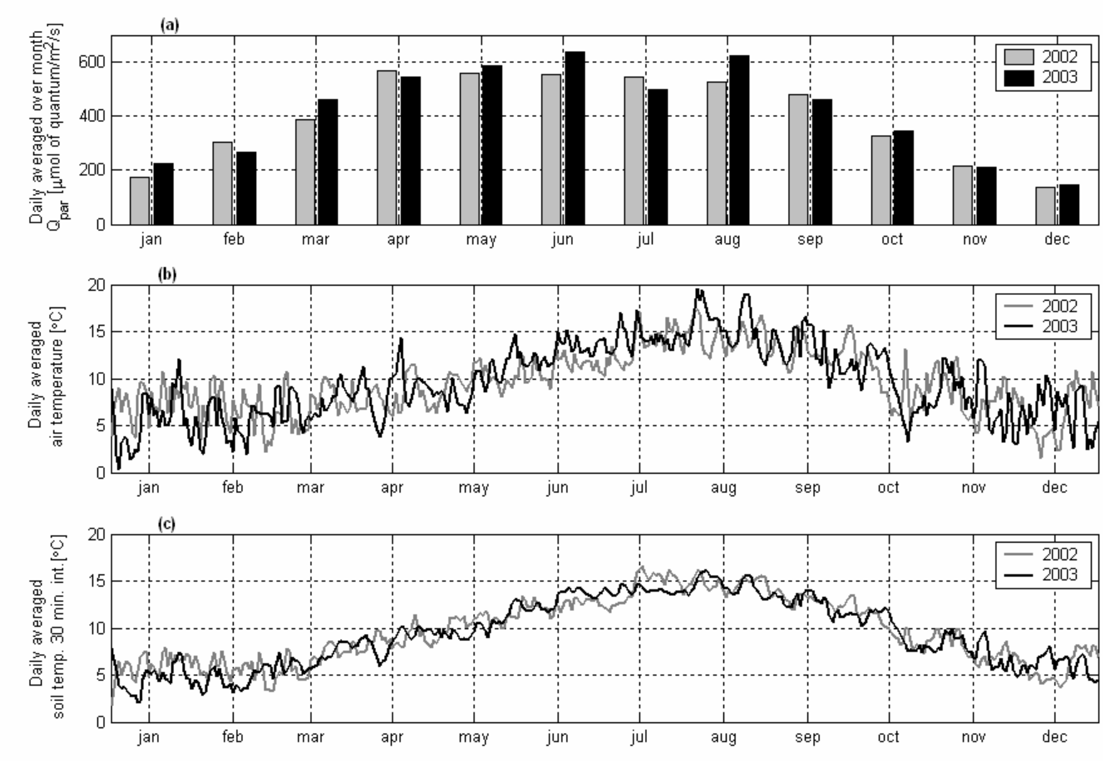
(a)
Daily averaged over month
Q_{par} [μmol of quantum/m²/s]
2002
2003
jan feb mar apr may jun jul aug sep oct nov dec
(b)
Daily averaged
air temperature [°C]
(c)
Daily averaged
soil temp. 30 min. int.[°C]

Figure 4.

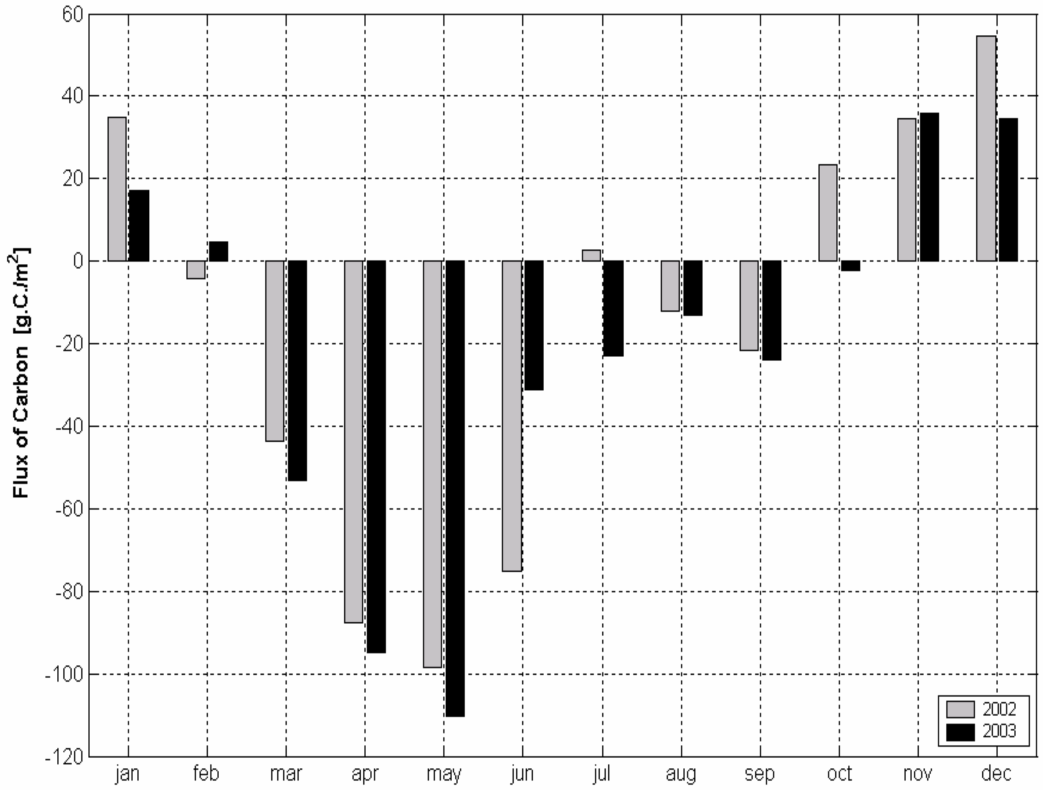
Flux of Carbon [g.C./m2]
60
40
20
0
-20
-40
-60
-80
-100
-120
jan
feb
mar
apr
may
jun
jul
aug
sep
oct
nov
dec
2002
2003

Figure 5.

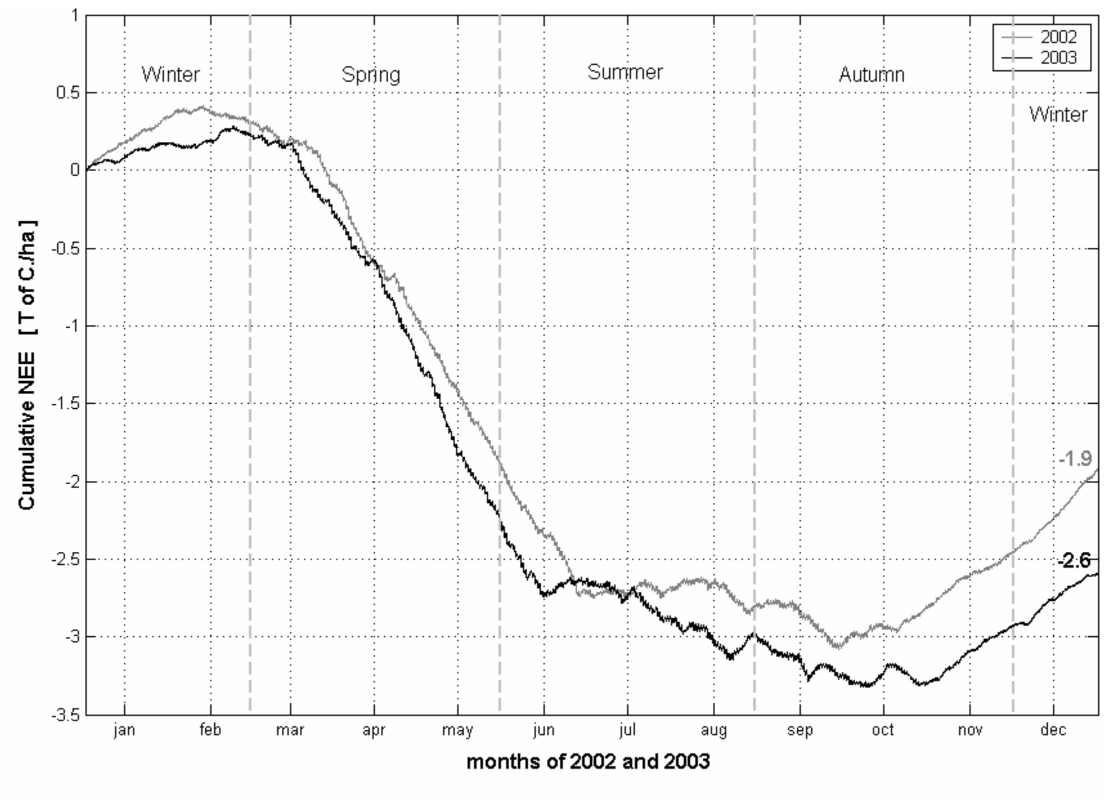

2002
2003
Winter
Spring
Summer
Autumn
Winter
-1.9
-2.6
Cumulative NEE [T of C./ha]
months of 2002 and 2003
jan
feb
mar
apr
may
jun
jul
aug
sep
oct
nov
dec

Figure 6.

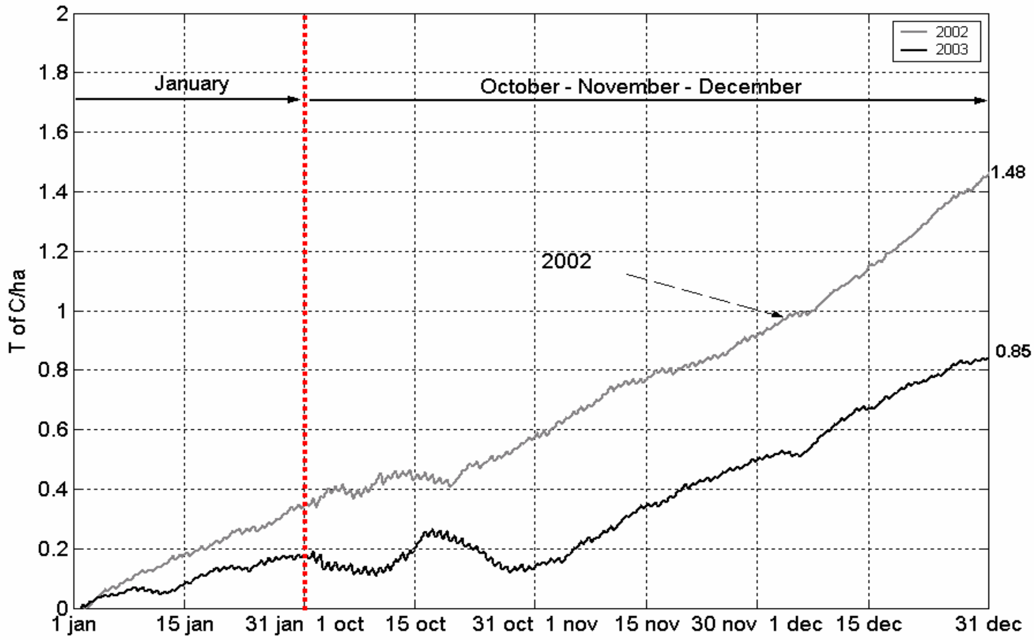

2
1.8
1.6
1.4
1.2
1
0.8
0.6
0.4
0.2
0
T of C/ha
2002
2003
January
October - November - December
1.48
0.85
2002
1 jan
15 jan
31 jan
1 oct
15 oct
31 oct
1 nov
15 nov
30 nov
1 dec
15 dec
31 dec

Table 1

Table 1. Values of day fitting regression parameters for use with Eqn.(3).

Year	Parameter	Months	Months	Months	Months	Months	Months
		Jan-Feb	Mar-Apr	May-Jun	Jul-Aug	Sep-Oct	Nov-Dec
2002	[illegible]	0.0173	0.031	0.030	0.018	0.029	0.019
2002	*c*	0.217	2.525	3.703	3.501	3.24	1.212
2003	[illegible]	0.0171	0.0298	0.033	0.032	0.030	0.015
2003	*c*	0.809	2.088	5.243	6.039	2.788	0.544

Table 2. Monthly summary of key variables in 2002 and 2003

Parameter	**Jan**	**Feb**	**Mar**	**Apr**	**May**	**Jun**	**Jul**	**Aug**	**Sept**	**Oct**	**Nov**	**Dec**	**Sum** (Mean)
02 Precip	254	231	73	137	178	99	48	73	45	244	255	150	**1785**
03 Precip	95	71	106	143	128	140	91	15	56	46	192	102	**1185**
02 PAR	175	302	388	567	558	552	545	527	480	329	217	135	**4805**
03 PAR	225	268	461	545	585	638	497	625	463	343	210	147	**5007**
02 Ta (Ts)	8 (6)	7 (6)	7 (7)	8 (9)	10 (11)	11 (13)	14 (14)	15 (15)	13 (13)	10 (10)	8 (8)	6 (6)	(9.63 -Ta)
03 Ta (Ts)	5 (5)	5 (5)	7 (7)	9 (9)	10 (10)	13 (13)	14 (14)	16 (15)	13 (13)	9 (10)	8 (8)	6 (6)	(9.64 -Ta)
02 VPD	0.115	0.156	0.154	0.230	0.212	0.230	0.271	0.271	0.266	0.155	0.113	0.094	(0.19)
03 VPD	0.138	0.129	0.175	0.227	0.200	0.281	0.252	0.366	0.252	0.186	0.121	0.111	(0.203)
02 ET	6.6	18.0	25.8	46.3	55.8	60.1	51.1	49.0	32.7	17.3	7.7	1.7	**370**
03 ET	8.3	12.8	23.9	39.5	64	65.2	50.7	47.9	30.2	13.4	7.0	4.8	**366**
02 PET	9.2	18.3	27.6	46.5	55.7	62.4	66.5	59.7	40.6	20.6	10.4	5.1	**423**
03 PET	8.8	14	31.6	46.9	60	75.1	64.8	75.3	42.6	22.2	9.1	4.8	**455**
02 θ_{30}	0.445	0.449	0.429	0.416	0.422	0.407	0.342	0.338	0.266	0.370	0.435	0.429	
03 θ_{30}	0.426	0.426	0.400	0.380	0.409	0.336	0.282	0.238	0.227	0.233	0.359	0.380	
02 LAI						-------	Cut 1st		Cut 30th	No grazing	No grazing	No grazing	
03 LAI						Cut 15th	----------		Cut 15th	grazing	grazing	grazing	
02 Fc	+35	-4	-44	-88	-99	-75	+2	-12	-22	+23	+35	+55	**-193**
03 Fc	+17	+2	-53	-95	-110	-31	-23	-13	-24	-2	+36	+34	**-260**

02 = 2002; 03 =2003; precip = precipitation; Ta = Air temperature in ^{O}C; Ts = Soil Temperature in ^{O}C at 5cm depth.
VPD = Vapour pressure deficit in kPa.
ET = EC measured evapotranspiration in mm. PET = Potential evapotranspiration using Penman-Monteith in mm.
θ_{30} = soil moisture (m3/m3) depth averaged over the top 0 to 30cm depth.
LAI = commentary on cutting and grazing times.
Fc = flux of carbon in g.C/m2.month (NEE).